REPORT NO.
UCB/EERC-80/28
OCTOBER 1980

EARTHQUAKE ENGINEERING RESEARCH CENTER

SHAKING TABLE TESTING OF A REINFORCED CONCRETE FRAME WITH BIAXIAL RESPONSE

by

MICHAEL G. OLIVA

COLLEGE OF ENGINEERING

UNIVERSITY OF CALIFORNIA · Berkeley, California

REPORT DOCUMENTATION PAGE	1. REPORT NO. NSF/RA-80 0366	2.	3. Recipient's Accession No. PB81 154304
4. Title and Subtitle Shaking Table Testing of a Reinforced Concrete Frame with Biaxial Response			5. Report Date October 1980
			6.
7. Author(s) Michael G. Oliva			8. Performing Organization Rept. No. UCB/EERC-80/28
9. Performing Organization Name and Address Earthquake Engineering Research Center University of California, Berkeley Richmond Field Station 47th Street & Hoffman Blvd. Richmond, Calif. 94804			10. Project/Task/Work Unit No.
			11. Contract(C) or Grant(G) No. (C) (G) PFR-7908257
12. Sponsoring Organization Name and Address National Science Foundation 1800 G Street, N.W. Washington, D.C. 20550			13. Type of Report & Period Covered
			14.

15. Supplementary Notes

16. Abstract (Limit: 200 words)

The program in this report involved testing of a one third scale 2 story reinforced concrete frame, having rectangular section columns, with inelastic biaxial motion induced through earthquake excitation on a shaking table. Close inspection of the experimental response, and comparison with previous test results on a similar frame under pure uniaxial motion, found that biaxial motion seriously reduced the column yield strength. Local and global response characteristics indicated a tremendous amount of interaction between the rectangular column's strong axis motion and weak axis response. Weak axis stiffness was reduced to less than one third the initial value, through strong axis interaction, associated with narrow hysteretic load-deformation response, characteristic of a low energy absorption mechanism.

Analytical correlation with experimentally measured response, considering response independently along the frame's major axes, was unsuccessful. Necessary modifications to current analysis techniques, for accurate modelling of multi-axial loading, including biaxial bending, of reinforced concrete members is discussed.

18. Availability Statement Release Unlimited	19. Security Class (This Report)	21. No. of Pages 205
	20. Security Class (This Page)	22. Price

(See ANSI–Z39.18)   See Instructions on Reverse   OPTIONAL FORM 272 (4–77) (Formerly NTIS–35) Department of Commerce

Shaking Table Testing
of a Reinforced Concrete Frame with Biaxial Response

By

Michael G. Oliva
Research Engineer
Department of Civil Engineering
University of California
Berkeley

October 1980
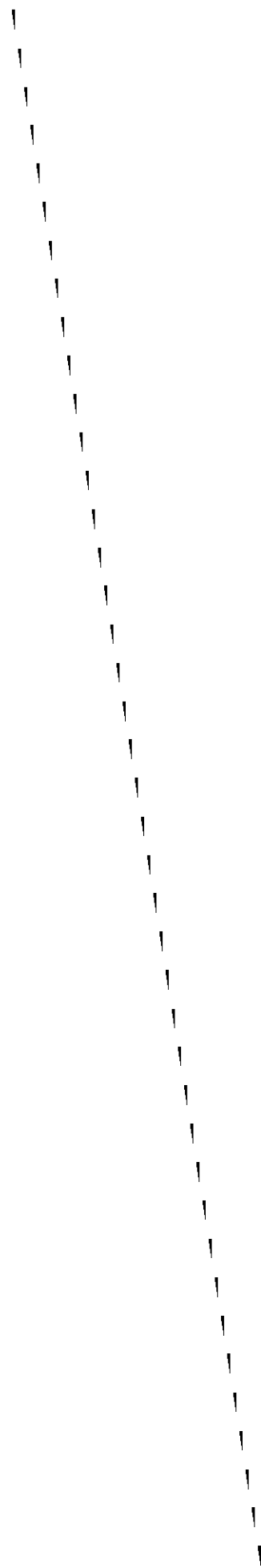
Shaking Table Testing
of a Reinforced Concrete Frame with Biaxial Response

Michael G. Oliva

Department of Civil Engineering
University of California

Abstract

The program in this report involved testing of a one third scale 2 story reinforced concrete frame, having rectangular section columns, with inelastic biaxial motion induced through earthquake excitation on a shaking table. Close inspection of the experimental response, and comparison with previous test results on a similar frame under pure uniaxial motion, found that biaxial motion seriously reduced the column yield strength. Local and global response characteristics indicated a tremendous amount of interaction between the rectangular column's strong axis motion and weak axis response. Weak axis stiffness was reduced to less than one third the initial value, through strong axis interaction, associated with narrow hysteretic load-deformation response, characteristic of a low energy absorption mechanism.

Analytical correlation with experimentally measured response, considering response independently along the frame's major axes, was unsuccessful. Necessary modifications to current analysis techniques, for accurate modelling of multi-axial loading, including biaxial bending, of reinforced concrete members is discussed.

Acknowledgements

Table of Contents

iv

Chapter 1

Introduction

The specialized area of earthquake engineering strives to develop system designs which will survive structurally under forces and deformations induced during ground shaking of the strongest likely intensity, while avoiding:

1. collapse of the structure itself,

2. loss of life due to failure of structural or non structural components acting structurally.

Unlike gravity loads, earthquakes transfer considerable kinetic energy to the system. In an elastic structure, the energy appears in the buildup of large resonant vibratory motion, limited solely by damping and duration of the shake. Energy stored in such a fashion will most often exceed strength and deformation capacities, resulting in one or both undesirable consequences. Seismic research is directed towards controlling the way such energy is manifested, through design for, and analytical prediction of, the response which will be developed under excitation.

An earthquake design philosophy has evolved in which energy absorption and dissipation mechanisms are integrated into the load resisting system. In most wood structures, the material itself has high energy absorption capacity and joints providing energy dissipation, even when designed primarily for gravity load. Research in steel has suggested development of critical regions within the structure where material energy absorption will occur with large local deformation. Methods of design in reinforced concrete have been proposed which likewise try to isolate energy absorption mechanisms within specific limited regions.

Reinforced concrete has frequently relied upon ductile moment resisting frames (DMRF) to provide vertical and lateral strength and stiffness in low to medium rise buildings. Elastic response to the lateral loads requires a significant strength capacity beyond that needed for gravity. Economic limitations, however, mandate inclusion of energy dissipation in the form of inelastic deformation to reduce dynamic internal forces and required lateral design capacity. The current DMRF design technique in concrete recognizes the critical importance of maintaining vertical load capacity of columns at all times to avoid sudden collapse. Hence, development of regions where inelastic behavior may occur is forbidden in column members. New structures are using a 'strong column-weak girder' approach [12]† where the combined bending and axial capacity of a column is designed to be higher than the sum of capacities of girders framing into it. Thus, inelastic action should be initiated in beams prior to columns.

---

† Numbers in brackets denote references listed at the end of the text.

While earthquakes create horizontal motions in randomly oriented directions, most structural design and analysis procedures consider only the independent response of a building along each of its principal axes. Minimum code design requirements, including the estimate of base shear, shear distribution and overturning moments, allow the assumption that forces along the separate main axes of a structure act non concurrently [12]. This approach is permitted because multidimensional analysis has been difficult and costly, there has been little information available regarding the load deformation behavior for reinforced concrete sections under biaxial bending, and it has been assumed that orthogonal peaks of motion are unlikely to occur simultaneously.

Independent uniaxial design of reinforced concrete columns has resulted in serious failure, however, particularly under seismic excitation. In frame structures, the multidimensional motion of earthquakes has its greatest effect on column loading. They are subjected to biaxial loads from both 2D lateral motion and structural torsion, with added varying axial loads due to overturning effects, in addition to the gravity forces. Previous experimental and analytic studies [20-26,30] using square and circular section columns, have noted that the biaxial bending during inelastic motion may significantly decrease stiffness and increase total drift. Ultimate and yield strength in any particular direction is decreased by the existence of simultaneous moments along another axis. Multiple loading with biaxial bending may cause inelastic deformation in columns, even with strong column-weak girder design, particularly if the multiaxial nature of the loading has not been considered during design.

Since a structure's response to a given earthquake is dependent on its strength, initial stiffness, damping and the overall relation between internal forces and deformation, which qualities define its hysteretic deformation capacity, variation of these characteristics under 2D lateral motion from those assumed with 1D motion may cause the response to differ from the assumed 1D response. One of the most graphic recent examples of deviation from 1D lateral response is the Olive View Hospital failure during the 1971 San Fernando earthquake. The inability of 1D analysis to explain the magnitude of displacement measured at the hospital (namely large residual drift) was mentioned in various investigative reports [25,27,28,29].

The work described herein is the first study to experimentally investigate the behavior of rectangular concrete columns under biaxial bending, and to test a large scale reinforced concrete frame with multiple columns under loading induced by earthquake motion. While a smattering of research reports documenting tests and analyses of circular and square columns under biaxial loading followed the Tokachi-Oki '68 and San Fernando earthquakes, there has been no significant work on rectangular section columns, even though they are in common use. Circular columns, having no principle axis of flexural rigidity, and square columns, (the quadrilateral section with the most similar characteristics) would be expected to exhibit less biaxial response coupling than rectangular columns. The very nature of a rectangular column, with different moments of inertia along its principle axes, should induce exaggerated interaction effects under biaxial loading. Detailed inspection of the local bending characteristics of the columns in the present test, found a surprising amount of stiffness degradation and bending

interaction due to concrete cracking, crushing and rebar elongation. A comparison of the internal resisting forces developed in the frame under biaxial bending with those from an identical previous frame tested under similar but uniaxial motion, found a definite apparent decrease in strength along the analogous axis when biaxial loading was present. Though interaction effects, such as reduced stiffness in one axis direction, were created by multiaxial loads in a particular column, the remaining columns had slightly different loads and different behavior. If numerous columns are joined in a single structure, the motion of any column will be constrained by that of the structure as a whole. All of the previously cited studies involved single columns tested under prescribed motion paths or analytic models of single columns with a lumped mass and earthquake excitation. In a structure such as tested in this program, where the columns are joined, the overall response may be less affected by individual interactions occurring in particular columns than has been witnessed in component tests.

If column response during a loading sequence remains within the so called elastic range, very little interaction would be expected, and an analytic prediction of response, based on a planar model of the structure with 1D bending, should provide accurate results. However, once the column reaches the inelastic deformation stage, some interaction (due to concrete cracking and rebar yield from load along one axis affecting the stiffness along the other axis) will occur, and a planar mathematical modelling, which considers motion along the two axes as independent, would be expected to predict erroneously. Aktan [25] and Pecknold and Suhawardy [31] claimed that as long as the analysis using a planar model predicted a maximum ductility of less than 2, then planar analysis should be acceptable. In the present program, planar analysis of an earthquake motion which caused inelastic deformation was attempted using a fairly sophisticated column modelling element which included inelastic moment rotation behavior and degrading stiffness [13], and resulted in a predicted peak first story displacement of 1.8 inches longitudinally, a displacement ductility of 3.4. In this case planar analysis was in fact not capable of effectively modelling the additional stiffness deterioration in the test structure caused by inelastic interaction of the multi-axial loads. However, actual displacements did not critically exceed the planar prediction, as postulated by Aktan, a result of the restraint provided by other columns under differing load.

The primary reason multidimensional analysis is not commonly employed is its complexity and cost. Until recently, very few mathematical techniques had been developed which could even model the biaxial bending behavior of a reinforced column, regardless of section shape. Two basic approaches have appeared within the last ten years. The first method [22,25,26,&30], explicitly models the column by dividing its cross section into a number of smaller areas (filaments). Each area is assumed to be uniaxially stressed and to have behavior governed by hysteretic stress-strain characteristics of the material it simulates. Force deformation characteristics of the column are then calculated by assuming the displaced shape of its axis, with internal forces calculated at various sections from resulting curvatures. Results are accurate, but the computation is too complex and costly for general use and concentrated end rotations due to effects such as bar slip within joints are not simulated. A second strategy [20,21,23,29] is appealing in both its elegance and its direct approach to simulating load-

deformation behavior. The model uses a flexure-rotation relation based on interaction equations between the biaxial moments, and a plasticity method to define moment vs rotation behavior. Though computationally less complex than the former, it is unable to include some of the specific effects (crushing of unconfined concrete, or yielding of particular bars) which are implicitly part of the filament type model.

In this program, the behavior of the section required special modelling, not met by the plasticity type elements, to duplicate interaction effects noted in the weak direction. Specific characteristics needed to model such weak axis interactions accurately are listed with observations and conclusions from the response study. Information on local behavior and overall structural response collected during the test sequence provides an excellent data base for correlation checks and development of new mathematical techniques to aid in prediction of inelastic response and structural safety during earthquake motions. ·

Chapter 2

Project description

Introduction

This report covers the experimental earthquake testing, investigation of response behavior, and analytic correlation of a large scale reinforced concrete frame with inelastic biaxial column bending. The structure used in this test program was identical to a frame studied previously under similar excitation, but with only uniaxial column bending [1]. The present frame was subjected to 3-dimensional motion, creating biaxial bending as well as varying axial load within rectangular section columns. This first detailed study of rectangular columns under biaxial bending was achieved by thoroughly monitoring the column response through various force and deformation measuring devices. A significant amount of interaction between strong axis and weak axis column motion was readily apparent. Attempts to model the structure's response with computer implemented mathematic techniques using traditional 2D planar frame modelling were unsuccessful when multi-axial interaction had a significant effect on the behavior.

Model frame-

The test model was a two story structure, rectangular in floor plan, and had floor slabs cast integrally with beams spanning in the longitudinal and transverse directions between four supporting columns which were also of rectangular cross section (Fig. 2.1). Basic design is of a strong girder-weak column type intended to induce inelastic deformation in the columns first. As a result of the rectangular floor plan, and columns oriented with their weak axis in the frame's short direction, the structure had different natural frequencies of lateral vibration along its two main axes. General frame properties are listed in Table 2.1.

Table 2.1

Material Properties

reinforcing steel	Grade 40, spec. min. yield 40ksi (276MPa)
concrete	spec. 28 day strength = 4000psi (27.6MPa)
	strength at test date = 4720psi (32.5MPa)

Design Column Ultimate and Yield Strength

size = 8.5x5.75 in. / strong and weak axis

M_u strong	197in-k	(22.3kN-m)
M_u weak	100in-k	(11.3kN-m)
M_y strong	146in-k	(16.5kN-m)
M_y weak	88in-k	(9.9kN-m)

6

Design Column Moment of Inertia *in.*[4]

strong axis	294. gross area
	129. cracked section
weak axis	135. gross area
	43. cracked section

Initial Lateral Vibration Frequencies (Hz)

	strong axis	weak axis
MODE1	3.44	2.07
MODE2	8.86	5.43
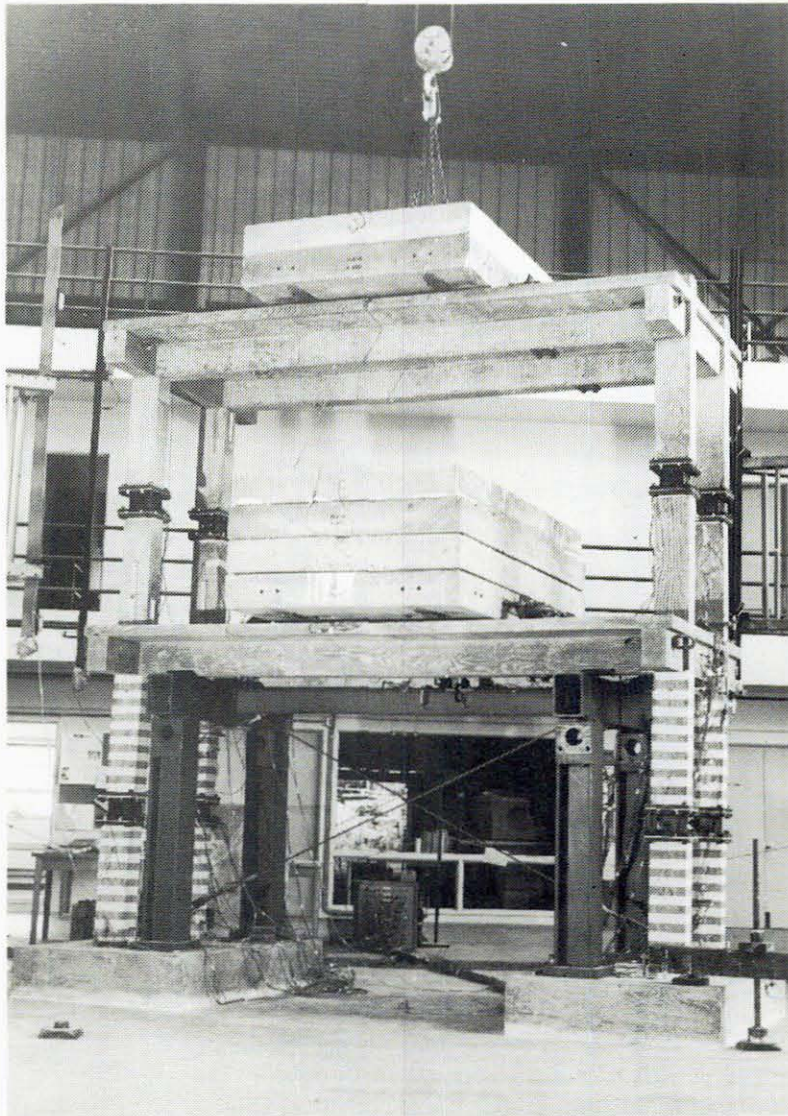
Figure 2.1 Experimental frame on shaking table,
with safety frame under floor in case of collapse.

Test sequence-

A ground displacement history, derived from the Taft, California 1952 earthquake record [8], was used as the primary test motion with magnification factors applied to provide various specific amplitudes. Between shaking table tests with the Taft earthquake motion, the structure's natural frequencies were measured using free vibration tests. Descriptive characteristics for the sequence of test motions are listed in Table 2.2

Table 2.2

Earthquake Test Sequence- Table Motion		
TEST	Peak Acc. (g's)	Peak Displ. (in.)
Taft100(1)	0.062	0.503
Taft100(2)	0.061	0.498
Taft1000	0.685	5.07
Pacoima	1.49	5.23
Frame repaired / epoxy injection		
Pacoima	1.37	5.25
Taft1000	0.711	5.06

Test results-

Considerable inelastic deformation occurred during the Taft 1000 large scale earthquake. The first mode lateral vibration frequency deteriorated by 46% in the strong axis and by 49% in the weak axis direction. Numerous bending type cracks developed at the joints near the ends of the lower story columns. Crushed concrete, part of the unconfined exterior cover, was visible at specific corners near the base of the columns. Very little visible damage was apparent in the beams other than cracking which had occurred during placement of the dead load mass blocks. Overall global response parameters of the frame may be seen in Table 2.3. Values of peak local quantities for the present (RCF5) frame are listed in Table 2.4 with comparable results from the previous uniaxial tests.

Peak Values of Local Quantities measured during T1000 test		
	RCF5	RCF2(W850)
Table accel.*	0.620g	0.570g
Column shear		
weak axis	4.63k	-
strong axis	7.28k	8.54k
Column moment		
weak axis	108in-k	-
strong axis	270in-k	n.a.
Column axial	46k	27k
Residual displ. first floor		
weak axis	0.058in.	-
strong axis	0.065in.	0.155in.
Peak displ. first floor		
weak axis	1.54in.	-
strong axis	2.12in.	2.04in.
Rebar strain (milli in./in.)	18.1	20.7
Avg. conc. strain (milli in./in.)	0.0158	n.a.
Column base rotation (rad.)		
weak axis	0.0226	-
strong axis	0.0223	n.a.
*Ground accel. component along strong axis of frame.		

Table 2.4 (left)

Table 2.3

Global Response Quantities		
	T100(2)	T1000
Table accel.	0.061g	0.685g
Strong Axis peak acceleration		
1st floor	0.144g	0.684g
2nd floor	0.198g	1.093g
peak rel displ.		
1st floor	0.1in.	2.12in.
Weak axis peak acceleration		
1st floor	0.041g	0.306g
2nd floor	0.072g	0.451g
peak rel. displ.		
1st floor	0.087in.	1.54in.
2nd floor	n.a.	2.05in.
Peak torsion	-	0.0043rad.

The amount of inelastic deformation is reflected in the values of peak column base rotation, peak rebar strain and estimated peak concrete strain. Indications of the effects of interaction during the biaxial frame test became apparent when shear vs. first floor displacement plots from the present structure were compared with those of the uniaxially tested RCF2 frame. Even though the present RCF5 frame was constructed of slightly stronger materials, it did not develop restoring forces, in the form of longitudinal shear or a vectorial combination of simultaneous shears along the two axes, as high as measured in the uniaxial RCF2 frame. Columns from both frames had identical initial stiffness, however, the columns under biaxial load differed from the uniaxial in having a crucially greater amount of stiffness degradation during inelastic response. Close inspection of the local bending behavior revealed further interaction. Bending response in the column weak directions exhibited obscure characteristics with little of the regular hysteresis behavior seen in most bending tests. The moment vs. curvature loops

became quite pinched, and traveled very erratic paths due to exaggerated strong axis motion interaction effects on the weak axis behavior caused by concrete cracking, crushing, and residual rebar elongation.

Analytical correlation-

A common inelastic computer analysis package (DRAIN2D [13]) was employed for response prediction, to be correlated with experimental frame results. The program has only 2-D planar frame analysis capability. Since codes generally allow seismic design based on application of simulated earthquake lateral loading independently along a structure's main axes, attempts at obtaining an analytical vs. experimental correlation were made with the same approach.

Mathematically predicted response was successfully correlated with the measured frame displacement history for the low amplitude Taft100(2) earthquake test. Interaction effects had a minimum of importance during the elastic motion of that shake, allowing the independent planar frame approach to be used with success.

Prediction of the frame's motion during an excitation which produced inelastic response, using independent planar frame modelling along the two major axes, resulted in poor correlation. With inelastic deformation, interaction effects significantly affect the overall structural response making independent frame analysis inappropriate. In short, stiffness degradation occurring along a particular axis of the structure can not be developed in the analytic model as a result of loading along that axis alone.

Concrete column mathematical modelling was attempted using an element included in the DRAIN2D computer program which allows bending moment- rotational stiffness degradation. However, appropriate estimation of the parameters needed to describe degrading characteristics accurately for the element would have been impossible without already having member test results in hand. No general guidelines have been developed which allow prediction of such parameters based on material characteristics and section dimensions.

Observations-

1) Results of the tests indicate that designers of reinforced concrete columns (particularly if rectangular), which may resist biaxial loading, should be cognizant of the possibility of reduced strength and increased degradation of stiffness compared to that expected under uniaxial load.

2) Prediction of loading and subsequent strength design, based on separate analyses along a structure's main axes, ignores the effects multi-axial interaction may have on the stiffness and natural vibration frequency.

10

3) Existing techniques of 3-dimensional frame modeling do not include all the necessary components, noted in the investigation of local response of the present tests, needed to describe column behavior under multi-axial inelastic loading for successful prediction of structural response.

4) Even planar analysis of concrete bending relies on member modelling elements with stiffness degradation (a necessity) that requires estimation of descriptive parameters for which no defining guidelines exist. Incorrect estimation of such parameters critically changed the predicted response. A commonly used computer program for reinforced concrete nonlinear dynamic analysis, upon which the correlation studies were based, was unable to simulate the response due to multi-axial interaction effects, and moreover required guesswork to establish parameters for the mathematical model resulting in a predicted response which was no more accurate than the guessed parameters.

Chapter 3

Model Description and Properties

Structural model

The entire project described herein was designed to closely parallel a previous concrete frame test program. That frame, described by Clough and Gidwani [1], and hereafter referred to as RCF2 (Reinforced Concrete Frame 2), was tested under uniaxial motion. Both the present skewed frame, Figure 3.1, and RCF2 model structures were built to nearly identical specifications. They are two story reinforced concrete frames with a single bay in each direction. The four columns are framed in the long direction by longitudinal symmetric section concrete "T" beams and in the short transverse direction by concrete single flange unsymmetric "T's" cast integrally with the floor slabs. The basic design is purposely of a strong girder-weak column type to initiate inelastic deformation primarily within the columns, however, even in strong column-weak girder design, inelastic action is expected to occur in columns due to the effects of combined multiaxial loading. Structural dimensions are indicated in Figure 3.2.

The primary difference between the research conducted on the RCF2 frame and the present model is in the type of motion allowed to occur in the frame during testing. The present model was allowed to displace freely in any direction and was mounted in a manner which would purposely induce multiple motions, while the RCF2 was only allowed to move along a single horizontal axis. As indicated in Figure 3.3, this model, RCF5, was mounted on the shaking table with its longitudinal axis at a 25 degree angle to the axis of horizontal motion of the table. Thus, horizontal movement of the table could induce horizontal response along each of the model's principal axes, whereas the RCF2 frame was mounted on the table with its longitudinal axis exactly parallel to the direction of motion as indicated in Figure 3.4. In addition, as indicated in Figure 3.2, 1" diameter (2.54cm) steel bracing cables were attached to the RCF2 frame in the transverse direction near the column at each floor level to constrain the structure against any transverse or torsional movement. The cables were simply hand tightened with a turnbuckle, supposedly providing enough slackness to allow longitudinal motion to occur unimpeded while restraining significant motion in other directions.

The basis for design of a model structure with these particular dimensions was originally described in a report by Hidalgo and Clough [2]. The structure was intended to represent a portion of a typical small (low rise) apartment or office building designed to meet most of the ductile requirements of the 1970 Uniform Building Code and the ACI-318-71 Code. Scaling between prototype and the model was according to the following ratios:
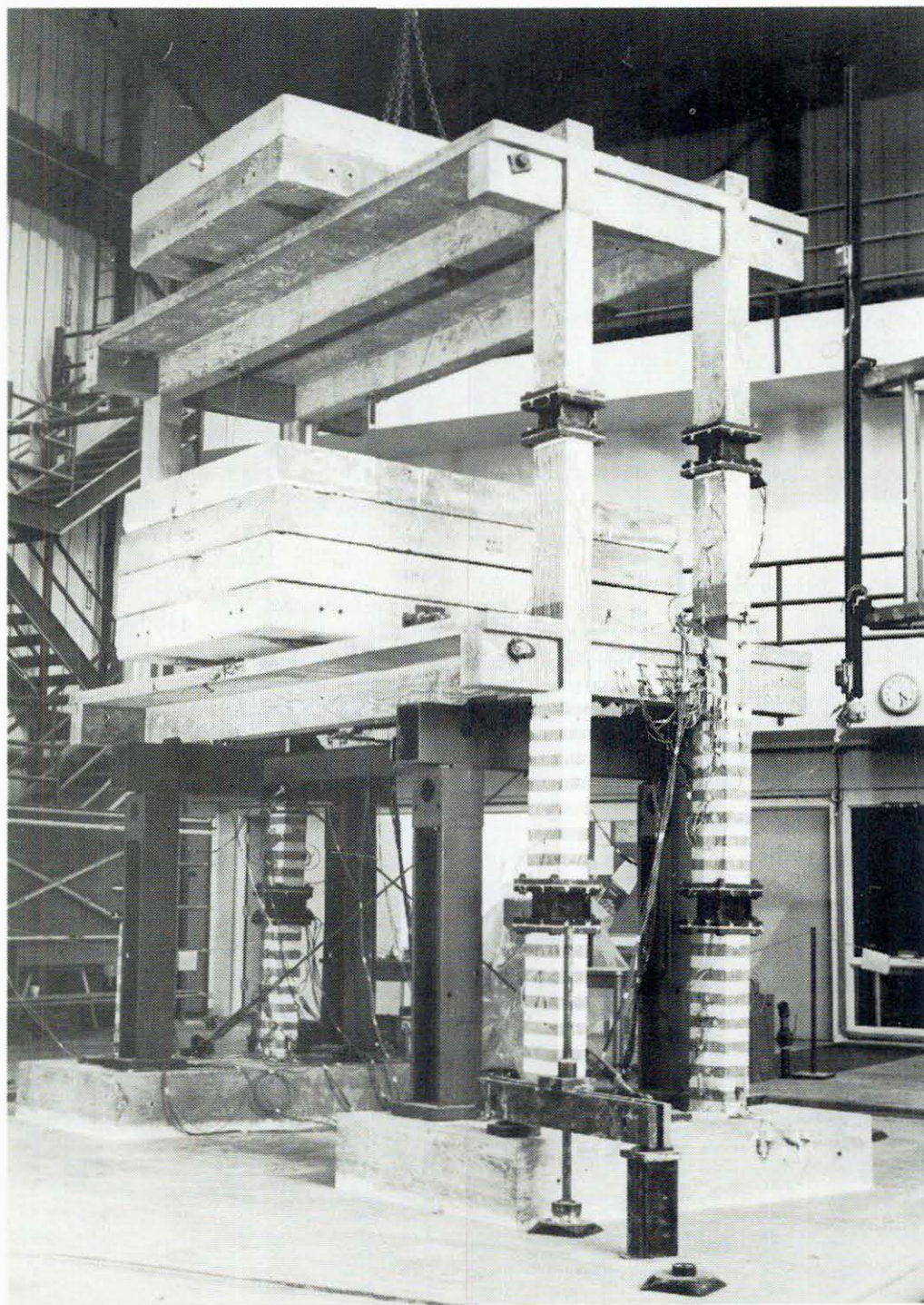
Figure 3.1 Skew mounted frame on table, viewed from north-east.
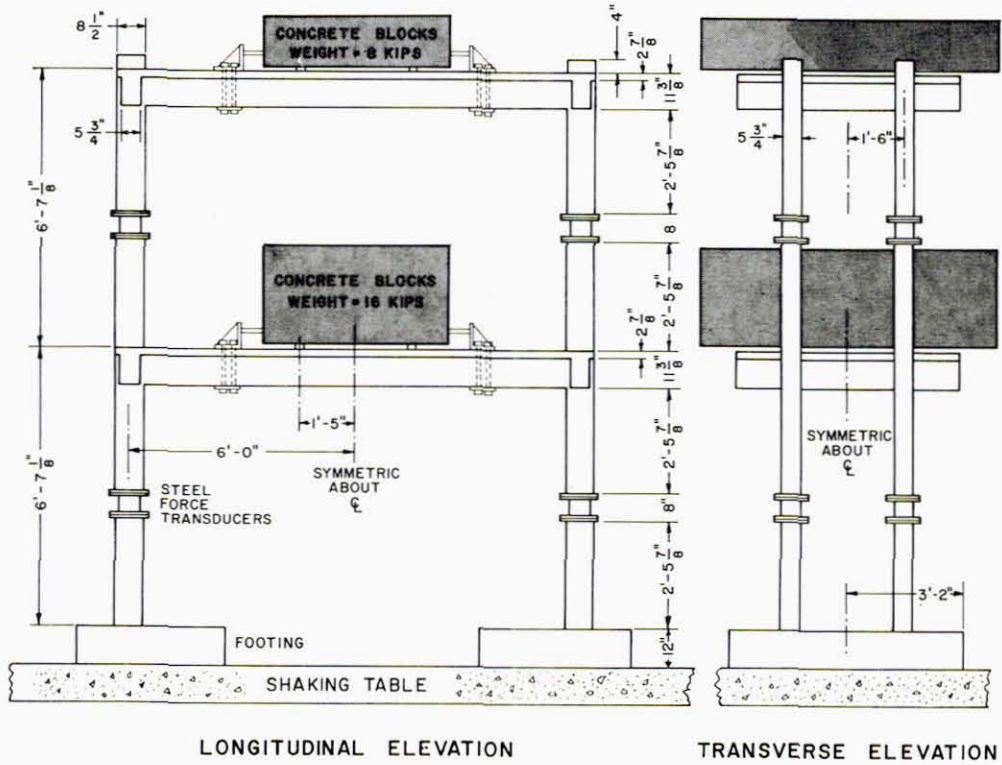
Figure 3.2 Overall dimensions and geometry of test frames, (top) present biaxial frame (RCF5), (Below) previous uniaxial frame (RCF2)
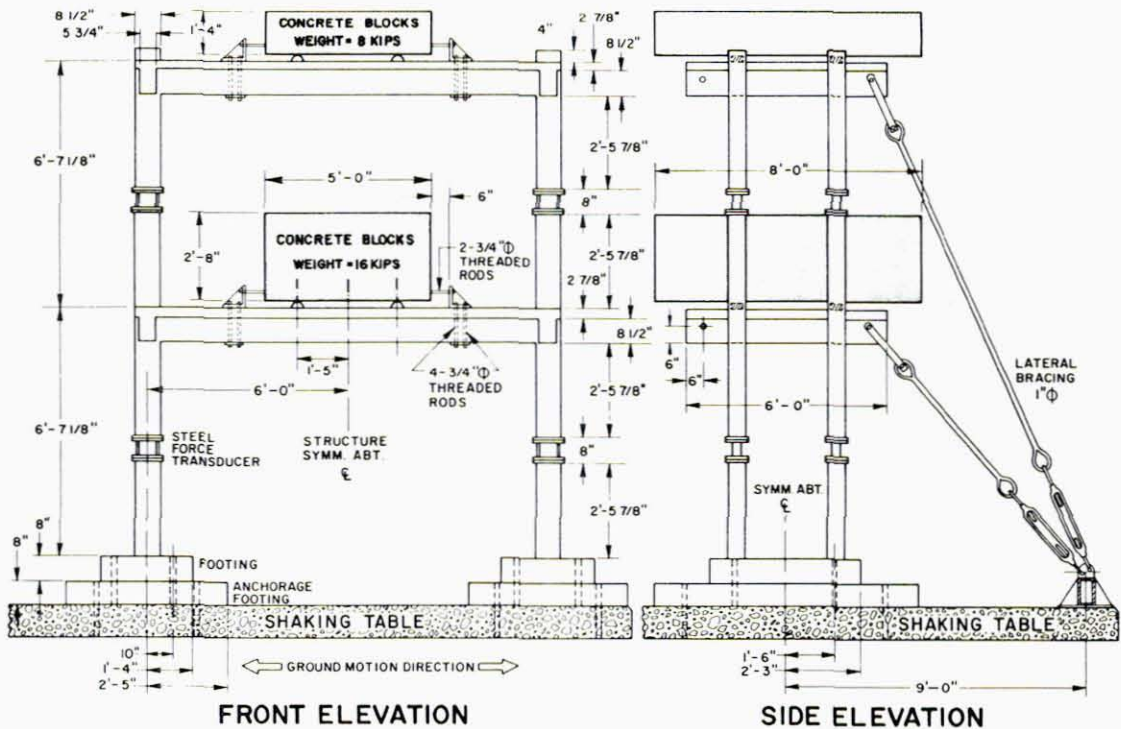
Length ratio	=0.707	Stress ratio (assumed)	=1.00
Area ratio	=0.50	Gravity ratio	=1.00
Strain ratio	=1.00	Acceleration ratio	=1.00

However, since normal reinforcing bars were used, the scaling of reinforcing area and therefore stress and strain, was altered by the available bar sizes. The same model configurations and dimensions were used in this test series to provide a direct comparison of damage and response between a structure undergoing simultaneous motion in two horizontal directions and a structure under similar magnitude of excitation responding along a single horizontal axis. The only difference in design of the two frames occurred in the size and detailing of the footings used in tying them to the table and can be seen in the detailed plans in *Appendix B*.

The original design was intended to represent a single bay of a long narrow building. To allow testing on the 20 ft. x 20 ft. (6.1m x 6.1m) shaking table and for economy, the model was built with dimensions approximately 7/10s those of a real building. This large scale modelling allowed use of "real" materials for construction (i.e. common reinforcing bars and normal concrete), thereby avoiding material modelling difficulties between prototype and model which generally occur in studies involving nonlinear behavior due to inelastic deformations. The scale also allowed design of a structural model whose natural response frequencies were within the table's range of excitation. Length scaling and a desire to simulate full dead load effects did require the addition of artificial masses at each floor level of the model frame. The weights of the structural frame sections, as measured before testing, and the added mass blocks are noted in Figures 3.2 and 8.2. A second deviation from the real building configuration was caused by the placement of force transducer units described in *Appendix C* at the mid-height of each column. This mid-height location, near the column's normal bending inflection point and stiffness of the same magnitude as the concrete column insured a minimum of influence on the structure's dynamic response behavior (see *Chapter 6*).

Model member configuration

As indicated previously, the test frame is composed of columns, symmetric and unsymmetric T beams, floor slabs, and footings. The prime purpose of the footings is to provide a means of attachment between the test structure and the moving table. To eliminate the unnecessary added complexity due to rocking, uplift, and sliding, which could comprise a separate study in itself, each footing is cemented down with a lime-gypsum based compound, and pressed against the table with an approximate pre-load of 90 kips (400 kN) creating good lateral restraint due to the bond and friction and causing an effective fixed base for the first story columns in the structure's initial condition.

The columns are rectangular in section with 4 longitudinal no. 5 reinforcing bars. (The no. 5 designation indicates the number of 1/8 inches in the diameter, ie.-no. 5 is 5/8 in. diameter.) Closed ties of no. 2 undeformed bars encircle the longitudinal bars at spacings required to insure that the shear capacity would be higher than the simultaneous moment capacity and to provide confinement for concrete under compression. A typical column cross section is drawn

Figure 3.3 Plan of biaxial test frame on shaking table.
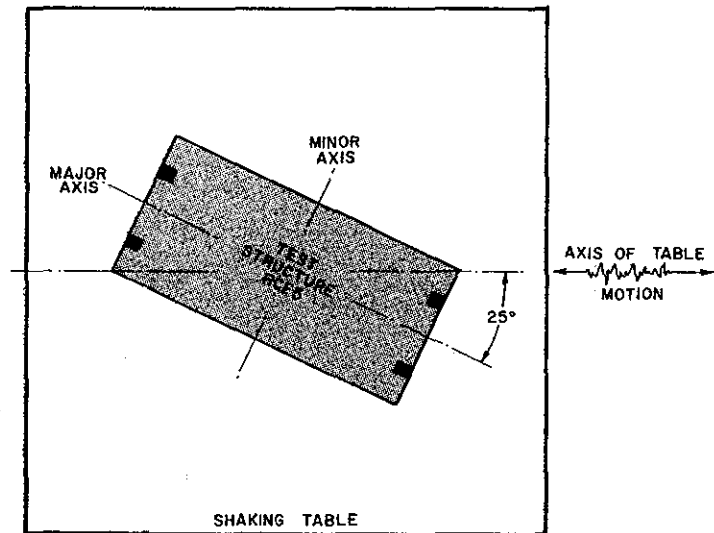
Figure 3.4 Plan of uniaxial frame on shaking table.
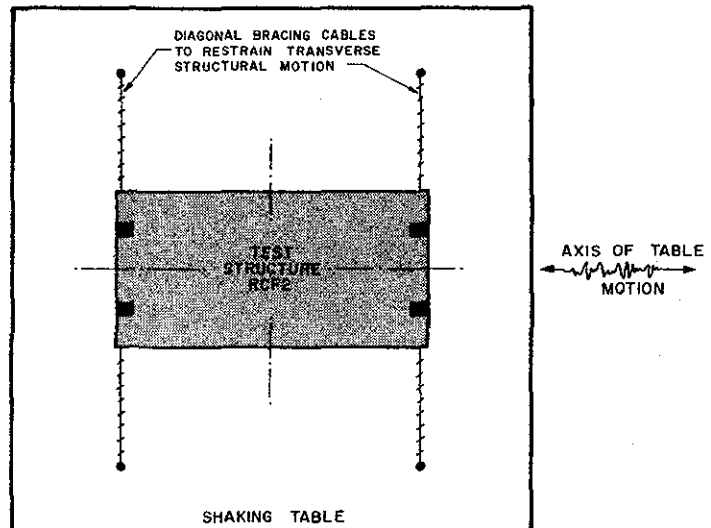
in Figure 3.5. All reinforcing steel was specified as ASTM Grade 40 material with minimum yield strength of 40 ksi (276 mPa) and not exceeding 50 ksi (345MPa).

Figure 3.5 Typical column cross section.
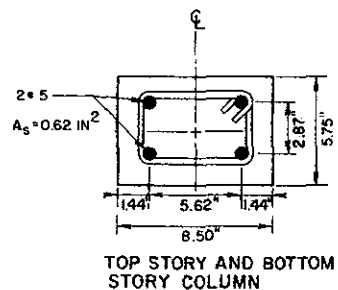
All of the T-beams are of similar cross-sectional dimensions with varying size and

16
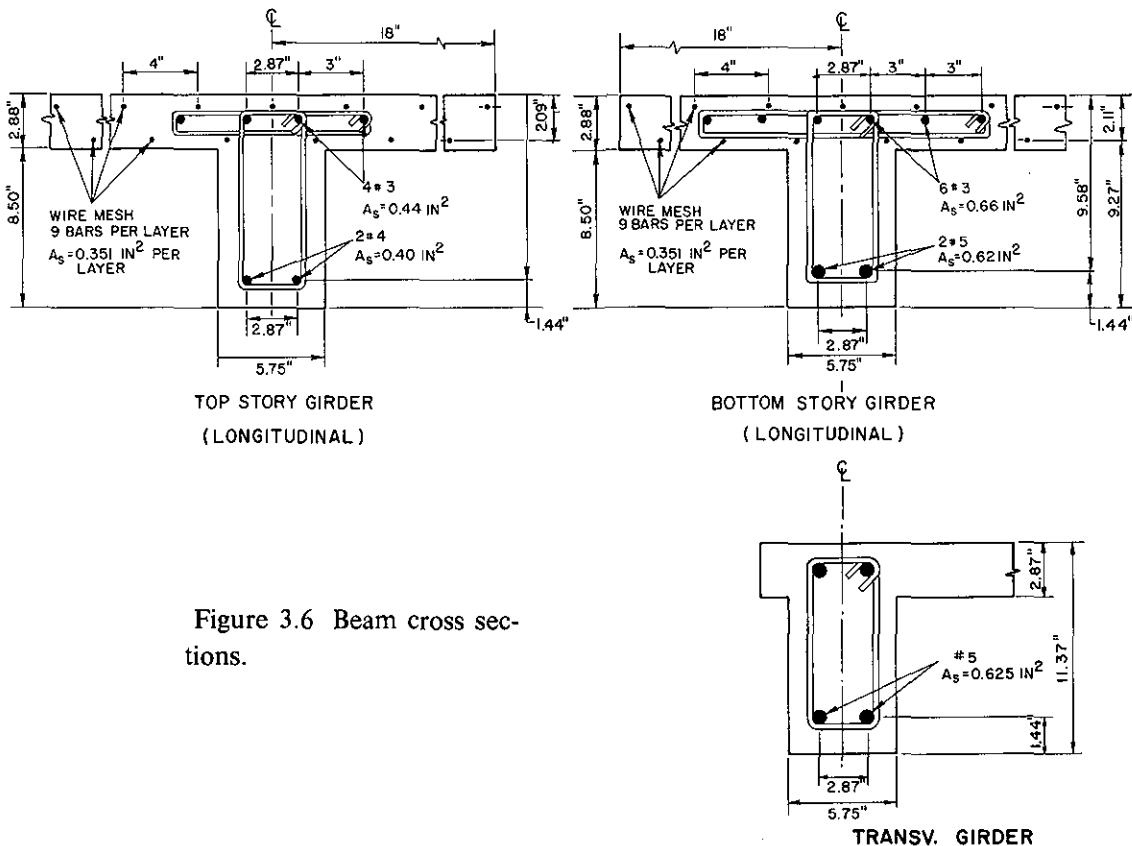
Figure 3.6 Beam cross sections.

amounts of reinforcement dependent on their location as seen in Figure 3.6. All the beams use either two no. 5 or two no. 4 reinforcing bars as bottom reinforcing and varying amounts of no. 3 or no. 5 bars in combination with slab mesh as top reinforcing.

The slabs are both 2 7/8 in.(7.3cm) thick, with top and bottom reinforcing of 4" x 4" (10.2cm x 10.2cm) mesh of 4 gage wire (0.23in, or 0.58cm diam.).

Material properties

Specimens of all materials were individually tested to determine their mechanical strength vs. strain properties. Specific details of the tests are included in the data and plots of *Appendix B* from which average stress-strain properties were obtained and are listed in Figures 3.7-3.9 of this section. The average stress-strain values are used in *Chapter 8* to define the mathematical models of member behavior used in structural computer analysis predictions of the exact member strength and frame response.

Reinforcing bars-

The general behavior of each of the types of reinforcing bars used in the structure can be characterized by specific quantities as shown in the stress-strain plot of Figure 3.7 and the listed

average values. All the steel reinforcing bars are deformed ASTM A615 Grade 40 steel bars except the no. 2 stirrups which were undeformed. Strain hardening moduli (E_{sh}) are given for the initial tangent slope after strain hardening commences.

RCF5 Steel Properties

size	dim (in.)	E (ksi)	f_y (ksi)	f_u (ksi)	ϵ_{sh} (in./in.)	ϵ_{su} (in./in.)	E_{sh} (ksi)
5	.625	30880	49.9	79.6	.0090	.121	1170.
4	.500	31080	49.2	73.8	.0160	.121	838.
3	.375	29200	56.7	80.1	.0185	.093	902.
2	.250	31460	58.2	85.1	n.a.	n.a.	n.a.

BAR NO.	E_S (KSI)	f_Y (KSI)	ϵ_Y	ϵ_{SH}	$f_{S_{ULT}}$ (KSI)	$\epsilon_{S_{ULT}}$
5	29.8	41.5	0.00140	0.0094	72.5	0.113
4	28.0	56.1	0.00201	0.0176	83.9	0.140
3	28.4	52.0	0.00183	0.0289	72.6	0.193
2	29.5	41.3	0.00141	0.0198	54.7	0.190

RCF2 STEEL PROPERTIES

Figure 3.7 Typical steel stress-strain curve from pseudo-static tensile test.

The reinforcing bars in the present frame were in general stronger and stiffer than those used in the RCF2 structure. Most significant is the high yield stress measured in all except the no.4 bars and the higher modulus of elasticity in all of the bars.

Wire mesh

The slab reinforcing wire mesh, also ASTM Grade 40, exhibited less ductility than the normal reinforcing bars due to brittle breaking at the welded intersection points. The typical behavior is represented by the plot and values shown in Figure 3.8. The general behavior of the mesh is fairly consistent for each of the two model frames with the exception of the lower initial elastic modulus measured in the wire of the present frame. There is no distinct point of yielding as seen in the regular reinforcing bars though the strain hardening moduli are very similar to that in normal bars.

Concrete

The concrete was purchased from a commercial readymix plant with a specified design requiring 28 day compressive strength of 4000 psi (27.6 MPa) with maximum aggregate size of 3/8 in. (0.95cm) and a slump of 5 in (12.7cm). The actual slump measured before and during the pour was 3 1/2 in.(8.9cm). Fourteen 6" x 12" (15.2 x 30.5cm) concrete test cylinders were taken at various stages of the frame pour and stored in conditions as identical as possible to those of the model frame. Cylinders were compression tested at 7 days, 14 days, 28 days and
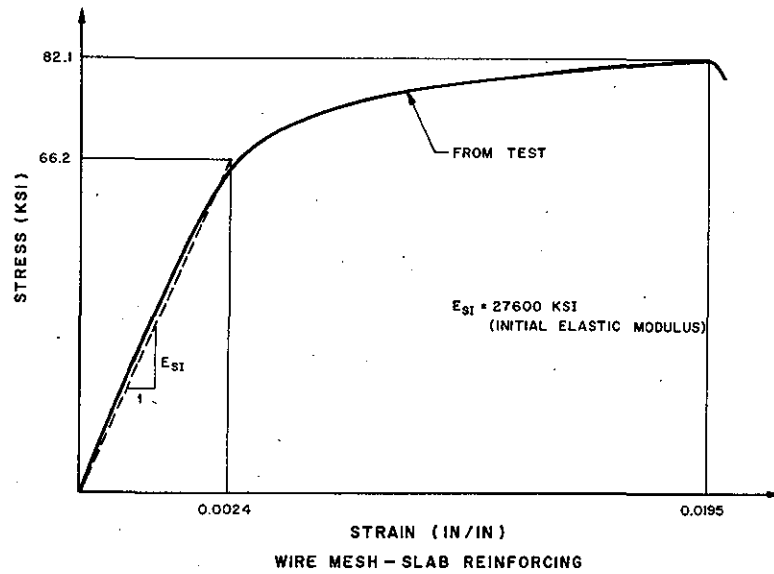
Figure 3.8 Stress strain curve for steel mesh, slab reinforcement.

near the time of testing of the actual structure at 244 days. Similar cylinders tested near the time of actual frame testing (91 days) for RCF2 indicated an average compressive strength of 4395 psi (30.3MPa). The concrete in the RCF5 frame had a 28 day strength of 3450psi (23.8MPa) and a 244 day strength of 4720psi (32.5MPa). Thus the actual concrete strength at time of structural testing was 7% higher in the present frame than in RCF2. Typical plots and average property values which generally characterize the concrete cylinder stress-strain mechanics for each of the concrete frames are given in Figure 3.9.
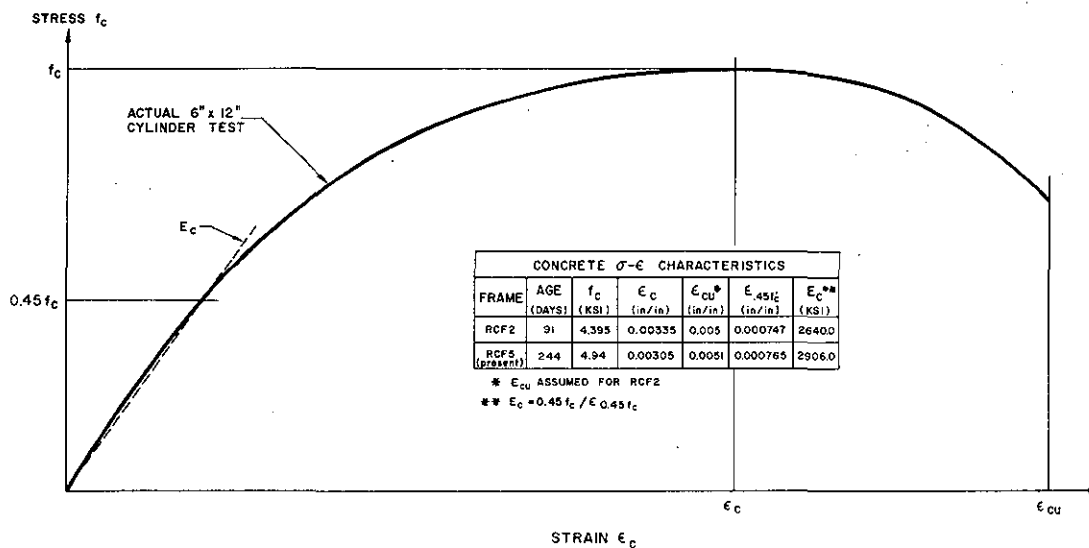
Figure 3.9 Characteristic compression stress-strain curve for concrete cylinders.

Member section properties

General section properties for the main members of the frames are calculated by various methods including use of the designed member geometry, actual built member geometry, and both the expected and measured material properties. Expected section strength for the columns was initially predicted using calculations including design dimensions, the expected steel yield stress (40ksi), the assumption that concrete can carry no tensile stress, and use of a concrete compressive stress block at 85% of the cylinder compressive stress over 85% of the depth to the neutral axis of a member in bending; resulting in the following estimates in the column's strong and weak axis directions:

M_u(strong) = 197in-k (22.3kN-m)

M_u(weak) = 100in-k (11.3kN-m)

with f_c'=4000psi and f_y=40ksi, design dimensions

strong and weak refer to the wide and narrow

column directions,

Which represents the design column strength for the RCF2 and RCF5 frames. Expected yield moments calculated similarly, though assuming a linear concrete stress-strain relation, are:

column

M_y strong=	146.in-k (16.5kN-m)		E_c=57000sqrt(f_c')
M_y weak=	88.in-k (9.9kN-m)		E=29000ksi
			f_y=40ksi
			design dimensions

A realistic estimate of column strength must use more exact member and material modeling, including the following:

a) average 'as built' column dimensions,

b) accurate description of concrete stress-strain behavior for the unconfined cover concrete with crushing and spalling,

c) accurate description of concrete stress-strain behavior for the confined core section such as that suggested by Kent [3] (see *Appendix B* , or Vallenas [11]),

d) use of a stress-strain relation for reinforcing steel which correctly reflects the rebar's real modulus, yield stress, and post-yield behavior including strain hardening and rupture.

This type of analysis is possible using the **RCCOLA** computer program for column analysis developed by Mahin [4]. In addition to the above criteria the program is capable of evaluating uniaxial moment-axial load interaction. Results for column strength and yielding (under zero axial load) for average measured 'as built' column dimensions and measured material characteristics are listed below.

Table 3.1

Column strength, no axial load, RCCOLA*

	RCF5		RCF2	
	(in-k)	(kN-m)	(in-k)	(kN-m)
M_u strong	250.	28.2	223.	25.2
M_u weak	124.	14.0	106.	12.0
M_y strong	168.	19.0	145.	16.4
M_y weak	103.	11.6	86.	9.7

*from RCCOLA column analysis program, Mahin[4]

Stiffness-

The relative stiffnesses of the column and beam sections, given in terms of the moment of inertia, can be estimated by using the original gross section area, transformed section, cracked transformed section or by explicit analysis including yielding, strain hardening, etc., as in the RCCOLA analysis program. Column stiffnesses, as calculated in *Appendix B* are listed below for the various methods of calculation.

Column moment of inertia- $in.^4$

axis	design dimensions			avg. built dim. RCCOLA	
	gross area	trans. area	trans. cracked	RCF5 elastic	RCF2 elastic
strong	294.	357.	129.	146.	159.
weak	135.	149.	43.	50.	52.

Table 3.2

In the actual structure the columns are under a static dead load of 10kips (44.5kN) compression. Structural overturning moments increase or decrease the column axial load significantly during dynamic shaking. Estimates of column strength and stiffness will vary depending on the axial load which itself will vary. Interaction diagrams, plotting maximum moment achievable while under a given axial load, are shown in Figure 3.10. The strengthening effect on moment resistance from addition of a small amount of axial compressive load is obvious. The change in capacity at different maximum compressive strain levels is a result of spalling and variation in material stress- strain properties with varying strain levels.

As mentioned, variation in axial loads affects column stiffness under bending. While increasing the bending strength, the added axial compression decreases the total ductility available. Both of these effects are detectable in the column moment-curvature plots seen in Figure 3.11. Small stiffening effects of a compression load, and softening due to tension loading are apparent as well. The concrete spalling and loss of a large resisting area of the section when the column is loaded in the weak direction creates a notable drop in moment capacity.

Additional illustration of column capacity, calculations and comparisons with RCF2 predicted characteristics are included in *Appendix B* along with calculations of beam strengths and stiffnesses.
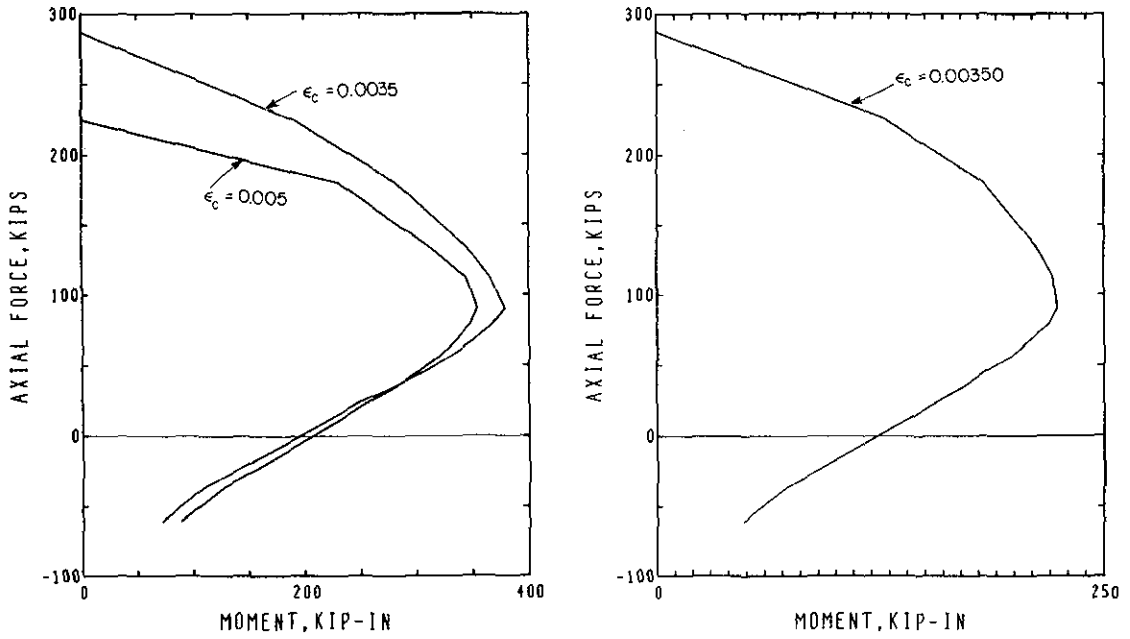
Figure 3.10 Predicted uniaxial moment vs uniaxial load interaction curves for various maximum extreme fiber concrete strains (left: strong axis bending, right: weak axis bending)

Figure 3.11 Predicted uniaxial moment vs curvature relation for various axial loads (- = axial tension).

(top) strong axis
(lower) weak axis
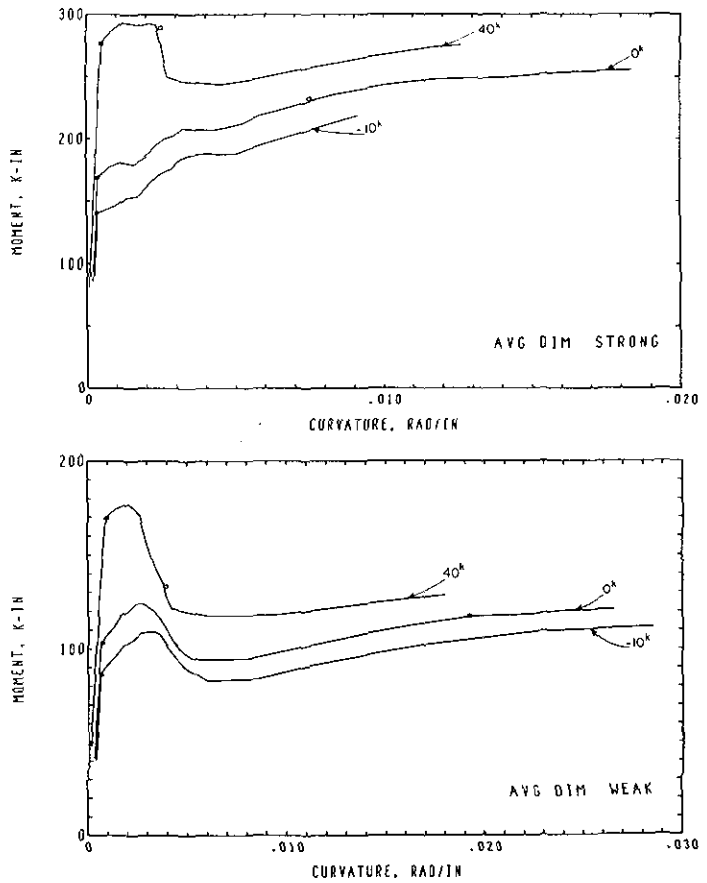
Chapter 4

Test Instrumentation

Over one hundred and forty measuring devices of various sorts were used to obtain a data description of the tests. The instruments, including accelerometers, force transducers, strain gauges, displacement measuring potentiometers and differential transformers, recorded the same types of basic data as obtained in previous tests and reports from these, [1], [2], may be consulted for a more thorough understanding of the instrumentation and data reduction process. Certain new forms of instruments, additional devices to measure biaxial motion and data analysis devices were applied in the present tests and are specifically noted. Detailed descriptions of each type of instrument and its range of applicability are included in *Appendix C*.

Table Motion

The actual table motion will always vary slightly from the input command signals due to the mechanical and hydraulic limitations of the system itself. Response of the table to a given command signal is limited by available displacement at low frequencies (0-2Hz), by velocity and oil flow capacities at mid-frequencies (2-15 Hz), and by maximum acceleration and oil pressure at high frequencies (15 Hz) as described by Rea et al [5]. Therefore, accelerometers and direct-current-differential transformer (DCDT) displacement measuring devices explicitly record the actual table motion including horizontal acceleration and displacement in the direction of motion, horizontal acceleration transverse to the direction of motion, vertical acceleration and displacement, and twist, roll, pitch angular accelerations.

Structural Response

The primary structural response quantities, floor displacements and accelerations, were measured at each floor level using linear variable potentiometers (POTS) and accelerometers. Three potentiometers per floor, mounted on reference frames off the table itself as diagrammed in Figure 4.1, provided the data required to calculate the longitudinal and transverse displacements at the center of each floor combined with the horizontal angular torsional displacement. Differences between the floor displacements and the measured table displacement provide relative structural values. Uniaxial accelerometers were mounted at the center of span of each floor on the east and south sides of the structure oriented in the transverse and longitudinal directions respectively. Additional accelerometers were placed in the two directions on the concrete mass blocks fixed upon each floor to detect differential accelerations due to rocking produced by bending of the supporting slab and beams. Force transducers measuring shear and moment along the two symmetry axes of the columns are located at midstory height of each
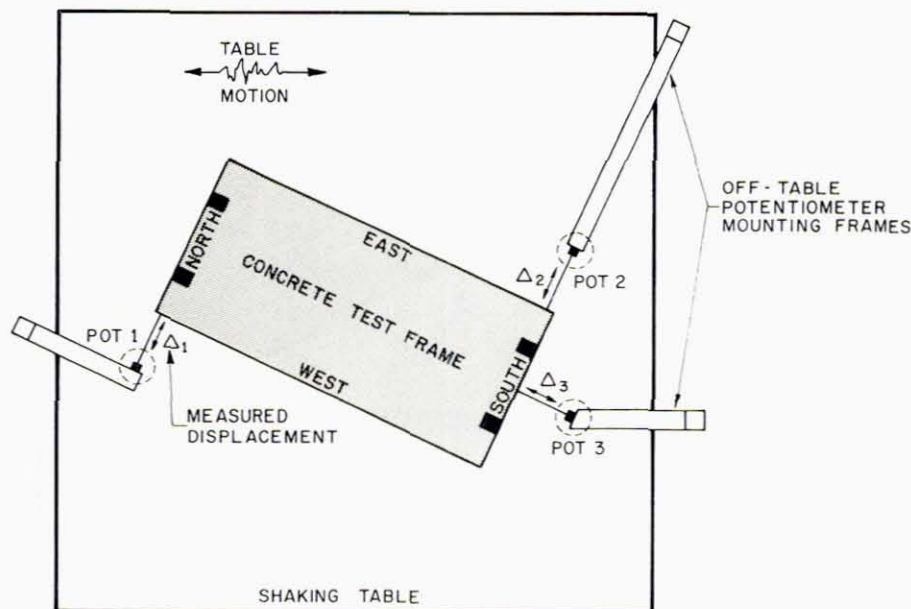
Figure 4.1 Location and attachment of 3 POTs at each floor.

individual column. The transducer outputs, from 4 or 2 active arm strain gauge- 4 arm Wheatstone bridge circuits, when multipled by appropriate calibration factors, provided direct force readout. Since the base shears, as output by the lower column transducers, are directly proportional to inertial forces during dynamic excitation, the consistency of the transducer's shear output can be checked by comparison to the mass acceleration data from the accelerometer output (see Chapter 6).

Member Behavior

Individual member response in terms of member rotations and component strains were measured, as in the previous tests, using DCDT's and strain gauges attached to reinforcing bars. Strain gauges, of elastic range and post yield type, as shown in Figure 4.2, were attached directly to many of the reinforcing bars in both columns and beams.

Figure 4.2 Strain gauges mounted on column reinforcing bar.

Most of the gauges were located at critical column-footing, column-beam or beam-beam joint interfaces. Combination of these gauge results at each column or beam end allowed calculation of curvature at that location. Additional gauges were applied slightly (3 in. or 7.62cm.) to either side of the critical interface gauge at certain locations as indicators of the amount of yield propagation and bond loss along the bars.

24

Direct current differential transformer (DCDT) displacement measuring instruments were mounted on columns and beams near the joints on opposite sides of the members to determine relative rotation between the member and joint through the differential DCDT displacements. At the column ends the DCDT's were mounted on threaded studs cast integrally into the columns at the center of each column face and located an average distance of 4in. (10.16cm) from the joint interface. Targets for the DCDT's were glued to the footing or beam bottom surfaces. The location and attachment at a typical column base is shown in Figure 4.3a. Beam DCDT's were mounted on frames as described in References [1] and [2] and shown in Figure 4.3b.

Figure 4.3a Column DCDT mountings.
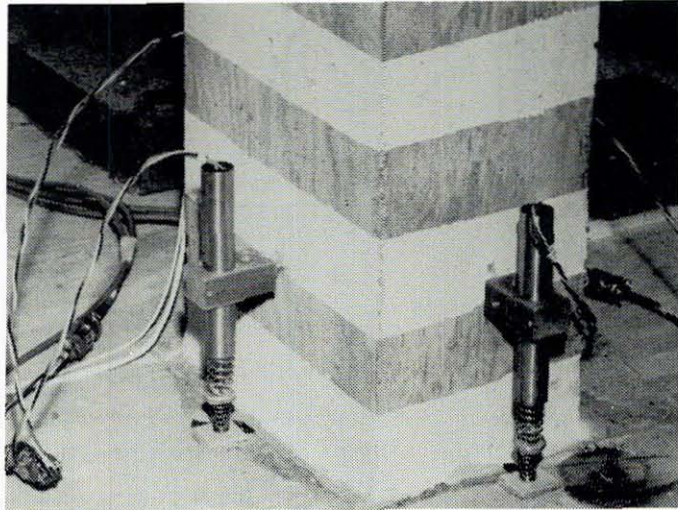
Figure 4.3b Beam DCDT mounting system.
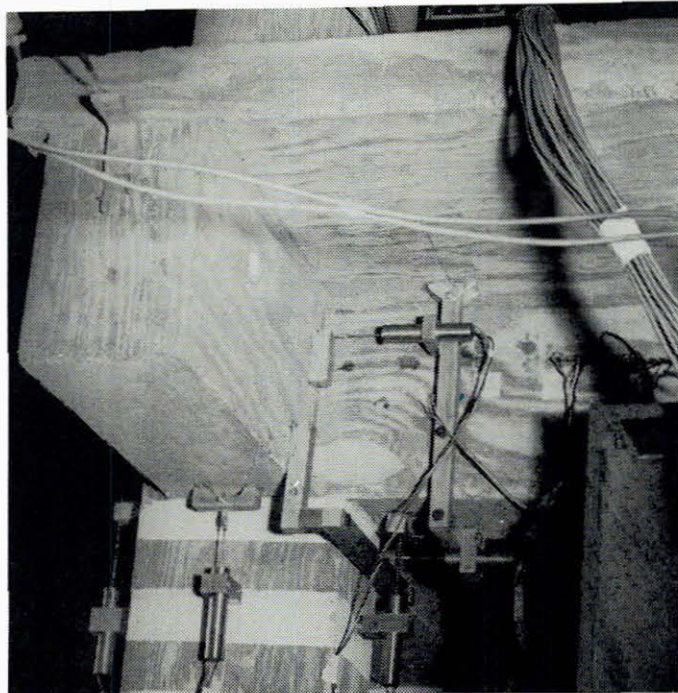
Data Acquisition

The data acquisition process was nearly identical to that described earlier, [2], and briefly summarized here. Extra devices to increase the number of data collecting channels and a new instrument to provide direct frequency analysis were utilized as well. The basic data acquisition system, a permanent facility at the Earthquake Simulator Laboratory, consists of multiple signal conditioners preceding a 128 channel signal scanner and analog to digital data conversion unit coupled to a minicomputer and disc storage unit on line with a magnetic tape deck. The balanced, nulled or conditioned signals from all of the individual instruments are read in bursts at 0.01952 second intervals with a phase lag of fifty microseconds between sequential channels and the signals are converted to digital data and sent to disc storage. Thus, on this system the data read rate is 51.23 times per channel per second (51.23 Hz.).

A second data acquisition unit was used in parallel with the system described above to provide an expanded data collection capability of 20 channels. The equipment configuration of the system was nearly identical to that above, except that the digital data was written directly on magnetic tape, skipping the disc storage step. Data collection on this system was run at exactly 50 Hz with 0.0200 sec. between each burst of channel readings.

Interfacing of the data collected on the two systems above was accomplished through the use of a channel common to both systems. A single peak on this common channel was used to define the time scale of the second system relative to the first. After matching the common time point in both systems, the data from the second system was converted to the same scan interval as the first system (0.01952 sec.) using a parabolic interpolation algorithm.

The new data interpretation device, a real time spectrum analyzer, was used to evaluate the structure's natural frequencies at various times during the testing sequence. Between tests, a pseudo white noise generator was used to deliver a low level noise command signal to the shaking table with the envelope characteristics shown in Figure 4.4. The response of the structure as interpreted through the four floor located accelerometers was viewed sequentially through the spectrum analyzer allowing determination of the natural frequencies from the spiked peaks as seen in Figure 4.5 for a particular accelerometer.

Figure 4.4 Spectrum of actual table motion with noise command signal.
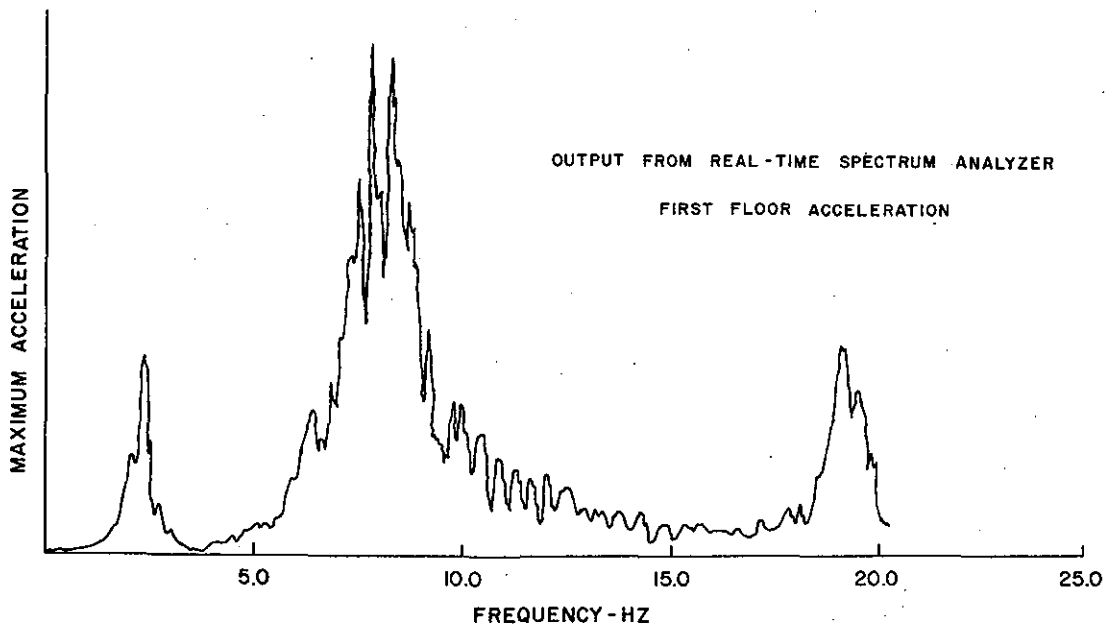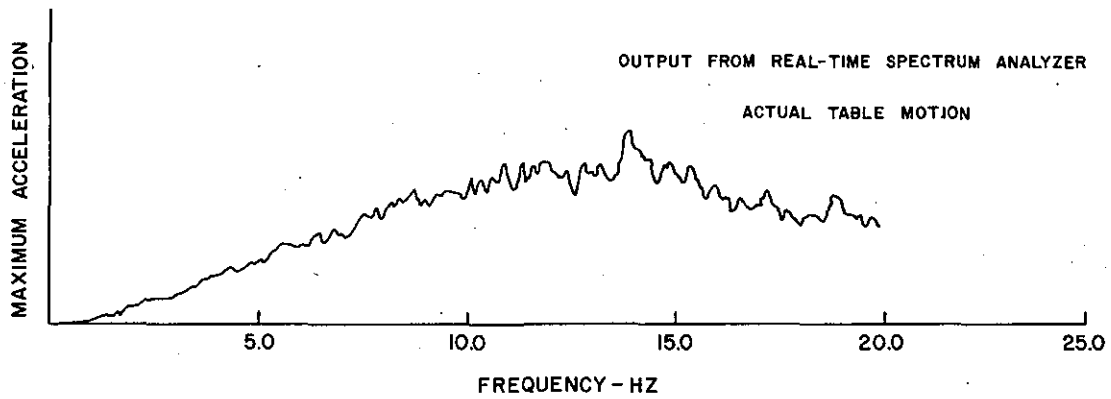
Figure 4.5 Spectrum of frame's response to table motion of Fig. 4.4.

Chapter 5

Experimental Program

The test program for this present frame included graduated shaking tests on the shaking table, intermediate testing of structural natural frequencies and damping, repairing of the damaged frame using commercial repair techniques followed by more shaking and frequency tests and finally static testing of the frame under lateral load to destruction. This overall sequence was generally similar to the RCF2 frame tests conducted previously and allows comparisons of results between the two projects.

Earthquake motion

The primary dynamic test motion applied at various amplitudes through the shaking table was a displacement record derived from the accelerogram of the Taft N69W component of the 1952 Kern County, California, earthquake. As described by Hidalgo and Clough (2), this particular signal was selected because of its broad frequency spectrum and long duration of strong amplitude motion. It has been used as the basic test signal in the previous reinforced concrete frame test programs, including the RCF2 testing. The shaking table's amplitude of motion under this signal can be continuously varied up to a maximum displacement of over 5 in. (12.7 cm.) by applying a scaling factor to the original Taft record. At the maximum (5 in.) displacement setting the peak table acceleration, (with structure-table interaction) would be approximately 0.7 g's or 4.4 times the measured acceleration of 0.16g in the Taft record.

Earthquake Test Sequence

Six earthquake tests were performed with the concrete frame on the shaking table. Four tests were initially executed causing significant inelastic motion and stiffness deterioration. The frame was subsequently repaired using a commercial epoxy injection procedure and retested with two strong motion shakes. The entire sequence of tests with descriptive quantities is listed in Table 5.1 with the analogous sequence used in the RCF2 test program.

A very low intensity shake was the first signal applied through the table with the intention of inducing minor cracking in the virgin frame to replicate the condition of a real structure which has seen service loading. The actual peak acceleration amplitude of the table during this test was 0.06 g. A second, identical test was conducted with the same peak acceleration. The data from this second test describes a normal frame's elastic response to a minor excitation.

The next severe shaking of the undamaged model under the same magnified signal simulated the effect of a sudden intense earthquake upon a normal frame structure forcing an

Table 5.1

Earthquake Test Sequence- Table Motion		
TEST	Peak Acc. (g's)	Peak Displ. (in.)
Taft100(1)	0.062	0.503
Taft100(2)	0.061	0.498
Taft1000	0.685	5.07
Pacoima	1.49	5.23
Frame repaired / epoxy injection		
Pacoima	1.37	5.25
Taft1000	0.711	5.06

RCF2 uniaxial frame	
TEST	Peak Acc. (g's)
Taft100w1	0.097
Taft850w2	0.57
Taft850w3	0.65
frame repaired	
Accelerations given are the same as components along longitudinal axis.	

inelastic response. The table's horizontal acceleration during the signal reached a peak of nearly 0.7 g or more than ten times the amplitude of the previous tests. The ground (or table) displacement reached 5.1 in. (13 cm.), nearly the limit of the shaking table facility.

In completion of this test sequence a final strong motion test followed with a similar intensity to study the effect of a severe aftershock. A new signal from the derived Pacoima accelerogram of the 1971 San Fernando, California, earthquake provided a different frequency input and a short duration of strong motion. Application of this signal was the first major variation from the RCF2 test sequence. The maximum horizontal acceleration of the table in a very sharp peak, was 1.49 g's. Sufficient damage was observed during this shake to warrant repair by an epoxy adhesive pressure injection technique prior to continued testing.

After repair the frame was subjected to a second test sequence starting with a high intensity run of the Pacoima record and followed with a duplicate of the strong Taft motion used previously.

Frequency measurement

The fundamental natural frequencies of the structure were acquired between each of the dynamic tests as a means of measuring the amount of stiffness decay and associated structural damage along with an indication of the effective modal damping. Natural frequency and damping values could serve a useful basis in establishing effective analytical models during subsequent response correlation studies. Three separate methods of frequency determination were employed and served as cross checks upon each other.

Free Vibration tests were accomplished by pulling the first and second floors of the structure horizontally along each of its principal axes under a static load applied through a cable with a sudden cutting of the pulling cable. The resulting response and vibration decay were monitored through appropriate accelerometers with variable filters and plotted in analog form through which frequency and logarithmic damping could be measured. The same signals were led to the spectrum analyzer and frequencies could be verified from the position of sharp response spikes. Digital data collected during the free vibrations was used as input for a Fast

Fourier Transform program in the system's minicomputer and the resulting spectra were plotted. The maximum amplitude of vibration of the second floor during these tests varied from 0.05 to 0.2g in top story acceleration.

Frequencies were also determined using the response decay phase in the motion of the structure during the earthquake shaking tests after the table motion had ended. The frequency under these conditions represented the real characteristics of the structure supported on a soft foundation. The "soft" foundation provided by the shaking table supported on its hydraulic actuators, passive stabilizers and air cushion interacting with the model structure has shown a tendency to reduce the apparent frequency of vibration of the structure below that on a fixed foundation. The frequencies again were measured from analog plots of floor accelerations and verified by the output of a spectrum analyzer. The amplitude of the vibration during the measurable signal decay period varied from 0.02g in the light shakes to 0.3g after the T1000 tests.

The third and simplest technique of natural frequency analysis used the pseudo white noise generator described previously to create a very low amplitude noise type vibration of the table; and response of the structure interpreted through the spectrum analyzer. The actual maximum structural accelerations induced were approximately 0.04g's.

It is important to note that the natural frequencies determined under low amplitude vibration conditions do not necessarily characterize the natural frequency of the structure at any particular instant during a large scale shaking. Inelastic or nonlinear behavior such as crack opening or bond slip continuously modify the structural stiffness, and therefore frequency, during large amplitude motions, but may not occur during small movements. Hence, the variation of natural frequency under low amplitude tests can only be taken as a coarse indication of structural damage.

Static Destructive Pull

Static horizontal displacement testing of the frame provided a final measure of its strength, the remaining stiffness and overall ductility. The structure was pulled horizontally at the second floor level. Constantly increasing displacement was slowly applied until the structure had deformed sideways more than two feet (0.61m). The measured force and displacement quantities are plotted in analog form in *Chapter 6*.

Chapter 6

Test Results

Visual damage description

The general nonhomogeneous character of concrete structures causes complex force resisting mechanisms which constantly change state during applied excitations. Under low level loading, the resisting mechanism may be simply dependent on the gross section properties or transformed combined concrete and steel section and essentially respond like a homogeneous linear elastic member. As loading increases, concrete cracks in tension regions, the concrete stresses are no longer linearly related to strains in the compressive region, steel stresses reach the yield point, steel to concrete bond deteriorates, the neutral axis moves, unconfined concrete crushes and spalls off the member face, all causing consecutive changes in the member stiffness. Some of the progressive deterioration mechanisms result in physically visible phenomena. Cracks appear in tension loaded concrete; concrete cracks open significantly when yielding produces large strains in tensile loaded steel and large steel yielding causes bar to concrete bond deterioration; concrete spalls when high compressive stresses occur in unconfined material. Observation of these effects allows some judgement as to what state of resistance mechanism the member is in at any point in time.

In addition to pinpointing local state of stiffness the listed visually detectable qualities provide an immediate indication of where within a full structure critical high force to member strength ratios are occurring. Unexpected types of cracking or cracking in unusual locations may signal the importance of response mechanisms which might not normally be considered.

Since the majority of structures damaged during earthquake motions are not instrumented to indicate exact load response history and the extent of deterioration of stiffness, it would be desirable if physical observation could be employed to some extent as a criterion for judging continued serviceability. Cracking would indicate development of lowered stiffness, easily repairable through epoxy injection. Concentrated multiple cracks may be indicative of local yielding in reinforcing and loss of bond in the yielded region difficult to fully repair with epoxy injection. Spalling of surface concrete implies a significant deterioration of strength and stiffness with loss of exterior rebar to concrete bond, requiring full rebuilding of the section. If such deterioration is present in a significant number of locations relative to the indeterminacy of the structure, a partial plastic mechanism may be formed, resulting in large deformation or collapse with continued loading. To this effect visual observations were made on the test model for use in correlation with actual measured data.

A. Taft 100(2)

The Taft 100(2) signal was the second low intensity shake applied to the structure with a peak acceleration of 0.06g's. This test was intended to excite the structure within its so-called elastic range. Very little cracking could be observed after completion of the test. A few micro-cracks developed at the extreme corners near the tops and bottoms of the first floor columns indicating that the effective section stiffness, in the column end region, should be based on cracked section properties for analysis purposes. No additional cracking was evident within the T-beams beyond the small amount of cracking (under positive moment) which had occured near the center of the longitudinal beams when the mass blocks were set on the floors.
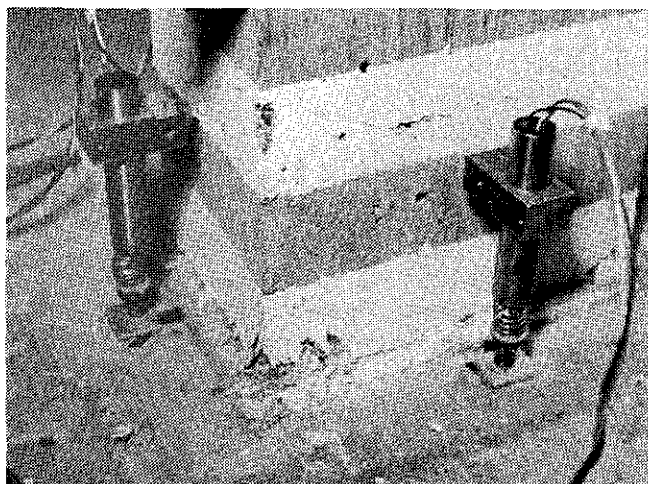
Figure 6.1 Crushing at lower column base, past T1000 test.

B. Taft 1000

The first large magnitude shaking of the frame was under the Taft signal with a maximum table acceleration of 0.7g. Considerable cracking occurred at member joints throughout the lower story of the frame. The bottom floor columns showed bending type cracks, as wide as 0.05in., particularly at the column corners within 6-8in from the top and bottom ends. Column cracking generally seemed to be concentrated at the very ends of the members. All of the columns had a crack around their full circumference at the column footing joint. Crushing of the concrete cover was definitely detectable at key points (see Figures 6.1 & 6.2) of high deformation including:

Crushing

        - southeast corner of column at the bottom, north B-frame lower column,

        - southeast corner of column at the bottom, south B-frame lower column,

        - southeast corner of column at the top, north B-frame, lower column,

        - northwest corner of column at the top, south A-frame, lower column,

Spalling accompanied the concrete crushing at the 2nd and 3rd locations listed above. The spalling in this test, occurring only at column corners, differed from the type seen in the RCF2 frame where spalling developed along the column face as expected in uniaxial bending.
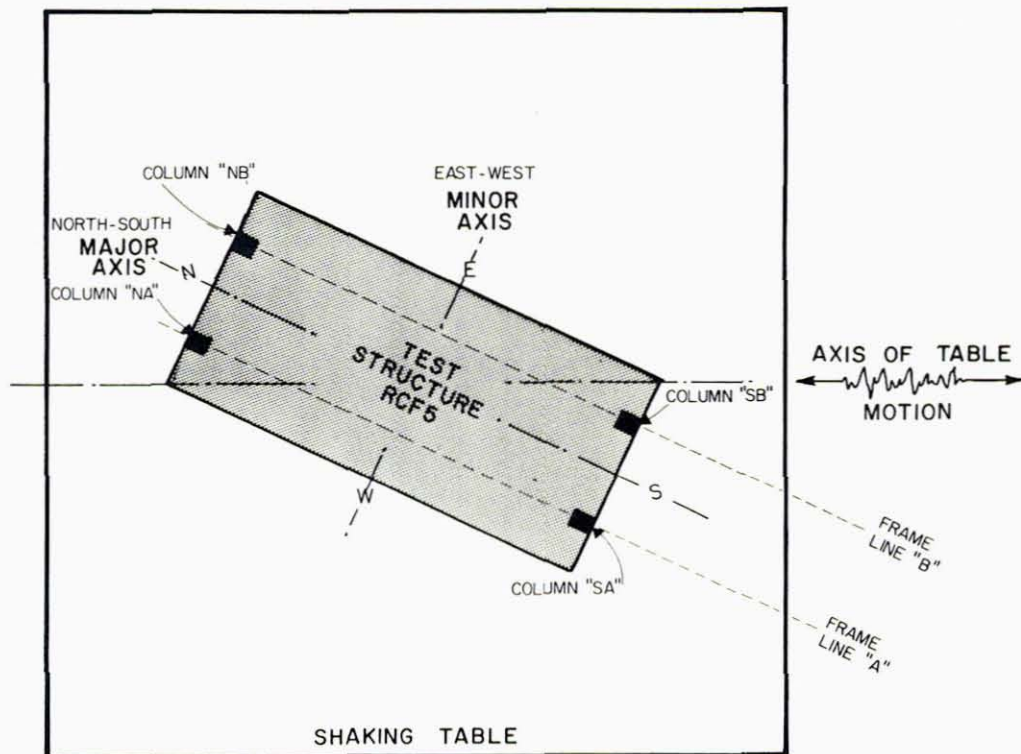
Figure 6.2 key to column and frame notation.

All of the lower columns had 0.025in. wide cracks at their top column to beam joints. At both the north A frame and south A frame column to transverse girder joints a crack opening of 0.05in (13mm) wide remained in the columns. Cracking due to bending was concentrated within the top 4in (10cm) of the column. There were no significant shear cracks in any of the columns and there was no cracking within the vicinity of the force transducers. Upper columns showed very little cracking except for small (less than 0.025in. wide) cracks at the joint with the first floor slab.

Damage to the transverse and longitudinal girders varied significantly from the RCF2 uniaxial frame. The RCF2 test damage after the first major shake was reported as follows [1]:

"also, cracks developed in the longitudinal girders near the column joints, extending from the bottom surface to the base of the slab. Some minor crack-ing occurred at the top of the first floor slab along the line of the transverse girder, ..".

In contrast, there was no visible slab cracking in this frame. A single crack, less than 0.025in. wide, appeared on the bottom of the transverse girder near the northwest column on the exterior cantilever beam segment and ran only 1in. (2.54) up into the beam. This lack of cracking deformation in the slab and beams seems to indicate that under the biaxial motion greater stiffness deterioration occurred in the lower columns than in the RCF2 test and most of the horizontal displacement of the frame may have been a result of inelastic hinge formation at the lower column extremities, allowing columns to bend or sway without causing significant beam deformation. Spalling, which was in evidence at the column bases, supports such a postulated

hinging effect at yield load.

Figure 6.3 Spalling along north face of SB column at footing, post Pacoima.
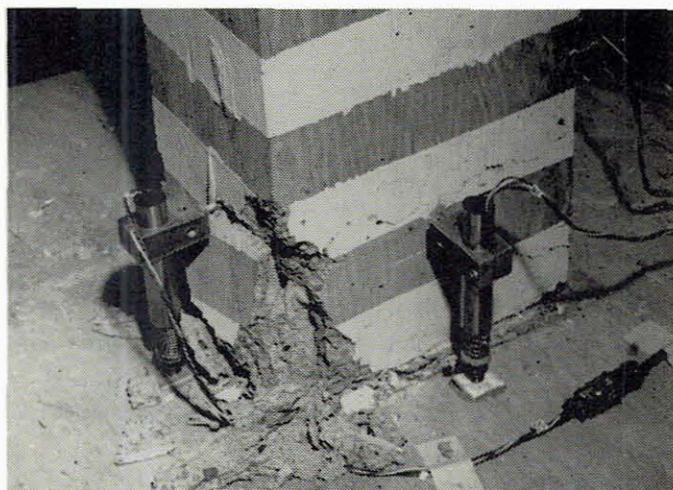
C.   Pacoima test

A considerable amount of additional damage was caused by deformation during the major "aftershock" Pacoima test. Extensive serious cracking, crushing, and spalling occurred at the column to footing joints. All of the columns except the south B frame column exhibited spalling along their entire north and south faces with damage concentrated at the corners as seen in Figure 6.3. The entire base of each column was cracked at the footing in a manner similar to that in the photo. Crack widths were as large as 0.10in. in most locations. There were very few cracks in the midsection of the columns, more than 8in (20cm) above the footing. Similar cracking and spalling existed at the lower level column tops such as that shown in Figure 6.4. Spalling was concentrated at the corners and the north and south faces. In Figure 6.5 the cracking pattern on the exterior north face of the north column can be observed to continue above the beam column joint; yet the cracks are definitely concentrated in the joint region. Extension of cracking into the joint was interpreted as indicating that either rebar yield and/or bar slip had developed within the joint region.

Again, there was very little cracking in the beams or the slab. The complete lack of significant beam cracks may be noted in Figures 6.4 and 6.5. The minor extent of slab cracking and upper column damage is obvious upon inspection of the typical joint shown in Figure 6.6 which shows a second story column and floor slab. The type of crack visible in the slab in the lower right hand corner should particularly be noted. Diagonal slab cracks intersecting the column near its interior corner have been noticed in previous tests of similar frames. They are a result of tensile force being from the rebar of the T-beam flanges to the slab concrete and carried by shear stress to the column itself. Shear stresses developed within the slab result in the diagonal crack (across the direction of principal tension) when stress levels reach a limiting magnitude, effectively separating the T-beam flanges from the column and decreasing the beam to column joint stiffness.

Figure 6.4 Cracking and spalling at first story SA column top, viewed from east, post Pacoima.
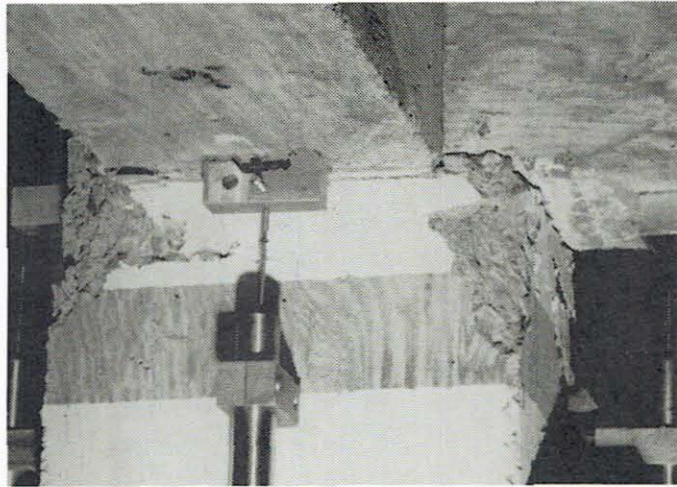
Figure 6.5 Cracking at first story column top, NB column, view from northeast.
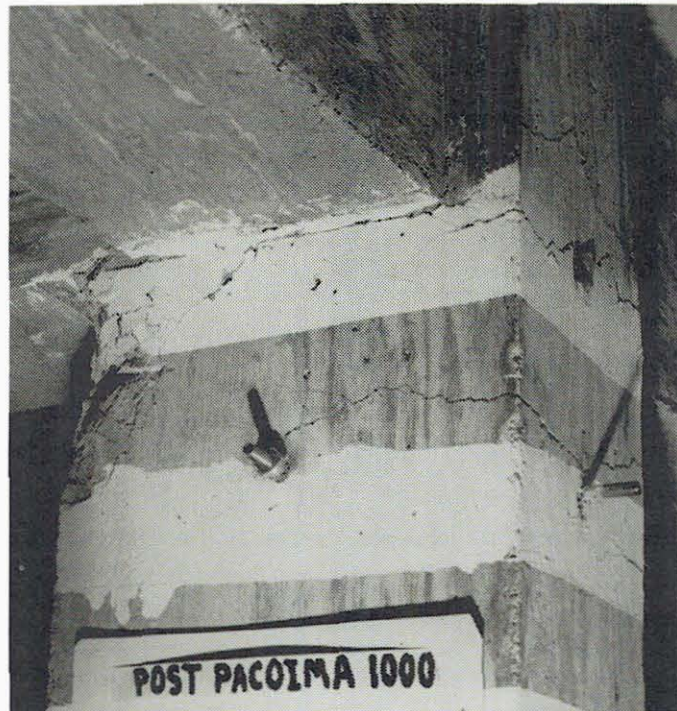
Repaired frame tests

After the Pacoima test, the epoxy injection repair took place followed by additional testing. Though the remainder of this dissertation will concentrate on the frame behavior during the first major Taft test (Taft 1000), it is of interest to examine the exaggerated damage which occurred in the first Pacoima test and the repaired frame tests to collect further clues toward understanding the types of damage mechanisms in operation.

The total extent of the column base damage after testing of the repaired frame is evident from Figure 6.7. The concrete cover is crushed and spalled to the point where the resisting

Figure 6.6 Cracking in first floor slab at base of NA second story column.

POST PACOIMA 1000
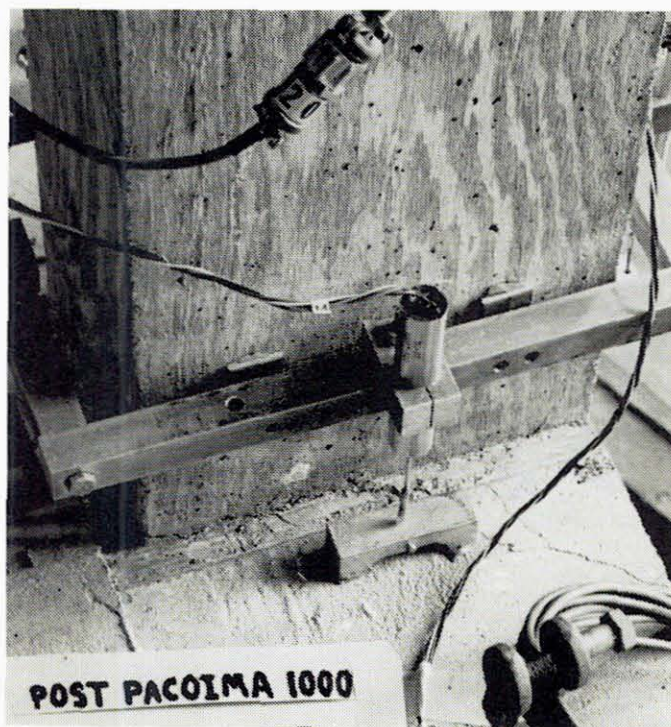
mechanism consists of the rebars with residual elongation after yielding and the confined concrete. The column tops were in an analogous condition, illustrated in Figure 6.8. A view of the same column from the north (exterior) side is taken in Figure 6.9. All the cover concrete in the joint region has loosened or spalled away from the north face of the column, indicating a loss of bond and existence of bar slip for the visible longitudinal column reinforcing bars (Figure 6.10). Though no catastrophic collapse occurred, the structure failed in the real sense that it was no longer able to provide required lateral stiffness.

Natural frequencies

The change in the model's basic natural frequencies after each test might be construed as an indication of the relative damage and stiffness deterioration caused by the preceding motion. In fact numerous existing buildings in California and elsewhere have been field tested under small amplitude forced vibrations to determine their natural frequencies. It is hoped that if any of the buildings experience strong ground shaking, effects of the shaking may be inferred from the change in frequency properties [6].

Variations of the present structural models' natural frequencies along the two principal axes are portrayed graphically in Figures 6.11 and 6.12. (Mode 1 lateral vibration refers to the characteristic displacement pattern in which the entire frame simultaneously moves in the same direction laterally. In mode 2 vibration, the directions of lateral motion for the two floors are opposite of each other.) A slight decrease in frequency is observable after the first Taft low
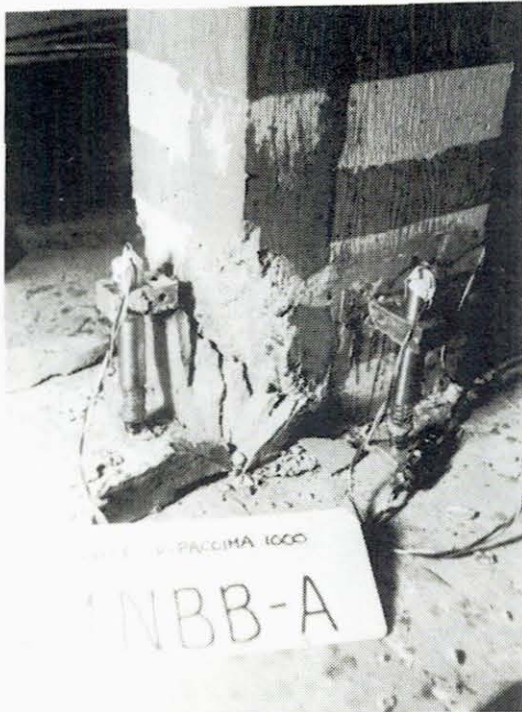
Figure 6.7 NB column at footing joint, damage to repaired column.
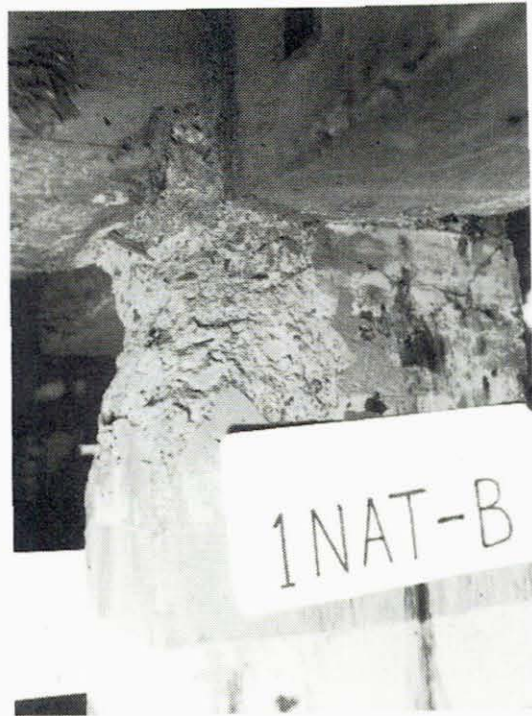
Figure 6.8 Extensive corner and face spalling at NA column top,
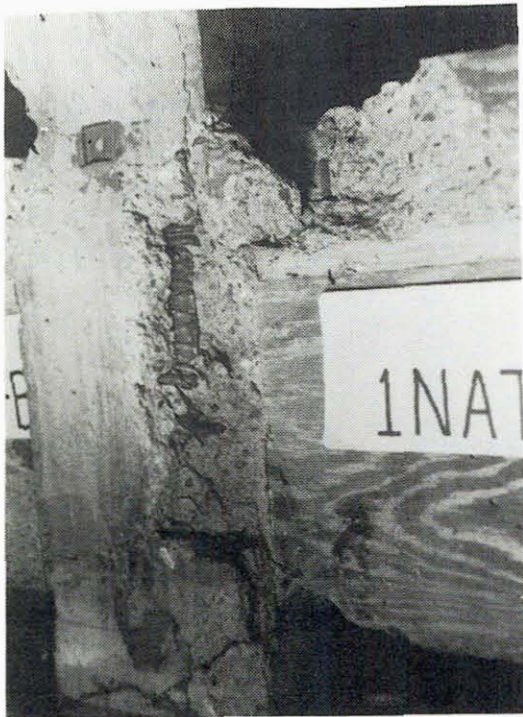
Figure 6.9 Loss of cover concrete and bar bond, torsion shear damage to first floor slab, NA column top.
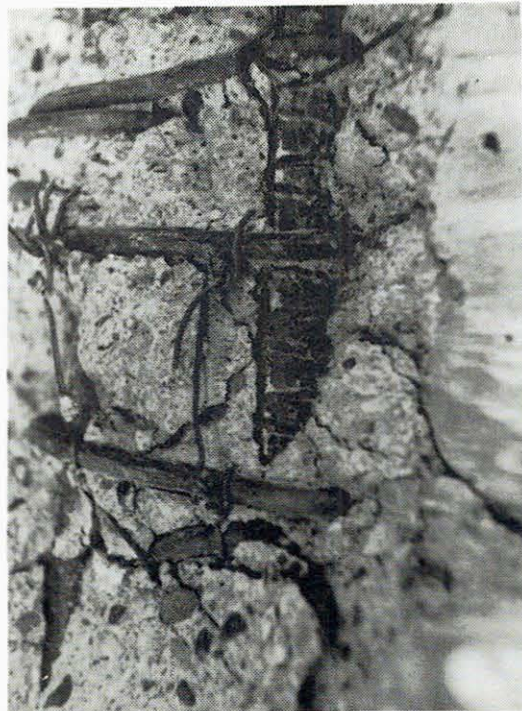
Figure 6.10 Closeup of bar and crushed concrete in NA column at first floor joint.

POST POST POST POST POST
ORIGINAL T 100 (1) T 100 (2) T 1000 PACOIMA REPAIRED PACOIMA

MODE 2

MODE 1

NATURAL FREQ.-Hz 10 5 0

NATURAL FREQUENCY VARIATION — LONGITUDINAL DISPLACEMENT MODES
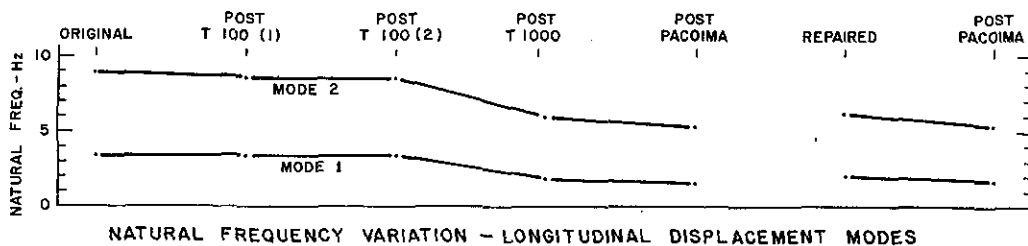
Figure 6.11 Longitudinal axis natural frequency variation.

POST POST POST POST POST
ORIGINAL T 100 (1) T 100 (2) T 1000 PACOIMA REPAIRED PACOIMA

MODE 2

MODE 1

NATURAL FREQ.-Hz 5 4 3 2 1 0

NATURAL FREQUENCY VARIATION — TRANSVERSE DISPLACEMENT MODES
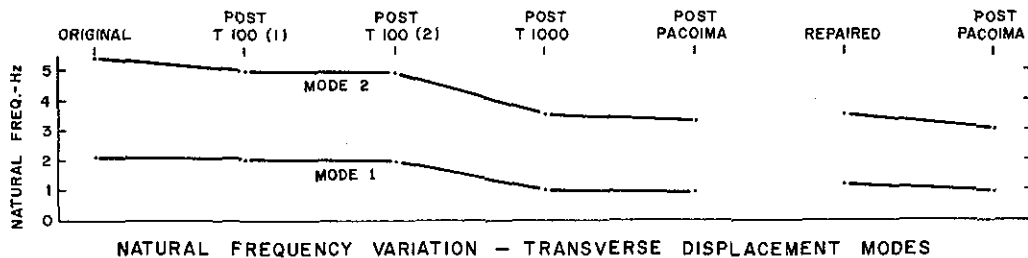
Figure 6.12 Transverse axis natural frequency variation.

magnitude shaking as would be expected if minor cracking occurred reducing the effective section size and moment of inertia at critical locations. The second low magnitude Taft signal caused virtually no change in frequency and hence it probably excited the structure in a nearly elastic manner without affecting further cracking. However the Taft 1000 strong motion signal reduced the first natural mode frequency along each of the principal structural axes by nearly one half. The second modal frequency in both directions was reduced by thirty per cent. The aftershock, in the form of the Pacoima record, resulted in a small additional decrease in frequencies. Considering the significant extra amount of visible damage in the form of column cracking and spalling that was recorded after the Pacoima test, it is surprising to find such a small decrease in frequency. Apparently the internal damage was caused during the Taft signal from the few major displacement cycles and the additional displacement cycles of the Pacoima signal forced already crushed concrete to spall giving the impression of extensive further damage.

The commercial epoxy injection repair procedure which followed the initial testing barely brought the structural natural frequencies above the level existing after the first large Taft test, especially along the transverse axis. If frequency is indeed an indication of structural damage levels, this repair procedure was quite inadequate to restore initial stiffness. After the first retest, with the Pacoima motion,the frequencies immediately fell near to or below their pre-repair levels. Average frequencies, the result of previously described measuring procedures are listed in Table 6.1.

Comparing results of the tests for structural frequencies run on the present frame with those from the RCF2 frame we find an indication of similar degradation. The first mode frequency in the longitudinal direction shows less of a decrease after the first small scale shaking but greater degradation during the first large scale inelastic test. Second longitudinal mode

Table 6.1
Frequency and Damping History

	Frequency Hz			Damping*		
	longitudinal		trans.	longitudinal		trans.
	RCF2	RCF5	RCF5	RCF2	RCF5	RCF5
MODE 1						
initial	3.80	3.44	2.07	1.28	4.78	·4.68
T100(1)	3.13	3.43	2.02	4.20	2.17	3.14
T100(2)	-	3.46	1.99	-	1.95	3.19
T1000	2.03	1.86	1.01	5.77	3.87	3.77
Pacoima	-	1.58	0.94	-	5.34	4.76
Repaired	2.58	2.03	1.21	2.67	3.93	4.54
Pacoima	-	1.70	0.93	-	4.18	6.09
MODE 2						
initial	9.80	8.86	5.43	1.59	1.87	-
T100(1)	8.70	8.60	4.95	·1.93	1.58	2.58
T100(2)	-	8.52	4.92	-	1.95	-
T1000	6.70	6.03	3.57	2.99	2.36	-
Pacoima	-	5.42	3.29	-	2.94	3.80
Repaired	7.22	6.20	3.51	2.00	2.64	-
Pacoima	-	5.40	3.02	-	3.68	. -

Damping given as a percent of critical.
Data indicated for state after given test signal.

Frequency ratios- f_1/f_2

	initial	T100(1)	T100(2)	T1000	Pacoima	Repair	Pacoima
LONGITUDINAL							
RCF2	0.39	0.36	-	0.30	-	0.36	
RCF5	0.39	0.40	0.41	0.31	0.29	0.33	0.31
TRANSVERSE							
RCF5	0.38	0.41	0.40	0.28	0.29	0.34	0.31

frequencies show the same behavior though less accentuated.

Damping, as measured by logarithmic decrement during free vibration decay, varies inexplicably in the first two measurements associated with all the vibration modes, but generally follows the variation seen in the previous RCF2 model during the remainder of the test sequence. Decay associated with the first and second modes of the structure was obtained by pulling the structure laterally, at the top and lower floors respectively, and suddenly releasing. The per cent of critical damping associated with second mode of vibration in the transverse direction was impossible to measure in certain instances due to difficulty in filtering undesirable associated frequencies out of the free vibration acceleration signal.
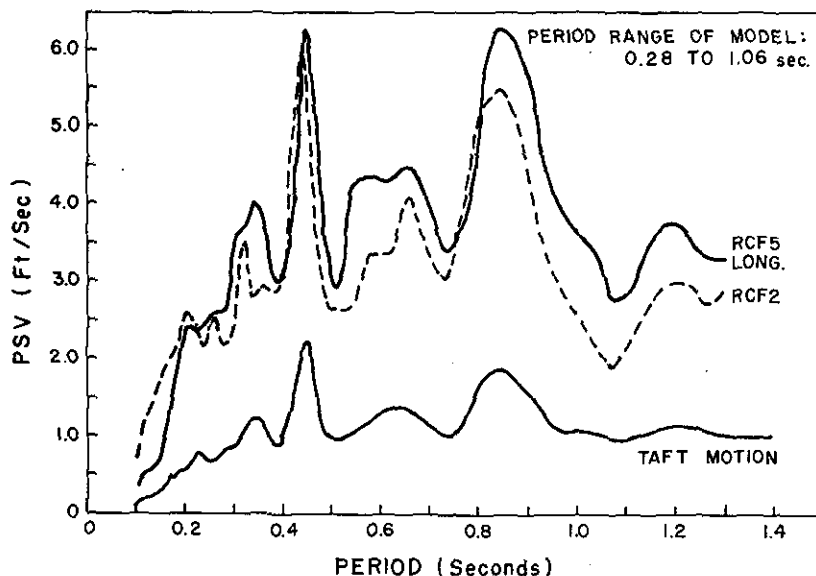
SPECTRAL PLOTS OF EARTHQUAKE MOTIONS WITH 2% DAMPING
Figure 6.13 PSV spectrum plots for original Taft earthquake, T1000 motion, RCF2 W2 motion, with 2% damping.

Structural response under earthquake shaking

The original Taft earthquake created damage in the Taft, California, area consistent with a Mercalli intensity of VII and specific damage at a near fault localized area indicating a scale XI intensity. The magnitude, judged from acceleration records, was calculated as 7.5 to 7.7. A pseudo velocity spectrum with 2% damping as derived from the accelerogram is plotted from CalTech [7] data in Figure 6.13. The earthquake records originally recorded at Taft Lincoln High (S69E) and distributed in corrected form (Cal Tech [8]), showed a peak acceleration of 0.18g's, velocity pulse of 10.6 in/sec. and maximum displacement of 2.5 in. in the initial thirty seconds.

Though the signals used in frame testing were based on the ground motion derived from the Taft earthquake record, the actual movement of the table was, in general, not identical to the historic record. Moreover, the motion is not exactly repeatable from one test motion to another. These variations result partially from mechanical limitations of the hydraulic pump, transmission and actuator system (as described previously). Differences seen from one test to another can also be caused by progressive aging and deterioration due to heating of components within the closed loop electronic control and feedback system and from model system dynamic interaction effects with models at slightly different frequencies.

Table motion:

Time histories of table displacement and acceleration for the T100 (2) and T1000 (Taft Signal) tests on the present frame and the W2 Taft 850 test on the RCF2 frame along with spectra plots are exhibited in Figures 6.31-47 at the end of this chapter. The following table lists common parameters used to characterize earthquake ground motions for the principal tests. The T100(2) shaking was very mild and similar to common weak earthquakes. The T1000

Table motion characteristics:

TEST	peak accel. (g's)	peak displ. (in.)	max. velocity pulse (in/s)	peak accel.* long. axis (g's)	peak accel.* trans. axis (g's)
T100(2)	0.062	0.503	4.01	0.056	0.026
T1000	0.685	5.07	32.46	0.621	0.289
W2 T850 RCF2	0.57	4.10	n.a.	0.57	0.00

Calculated as components of the peak acceleration.

shaking contained a velocity pulse of 32.5 in/sec (82.5cm/sec) three seconds into the signal with a second pulse of 31.1 in/sec (79.1cm/sec) under the peak acceleration at six seconds. The effective ground accelerations along the frames' two principal axes were calculated as the vector components of the table acceleration. The peak acceleration of the RCF2 test was slightly lower than the longitudinal axis component of the present frame. Thus if the frame damage is proportional to peak inertial force, the present frame would be expected to show a slight bit more damage regardless of biaxial effects. However, high frequency spikes in the acceleration are not always correlated with the occurrence of maximum damage. More often, inelastic response and damage follow from a short sequence of lower amplitude shaking near the structure's natural frequency, building up elastic resonant response, followed by a sizeable energy pulse, creating inelastic deformation.

HORIZONTAL TABLE DISPLACEMENT
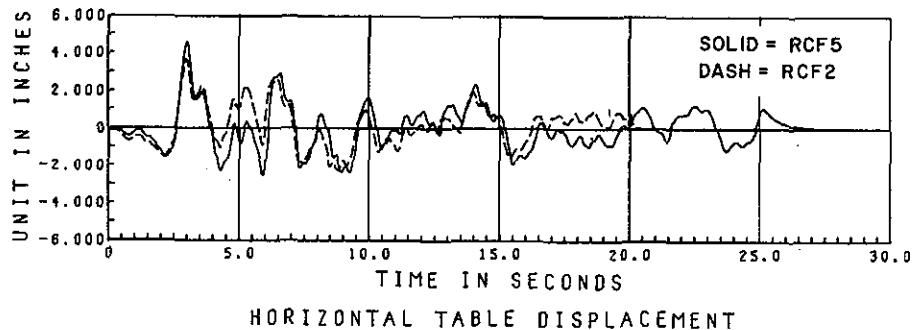
Figure 6.14 Table displacement in the RCF5 T1000 and RCF2 850 W2 tests.

The frequency content of the test signals may be inferred from the approximate velocity response of a one degree of freedom system to the motion as presented in a pseudo-velocity response spectrum plot. The spectra for the major tests and the original Taft motion are plotted in Figure 6.13 for a system with 2% of critical damping. The RCF5 plot was calculated from the component of motion along the longitudinal axis of the frame to allow comparison with the RCF2 spectrum. The two spectra are very similar in character and indicate comparable

frequency content though the RCF5 signal tends to be slightly stronger especially in the lower frequencies (longer periods). The ground (table) displacement components along the longitudunal axes of the frame are plotted in Figure 6.14 for the same tests. The two motions have a strong resemblance though the RCF5 test displacement is again slightly greater. Towards the end of the shake, after 15 seconds, the two displacement records have a distinct relative baseline shift. The shifting baseline, caused by low frequency components (greater than 1Hz), has very little effect on structural response.

Test model response

The overall response of a structure to applied load is often described in terms of various *global* parameters such as floor accelerations, base shear, floor displacements and story drift. Values for such parameters are tabled for comparison of the motion during the prime tests.

Global **structural response**

	Frame and test signal			Table 6.3
	RCF5 T100(2)	RCF5 T1000	RCF2 850-W2	
table acceleration*	0.055	0.620	0.570	
longitudinal axis:				
acceleration peak(g)				
1st floor	0.144	0.684	0.798	
2nd floor	0.198	1.093	1.107	
rel.displacement peak(in.)				
1st floor	0.108	2.12	2.04	
2nd floor	-	-	2.73	
transverse axis:				
acceleration peak(g)				
1st floor	0.041	0.306	-	
2nd floor	0.072	0.451	-	
rel. displacement peak (in.)				
1st floor	0.087	1.54	-	
2nd floor	-	2.05	-	
torsion (radians)				
1st floor	-	0.0043	-	

*acceleration component along longitudinal axis;

Of the one hundred and forty-one data measuring devices monitored during testing, the results from only one instrument were detected as inoperable. Unfortunately, the potentiometer measuring longitudinal motion at the south end of the frame at the second floor had a poor electric wire connection resulting in an intermittent open circuit during the T100(2) and T1000 tests of the present frame. However, since the majority of the inelastic deformation occurred below the first floor, mainly in the first floor columns, this was not a critical loss. Plots of floor accelerations and displacements in time-history form can be found in Figures 6.37,38,41 and 42 at the end of this chapter.

Histories of the first floor deformations in Figures 6.15 and 6.16 immediately indicate the difference in the model's natural frequency of vibration along the two principal axes. The difference is obvious in the plots mainly because the model is responding primarily in its two

1st FLOOR DISPLACEMENT RELATIVE
TO THE TABLE—LONGITUDINAL AXIS
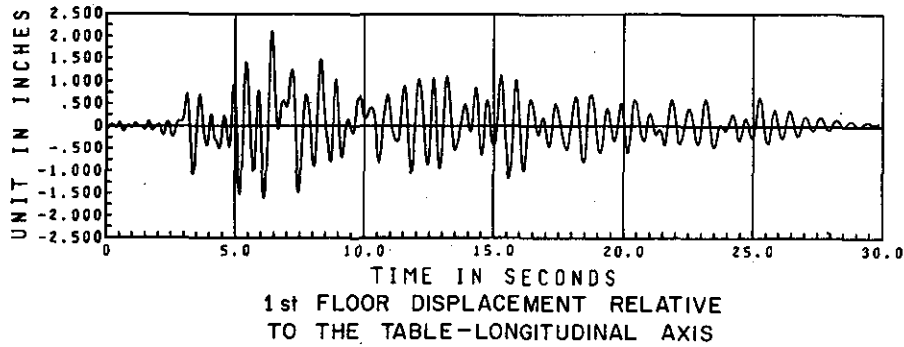
Figure 6.15   1st floor longitudinal displacement, T1000 test.

1st FLOOR DISPLACEMENT RELATIVE
TO THE TABLE—TRANSVERSE AXIS
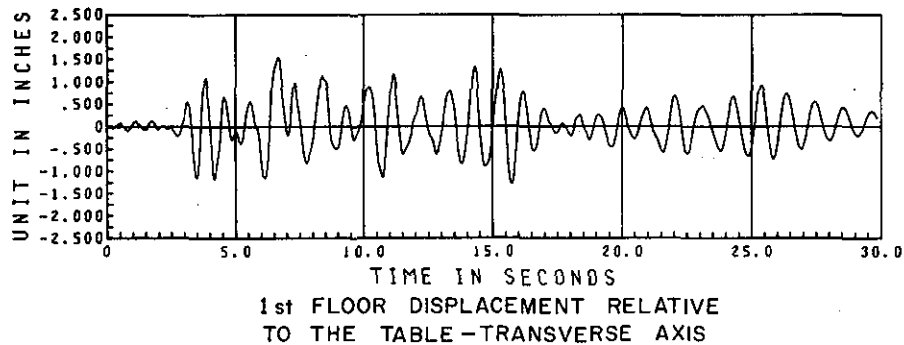
Figure 6.16   1st floor transverse displacement, T1000 test. .

first lateral vibration modes. If a significant amount of displacement occurred in the second lateral vibration modes, the obvious wave form in the Figures would be obfuscated by the higher second mode frequencies. The predominance of first mode response is further verified by the floor acceleration plots (Figures 6.37,38,40, and 42) where second mode effects should be accentuated due to the ω^2 effect. The true biaxial nature of the displacements becomes apparent if the motion is viewed from above the frame producing a displacement path trace as plotted in Figure 6.17.
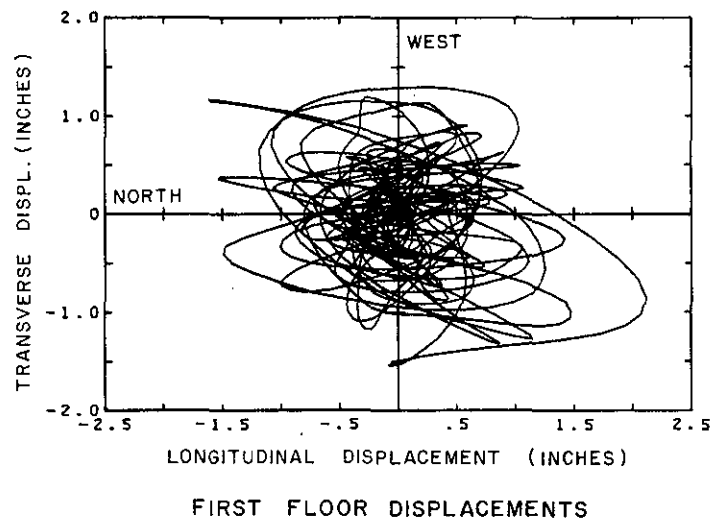
Figure 6.17 First floor displacements as viewed from above.

FIRST FLOOR DISPLACEMENTS

As mention previously, the response of a structure may be more often a function of the excitation frequency (vs.the structure's natural frequency) than of the peak acceleration of the ground motion. The lack of correlation between the times of buildup and decay in the 2 displacement histories along the axes of this structure (Fig. 6.15 & 6.16) is indicative of such dependence. While the transverse axis motion builds up to high levels at 3.5sec. or at 25.4sec., the longitudinal motion is low; and vice-versa, the longitudinal motion builds up at 13sec. and 18sec. while the transverse motion is low. However, both axes show peak displacement near 6 seconds, due to some resonant build-up, followed by a large energy sequence in the ground motion. The close tie between resonant amplitude buildup and input signal frequency can also be seen by comparing the response with records produced by Shoja-Taheri [9], in which the Taft signal is separated into components of small specified bandwidths.
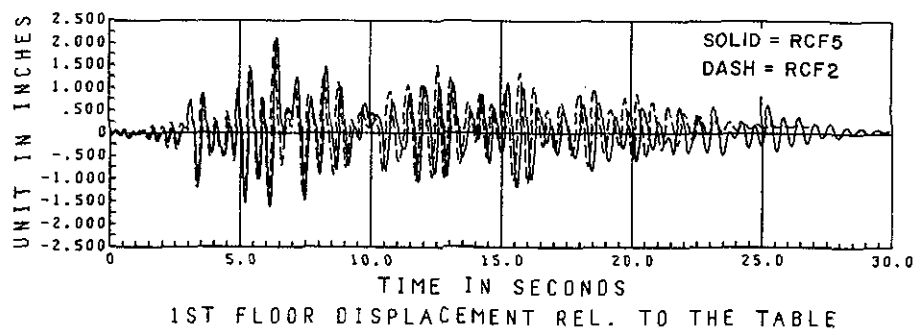
Figure 6.18 First floor longitudinal displacement, RCF5 and RCF2.

Displacements along the longitudinal axis of the RCF2 and RCF5 frames are superimposed in Figure 6.18 from the T1000 test. The two models show nearly identical displacements until the negative peak at approximately 6.2 seconds. At that instant the RCF5 frame has a peak in displacement along the transverse axis as well as the longitudinal and apparently suffers greater stiffness deterioration than RCF2 as evidenced by the decrease in frequency relative to the RCF2 frame over the remainder of the test.

Figure 6.19 Enveloping cycles of column shear vs displacement response, NA column.
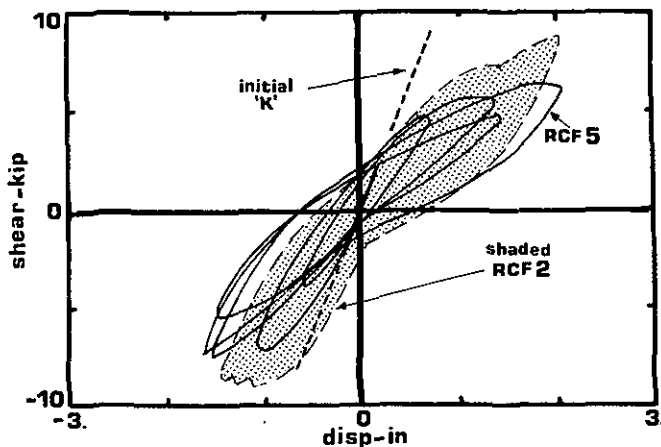
column shear - displacement

A comparison of the overall stiffness and strength of the present frame versus the RCF2 frame can be seen in Figure 6.19.   Major enveloping cycles of column displacement-shear, in the longitudinal direction, (similar to displacement-base shear) are plotted with the RCF5 results solid and RCF2 results in dashed lines and shaded. It is of interest to note that:

1) both frames have essentially identical initial elastic stiffness;

2) the present frame shows a lower yielding level;

3) the present frame tends to have greater stiffness degradation.

Even though individual materials in the present frame were slightly stronger than those used in the RCF2 test, the yield capacity of the present frame, under biaxial bending, was substantially lower than under uniaxial load. Not only was the longitudinal shear capacity lower, but the maximum principal shear, a vectorial combination of the shears occurring simultaneously along the two axes, was just 7.44kips, definitely lower than the 8.5kip shear capacity developed in the uniaxial RCF2 test. Such capacity reduction under multi-axial load may have serious consequences in columns designed using the code approved method of design in which independent lateral load analysis is used along a structure's principal axes [12]. Though the plot (Fig. 6.19) is of shear and displacement, it is important to understand that the major part of the displacement is a result of column bending and the three points given above are appropriately applied to the bending behavior.

Figure 6.20
Figure 6.21

PSV spectra for the T1000 ground motion with first mode frame natural frequencies noted.
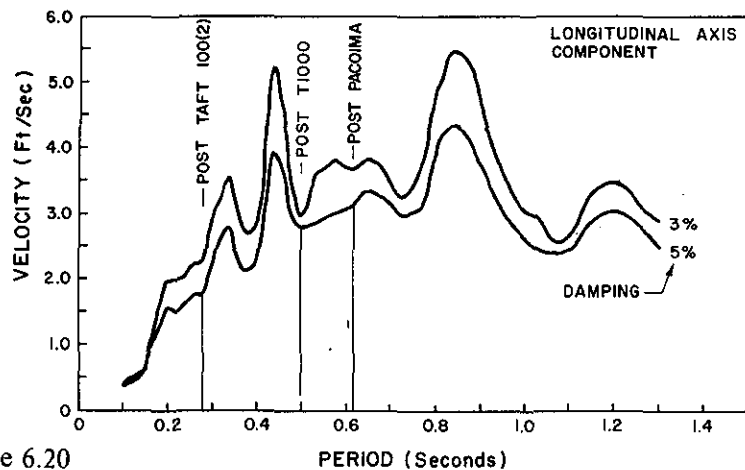
Figure 6.20

Variation of natural period of the structural model during several of the shaking tests is shown with plots of the pseudo-velocity spectra (with 3% and 5% of critical damping) for the component of ground motion along each of the model axes in Figures 6-20 and 6-21. In both axes the structure's period moved past relative peaks of the spectra plots. In general, based on results of concrete frames previously tested [1],[2], [10], the natural period during a major test decreases toward and remains in a valley of the spectra plot; strong shaking provides energy at the necessary frequency - creating inelastic stiffness deterioration and moving the natural period to an adjacent valley with insufficient additional energy input to cause further damage.
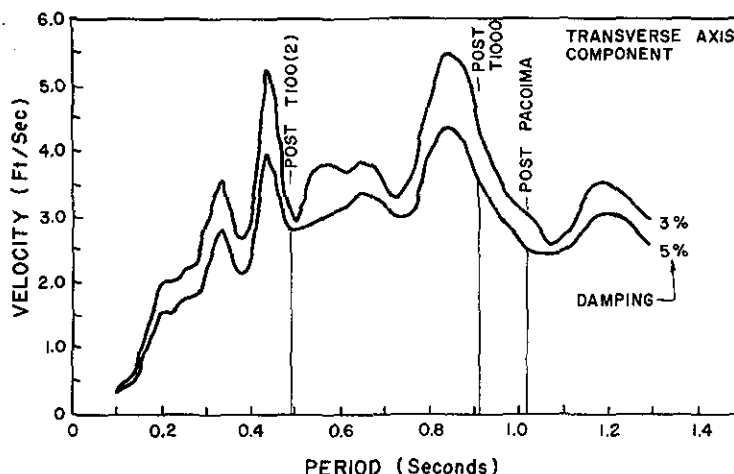
Figure 6.21

Model local response

Additional quantities describing the overall response of the present frame and providing a comparison with the previous test are listed in Table 6.3.

Table 6.4

Peak Values of Local Parameters-

T1000:RCF5 frame

850-W2:RCF2 frame

test	peak accel* (g)	max. shear column NS (k)	max. shear column EW (k)	max. moment column NS (in-k)	max. moment column EW (in-k)	residual displ. after test l-long. (in)	residual displ. after test l-trans. (in)
T1000	0.620	7.28	4.63	270	108	0.065	0.058
850-W2	0.570	8.54	-	-	-	0.155	-

test	max. strain column** milli in./in	residual strain column** milli in./in	max. rotation column*** (radians) NS	max. rotation column*** (radians) EW	res. rotation (radians) NS	res. rotation (radians) EW	max. axial load (kips) comp.	max. axial load (kips) ten.
T1000	18.1	6.6	0.0223	0.0226	0.0016	0.0035	45.6	-29.3
850-W2	20.7	6.9	-	-	-	-	27.3	-5.5

* acceleration of ground along longitudinal axis;

** strains from no.5 reinforcing bars;

*** rotation in bottom 4" of column, for column 1NAB;

The maximum column moments given in the table occurred at the base of the 1NA column. Maximum moments measured at the column midheight, center of the force transducers, were 34.8in-k (3.9kN-m) in the north- south or strong axis and 13.5 in-k (1.5kN-m) in the east-west weak axis direction, indicating that the column moment inflection point never deviated far from center. The maximum N-S moment (270in-k, 30.5kN-m) is higher than the statically predicted column strength of 250in-k (28.2kN-m) as described in *Chapter 3*, this variation will be investigated further in *Chapter 7*.

A difference in residual first floor displacements found in the RCF2 and RCF5 T1000 tests, and listed in Table 6.3, is noticeable in Figure 6.18; the cause is not readily apparent. The resonant build-up, peaking at 12.5 seconds and again at 15.8sec. seems to add progressively small amounts of permanent lateral drift which remains through the following response.

Column rotation was measured over a 4 inch (10.2cm) gauge length at the column bases. If the entire listed maximum rotation was considered to occur in a concentrated hinge at the column base, the resulting displacement (if the column were a cantilever beam) at the opposite end of the column would be 1.52in.(3.85cm) with a residual displacement of 0.24in (0.6cm). Since similar regions of concentrated rotation, though smaller in magnitude, form at the column tops as well, a fair proportion of the 2.12in. (5.4cm) of lateral first floor displacement becomes explainable.
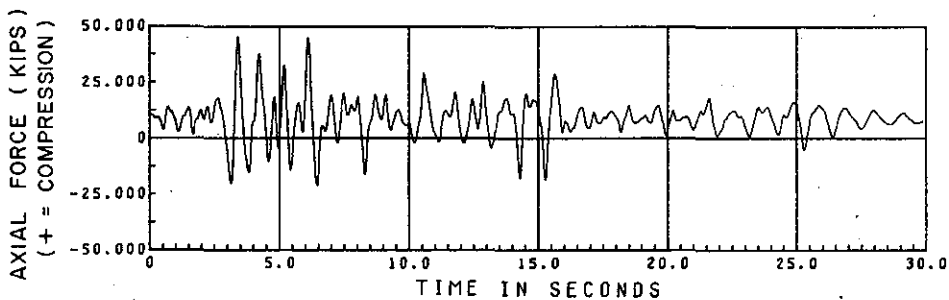
Figure 6.22 History of NA column axial force.

Because of biaxial motion in the present frame, dynamic overturning moments formed along both of the structural axes. When peak amplitudes occurred simultaneously, select columns were subjected to double components of axial loading, increasing or decreasing the summed axial load nearly twice as high as, or well below the RCF2 tests (Table 6.3). The higher axial loads interacting in the columns change the moment capacity (see the moment-axial load diagrams, *Chapter 3*

Fig. 3.10) accentuating the overall change in bending behavior under biaxial motion. The axial load history of the 1NA column is plotted in Figure 6.22.

A check on the accuracy of the shear channel of the column force transducers was possible by comparing the total base shear as a sum of the individual transducer outputs, with the total calculated inertial force. The inertial force was computed from the accelerometer data at each floor and on the mass blocks multiplied by the proportion of structural mass associated with each accelerometer. Figures 6.23 and 6.24 compare the calculated inertial force and the transducer output. The summed transducer shear output is plotted in a solid line and the inertial forced dashed. (The agreement is so close that the two histories are nearly indistinguisable.)
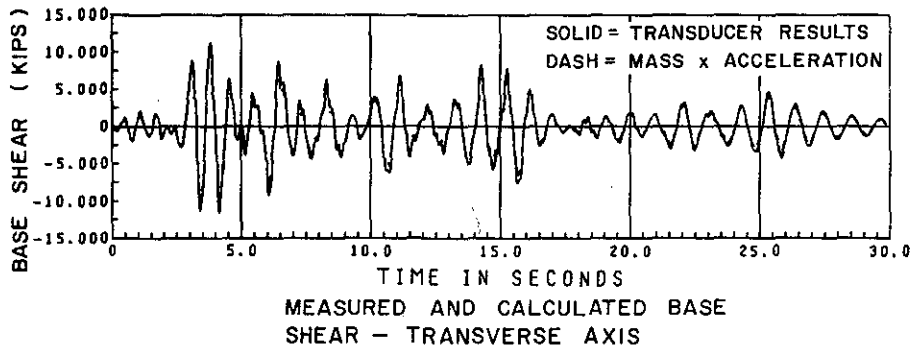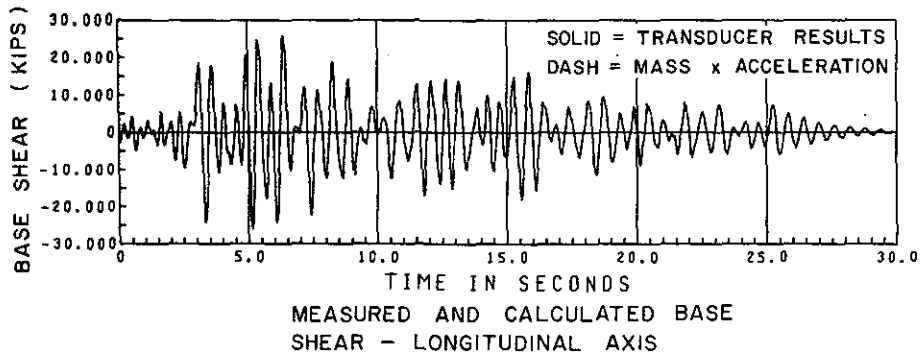
Figures 6.23 & 6.24   Comparison of transducer measured shears and inertial force.

Static pull to destruction

After completion of dynamic testing the structure was subjected to a lateral force applied statically at the top floor level in the longitudinal direction (with the force transducers removed). The only data measured consisted of force and structural floor displacement. A plot of the load-deformation response, as shown in Figure 6.25, indicates the amount of ductility available in the model frame. (Overall displacement ductility, measured from the plot of Fig. 6.25, was 4.2 times the yield displacement of 5.6in..) Figures 6.26 through 6.28 illustrate the amount of deformation obtained (nearly 24" at top floor), and the column to beam inelastic hinging behavior at member ends.
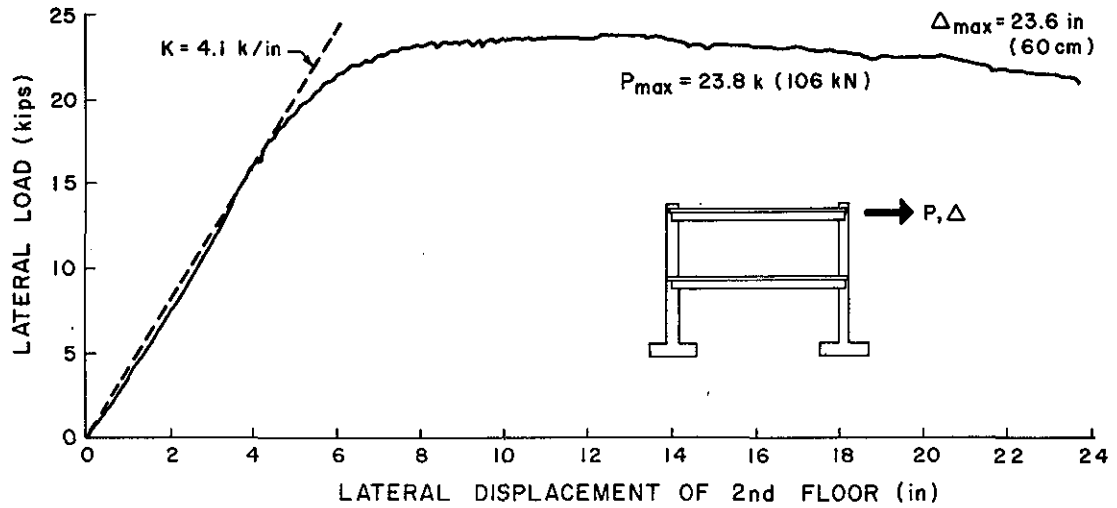
Figure 6.25 Lateral load vs displacement plot, pseudo-static test.
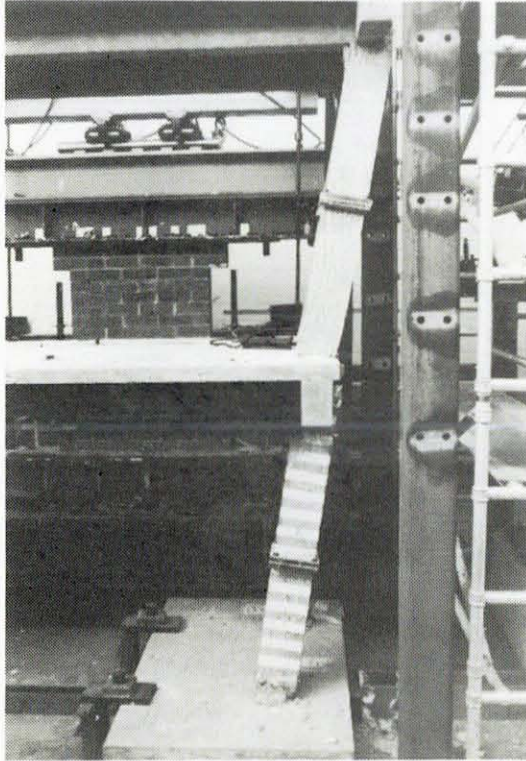
Figure 6.26 North frame.
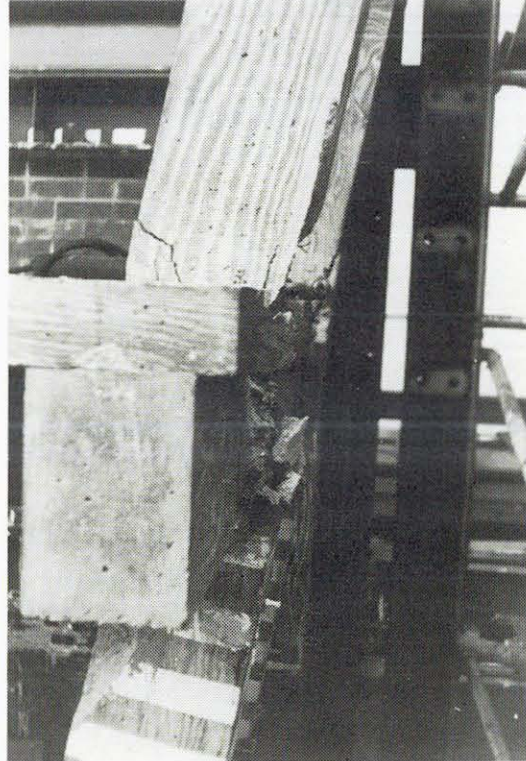
Figure 6.27 First floor column joint.
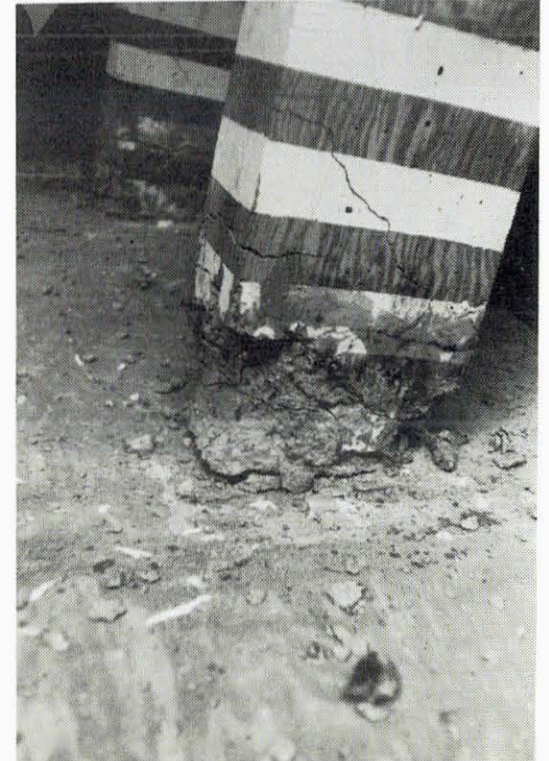
Figure 6.28 Column footing joint.

Figures 6.26-6.28 Frame damage after
pseudo-static lateral test, approx. 24 in.
displacement at second floor.

Summary

Visual observation of physical evidence of damage, such as concrete cracking, crushing, or spalling, and formation of concentrated regions of high deformation, was attempted as a means of evaluating the amount of damage created during any test. While such damage inspection provided a general indication of where inelastic energy dissipation mechanisms formed within the frame, it did not effectively evaluate the amount of damage which had occurred. After the Pacoima test, first story columns showed considerable concrete spalling at their bases which led to a conclusion that sizeable stiffness degradation developed during the test. However, frequency data indicated that the actual damage (and stiffness deterioration) had occurred during the preceding Taft1000 test.

The frequency measurements produced quantitative information regarding the extent of damage in the model, but essentially provided no definite information regarding where or how the deterioration occurred.

Combination of visual inspection and frequency testing of an earthquake damaged system could provide much of the information required to evaluate future structural safety. The qualitative knowledge of approximate section condition (e.g. effective moment of inertia) and location of inelastic deformation from visual inspection may be used to develop an analytic mathematical model of the system. Calculated natural frequencies from the analytic model could be correlated with quantitative measured frequency data. The resulting analytic model, with correct frequency characteristics, could then be used to predict structural response and member load levels during future excitations as a means to judge future safety.

Column lateral strength, measured in the present biaxial tests, was substantially lower than measured under uniaxial load. In addition, column stiffness, as determined through frequency tests and load-deformation relations, deteriorated to a greater degree under biaxial load than under uniaxial. Both effects have serious implications regarding lateral load capacity of, and design procedures for columns under earthquake loading. Accepting the random nature of earthquake induced horizontal ground motion, it is obvious that columns, particularly in buildings which rely on ductile moment resisting frames for lateral strength, will experience biaxial loads. If columns are designed to resist loads along their principal axes directions independently, their capacity may be insufficient to resist induced multi-axial loads. Even when columns are designed to successfully handle biaxial loading, reduced lateral stiffness, caused by inelastic interaction, may result in structural failure.
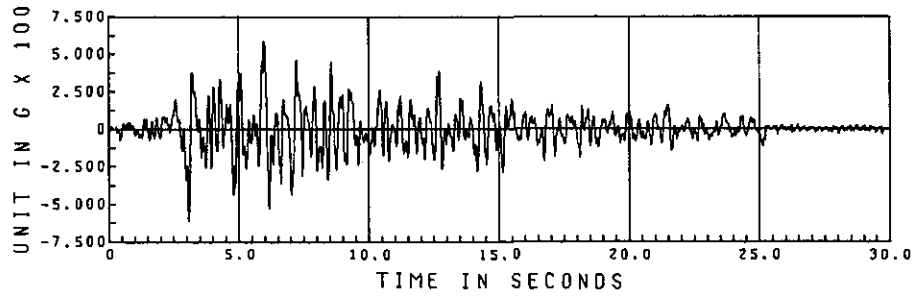
Figure 6.29 Taft 100(2) table acceleration history.
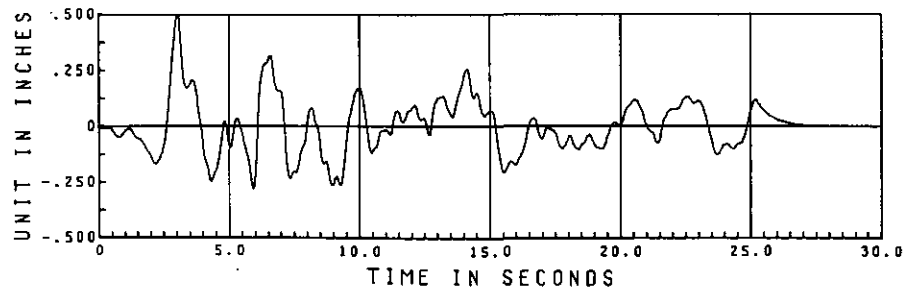
Figure 6.30 Taft 100(2) table displacement history.
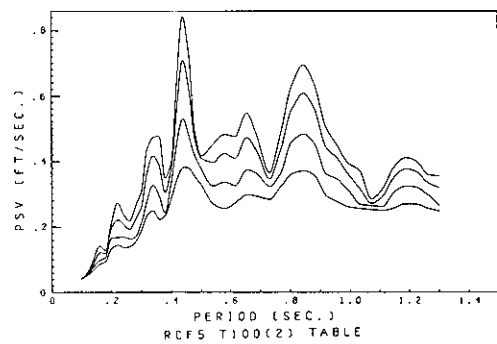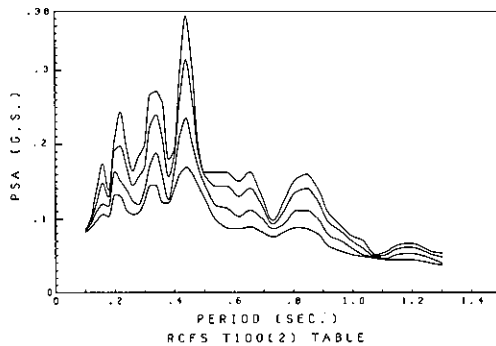
Figures 6.31 & 6.32 PSA and PSV spectra plots for T100(2) table motion, 2%, 3%, 5%, and 8% damping (top to bottom).

HORIZONTAL TABLE ACCELERATION
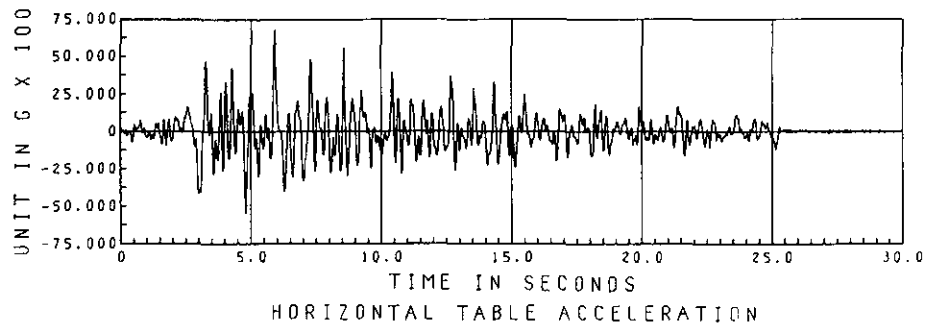
Figure 6.33 Taft 1000 table acceleration history.

HORIZONTAL TABLE ACCELERATION
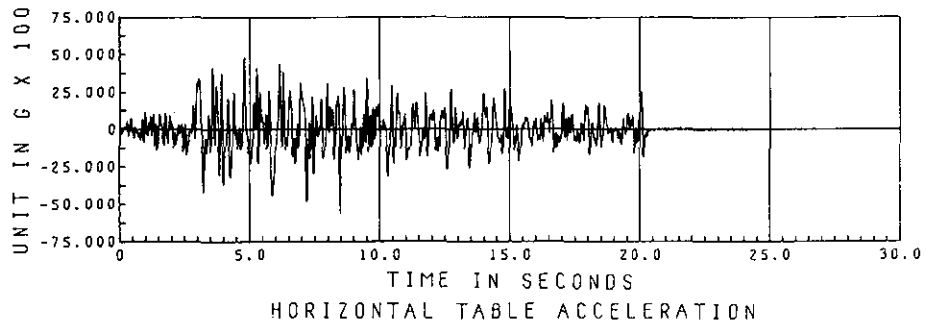
Figure 6.34 RCF2 T850W2 table acceleration history.

HORIZONTAL TABLE DISPLACEMENT
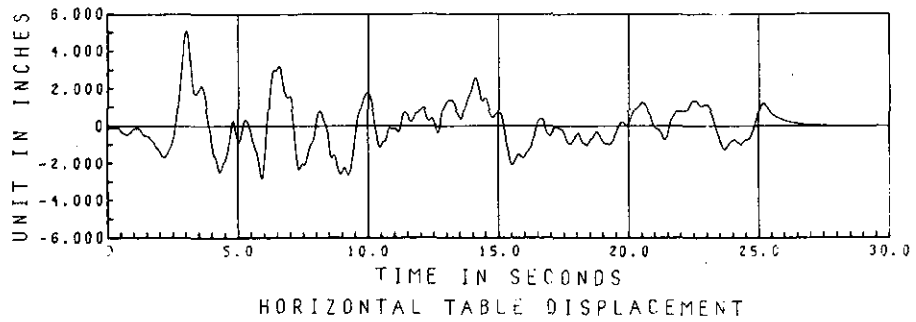
Figure 6.35 Taft 1000 table displacement history.

HORIZONTAL TABLE DISPLACEMENT
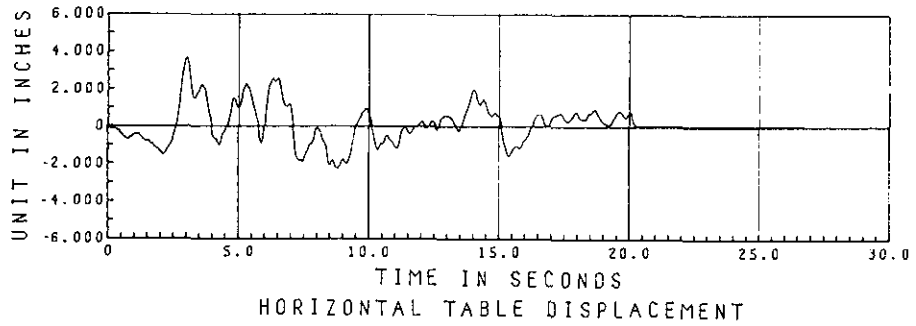
Figure 6.36 RCF2 T850W2 table displacement history.
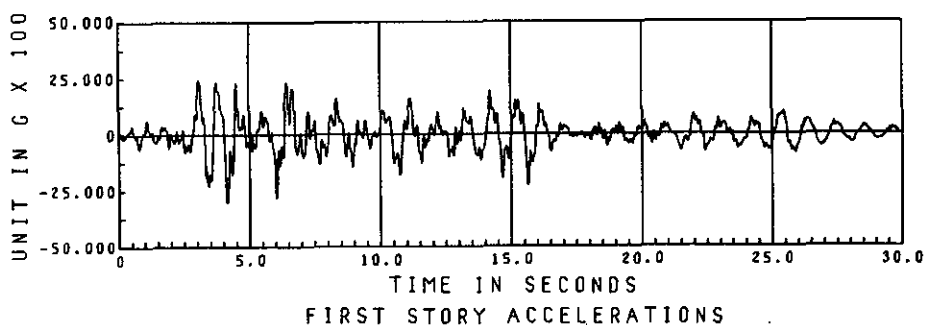
Figure 6.37 First story transverse acceleration history, T1000 test.
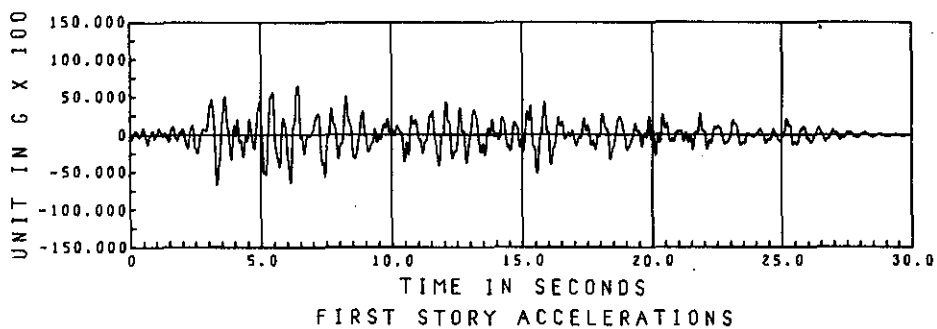
Figure 6.38 First story longitudinal acceleration history, T1000 test.
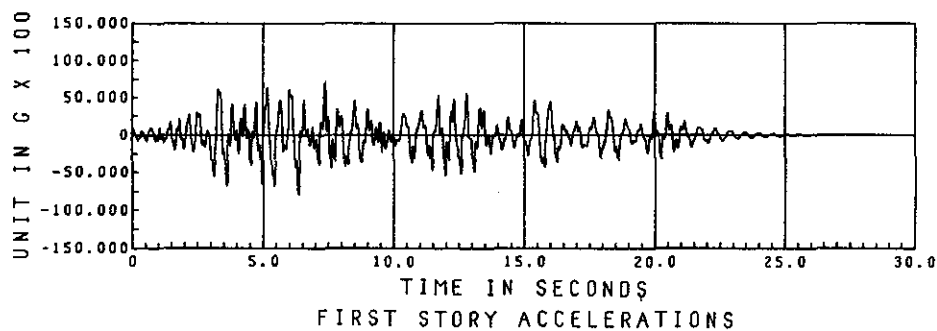
Figure 6.39 First story longitudinal acceleration history, RCF2 W2
(opposite sign of that used in Figure 6.38)
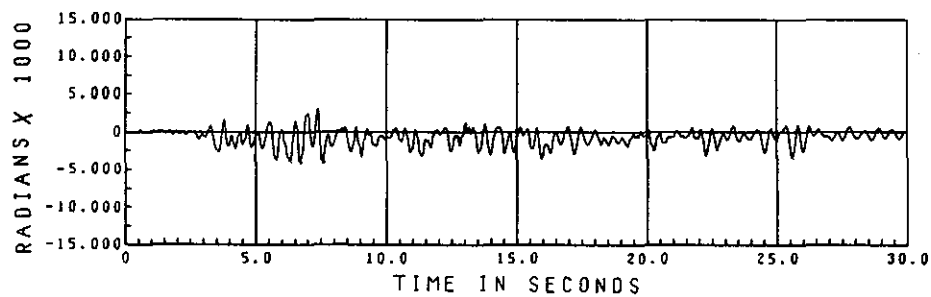
Figure 6.40 First story torsion history, T 1000 test.
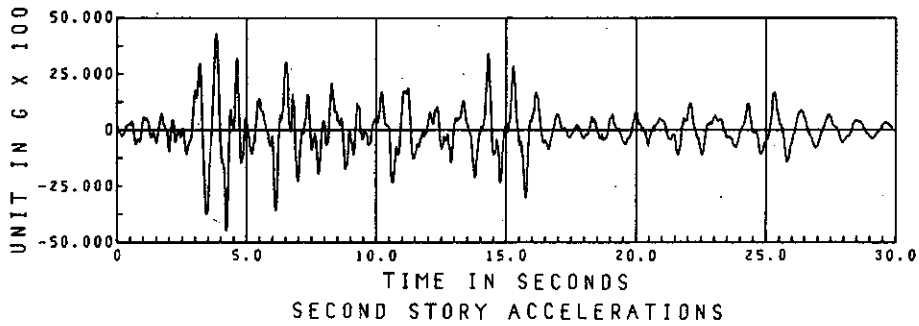
Figure 6.41 Second story transverse acceleration history, T1000 test.
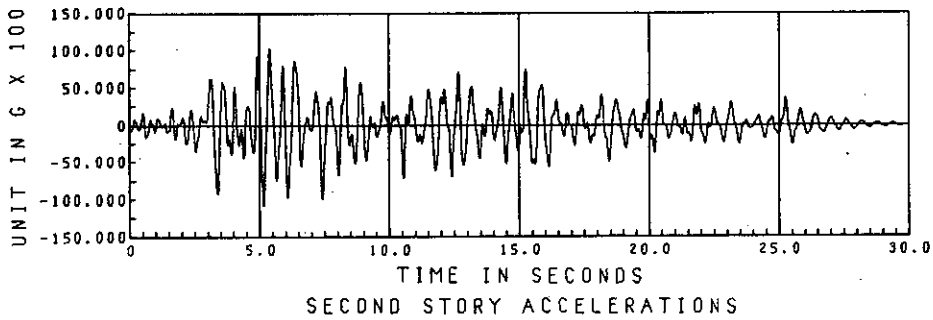
Figure 6.42 Second story longitudinal acceleration history, T1000 test.
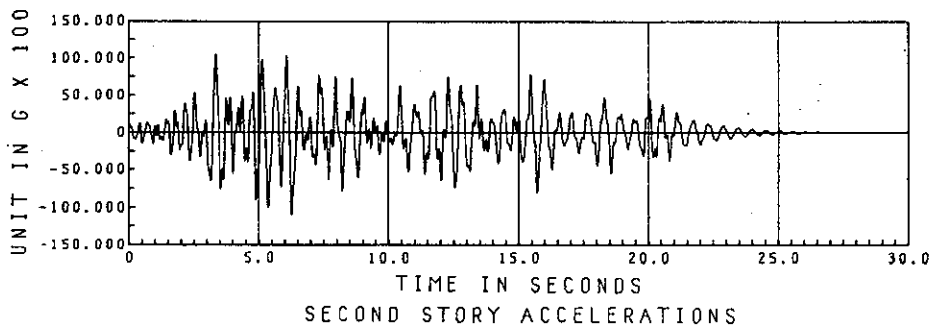
Figure 6.43 Second story longitudinal acceleration history, RCF2 W2
(opposite sign of that used in Figure 6.42)
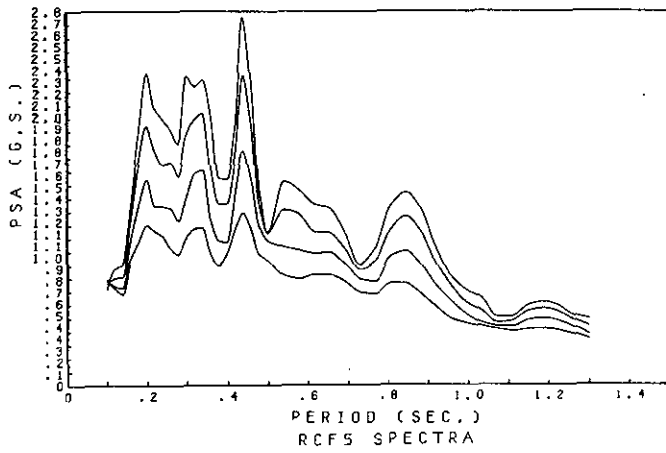
Figure 6.44 RCF5 PSA spectrum.
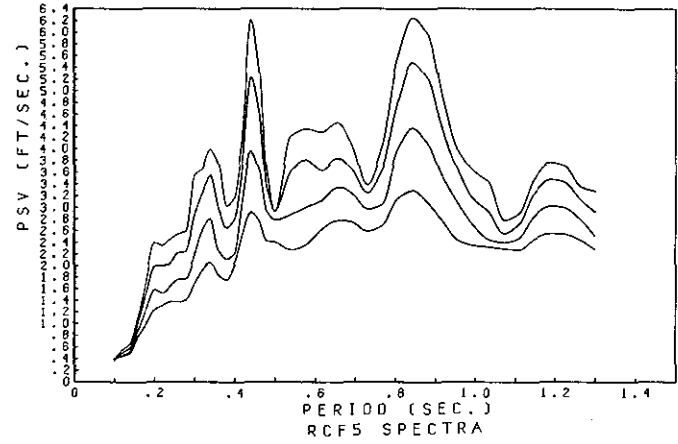
Figure 6.46 RCF5 PSV spectrum.
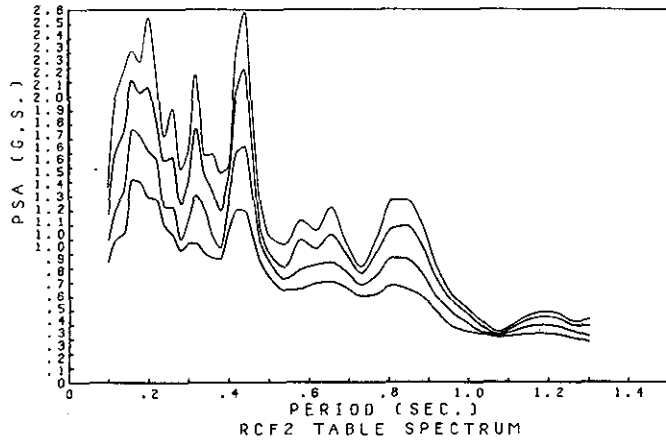
Figure 6.45 RCF2 PSA spectrum.
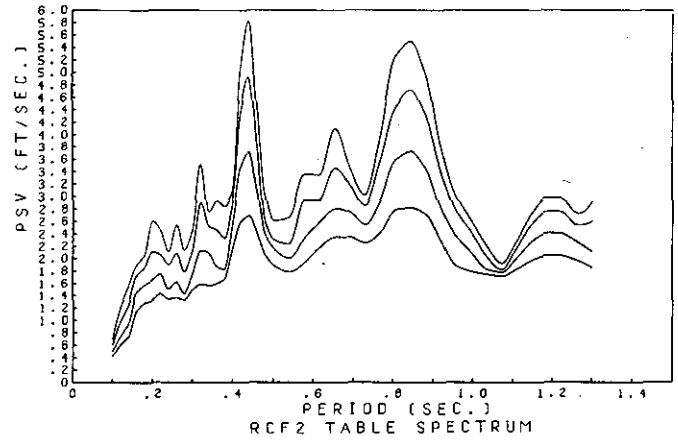
Figure 6.47 RCF2 PSV spectrum.

Figures 6.44-6.47 Response spectra for T1000 and RCF2 W2 table motions with 2%, 3%, 5% and 8% damping top to bottom.

Chapter 7

Local Behavior

The overall response of a structure is just a summing or coupling of the behavior under excitation from the multiple elements, such as columns or joints, which form the structure. Thus, it is the characteristics of individual elements which basically determine the reaction of the whole structure to any applied deformation or loading. Local behavior is of particular interest in the present test. The natural loading, including biaxial bending, in the columns and axial force due to overturning moments, with full inelastic load reversals occurring in a fraction of a second, allows an opportunity to study column behavior in a test situation which has not been adequately achieved previously.

Section 1: General Column Mechanics

A set of load-deformation relations comprise the characteristics necessary to describe the local column behavior. The exact form of such a relation is difficult to define for reinforced concrete elements; even in the case of uniaxial loading, formulation of a moment bending response description requires complex modeling. Under biaxial inelastic motion, coupling of separate deformations, such as increased rotation about both axes due to yielding of reinforcement caused by combined moments, could render simple combination of two uniaxial response descriptions, where yielding might not occur under either of the individual moments, inappropriate. The loading and deformation of the columns in the present test have been closely monitored to obtain a history of local behavior and to define the response characteristics. The description of those results in the remainder of this Chapter will consider only the Taft 1000 earthquake test.

Column loads

Column force transducers provide a direct measurement of the four primary force quantities, two bending moments and two horizontal shear components, at the mid-height of the columns. Application of equations of force equilibrium allowed determination of moments at the top and bottom column extremities. Column axial loads were calculated through a combination of equal compressive forces from the measured model self-weight and additional axial components varying in each column resulting from inertial overturning moments acting in the frame's two principal axes. (The overturning moments came from a summation of the

products of lumped

mass elevations multiplied by inertial forces, which were calculated as the lumped mass times its acceleration.) Column torsion force was not measured. Though slight torsional rotation of the individual columns did occur, the effects of torsional loading and deformation on individual column elements has been neglected in this program. The relative size of the bending and axial forces (as noted below) justifies the assumption that it was these which primarily controlled the response. Maximum forces occurring (not necessarily simultaneously) in many of the column members are listed in Table 7.1 with their frame location keyed in the sketch of Figure 7.1.
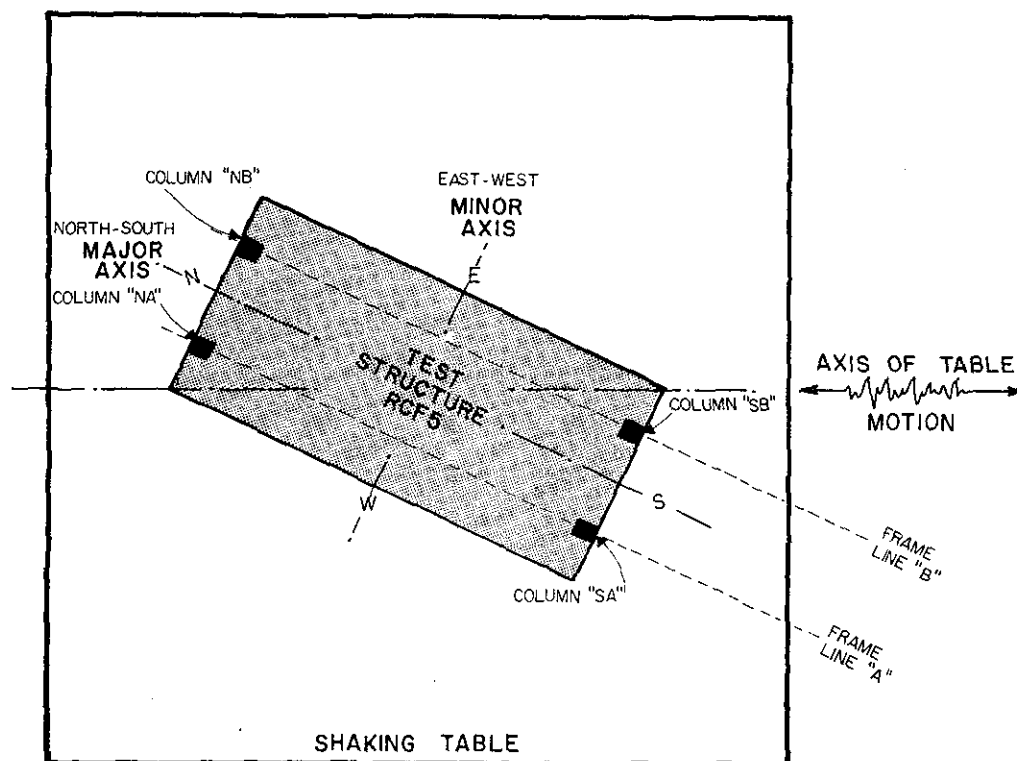
Figure 7.1 Key to column and frame notation

Column deformations

Lateral displacement at the column ends was calculated from the measured relative displacements on the first floor level assuming that the floor acted as a rigid diaphragm in its own plane. Column bending was monitored by calculating the differential output from displacement measuring DCDT's mounted on the column faces with a 4in. gauge length to give local member rotation. The individual strains in each of the column rebars was measured and their differential values were combined to give a second measure of rotation or curvature. Peak rotations, displacements and measured strains at various parts of the model frame are listed in Table 7.2.

Table 7.1

Peak Column Forces-Taft test (T1000)

	Column Shears (kips)				
	1NA	1SA	1NB	1SB	2NA*
north-south (strong axis)	7.15	7.28	7.17	6.91	4.04
east-west (weak axis)	3.34	3.83	4.63	3.34	1.75

	Column Moments (in-kips) (at column base/ at column top)				
	1NA	1SA	1NB	1SB	2NA
north-south	-271/245	-268/240	-233/-224	232/-203	87/180
east-west	108/-114	122/-126	1 52/-150	108/-110	53/-59

2NA refers to second story column.

	Column Axial Loads (kips)			
	1NA	1SA	1NB	1SB
compression	45.6	33.8	42.1	39.2
tension	-21.3	-24.2	-16.0	-27.0

Maximum "principal" forces- column 1NA
(vector combination of simultaneous components from the two axes)
Shear: Vp= 7.44 kips
Moment: Mp= 274 in-kips

Table 7.2

Peak Column Displacements- Taft test (1000)
(units in inches)
first story columns:

displacement	NA	SA	NB	SB
north-south (strong axis)	2.14	2.14	2.10	2.10
east-west (weak axis)	1.50	1.81	1.50	1.81
principal*	2.31	2.35	2.27	2.32
horizontal drift(%)**	3.4%	3.5%	3.4%	3.4%

torsional rotation of all columns = 0.0043 radians

principal displacement = vector sum of orthogonal components;
based on principal displacement. drift=displacement/column height;

Peak Column End Rotations - Taft test (T1000)
measured over 4in. gauge
(units in radians)

column:	north-south	east-west
1NA bottom	0.0223	0.0226
1SA bottom	0.0223	0.0208
1NB bottom	0.0220	0.0161
1SB bottom	0.0224	0.0210
1NA top	0.0120	0.0126
1SA top	0.0119	0.0169
2NA bottom	0.0053	0.0035

Peak Column Strains - Taft test (T1000)
(milli in./in.)

column:	bar location			
	north west	north east	south east	south west
1NA bottom	8.45	18.14	13.71	15.31
1NA top	14.03	11.72	16.22	10.92
1SA bottom	9.52	13.59	14.66	16.79
1SA top	13.60	7.24	3.86	2.47

Peak Beam Strains-Taft test (T1000)
(milli in./in.)

location:	top bars	bottom bars
transverse beam at column 1NA	0.83	1.14
long. beam at column 1NA	2.02	1.58

As mentioned in *Chapter 6,* a simple rotation at a column base of 0.022 radians could cause a deflection at the column top of 1.49 in. (3.8cm.) if the column were a cantilever. Nearly 70% of the actual first floor column drift would be immediately explained by such a mechanism. In fact the column top peak rotations, noted in the previous table, occur simultaneously with the peaks at the bottom, actually forming a double hinged column. A rotation of 0.022 radians was measured over the bottom 4 in. of the columns from the DCDT data.

Presumably the displacement data from any three non-colinear devices at any horizontal section of a column should be sufficient to define the rotation about horizontal axes of an initially horizontal plane cut through the column at a section relative to its initial position. Having four displacement or strain measuring devices at each section allowed a check to be made on the plane deformation calculated from the output of any three of the devices. The displacement or strain output from all four devices located around the column at any section were incorporated into a least squares plane fitting computer algorithm, with the sum of squared errors taken as an indication of goodness of fit. Rotation along the two horizontal axes of the column section was defined by forming a unit normal vector to the rotated plane and resolving it into components along the column's own axis and the original horizontal axes of the section. Data sets from reinforcing bar mounted strain gauges and column face located DCDT's were both analyzed in this manner.

The fit of a plane surface to the DCDT measured column deformations was exceptionally close, even during large inelastic rotations, and was a pleasing verification of the basic engineering first order theory that plane sections remain plane after loading. An estimate of the algebraic equation for the deformed plane of the lower north A-frame column, based on the DCDT measured displacements over a 4 in. (10.2 cm.) gauge length, had a peak sum of squared error equal to 0.0000313 *in.*^{2} at a time when the measured displacement on the north face was 0.215 inches. If the full error existed in any one of the DCDT locations it would be less than 2.6% of the maximum measured displacement at that instant.

Estimates of a deformed surface based on the strain gauge data produced results indicating distortion of the assumed plane. The sum of squares of the errors between the actual and the predicted strains from the estimated plane of deformation peaked with a value of 0.0000644 (strain squared) when the measured strain was 0.015. If that full discrepancy had existed at one of the bars it would represent an error 0f 0.008 or 52% of the maximum strain measured at that time. Local measurements of the column curvature based on such estimates of the deformed plane have an unacceptable amount of error.

The natural non-homogeneous state of reinforced concrete should lead one to expect a certain amount of nonuniform behavior at the the local level. The section distortion indicated by the strain gauge measurements could be caused by local irregularities such as the discrete cracking of concrete rather than a uniform straining in tension regions. Strain gauges placed at locations on bars where concrete to re-bar bond deterioration has occurred will show significantly different behavior than gauges on other bars at the same section with bond still intact. In contrast, the DCDT's average the effect of such discrete phenomena over a longer gauge length and avoid accentuating irregularities while providing a record of the desired member rotational behavior. All the reinforcing bar peak strains listed were measured at column-footing, column-beam, or beam-column joint interfaces. The peak deformation, at 1.8% strain, represents more than eleven times the yield strain. Moreover, alternate yielding in tension and compression actually produced an unknown accumulated amount of inelastic strain, considerably beyond that represented by a single cycle to eleven times the yield strain.

The additional strain gauges placed to either side of the joint interface gauge on a few of the reinforcing bars provided further indication of reinforced concrete's non-homogeneity. The south-east rebar at the top of the 1SA column is featured in Figure 7.2. Strains measured by a gauge at the column-beam joint are described by the short dashed line, strains 3 in. into the joint by the long dashed line, and strains 3 in. out in the column by the solid line. The bar yields significantly in the column but not in the joint or at its interface. Specific location of yielding in bars depends extensively on location of discrete tensile cracks in the concrete. Yielding of this gage away from the column joint may well be a result of crack formation.

Figure 7.3 shows results from the north-west bar at the bottom of column 1NA. Here, the solid line is the lowest gauge 3in. inside the footing, the short dash is the middle gauge- at the column footing interface, and the long dash is located 3 in. up in the column. The straining is similar to Figure 7.2 though the middle gauge shows some yielding.
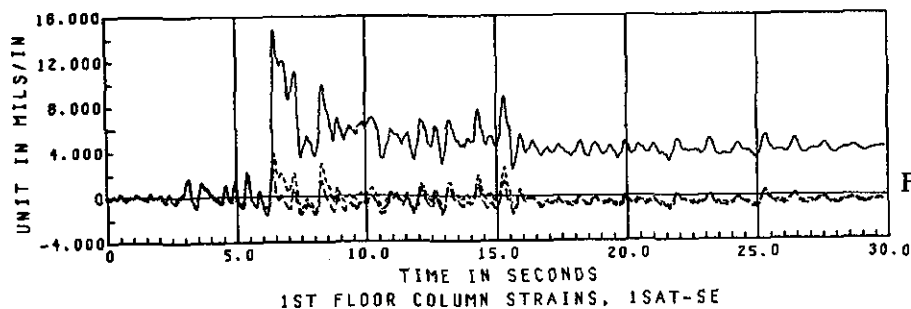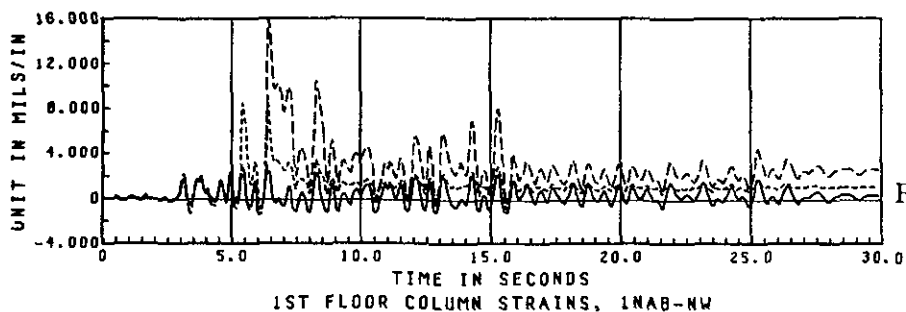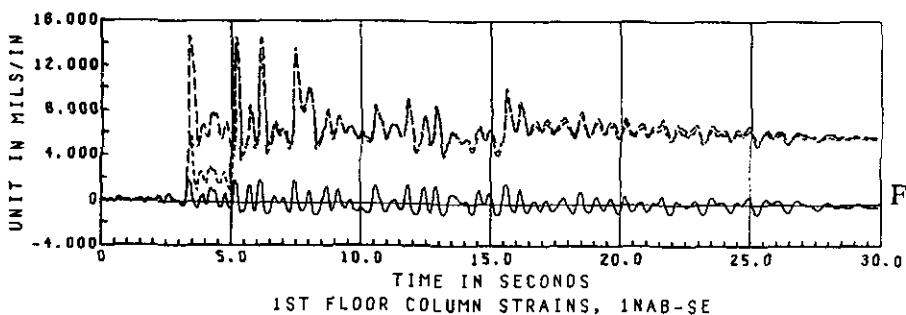
Figures 7.2-7.4 Rebar strains near column end joints.

Figure 7.4 comes from the south-east gauge set in the same column as the previous plot, *ie.* the rebar diagonally opposite to that of Figure 7.3. Strain gauge representation is identical. Here both of the nonfooting gauges show yielding at approximately 4.25 seconds though in differing amounts. Then, at 5.2 seconds, the rebar at the interface yields further after which the gauge at the interface and in the column show nearly identical strains with a residual offset of approximately 0.57% (strain of 0.0057). Certainly the concrete cannot withstand such tensile straining without considerable cracking. The high strain combined with virtually no change over the 3 inches separating the gauges is indicative of a loss in concrete-steel bond around this bar. Similar behavior had probably occurred in numerous other ungauged bars at the column bases.

The poor fit of a plane surface to the distorted rebar strain data could be a direct result of the phenomena seen in the Figures 7.2, 7.3, and 7.4. Some of the bars may yield at the joint interface while others remain elastic at the interface and yield at a location slightly inside the member as seen in Figure 7.2. Or, bond loss over short distances may occur in certain bars and

not others. In either case, the strain gauges cannot be used to provide an accurate estimate of the local column curvature.
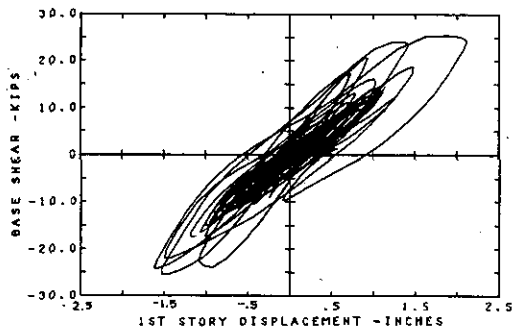
Figure 7.5a North-south displacement vs base shear, first floor.
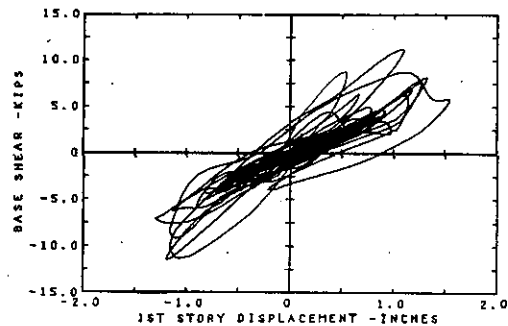
Figure 7.5b East-west displacement vs base shear, first floor.

Column load-deformation relations

A comparison between the changes in load and the related displacements in individual elements throughout the frame's response history might directly indicate the element's behavior characteristics. In real buildings the structure is often categorized by the floor displacements or relative floor drifts developed under lateral loading. Such a comparison for the present model frame is illustrated in Figures 7.5a,b. Figure 7.5a, longitudinal first story displacement vs. base shear, exhibits:

-definite yielding, particularly in positive or south direction with an estimated displacement ductility of 2.4 along the strong axis,

-several nearly full displacement reversals.

It is obviously impossible to follow the load deformation response timewise in Figure 7.5a due to the numerous cyclic reversals during the response history, plotted atop one another. However, a similar response plot, for a particular column, may be observed in detail through step by step plots presented later in this chapter. Figure 7.5b of transverse shear vs. displacement, does not include identifiable yield behavior, although numerous large displacement cycles, resulting from biaxial interaction, are evident. To obtain structural characterizations analytically, as shown in Figure 7.5, it is necessary to describe the individual column behavior in terms of the lateral displacement expected at one end relative to the other, when a lateral force is applied. The overall structural response will then follow as a sum of the column results.

The lateral load response at a structure's floors is normally given by the product of a stiffness factor and the structure's lateral displacements. But the individual column load response depends on the whole structure's torsional motion as well as the lateral displacements. Figure 7.6 shows traces of the individual column displacements as seen from above the frame. The difference in movement between the columns is due to varying additional lateral components caused by the frame's torsional twist. The peak torsional rotation of 0.0043 radians would cause a lateral movement of 0.31 in. (0.79 cm.) in the columns. The force and
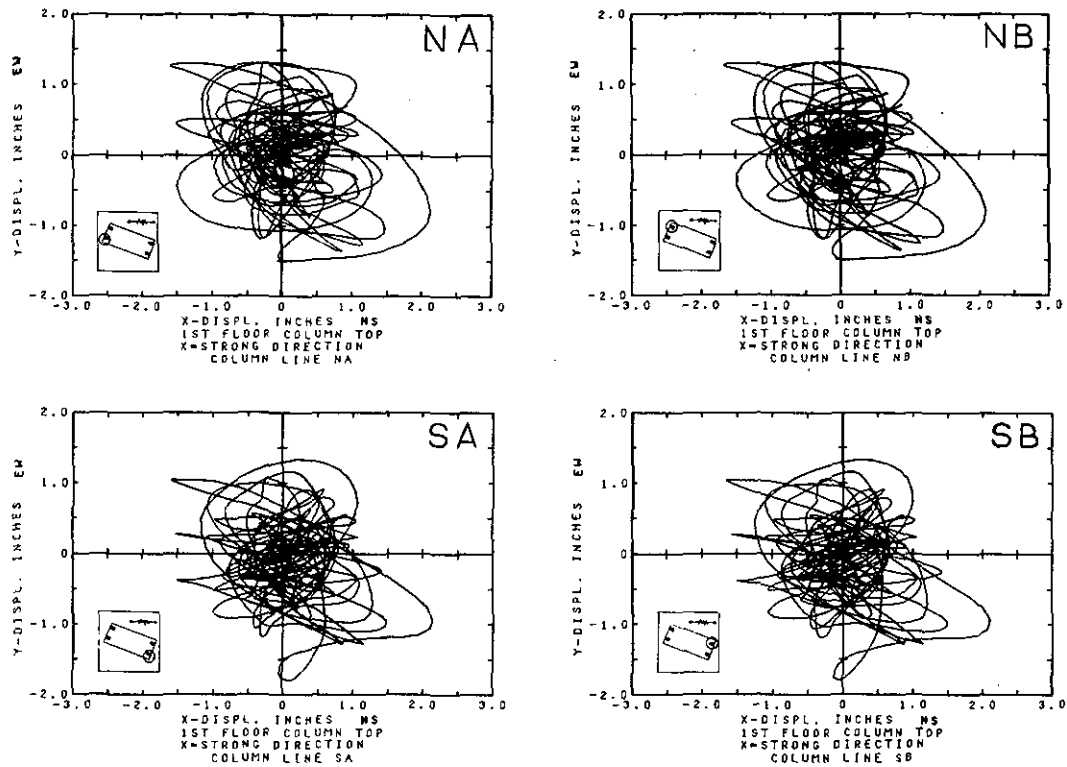
Figure 7.6 Column displacements, (+x = south, +y = west).

deformation quantities in each of the columns should differ slightly with the varied overall displacements.

Figure 7.7 Strong axis shear and displacement of NA column.
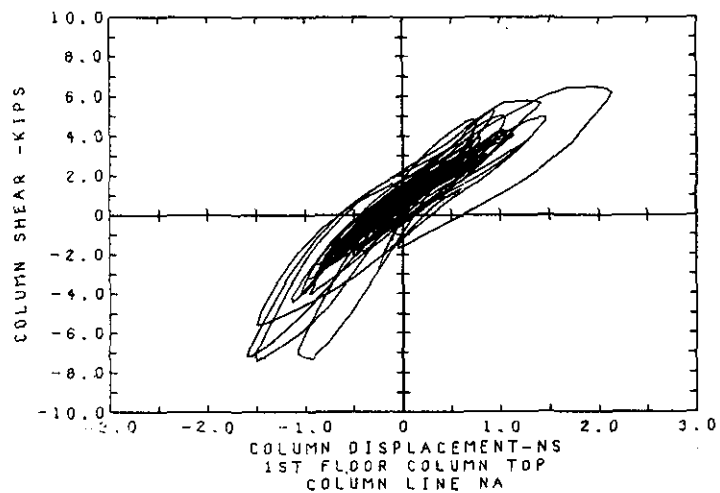
Column lateral load - displacements

The displacement under lateral load (shear) relation along the strong N-S axis of one of the column elements is shown in Figure 7.7 from the T1000 test. The stiffness in the north-south direction starts out as 11 kips/inch (19.2 kN/cm) but begins to degrade in the first large displacement cycle and remains near 3.1 to 3.3 kips/inch (5.7 kN/cm) through most of the test after the initial strong motions at 6.3 seconds. The actual stiffness appears to depend on the sign of the shear. Under negative shear, the slope of the curves (= stiffness) is slightly higher, especially during the initial strong motion or large displacement cycles. This may be attributable to increased axial compressive force, a result of the frame's dynamic overturning moment in the north-south direction, since it is co-incident with motions causing a negative shear. Definite yield-type response may be observed as well. The "yield" level seems to depend on the sign of the shear just as the stiffness did.

Figures 7.8-7.10 Column strong axis shear vs displacement, NB, SA and SB columns respectively.
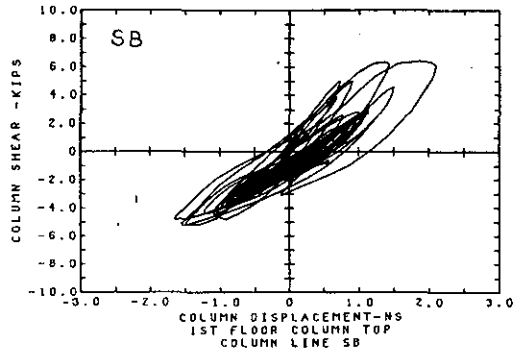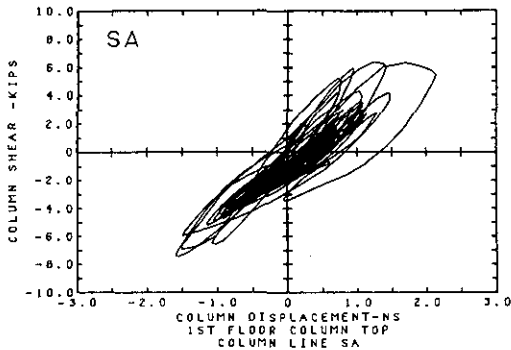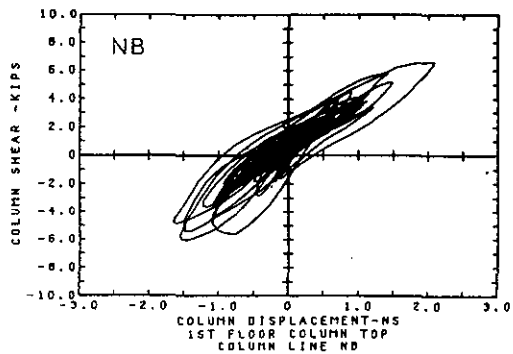
The cause of the apparent load versus displacement response cannot be explained quite so easily, though. Figures 7.8, 7.9, and 7.10 show the simultaneous load-shear displacement response of the other three columns of the frame. The same axial loading due to north-south dynamic overturning moment occurs in the north A-frame and north B-frame (NA and NB columns), and thus the effect should be similar. However, comparison of Figures 7.7& 7.8 indicates distinct differences. In general, there still seems to be slightly higher stiffness under negative shear in both the plots but the load behavior under negative shear is significantly different. In the NA column, Figure 7.7, the shear peaks of the three highest cycles go higher than -7.0 kips (31.1 kN) while the NB column of Figure 7.8 has all three of the correlated

peaks less than or equal to -6.0 kips (26.7kN). The loads and displacements under the two sets of peaks are listed in the following table.

Peak	Time secs.	Shear NS kips		Axial Load kips		Displ. NS inches	
		NA	NB	NA	NB	NA	NB
peak 1	3.34	-7.3	-5.6	32.9	13.1	-0.92	-0.75
peak 2	5.17	-7.4	-6.0	32.8	19.8	-1.51	-1.54
peak 3	6.11	-7.2	-4.8	45.4	3.5	-1.59	-1.65
peak 4	7.44	-5.6	-5.4	18.6	29.1	1.50	1.48

Table 7.3

In each of the three initial negative peaks (Fig. 7.7, 7.8), the actual compressive force is considerably higher in the NA column than in the NB column, a result of the overturning moments in the north-south and east-west directions combined. The column displacements, listed with the axial load and shear values in the preceding table, are very close or nearly identical in both columns. The higher shear or lateral load level at similar displacements is indicative of a higher effective lateral stiffness under axial com pression. Examination of load and displacements in the two simultaneous fourth negative peaks shows that the shear in both columns under very similar displacement is nearly the same, indicative of identical lateral stiffness, in this instance with the NB axial load increased.

Additional differences in the response behavior may be due to the variation in the column displacements mentioned earlier. Certain specific characteristics, such as the continued increase in displacement under decreasing lateral load, as seen in the first major negative peaks of Figures 7.7 and 7.8 are results of multi-axial interaction effects and will be investigated thoroughly in the latter half of this chapter.

The major enveloping cycles of the NA column from Figure 7.7 are compared with the shear displacement results from the same column location of the previous uniaxial RCF2 test frame in Figure 7.11 (reproduction of Figure 6.19 in the preceding chapter). If the parameters affecting the lateral load versus deformation relation for the columns in either of the two frames are:

Figure 7.11 Enveloping cycles of strong axis shear vs displacement, NA column, T1000 and RCF2 W2 tests.

column shear - displacement
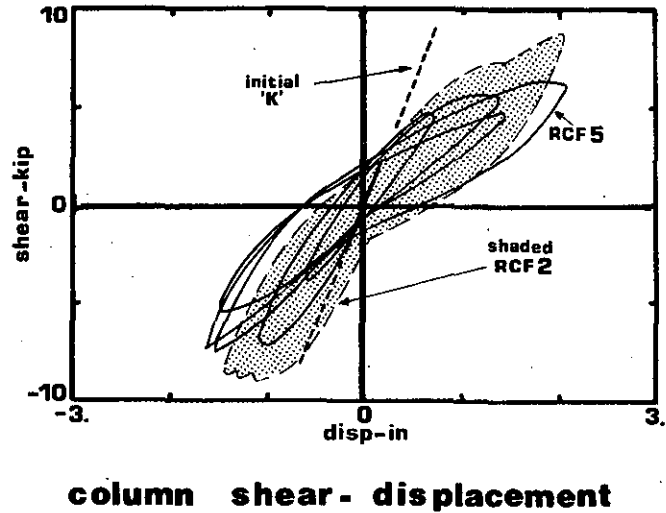
a. lateral shear,

b. lateral displacement,

c. axial load,

as considered in the preceding comparison of behavior of the columns in the present test, then one could expect that the additional axial compressive or tensile loads caused by the east-west dynamic overturning moments would explain deviations between the column behavior in the two test frames. However, even with the additional component of axial compressive load (east-west overturning), which the uniaxial RCF2 column did not have, in the first three negative peaks, (axial compression was greater than the maximum, 27k, in RCF2). The stiffness and maximum shear are less than seen in the RCF2 column; but the higher axial compressive load should have caused the exact opposite results.

This unexpected lower strength and lower stiffness in the column of the present skewed frame must be the result of additional unconsidered parameters, beyond the three mentioned previously, namely interaction effects due to the lateral force and displacement components occurring in the second minor axis direction. Even when the two simultaneous shear components in the column were combined, the resultant 7.4k maximum shear was less than measured during uniaxial testing.

Lateral load versus displacement behavior along the weak (east-west) axis of the NA column is plotted in Figure 7.12 for the same test period as used in the north-south axis of Figure 7.7. In this Figure positive shear is coincident with axial compression due to dynamic overturning moments in the east-west direction. Once again, a steeper slope, indicative of higher stiffness can be detected when the column is under positive shear and compression due to east-west overturning effects. There is no definite "yielding" behavior obvious along this axis although certain irregularities in stiffness are apparent. Initial lateral EW stiffness of the NA column was 3.4k/in. but degrades after 6 seconds and remains approximately 1.1k/in there

Figure 7.12 Weak axis shear and displacement of NA column.
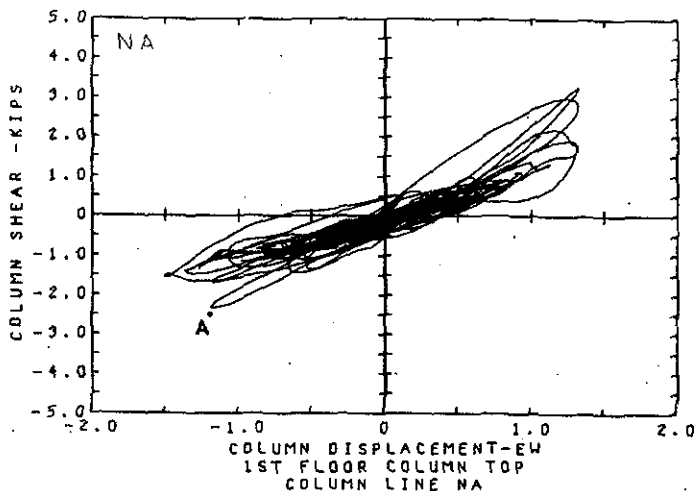
after even though no normal yielding was detectable. The substantial decrease of stiffness in this weak direction was a result of inelastic deformation developed through the strong axis response, as will be seen in Section II of this chapter.

Figures 7.13-7.15 Column weak axis shear vs displacement, NB, SA, and SB columns respectively.
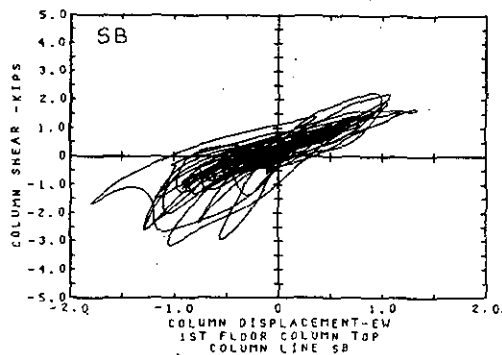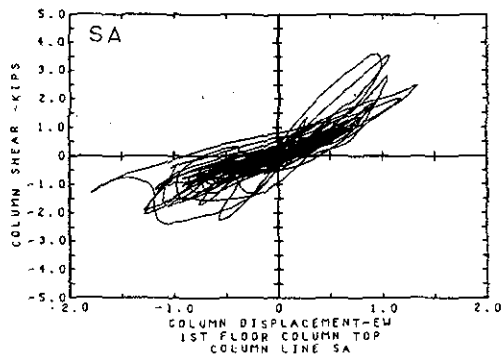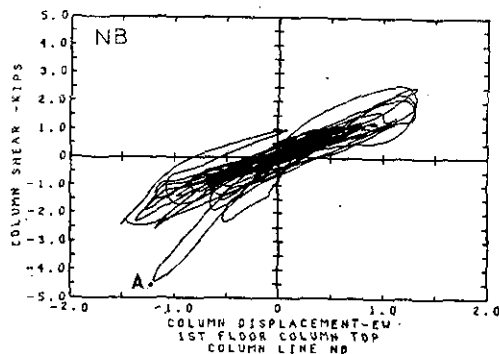
Similar response histories for the remaining three lower story columns are included in Figures 7.13, 7.14, and 7.15. Greater displacement variation between columns can be seen in this weak axis direction than in the previous strong direction because the structure's torsional rotations are multiplied by a longer "arm" in determining the structure's contribution to the total east-west displacement in each column. Once again unexplainable differences are apparent when

results from the various columns are compared. For instance, the negative shear peaks marked 'A' in Figures 7.12 and 7.13 which occur simultaneously. The forces and displacements exist- ing at the two peaks are listed below. Though the peaks have exactly identical east-west dis- placement, and displacement in the orthogonal axes of -0.208in.(NA) and -0.146in.(NB), the shear in the NB column (Fig.7.13) is nearly twice that measured in the NA column, indicating that one column has an effective lateral stiffness twice as high as a similar one while deformed equally. Since the north-south shears in both columns are comparable the contrasting stiffness must be a result of the very high axial compressive load (90% of the maximum compressive peak) occurring in the stiff NB column while the NA column has a small amount of tensile force.

"A" - EW Column loads, displacements at 3.81 seconds

Column	VEW kips	VNS kips	AXIAL kips	DISPL-EW inches
NA	-2.3	-1.0	-14.8	-1.16
NB	-4.5	-1.2	40.0	-1.16

Table 7.4

Column local moment-rotation relations

Since column lateral displacements are caused primarily by bending and are affected by end support conditions- *ie*. the end continuity and end moments, it is necessary to define the amount of lateral bending which will occur under given bending moments as a basic component of the element load deformation characterization. In dynamic lateral vibrations, primarily of the first natural mode, a column with an initially 'fixed' base and stiff girder at the top will nor- mally have a bending inflection point and change of sign of moment near its mid-height. The measured peak moments at the column mid-heights in the present test were never higher than 20% of the peak moments at the column ends. Therefore most of the inelastic non-linear bending response occurred in concentrated rotational hinging measured by the DCDT devices over a 4 inch gauge length, at the column top and bottom extremities. (Strong-girder and weak column design was purposely implemented in this frame to initiate and localize inelastic defor- mation in the columns. Normal ductile moment resisting frames are required to use the oppo- site design approach, however, biaxial loading may still cause unexpected inelasticity within the columns.) The bending moment and rotation response in the major north-south direction is illustrated in Figure 7.16 for the base of the north A frame column. Once again, the behavior seems to show a slight stiffening effect when under negative north-south moment which corresponds to compressive axial loading resulting from north-south dynamic overturning moments. The overall characteristics of the moment-rotation diagram in Figure 7.16, particu- larly including the major cyclic peaks, are in general very similar to the north-south shear- displacement response cycles for the same column as seen in Figure 7.7. Knowing that the column base-moment corresponds directly to the column shear, the similarity between the shear - displacement and the moment - rotation response substantiates an analogous situation between column top displacement and base rotation due to bending. As mentioned previously,

Figure 7.16 Strong axis moment and curvature of NA column at footing.
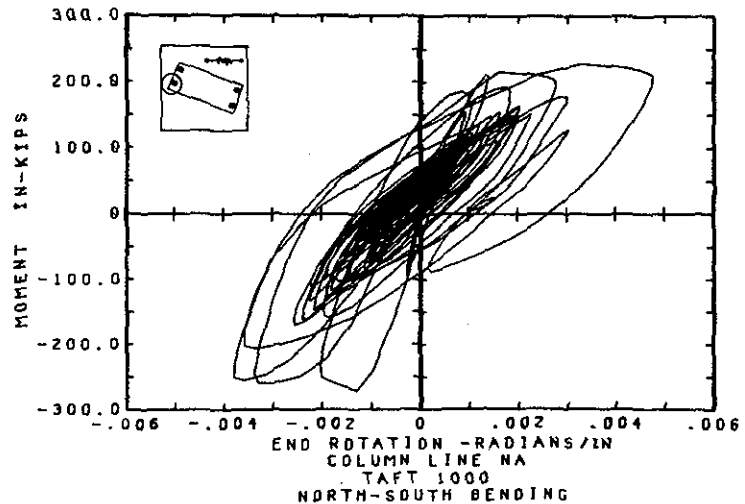
the peak positive rotation plotted in Figure 7.16, if multiplied by the distance to the column-top, would produce more than half the peak positive displacement plotted in Figure 7.7 (see Figure 7.17). Moment versus rotation plots for the remaining three columns are similar to Figure 7.16 and are displayed in Figures 7.62, 63 and 64 at the end of this chapter.

Figure 7.17 Effect of column base rotation.
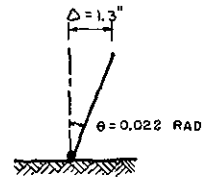
The progressive degradation of the column stiffness becomes clear when the thirty second response plot of Figure 7.16 is separated into four consecutive segments or 'windows', of five seconds duration each, as in Figure 7.18. Within the first frame the initial uncracked (67000 in-k/rad) column strong axis stiffness and the cracked (36000 in-k/rad) column stiffness are readily apparent. Overall shape of the hysteretic load-deformation loops would be described as having a pinching effect, i.e. the loops tend to squeeze together near the level where the sign of the moment reverses. Increased pinching effect is associated with development of a less efficient energy dissipation mechanism since the energy absorbed during cyclic structural deformation is proportional to the area enclosed by the hysteretic load vs. deformation path. After the inelastic yield cycles of the second window, the member has a varying stiffness depending on the instantaneous load level and previous loading history. The medium amplitude cycles in windows or frames 3 & 4 exhibit such varying stiffness; moreover the loading path under negative moment can be seen in frame 3 (also true in frame 4) to be consistently directed toward the previous peak moment rotation point shown by the dashed lines.

The moment rotation behavior of the same column (north A-frame) in the weak axis direction is significantly different. The response, Figure 7.19, seems to lack any simply described phenomena as existed in the strong direction behavior of Figures 7.16,7.18. The
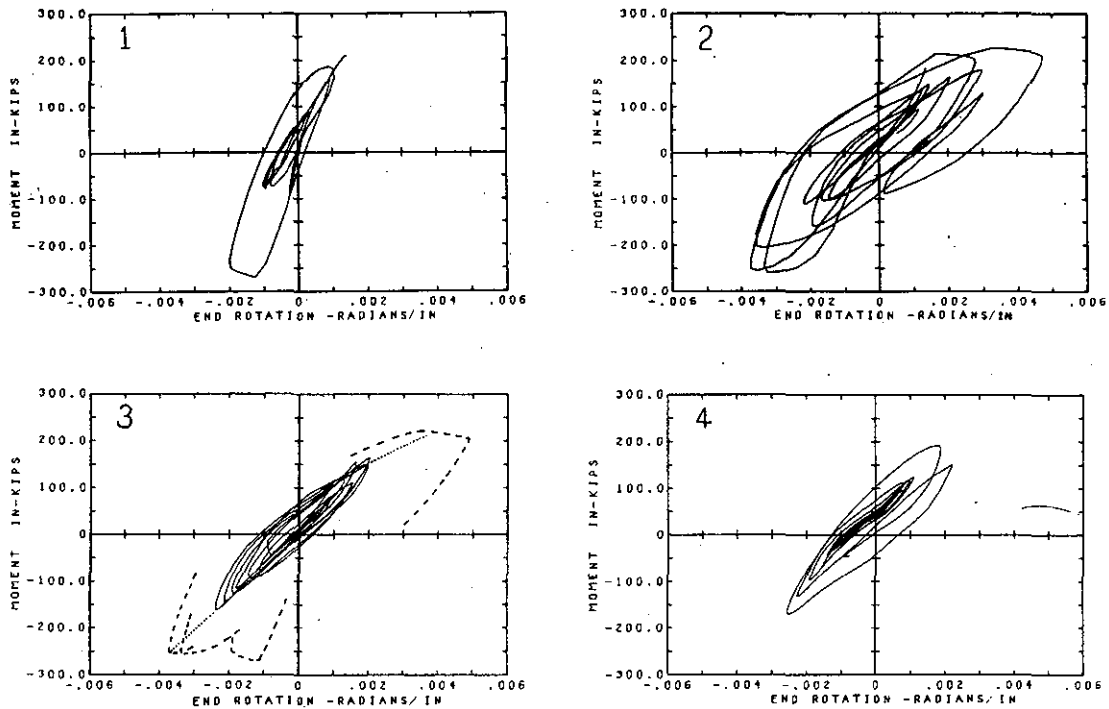
Figure 7.18 Strong axis moment and curvature of NA column at footing, sequential 5 second intervals.

Figure 7.19 Weak axis moment and curvature of NA column at footing.

COLUMN LINE NA
TAFT 1000
EAST-WEST BENDING
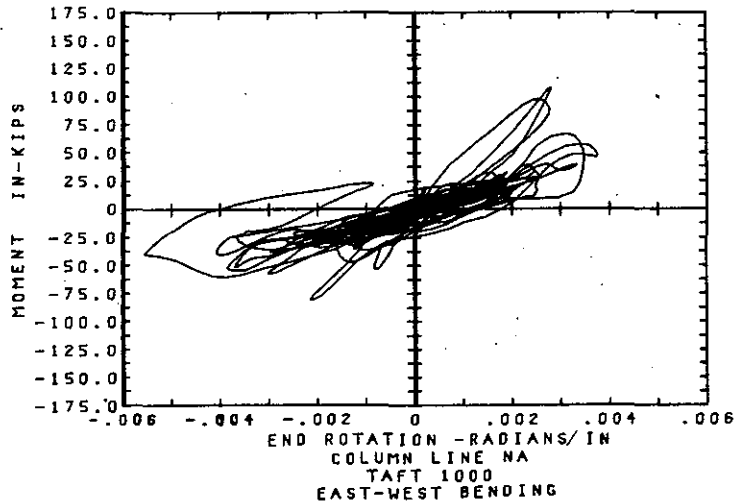
response is also broken into four consecutive intervals of five seconds each in Figure 7.20. An uncracked stiffness of 72000 in-k/(rad/in) is apparent in the first frame's initial motion. From that point and on, the motion tends to be quite irregular, especially in the second frame, the same interval within which the response in the major strong axis had large inelastic excursions. Average stiffness in the second, third, and fourth plot segments had deteriorated to less than one third of the initial, a very substantial reduction, without significant yield occurring! Furthermore, characteristics of the weak axis motion, illustrated in Figure 20, indicate considerable
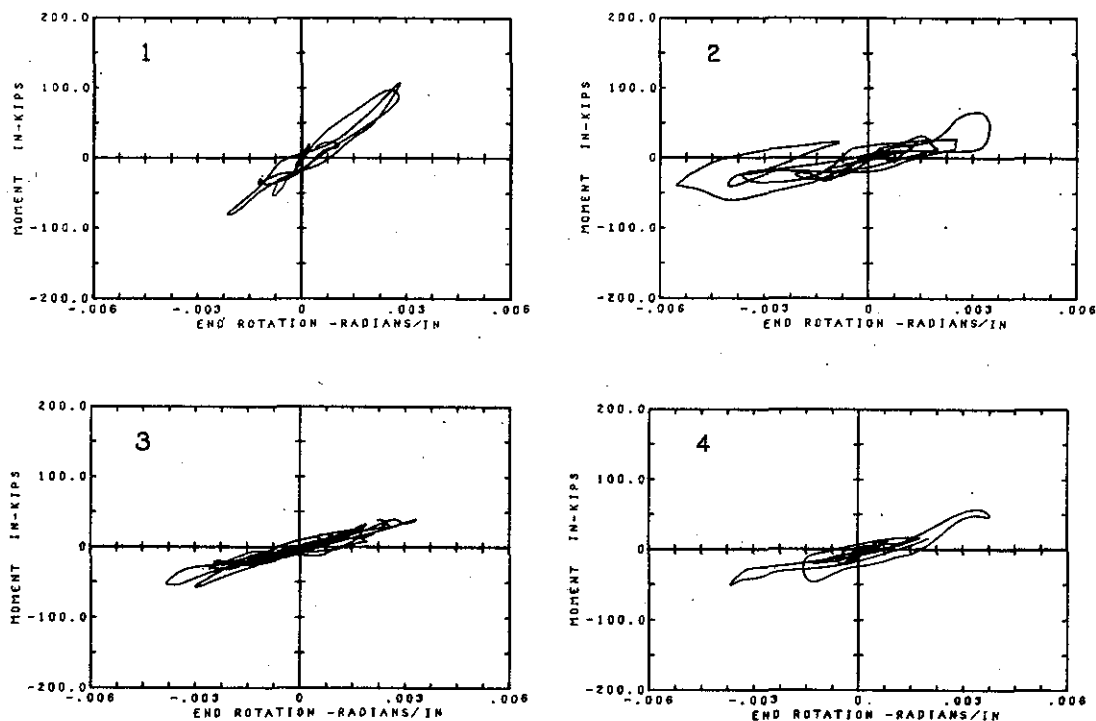
Figure 7.20 Weak axis moment and curvature of NA column at footing, sequential 5 second intervals.

deformation with little energy dissipation. Such action in a real building could result in serious non structural damage due to high floor drift and a resonant response unconstrained by inelastic energy dissipation. The peculiar response along the weak axis results partially from the effect of axial load as seen previously in the shear displacement behavior and additionally, from interaction between the simultaneous bending moment and inelastic rotation occurring along the perpendicular strong north-south axis. Bending behavior in the east-west direction of all the columns had obscure characteristics which are illustrated in Figures 7.65, 66 & 67 at the end of this chapter. The bending, shear and axial response and interactions within the north A frame column are investigated and explained in further detail in *Chapter 7- Section 2*.

Axial interaction

The effect of axial load on bending strength is normally considered in the design of concrete beam column members. Effects of axial loading are frequently considered when estimating the curvature under bending and available curvature ductility, though with only uniaxial bending. It has already become obvious that the axial load, particularly the varying component from the two overturning moments, had a significant effect on the load deformation mechanism existing in the individual columns of the present test frame. A time history of the dynamic plus static axial load in the north A frame first story column is plotted in Figure 7.21. The static component, due to the dead weight of the model and the attached mass blocks was 8.93 kips (39.7 kN) in each column. Large axial forces, including axial tension were added to the static load, particularly from the east-west overturning moment because of the close column
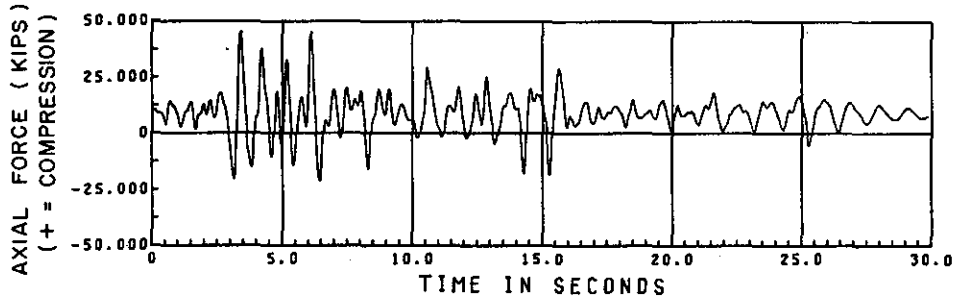
Figure 7.21 NA column axial load history.

spacing in that direction. While the unrealistically close column spacing in the present frame exaggerated effects of overturning moment in the weak axis direction, large varying axial forces and their exhibited interaction effect must be considered in design for seismic resistance.
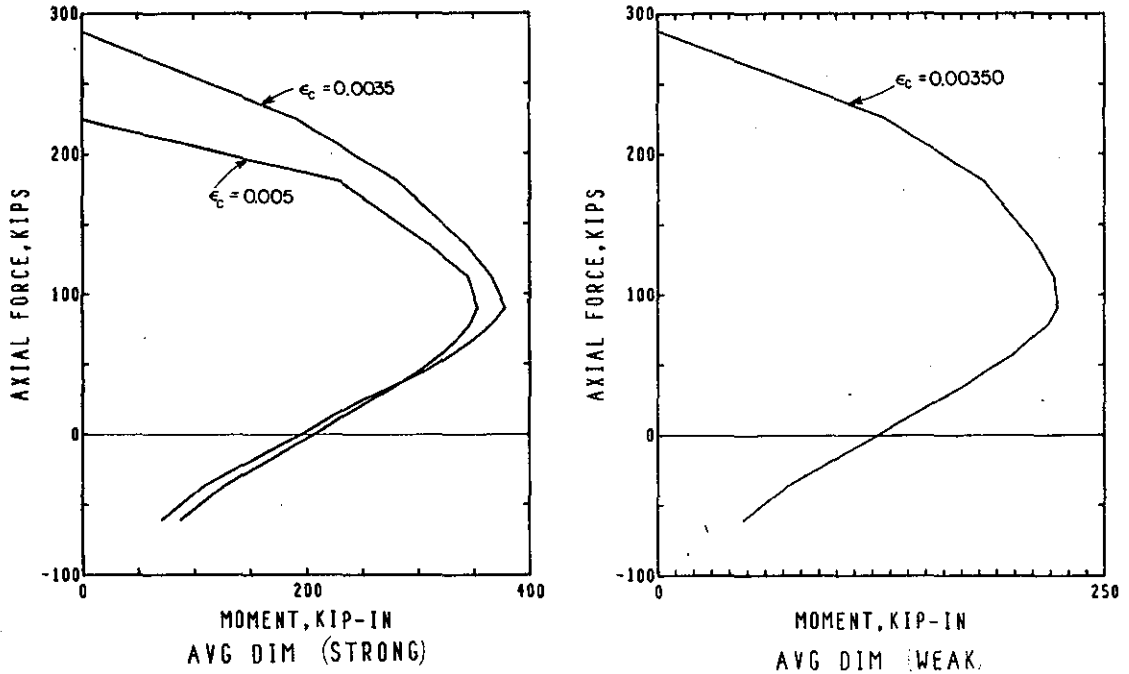
Figure 7.22 Predicted uniaxial moment- axial load interaction curves, for various maximum extreme fiber concrete strains, strong and weak axes.

Figure 7.23 3D moment vs moment vs axial load interaction surface.
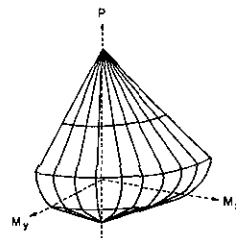
The importance of axial loading on the column's lateral response behavior is easily presented in the form of the familiar uniaxial moment- axial load interaction diagrams of Figure 7.22. The actual limit states under biaxial bending would be represented by 3-dimensional interaction surfaces for the various deformation conditions such as reproduced in Figure 7.23. Regardless of the method used to develop the 3-d surface (see *Appendix A*), the moment capacity along each of the principle axes of a rectangular section, under any specified axial load, will be a maximum when the other orthogonal moment component is zero. Thus, the uniaxial interaction diagrams of Figure 7.22 will act as conservative envelopes for the immediate capacity at any instant during the column's response history if they are compared to the two principle axis components of the biaxial bending moment.
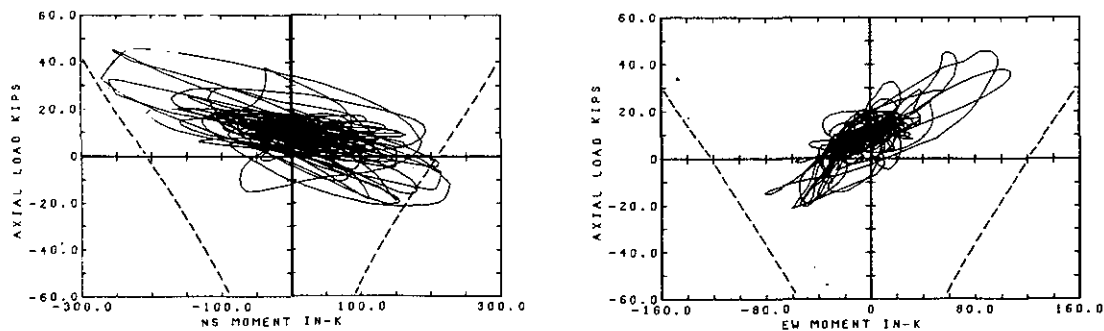
Figure 7.24 NA column simultaneous moment and axial load, left: strong axis, right: weak axis, dashed line = predicted curve for 0.005 extreme fiber strain.

A trace of the moment component and simultaneous axial load value for the two axes of the North-A frame column can be viewed in Figure 7.24. Segments of the uniaxial interaction curves as calculated in *Appendix B* and based on average column dimensions, are shown as dashed lines in Fig. 7.24. It is quite apparent that deformation limit states represented by the uniaxial N-S interaction plot were exceeded a significant number of times and the actual 3-D surface would have been crossed at least as often. The deformation existing at a maximum concrete surface strain of 0.005 would include a considerable amount of inelastic behavior including spalling and crushing of the concrete cover and yielding of the reinforcing bars with concrete cracking in the bending tensile regions.

Explanation of the super capacity seen in the excursions beyond the uniaxial interaction plots in Figure 7.24 will be left until Section 2 of this chapter where moment-axial load interaction relations will be predicted for the specific dimensions of the column where the moment and axial load exist.
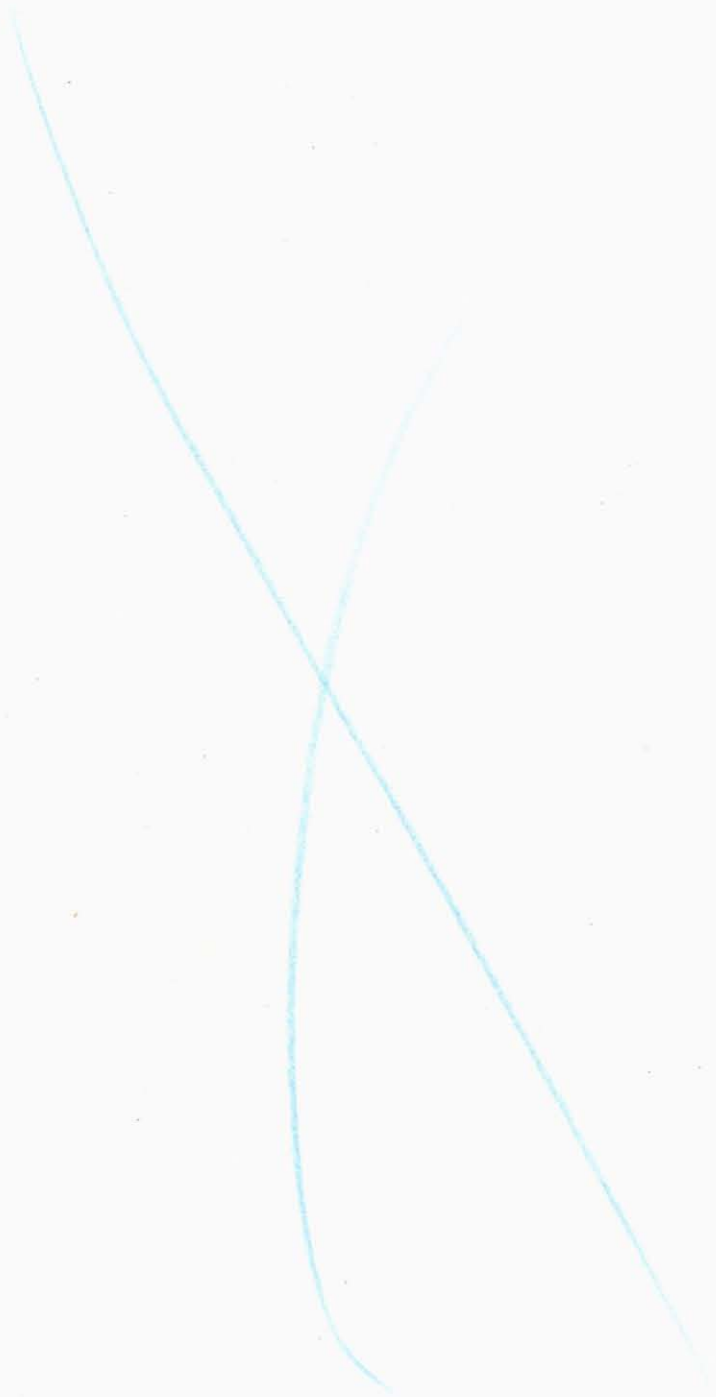
Section 2: Local Mechanics of a Specified Column

Local load deformation response and its variation during the Taft 1000 (peak ground accel. =0.685g) test should provide the detailed information necessary to understand the "irregular" behavior noticed in the previous section and to describe the predominant mechanisms involved in multiaxial response coupling. Since the instantaneous response of a member which is undergoing or has seen inelastic deformation is dependent on it's past history (i.e. cracking, spalling, residual steel strains), the local response of a specified column will be followed step by step through the earthquake shaking sequence.

Description of response characteristics

The behavior of the North A-frame first story column at its base near the footing joint (1NAB) will be investigated in this section by a close examination of:

1.) simultaneous moments acting in the north-south (strong, major) axis and the east-west (weak, minor) axis,

2.) simultaneous axial load,

3.) comparison of simultaneous axial load and moment along each axis with the predicted uniaxial moment-axial load interaction envelope,

4.) simultaneous moment-average curvature values along both axes,

5.) average corner concrete strains estimated from average column base deformation,

6.) reinforcing bar strains and estimated strain rates,

7.) reinforcing bar stress estimated from measured strains.

Items 1,2,3, and 4, simultaneous moments, moment-axial interaction and moment-average curvature, will be shown in plotted form along with a listing of values at critical points. The values for the remaining items will be listed near critical points.

Moments, axial forces and column curvature were determined at the column base as described in the previous section of this chapter. Data from the four DCDT's mounted at the bottom defined the deformed location of a plane through a column section 4 inches from the base relative to the footing, as outlined in Section 1. Average concrete corner strains were calculated from the amount of corner deformation over the 4 in gauge, as an indicator of the degree of cracking (tensile strains) and the amount of concrete providing compressive resistance at any instant.

Strains in reinforcing bars were measured at the column to footing joint. Strain rates, estimated from strain values at sequential time points, indicated whether increased strengths could be expected as a result of dynamic loading. Stress values for each of the bars were calculated from the strains using a trilinear stress-strain relation including an elastic portion, a

"Bauschinger" effect portion with 20% of elastic stiffness and a strain hardening portion as fully described in *Appendix B*.

Predicted uniaxial moment-axial load interaction plots were based on section strength analysis using the actual dimensions at the 1NAB column with reinforcing bars located as measured immediately prior to concrete placement. Confined concrete was assumed to possess a stress-strain behavior as proposed by Kent [3]; unconfined concrete was modeled after the concrete cylinder results with crushing and complete loss of strength at a strain of 0.0051. The theoretical moment-load interaction envelopes are shown for various maximum strain levels at the extreme compression fiber. Further details of the column theoretical strength modeling are to be found in *Appendix B*. Figures 7.25 and 7.26 display the moment-axial interaction envelopes and expected moment curvature behavior for the 1NAB column with uniaxial north-south moment. Figures 7.27 and 7.28 include similar results for east-west moments. Again, the predicted effect of axial load on the column moment curvature resisting mechanisms should be noted. A maximum axial compressive load of 45 kips occurred in the 1NAB column.

Time Windows

The response data was divided into discreet time "windows" for plotting purposes to allow a clear view of the plot trace without overplotting from subsequent excursions. The length of each "window" was arbitrarily defined as the time required for the moment in the north-south strong axis to change through one cycle, from maximum positive value to the next following positive peak value.

Figure 7.25 Strong axis uniaxial moment-axial load interaction, NA column.
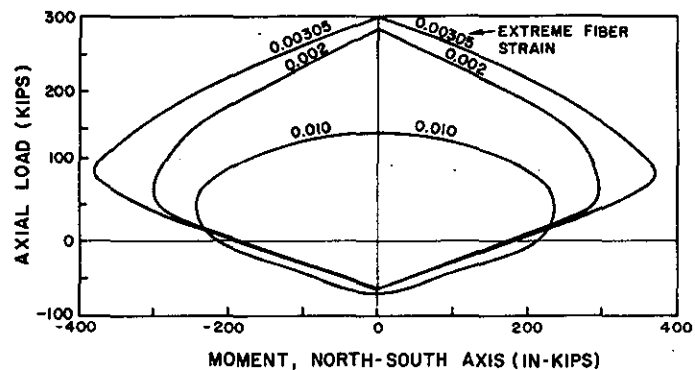
Figure 7.26 Strong axis uniaxial moment curvature and axial load, NA column.
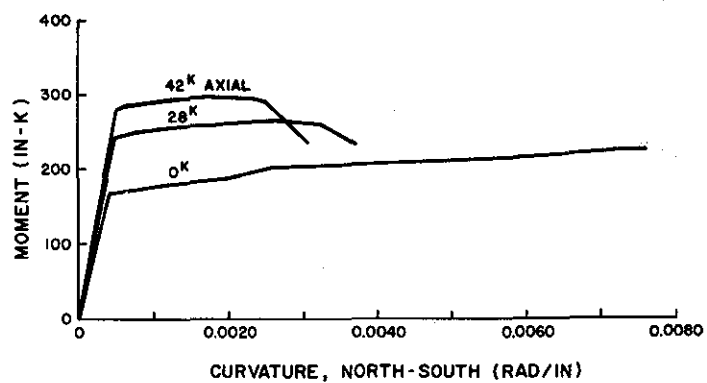
Figure 7.27 Weak axis uniaxial moment-axial load interaction, NA column.
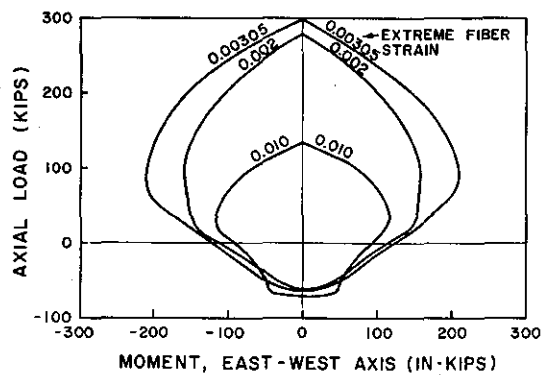
Figure 7.28 Weak axis uniaxial moment-curvature and axial load, NA column.
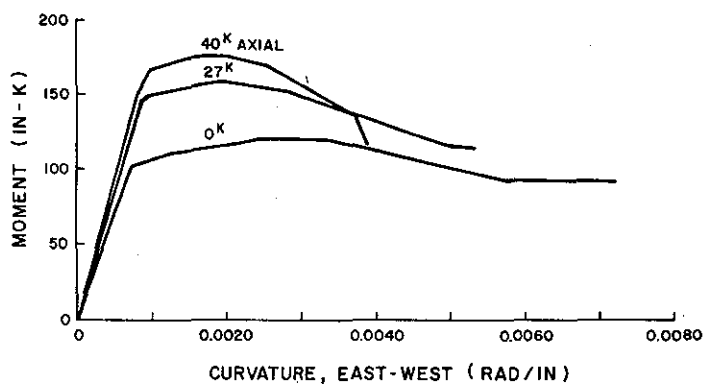
Column 1NAB local behavior

Window 1, time 0.0 to 3.14 seconds, Figures 7.29-7.32

The column responds elastically until the first major displacement excursion in the southeast direction between 2.95 and 3.14 seconds. At 3.104 seconds strain data indicates the northeast bar initiates yielding and remains in yield condition to 3.143 seconds. The other bars remain elastic throughout with only the southeast bar showing compressive stress. The calculated average concrete compressive strain value of 0.0044 in the southeast corner occurs simultaneous with a crossing of the 0.002 maximum strain envelope on the uniaxial moment axial load interaction plot. At the same instant the other column corners are under tensile strains indicating definite concrete cracking across most of the north column face. Though bar yielding and possibly some concrete compressive crushing occur in one corner there is very little evidence of significant non-linear behavior in the moment-curvature plots for either the strong north-south axis or the weak east-west axis. The change in stiffness is representative of deterioration from gross section to cracked section stiffness, though the actual cracked section has a skewed neutral axis as obvious in the strain data below.

units:	loads = in-k,kips	+ = tensile
	stress = ksi	- = compression
	strain (x 0.001)	
moment N-S, + = comp. south		
moment E-W, + = comp. west		

Internal Forces

time	M_{NS}	M_{EW}	Axial
3.143	153	-52	20

	reference corner			
time	NW	NE	SW	SE
steel stress				
3.143	50.0	42.1	17.6	-4.2
conc strain				
3.143	8.62	3.99	0.69	-4.38

Key to time	key:	A
pts. on plots	time:	3.143
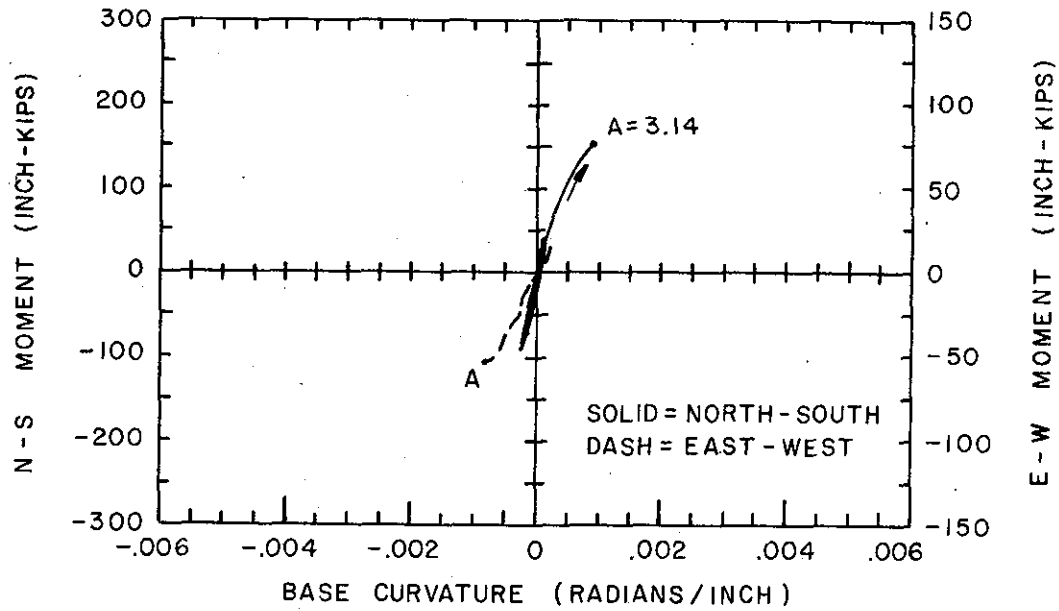
Figure 7.29 Column moment vs curvature, NS (strong) and EW (weak) axes.
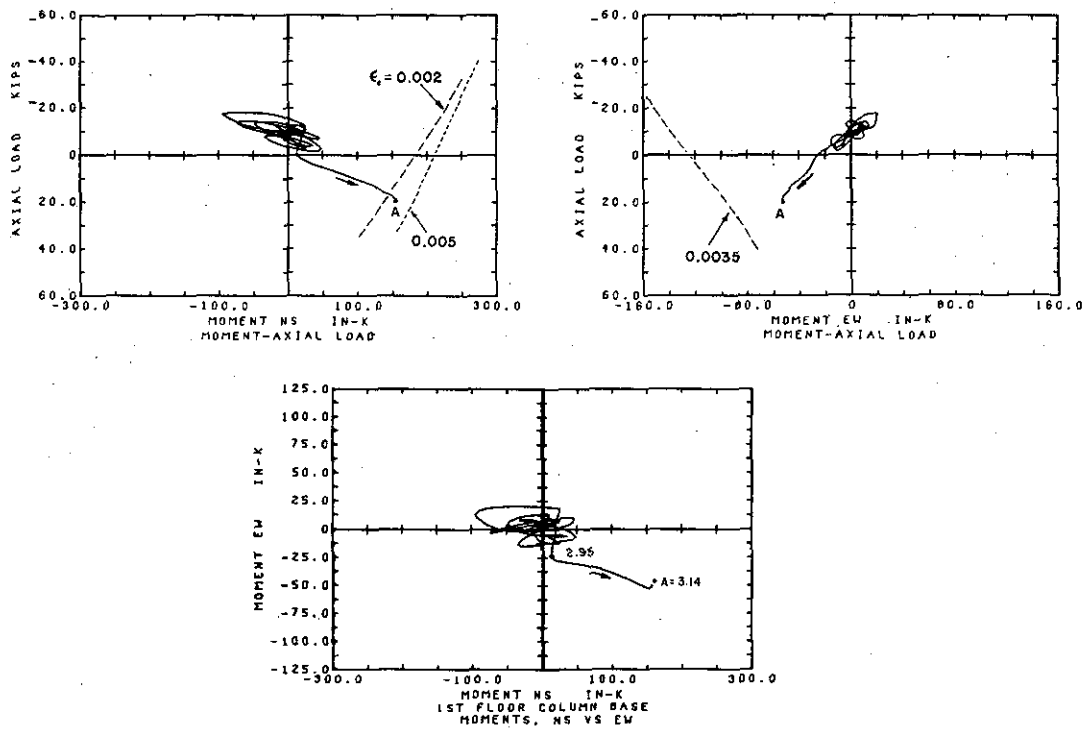
Figures 7.30 - 7.32 clockwise from top - left: moment NS-axial, moment EW- axial, moment NS-moment EW.

Window 2, time 3.16 to 3.61 seconds, Figures 7.33-7.36

At 3.24 seconds (point A) a sudden softening occurs in the east-west bending stiffness visible as a small step on the E-W moment curvature plot. The moment in the north-south direction is simultaneously changing sign from positive with south compression to negative and north compression causing a changed effective section and neutral axis orientation. As the column N-S moment increases, the NW corner also closes with only small additional strain in the already closed NE corner, causing an apparent west(+) rotation. With the full north face closed the column stiffness resumes its previous appearance.

At 3.37 seconds (C), another small decrease in the bending stiffness is apparent. The increasing west moment again causes the NE corner to open simultaneous with yielding of both the south side bars due to the high N-S moment resulting in a revised effective cross section and section stiffness.

During the same time period (3.34 to 3.40 seconds) the north-south moment reached a negative peak coincident with a very large axial force due to combined overturning moments along the two structural axes. The two south bars, in tension, begin to yield at 3.33 seconds and the N-S bending stiffness would ordinarily be expected to decrease. However, as obvious in the N-S moment-curvature plot, the stiffness actually becomes negative with continued curvature under a decreasing moment. Referring to the moment-axial load plots and the effect of axial load as seen in Figure 7.26 it is obvious that an effective decrease in column strength is possible. With the increasing axial load near -40 kips and curvature ranging from 0.001 rad/inch at 3.34 to 0.002 rad/inch at 3.37 it is apparent that significant concrete crushing should be occurring, especially in the NW corner where the biaxial moments compound the compressive strain. The curvature is nearing the point where compressive bar yielding could severely decrease the column strength (Fig.7.26). The measured average concrete compressive strain of -0.0101 at 3.42 seconds and associated compressive failure verifies a loss of strength due to combined tensile yielding and concrete crushing with "cover" strength loss.

Finally, from 3.46 to 3.51 seconds (E to F), the EW bending shows an effective negative stiffness. No bars are yielding at this point. The moment in the NS direction changes sign at 3.48 seconds. A decreasing north moment leaves the full column section with an open crack while loads are carried on the reinforcing bars which have residual elongations from previous yielding. Until the SW corner starts closing and carrying compression in the concrete at 3.50 seconds the section rotates in the east west direction.

Internal Forces			
time	M_{NS}	M_{EW}	Axial
3.24	-4.7	-28	+2
3.34	-271	39	-33
3.37	-250	72	-41
3.40	-234	84	-46
3.46	-85	98	-40
3.51	95	84	-26

	reference corner			
time	NW	NE	SW	SE
steel stress				
3.38	-19.3	23.8	52y	52.4y
conc strain				
3.42	-10.1	3.12	6.2	19.9
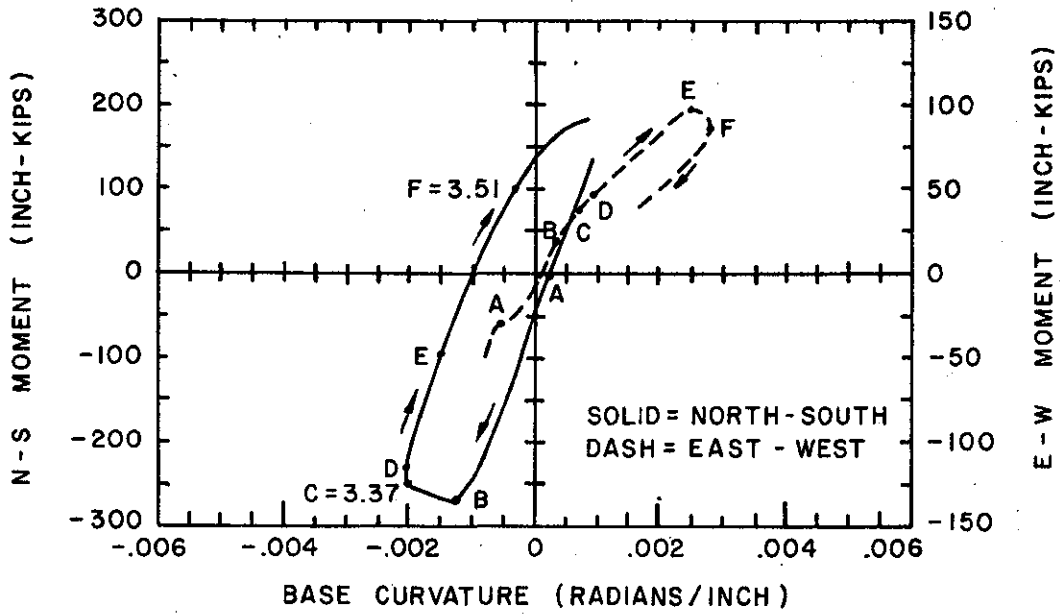
Figure 7.33   Column moment vs curvature, NS (strong) and EW (weak) axes.

Key to time	key:	A	B	C	D	E	F
pts. on plots	time:	3.24	3.34	3.37	3.40	3.46	3.51
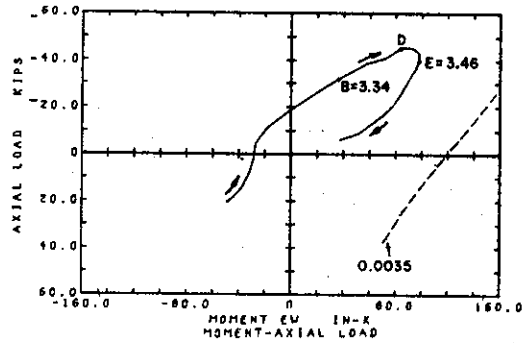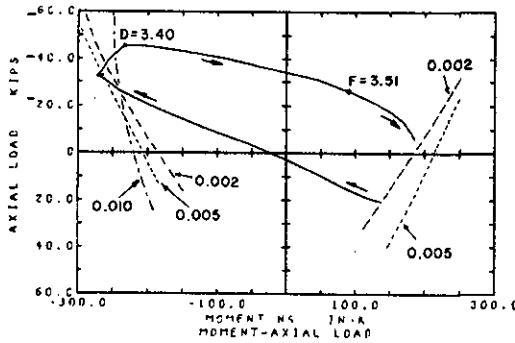
units:	loads=in-k,kips	+=tensile
	stress=ksi	-=compression
	strain (x 0.001)	
moment N-S, +=comp. south		
moment E-W, +=comp. west		
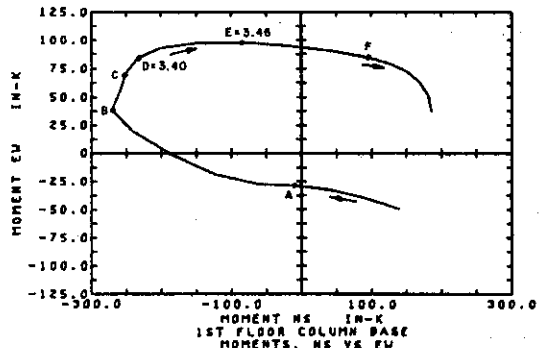
Figures 7.34-7.36   clockwise from top - left: moment NS-axial, moment EW- axial, moment NS-moment EW.

Window 2, Figures 7.37-7.40,

Plots of curvature vs curvature, displacement vs displacement, shear vs shear and shear vs displacement are shown for the same time section as the previous window plots. In general, the shape of the shear NS vs shear EW and the corresponding moment vs moment plots are nearly identical- as expected considering the close relation between column shear and moment. Comparing the column top displacement with the column base curvature plot, a significant similarity is apparent. Considering the close match between shear and moment response and the match between displacement and curvature deformation, the shear displacement plots tend to be similar in characteristics to the moment-curvature plots though the shear-displacement plots have the sharp corners smoothed since the displacement results from cumulative deformation over the height of the column.

There is very little useful additional information within Figures 7.37 - 7.40 that is not presented already in the previous plots, Figures 7.33-7.36. For the remaining time windows only plots of the first type will be shown, ie- moment vs moment, moment-axial and moment vs curvature.
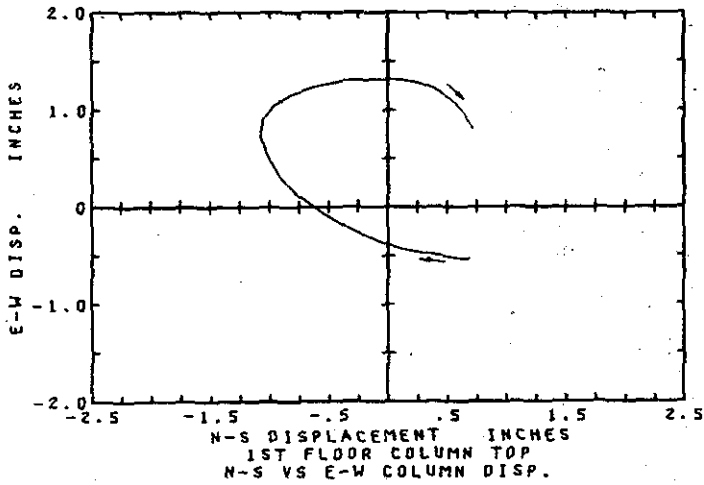
Figure 7.37 Column displacement, EW vs NS
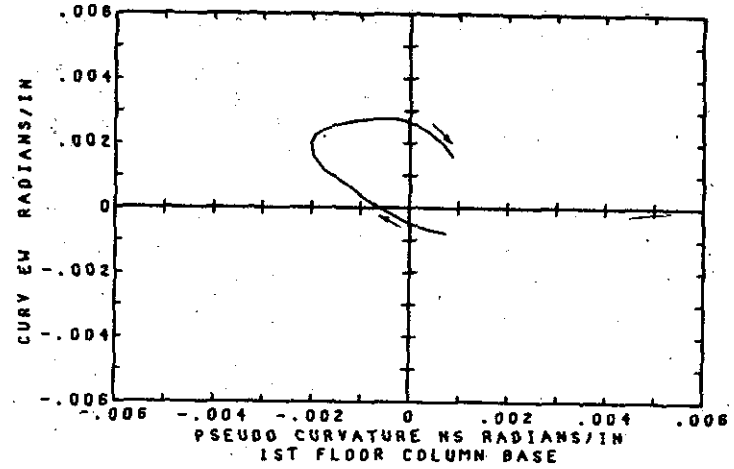
Figure 7.38 Column curvature, EW vs NS.
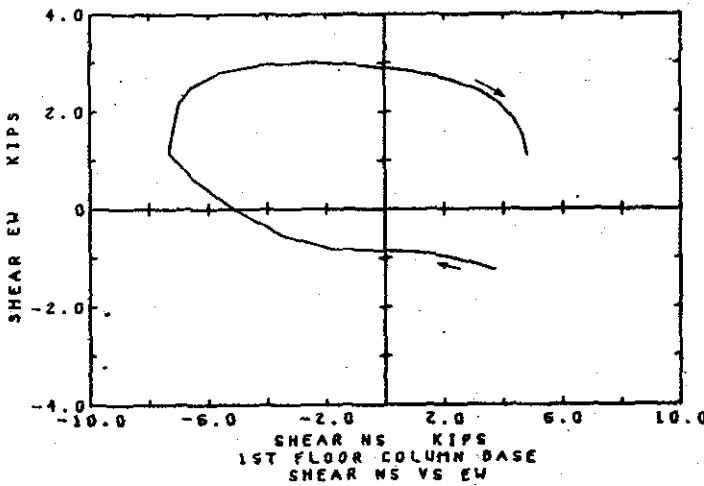
Figure 7.39 Column shear, EW vs NS.
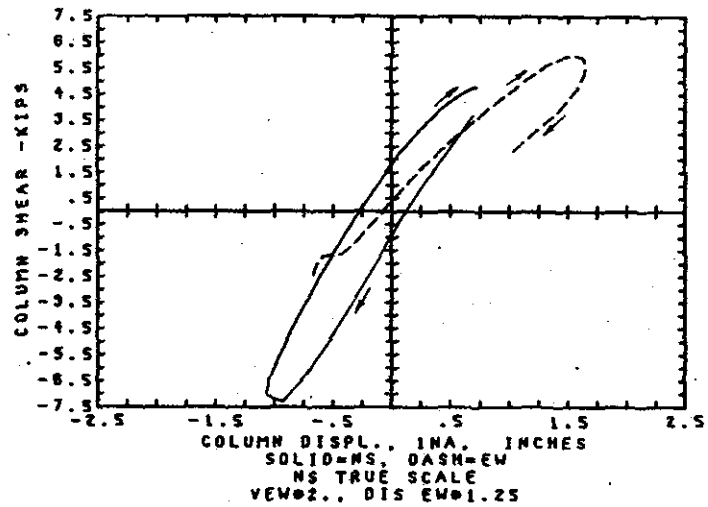
Figure 7.40 Column shear vs displacement.

Window 3, time 3.63 to 4.08 seconds, Figures 7.41-7.44,

In the previous window it became apparent that strong axis motion had a significant influence on the weak axis motion- particularly when strong axis unloading followed an inelastic deformation. This is conceivably due to non uniform yield deformation in the reinforcing bars under combined loading and residual strains with column concrete section being cracked open. Since the "arm" between the reinforcing bars in the east-west direction is only 2.4 inches, while the arm in the north-south direction is 5.1 inches, the east-west direction has considerably less stiffness and will undergo twice the curvature for a given bar strain than the north-south direction will show when the concrete section is cracked open and resistance is dependent on the bars alone without compressive concrete.

In the present window the north-south moment changes from positive to negative at 3.76 seconds after a small elastic peak positive moment. In this case there seems to be none of the rocking or rotation in the east-west direction as had been seen in the previous window. In fact, at 3.76 seconds (A), and slightly before and after, both the NE and SE corners should be closed based on the deformation data, with the concrete in compression under the east-west moment, and no sudden east-west rotation should be expected.

By 3.81 seconds the east-west moment has reached a peak value with a simultaneous peak axial tension (due to EW overturning) causing inelastic tensile deformation in the NW and SW bars.

As the EW moment and NS moment decrease from maximum negative peaks, a point is reached at 3.96 seconds (C), where both the north-south and east-west moments are changing sign or directions. With the decreasing moment the only remaining closed corner at the northeast, re-opens, leaving an open fully cracked section. A decrease in stiffness is again apparent in the east-west moment vs. curvature plot. At 4.06 seconds (D), the SW corner closes under compression from the new bending moments and an increasing stiffness may be seen on the EW moment-curvature plot.

units:	loads = in-k,kips	+ = tensile
	stress = ksi	- = compression
	strain (x 0.001)	
moment N-S, + = comp. south		
moment E-W, + = comp. west		

Internal Forces

time	M_{NS}	M_{EW}	Axial
3.76	-5.8	-70	12.3
3.81	-45.	-84.	14.8

Key to time	key:	A	B	C	D
pts. on plots	time:	3.76	3.81	3.96	4.06
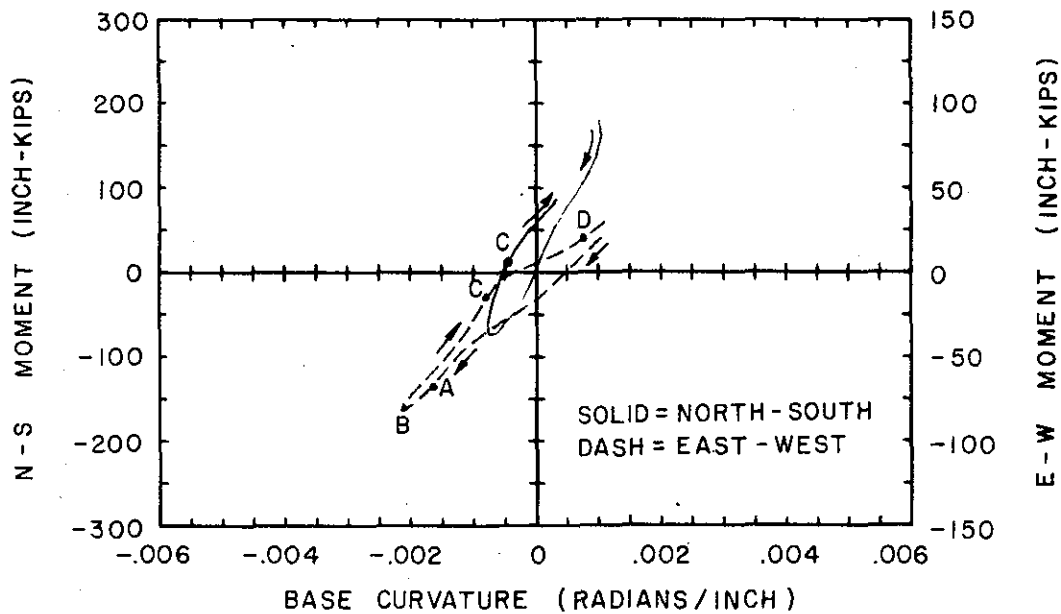
Figure 7.41 Column moment vs curvature, NS (strong) and EW (weak) axes.
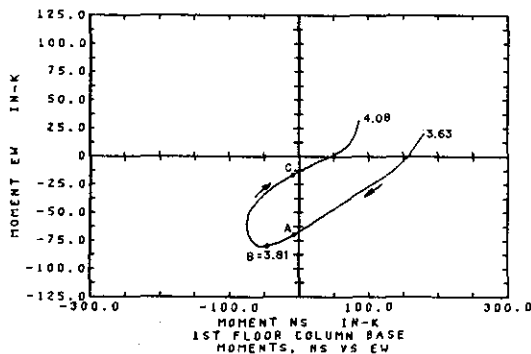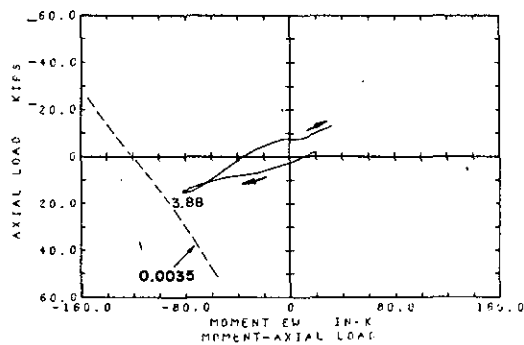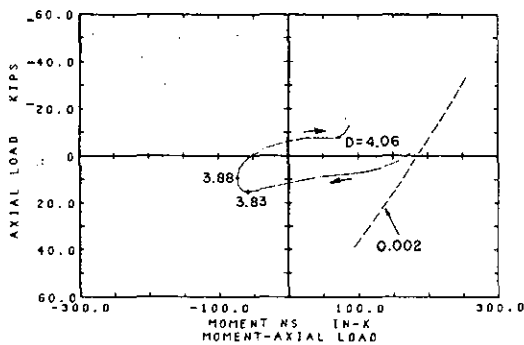
Figures 7.42-7.44   clockwise from top - left: moment NS-axial, moment EW- axial, moment NS-moment EW.

Window 4, time 4.10 to 4.57 seconds, Figures 7.45-7.48,

A single unusual feature of note during this period occurs in the east-west moment vs curvature plot at approximately 4.45 seconds (B). Once again there is an abnormal change in the bending stiffness. This variation follows a positive peak of the EW moment at 4.18 seconds. At 4.47 seconds (C) the NS moment changes from negative to positive. With the decrease in the NS moment, a concurrent low M_{EW} and axial force below the dead load level at 4.45 seconds, the previously closed NW corner opens and the stiffness becomes that of a fully cracked beam with rebars resisting bending. By 4.55 seconds (D), the SE corner has closed in compression and the section stiffness has increased.

units:	loads = in-k,kips	+ = tensile
	stress = ksi	- = compression
	strain (x 0.001)	
moment N-S, + = comp. south		
moment E-W, + = comp. west		

Internal Forces

time	M_{NS}	M_{EW}	Axial
4.18	-15	108	-34.8
4.45	-23	-17	-7.8
4.55	79	-35	7.1

Key to time	key:	A	B	C	D
pts. on plots	time:	4.18	4.45	4.47	4.55
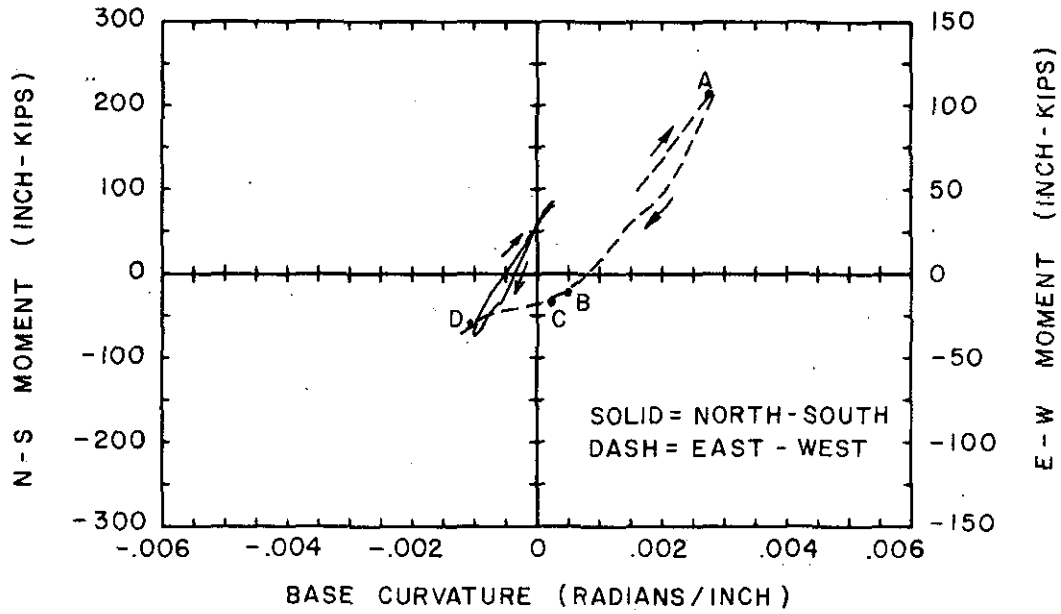
Figure 7.45 Column moment vs curvature, NS (strong) and EW (weak) axes.
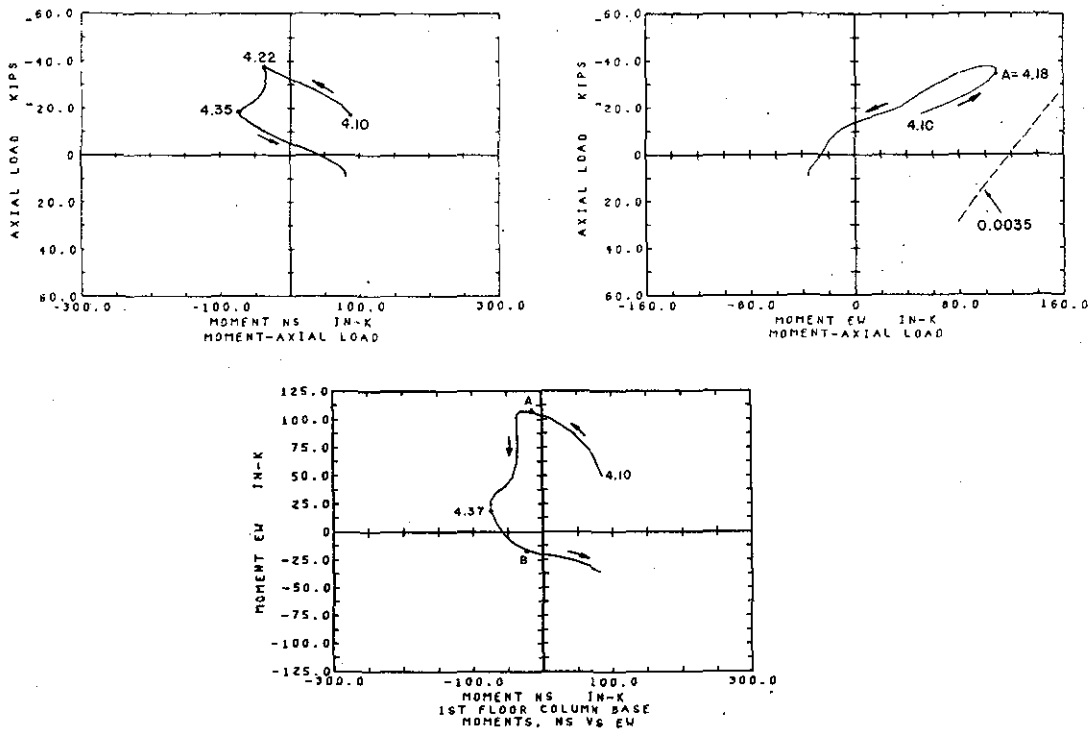
Figures 7.46-7.48   clockwise from top - left: moment NS-axial, moment EW- axial, moment NS-moment EW.

Window 4a, time 4.41 to 4.82 seconds, Figure 7.49

This special interval, which overlaps windows four and five, allows a clear study of the behavior of the column bending mechanism in the east-west (weak) direction, particularly between 4.62 and 4.67 seconds. At the end of window 4, time equals 4.57 seconds (B), the moment in the east-west direction has reached a negative peak value. The next window shows an unloading from that peak for a very short interval, until 4.62 seconds (C) with both M_{EW} and the east-west curvature decreasing. However, shortly after 4.63 seconds M_{EW} begins increasing again while the curvature continues to decrease. If one assumes that the global displacements of this column are principally defined by the motion of the frame as a whole, due to frame inertial effects and the summed restoring forces provided by all the columns, then the local curvature deformation is essentially being dictated by the frame and the local restoring force (moment) is the result of the instantaneous column stiffness.

The experimental data indicates that all of the rebars should be within the purely linear stress-strain range during this period (4.55-4.70 seconds) with no Bauschinger degrading or yielding. Predicted concrete compressive strains are quite low and certainly far from a level (crushing) which might cause non-linear column bending response. In terms of normal individual material behavior the column stiffness would be expected to show a linear response. Once again the effects of residual deformations in the bars and concrete cracking in the composite beam-column seem to affect the behavior at low load levels, particularly in the weak east-west direction.

Measured data, listed in the accompanying table, shows both low moment and axial (below dead load level) load during the interval of unusual response, 4.62 to 4.67 seconds, including reversal of M_{NS}. During this period the southwest rebar changes from compressive to tensile stresses, the NE corner concrete closes in compression (4.62 sec.) and the SE corner concrete cracks open at 4.64 seconds. Under a decreasing south moment the column is now rotating towards the north. After the NE corner closes, the section gains an asymmetrical stiffness about the east-west axis and the north rotation tends to create a rocking in the west direction as well. Since overall column deformation is governed by movement of the frame as a whole, an internal column moment ($-M_{EW}$) must develop to constrain the natural rocking effect.

Internal Forces

time	M_{NS}	M_{EW}	Axial
4.55	79	-35	7.1
4.57	81	-36	9.5
4.59	72	-33	10.7
4.61	56	-29	10.1
4.63	37	-29	8.8
4.64	16	-33	6.0
4.66	-7	-36	2.5
4.68	-29	-36	-1.0
4.70	-47	-34	-4.4

	reference corner			
time	NW	NE	SW	SE
steel stress				
4.59	26.	6.	-1.	-31.
4.61	22.	3.	0.	-28.
4.63	18.	0.	3.	-24.
4.64	14.	-3.	7.	-19.
4.66	10.	-6.	12.	-13.
conc strain				
4.61	7.00	0.12	5.81	-1.10
4.63	6.25	-0.45	6.17	-0.53
4.64	5.43	-1.06	6.63	0.18
4.66	4.61	-1.55	7.13	1.03
4.68	3.52	-1.82	7.43	2.20
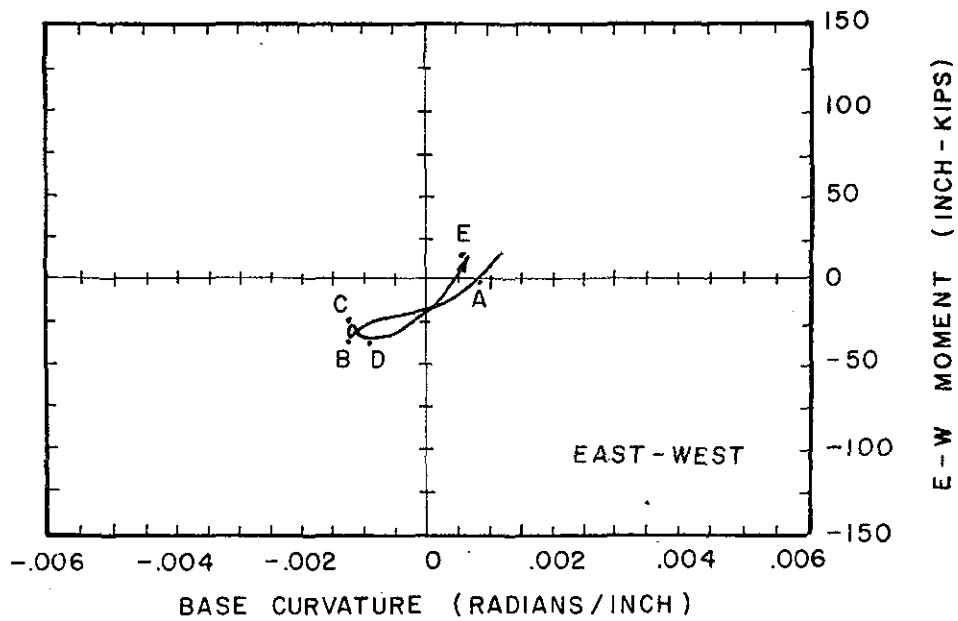
Figure 7.49   Column moment vs curvature, EW (weak) axes.

Key to time	key:	A	B	C	D	E
pts. on plot	time:	4.41	4.57	4.62	4.66	4.82

units:	loads=in-k,kips	+=tensile
	stress=ksi	-=compression
	strain (x 0.001)	
moment N-S, +=comp. south		
moment E-W, +=comp. west		

Window 5, time 4.59 to 4.96 seconds, Figures 7.50 to 7.53

By the start of this period the column has already been subjected to a fair amount of inelastic deformation. The reinforcing bars had residual tensile strains of 0.0005 in the NW corner, 0.0008 at the NE corner, 0.0023 at the SE and 0.0032 in the SW corner. Calculated compressive strains in the concrete have reached peak values of 0.010 at NW, 0.004 at NE, 0.004 at SE, and 0.005 at SW with all of the corners having had nominal tensile strains greater than 0.008 indicating full cracking.

The initial irregularity in the EW moment-curvature plot (4.64 secs.) has been described in the previous section. A second similar motion occurs between 4.85 and 4.94 seconds (B and D) in the east-west response. Again, an increasing M_{EW} occurs with a decreasing curvature in the east-west direction. The rapidly increasing north-south moment causes the SW corner to close first in compression (the SW bar was under high compressive strain) causing a rocking effect which decreases the west curvature and forces development of an increased west moment since the column is constrained to follow deformations of the entire frame.

units:	loads=in-k,kips	+ =tensile
	stress=ksi	- =compression
	strain (x 0.001)	
moment N-S, + =comp. south		
moment E-W, + =comp. west		

Internal Forces

time	M_{NS}	M_{EW}	Axial
4.85	64	17	-13
4.90	166	23	-4
4.94	211	18	3

	reference corner			
time	NW	NE	SW	SE
steel stress				
4.86	4.	11.	-37.	-25.
4.90	30.	37.	-38b	-36b
conc strain				
4.86	0.33	6.47	-1.86	4.21
4.90	5.20	9.60	-2.89	1.27
4.94	8.61	11.3	-2.97	-0.58

Key to time	key:	A	B	C	D
pts. on plots	time:	4.64	4.86	4.90	4.94
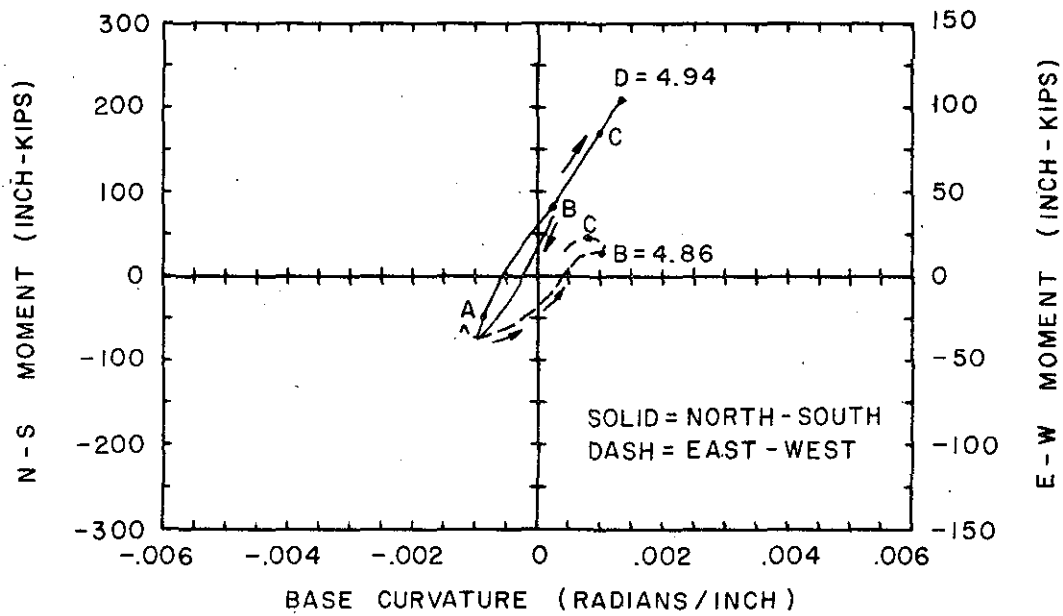
Figure 7.50   Column moment vs curvature, NS (strong) and EW (weak) axes.
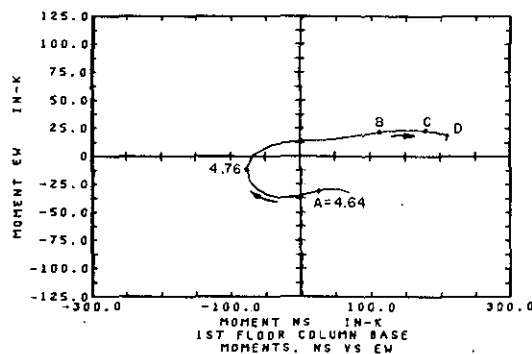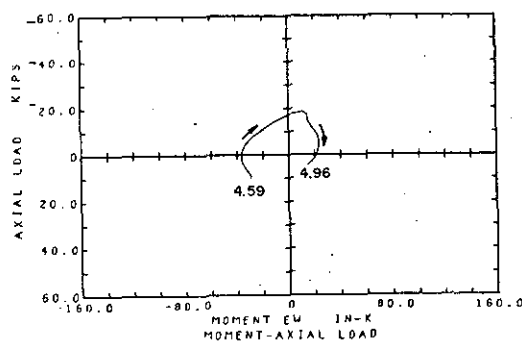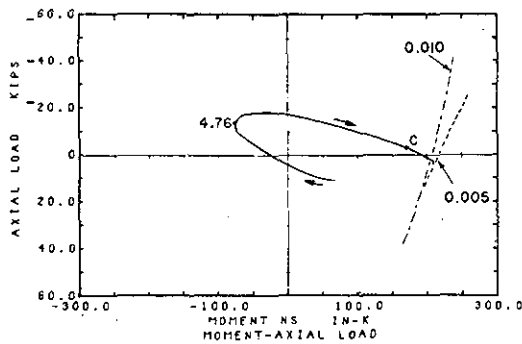
Figures 7.51-7.53   clockwise from top - left: moment NS-axial, moment EW- axial, moment NS-moment EW.

Window 6, time 4.98 to 5.39 seconds, Figures 7.54-7.57

The second large moment in the north-south direction reaches its peak at 5.16 seconds and tends to be the dominant feature at first inspection of the response plots. However, again one can detect an unusual motion in the east-west direction between 5.05 and 5.09 seconds (A to B) under a very small M_{EW}. As in previous cases this motion occurred as the strong axis-moment changed sign and increased from -1.7 in-kips at 5.05 secs to -168 in-kips at 5.09 secs. The changed moment was accompanied by rapid straining of the compressive rebars until the previously open compression face crack closed. In addition, the new tensile rebars (in the south face) changed from compressive to tensile stress at 5.06 seconds. The reversal of stress may cause a finite amount of slip between the bars and concrete until the bars reseat themselves, since the high bar strains which have occurred prior to this interval (-0.00626 at SW) undoubtedly caused some crushing of concrete adjoining the bar.

Also, since both M_{NS} and M_{EW} are nearly zero at 5.05 seconds, the deformation data are essentially indicators of residual column curvature and strain following previous inelastic motions. Column curvature at 5.05 was -0.00313 NS and 0.00374 EW radians per inch.

By 5.11 seconds (C), the north-south moment vs. curvature plot starts to show a typical rounding associated with the initiation of column yielding. Since the residual strains in the NW and NE bars were quite low (see data at 5.05 seconds) the north face concrete starts carrying a large portion of the compression force before the two north bars can reach their yield point. In fact, at 5.13 seconds (D), the uniaxial NS moment-axial load plot reaches the limiting interaction curve for maximum north face compressive strain of -0.005. The actual column concrete strains reached are -0.0071 in the NW corner and -0.0013 at the NE corner. Between 5.13 and 5.17 the axial load, M_{NS} and M_{EW} all increase slightly with the M_{NS} axial load plot seemingly moving parallel to the ϵ_c =-0.005 uniaxial interaction curve. A small underestimate of the steel yielding point in the SW and SE bars (at 5.11 and 5.13 seconds respectively) may exist since strain rates in those bars reach nearly 20% per second, ie "dynamic straining".

After unloading from the high north moment, the north-south bending stiffness shows a distinct decrease at 5.29 seconds. At this point, the stress in the NE bar reverses from compression to tension and both the SE and SW bars reach the "Bauschinger" range, near compressive yield, where stiffness decreases. By the next time step, both bars have started compressive yielding.

At 5.37 the two north face tensile bars enter the Bauschinger level as well, with yielding occurring by the next time step and the north-south moment curvature plot showing a yield effect. The slope or stiffness in the north-south direction is negative. Considering the north-south moment vs axial load plot, the column loads have crossed the uniaxial interaction plots at concrete strain levels of -0.002, -0.005 and -0.010. Measured data indicate a maximum strain of -0.0034, above crushing level in the SE corner. The apparent negative stiffness is the result of concrete crushing and reduced moment capacity (while axial load is increasing). Since the predicted interaction curves were calculated using a statically obtained steel stress-strain relation, an underestimate of the column strength would occur if the actual loading were at a speed

causing fast dynamic strain rates. Under rapid straining the apparent steel yield strain is higher than under statically applied loading. Between 5.37 and 5.39 seconds the strain rate in the NE and NW bars was greater than 22% per second.

Internal Forces

time	M_{NS}	M_{EW}	Axial
5.05	-2	1	-10
5.09	-168	-2	-18
5.11	-223	-1	-24
5.13	-249	4	-26
5.17	-260	16	-32
5.37	215	1	7
5.39	211	-9	11

	reference corner			
time	NW	NE	SW	SE
steel stress				
5.05	-22.	-23.	-6.1	-8.7
5.13	-30.	-16.	56.y	55.y
5.29	-12.	-2.3	-33.b	-32.b
5.37	41.b	49.b	-44.	-46.y
steel strain				
5.05	0.165	0.497	2.58	4.31
conc strain				
5.05	-0.55	1.64	2.07	4.35
5.13	-7.12	-1.33	1.35	1.99
5.17	-9.17	-1.52	1.87	2.71
5.37	13.4	12.1	-0.40	-2.12
5.39	18.9	16.2	-0.15	-3.43

units:	loads=in-k,kips	+=tensile
	stress=ksi	-=compression
	strain (x 0.001)	
moment N-S, +=comp. south		
moment E-W, +=comp. west		

Key to time	key:	A	B	C	D	E	F	G	H
pts. on plots	time:	5.05	5.09	5.11	5.13	5.17	5.29	5.37	5.39
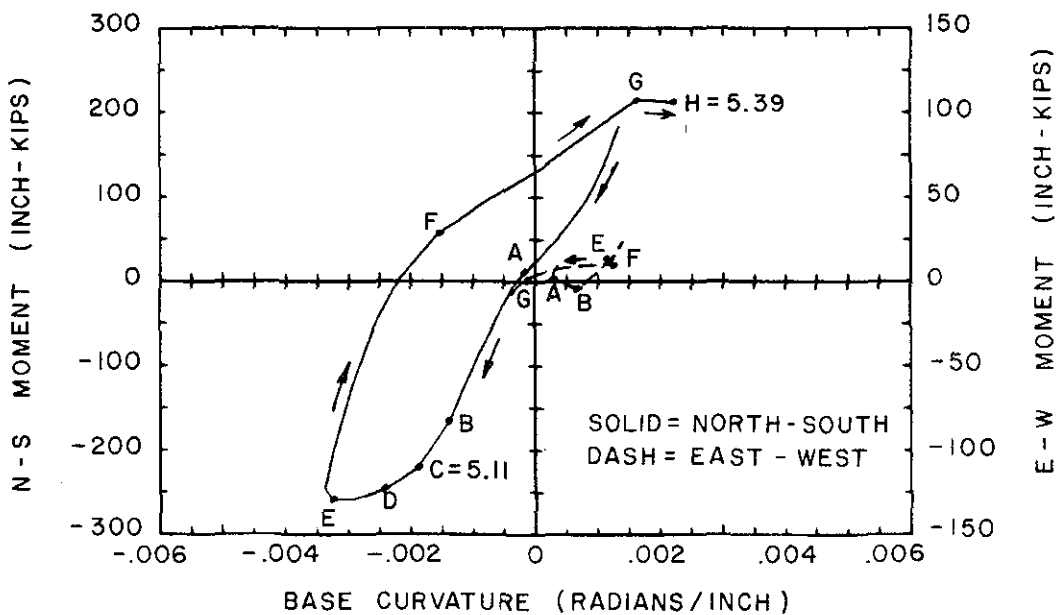
Figure 7.54 Column moment vs curvature, NS (strong) and EW (weak) axes.
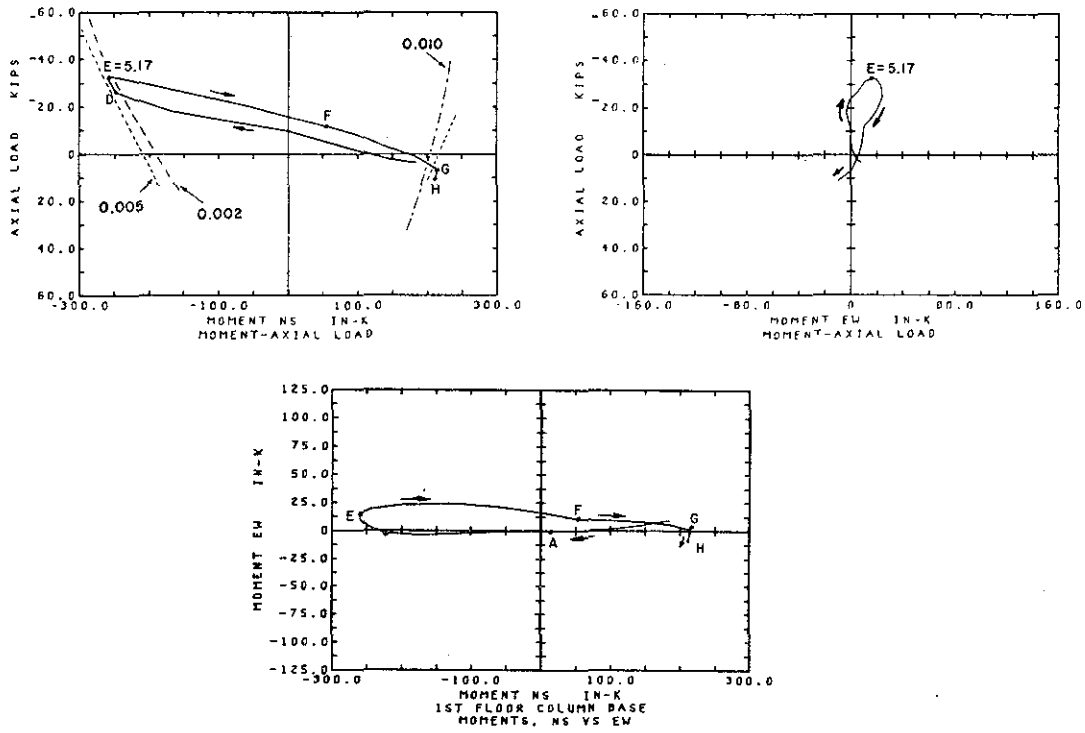
Figures 7.55-7.57 clockwise from top - left: moment NS-axial, moment EW- axial, moment NS-moment EW.

Window 8, 5.93 to 6.38 seconds, Figures 7.58-7.61

The response behavior during this period re-emphasizes most of the multi-axial interaction effects and inelastic yielding seen in the previous windows. Looking at the east-west moment vs curvature plot, the window starts with a phase of very low stiffness between 5.93 and 5.99 seconds (A to B). At the start of this phase (5.93 seconds) the column is under a low axial load with high residual elongations in the rebars. The entire concrete section has been cracked. With the medium size south moment (119 in-k) and small M_{EW} the SW bar was yielding in compression and the SE bar is near compressive yield. By 5.99 seconds, M_{NS} has reduced to zero and the NW corner concrete has closed the previous open crack under an increased axial compression with the small west moment. The SW bar was under elastic compression while the SE bar reversed the previous near yield compression to tensile stress. The steady M_{EW} with continuing west rotation was a result of the large change in strain of the yielding NW bar under the increasing axial compression and decreasing south moment.

After the NW corner concrete closes and begins carrying compressive stress at 5.99 seconds (B), the effective section stiffness increases and becomes unsymmetric. The increasing north moment after 5.99 tends to cause a coupled north and east rotation of the unsymmetric effective section. Since the actual deformation is constrained by the entire frame an additional west moment has formed to prevent the easterly rotation which would occur in an unrestrained beam with unsymmetric section under increasing moment and deformation along one axis. Thus between 5.99 and 6.05 seconds (C), the east-west motion shows a sudden stiffening effect due to the actual increased stiffness of the column and the increase in west moment required to restrain the section deformation.

Looking now at the behavior in the north-south direction, the column shows a change in stiffness signifying "yielding" under north moment at 6.05 seconds. At that point the NW bar has a low Bauschinger stiffness and is near compressive yielding; the SE bar has just started yielding in tension and the SW bar is near tension yielding. At 6.05 seconds only the NW corner concrete is closed and carrying compressive stress with a strain of -0.0102.

The yielding reduces the stiffness in the east-west direction as seen in the plot interval between 6.05 and 6.07 seconds (C to D) crushing occurs in the NW corner with its strain reaching -0.0124 (previous max was -0.0101 in window 2 at 3.42 seconds). Between 6.03 and 6.11 seconds the stress in the SW bar increases 53 ksi while the SE bar, which is yielding through most of the interval increases 13 ksi. The differences in the stress increases of the two bars, which elongate with nearly identical change in strains, causes an effective moment in the east direction. The combined result of loss of strength due to inelastic deformation and creation of an effective east moment allow the continued curvature under decreasing west moment seen between 6.07 and 6.11 seconds in the east-west moment vs curvature plot.

The north moment reaches a peak value of -255 in-k at 6.11 seconds simultaneous with a peak axial compression of 45.4 kips. The two load values appear in the M_{NS}- axial load plot just across the predicted uniaxial interaction strength curve based on a maximum compression strain of -0.010. The M_{EW} axial load plot shows fairly large forces along the column's weak

axis at the same instant the peak north moment exists. The biaxial moment-axial load interaction surface predicted for a -0.010 compressive strain would certainly have been crossed as well. Calculated concrete strain based on curvature data at 6.11 seconds was -0.0153 in the NW corner. Unlike the previous cases, where the predicted interaction surface was passed, in this case the strain rates, 8.8% per second in tensile steel and 11.3% per second in compression concrete, do not fully explain the measured overstrength.

With a reversal in the north-south moment at approximately 6.25 seconds (F), once again a definite change in the north-south bending stiffness is apparent in the moment-curvature plot. At that point the two south rebars, both having just previously yielded in tension with residual elongation are reaching a state of compression yield while the concrete at the south face is still with open cracks and the northwest is the sole corner with concrete compressive strain.

Between the time when the compression bars start yielding (6.25) and 6.33 seconds (G) the east-west moment vs curvature plot once again has a plateau of "zero stiffness" where the west curvature is decreasing with no change in M_{EW}. During this entire period the column, at its base, essentially stands on the four reinforcing bars alone; since previous inelastic cycles have elongated the bars and completely cracked the concrete. The stiffness in the east-west direction becomes very small because of the short distance between the east and west moment resisting bars.

At 6.34 seconds (H), the concrete in the SE corner closes causing development of an unsymmetric stiffness which in turn forces formation of an east moment since east-west deformation is constrained to follow the deformation of the frame as a whole. The stiffening and developed moment are both evident in the sudden slope change of the east-west curvature plot.

As mentioned, the SE corner closes at 6.34, the same instant the two north rebars start yielding with tension stress, again decreasing the M_{NS} curvature slope. By 6.38 the SE corner concrete has reached a higher compressive strain than measured previously, -0.0073, indicating concrete crushing, and producing the slight negative slope due to loss of strength with increasing deformation. As the crushing occurs between 6.36 and 6.38 seconds, the plot of M_{NS} vs axial load again moves parallel to the predicted interaction curve. Tensile steel strain rates between 6.32 and 6.38 seconds average 12% per second; not high enough to justify the strength increase beyond the predicted interaction curve.

Internal Forces			
time	M_{NS}	M_{EW}	Axial
5.93	119	17	-6
5.99	2	25	-16
6.11	-255	59	-45
6.25	48	14	-14
6.33	195	8	5
6.34	211	4	7
6.38	223	-36	16

	reference corner			
time	NW	NE	SW	SE
steel stress				
5.93	6.2	38.	-44.y	-31.
5.99	-29.	3.2	-25.	1.4
6.05	-47.b	-15.	35.	56.y
6.11	-49.y	-17.	58.y	58.y
6.25	-10.	1.0	-33.b	-25.
6.34	53.	58.	-36.	-46.y
6.38	55.	61.	7.7	-31.
steel strain				
6.05	-0.34b	7.28	8.65	9.63y
6.11	-0.823y	7.25	11.3y	12.1y
conc strain				
5.93	10.2	13.3	-0.64	2.13
5.99	-0.52	10.2	0.41	11.1
6.05	-10.2	6.32	6.88	24.0
6.07	-12.4	5.88	9.55	28.4
6.11	-15.3	4.75	14.5	35.5
6.25	-9.14	9.94	5.96	25.5
6.34	19.6	19.9	-0.78	-1.12
6.38	37.4	27.5	3.55	-7.33

units:	loads=in-k,kips	+=tensile
	stress=ksi	-=compression
	strain (x 0.001)	
moment N-S, +=comp. south		
moment E-W, +=comp. west		

Key to time	key:	A	B	C	D	E	F	G	H	I
pts. on plots	time:	5.93	5.99	6.05	6.07	6.11	6.25	6.33	6.34	6.38
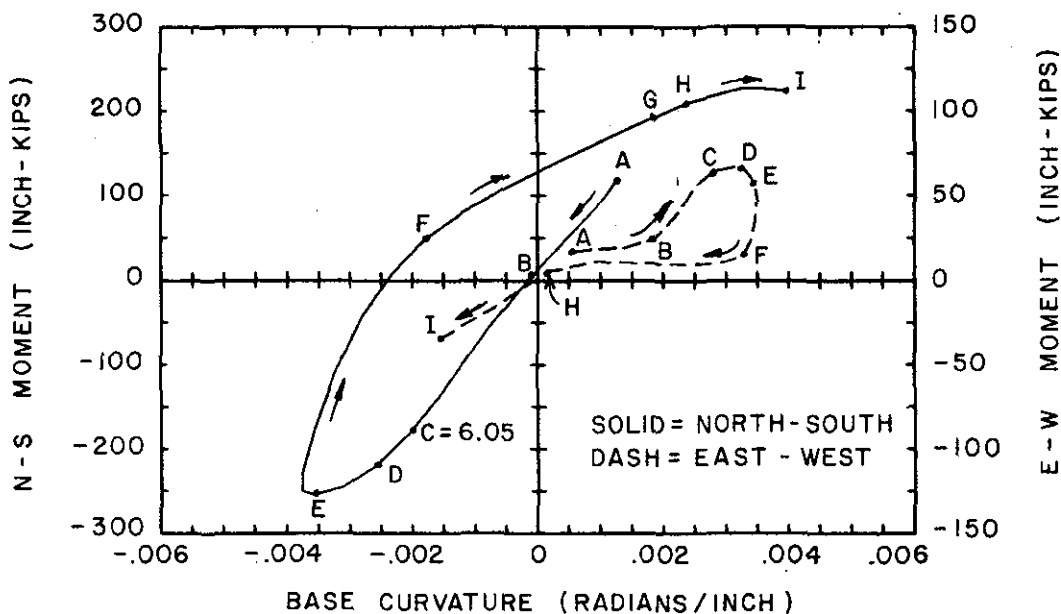
Figure 7.58 Column moment vs curvature, NS (strong) and EW (weak) axes.
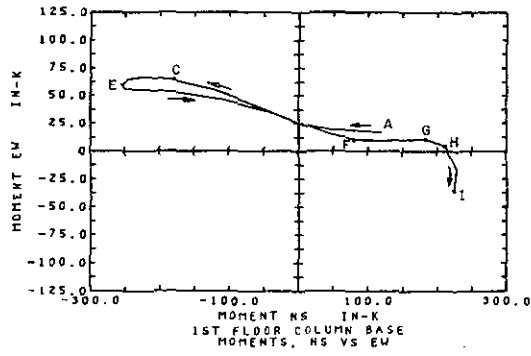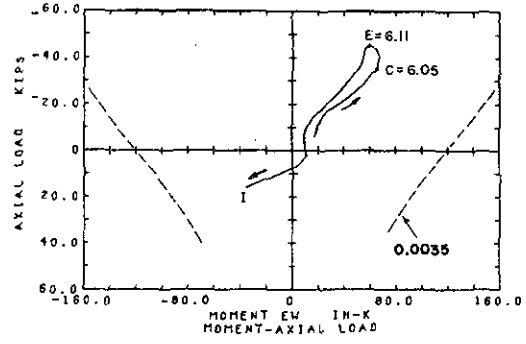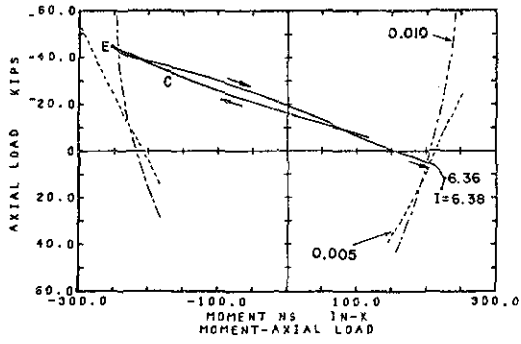
Figures 7.59-7.61 clockwise from top - left: moment NS-axial, moment EW- axial, moment NS-moment EW.

Summary: observed local response qualities

Response along the weak axis of the rectangular column was found to be greatly affected by motion along the column's strong axis. While the initial weak axis stiffness was 3.4k/in., a decrease to a stiffness of 1/3 the initial, while under low load, was due to inelastic damage within the column section caused by strong axis motion. The major part of that damage occurred during the initial fifth of the earthquake motion, thus, the weak axis response remained at the low stiffness level through most of the shaking.

Unfortunately, the particular type of response (Figure 7.20) associated with the low load-low stiffness weak axis column motion, is specifically of a low energy dissipation character. Hence, once strong axis motion causes inelastic damage within the rectangular column section, and the weak axis stiffness deteriorates, resonant motion of fairly large amplitude may build up in the weak axis direction- a result of inefficient mechanisms for energy dissipation.

Implications of such lowered stiffness and associated large displacement must be considered in seismic resistant design. Besides the obvious possibility of serious damage occurring with failure of non structural components, such glass, plaster, etc., the possibility of structural overload in the absence of energy absorption or dissipation must be kept in mind. In addition, loss of weak axis lateral stiffness under biaxial load may increase the danger of catastrophic structural failure under the multiaxial loading combined with P- Δ effects.

Analytic modelling of weak axis response by simulating the characteristics such as concrete cracking, bar elongation and rocking, which were seen to influence the behavior strongly would be extremely complicated. Comparison of Figure 7.5b, which exhibits the shear displacement in the weak axis direction on the first floor, and Figure 7.19, which plots behavior for one of the columns, indicates that the inelastic interaction effects apparent in an individual column become somewhat masked when averaged with other columns to form structural response behavior. The averaging effects of multiple columns in a structure may slightly decrease the global importance of interaction and allow use of a somewhat less sophisticated analytical model to achieve acceptable response prediction.

Inelastic structural behavior is often quantified by definition of a 'ductility', frequently displacement ductility, the total structural displacement divided by yield displacement. In the present frame, displacement ductility along the longitudinal axis was effectively 2.4. However, in a situation with biaxial bending, ductility loses its meaning as a measure of inelastic deformation to a large extent, particularly with non axisymmetric sections such as rectangular columns. A rectangular column would essentially have varying ductility dependent on the specific direction, with respect to its principal axes, one considers. Definite unique ductilities could certainly be assigned along the principal axes. However, even then ductilities may have little real meaning as a measure of inelastic deformation since, as noted in the present tests, inelastic motion along one axis may create lowered stiffness and allow large deformations along the orthogonal axis, resulting in a high ductility rating along that axis, though there may have actually been no inelastic deformation developed through loading along that axis itself.

The step by step inspection of the local load deformation response at the base of the north-west first floor column allowed a detailed look at certain seemingly irregular characteristics of the column restoring force mechanism. In addition to the apparent bending and shear stiffness increase under axial compression load mentioned in Section 1, the following local characteristics indicate additional load interaction effects.

(1) The most frequently seen irregularity was a change in the apparent EW (weak axis) column bending stiffness, concurrent with a reversal in the sign of the strong axis column moment. This particular behavior started occurring after the initial column yield in bending under a large motion, causing the first non-linear action.

    a. After bar yielding has occurred, residual elongations remain keeping the concrete section cracked open under low loads. The effective column section at the crack location simply consists of four reinforcing bars. Since the distance between bars on the east and west faces was fairly small, the column showed a low instantaneous bending stiffness in the east-west or weak direction. A given change in strain in any of the four bars caused by a combination of axial forces, M_{NS} and M_{EW} would create twice as much change in the east west as in the north south curvature.

    b. The residual deformations frequently resulted in the formation of an unsymmetrical stiffness about the NS axis when the moment and curvature in the NS axis direction were changing. This usually occurred when a previous tension crack on the north or south face began to close due to a moment reversal with either the west or east corner closing before the other and causing an unsymmetric EW stiffness due the newly effective concrete area in one of the corners. Continued bending in the NS direction would then tend to cause a secondary rotation in the EW direction and the constraint on the column deformation imposed by the frame as a whole would require formation of an internal EW moment opposing the secondary rotation. Unexpected moment changes and curvatures were detected along the EW axis under such conditions.

(2) When reinforcing bars reached their yield points due to restoring forces along one axis, the response in the other perpendicular direction showed a loss of stiffness as well. The bar yielding was normally caused by NS moments or combination of M_{NS} and M_{EW} with axial loading, and the secondary results of yielding were frequently seen in the EW bending stiffness.

(3) During sequences where high bending moments (particularly M_{NS}) occurred simultaneously with high axial force, (and the predicted limiting moment-axial curves were reached) the actual loads seemed to change in a manner which resulted in their following the shape of predicted limiting uniaxial moment-axial interaction curves. Generally, the axial load would continue to increase due to the structure's overturning effect and the column internal moment decreased, though curvatures continued to increase, producing an apparent negative bending stiffness.

(4) Under the rapid earthquake induced dynamic motion, strain rates in some of the column reinforcing bars reached 22% per second (0.22 strain per second). Such rates can be considered "dynamic" and stress-strain relations from static tests would underestimate the yield level stress.
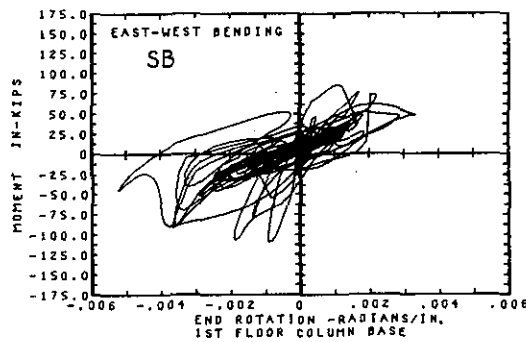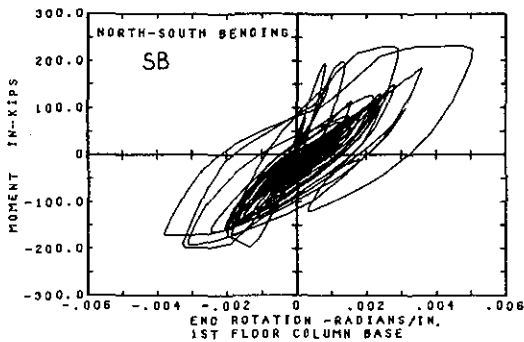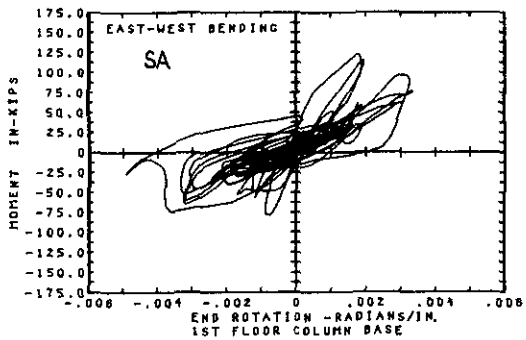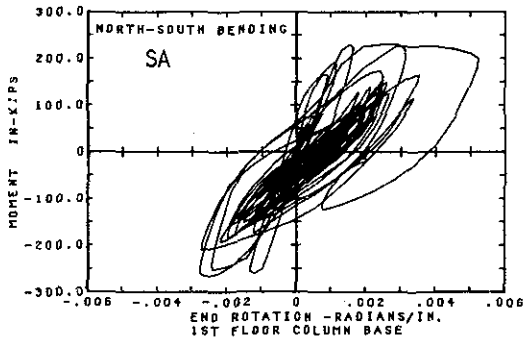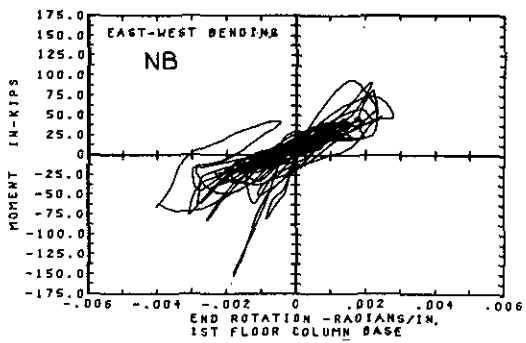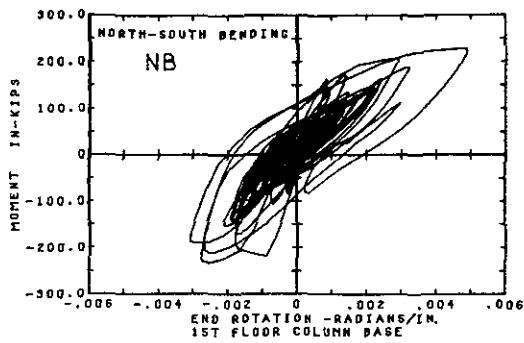
Figures 7.62-7.67 Strong axis (NS) moment vs curvature and weak axis (EW) moment vs curvature of NB, SA and SB columns at footing.

Chapter 8

Analytical Modelling and Correlation

Analysis of a structure requires a model describing the spatial geometry, connectivity, stiffness, strength, and mass in mathematical form and an algorithm capable of solving the equations of motion for the model under a given excitation. The spatial geometry, connectivity, and mass are readily described using discrete elements joined to match the obvious shape and weight of the prototype. Modelling the behavior in terms of stiffness and strength, requires an understanding of the response characteristics of each of the discrete elements included in the spatial geometry of the structure, -beams columns, footings, slabs and their joints. An element in a structure undergoing small deformations may have behavior which can be accurately described by a simple unique linear or non- linear relation between internal force and element elongation. More likely, especially under heavy loading or earthquake excitation, the element behavior will be irregular and history dependent, and the analyst may find she/he has few guidelines for defining mathematical behavior. When the model itself is defined, with equations established through element characterization and connectivity, various dynamic or static algorithms of proven accuracy may be used to solve the equilibrium equations.

In the present structure, attempts have been made to correlate analyses with the measured test response for the T(100(2) "elastic" and the T1000 "inelastic" test motions. The actual measured shaking table horizontal acceleration history was used as the excitation input for each set of analyses. While the structure's global response, in the form of first floor displacements, was the prime descriptive quantity considered in the correlation, certain aspects of local element behavior were compared as well.

The second purpose of this project was to evaluate the correlation between measured and analytically predicted response. Overall the intent of the correlation procedure was not to search for a mathematical model which would duplicate the measured response, but to select certain 'rational' models based on predicted element characteristics by the use of commonly available techniques for element section analysis and compare such predicted structural responses with the experimental results. However, during analysis of response to the strong T1000 motion, a lack of established guidelines for estimating parameters controlling element behavior and particular shortcomings in the element behavior resulted in a certain amount of trial and error procedure.

Elastic analysis, T100(2)

Concurrent multi-axial forces during elastic column motion should cause no detectable interaction between the response along the various axes. If such interaction is negligibly small, then separate 2 D analysis of the beam-column frames along the structure's major axis would provide accurate estimates of the lateral displacement response to horizontal earthquake motion. Code defined methods [12] of design for lateral loading often assume loading along the principal axis of a structure will be resisted separately by frames or walls parallel to the direction of loading. Of course the results of such independent frame analyses neglect the combined components of axial force and deformation in the columns caused by structural overturning moments along the two major axes.

The analytical model selected for elastic correlation consisted of a single beam-column frame in each direction: along the structure's longitudinal and horizontal axes. The two 2D frames resulted in a total analytical approach which is simpler to describe mathematically than a 3D model, and provided an opportunity to determine if interaction due to concurrent multiaxial loading (particularly bending) is significant during elastic response.
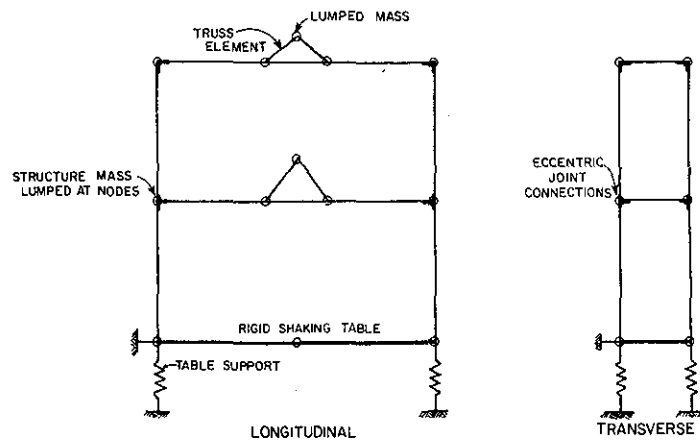
Figure 8.1 Overall geometry of analytic model, circles indicate nodes.

The spatial geometry of the longitudinal and transverse analytic models is outlined in Figure 8.1 with the masses as detailed in Figure 8.2. Centerline dimensions were used for column spacing and nodes were placed at levels of intersection with the neutral axes of the beams. Column-beam joints were originally considered rigid and short eccentric connections of length equal to the dimension to face of the beam or column extended from the joint nodes (as represented by heavy line segments at the joints in Figures 8.1 & 8.2). Simulation of rocking of the added mass blocks supported on the longitudinal beams was attempted by locating lumped masses at a height above the floors equal to the distance to the center of mass of the actual blocks. Such lumped masses (Figure 8.2) were tied to the floor beams at locations identical to the actual supports by stiff truss members. Columns were modelled by single elements, one story height in length. The longitudinal T beams were split into 3 segments for modelling purposes. Since the effective moment of inertia of a T beam depends directly on the sign of the bending moment, designating a value for section inertia becomes difficult if moment
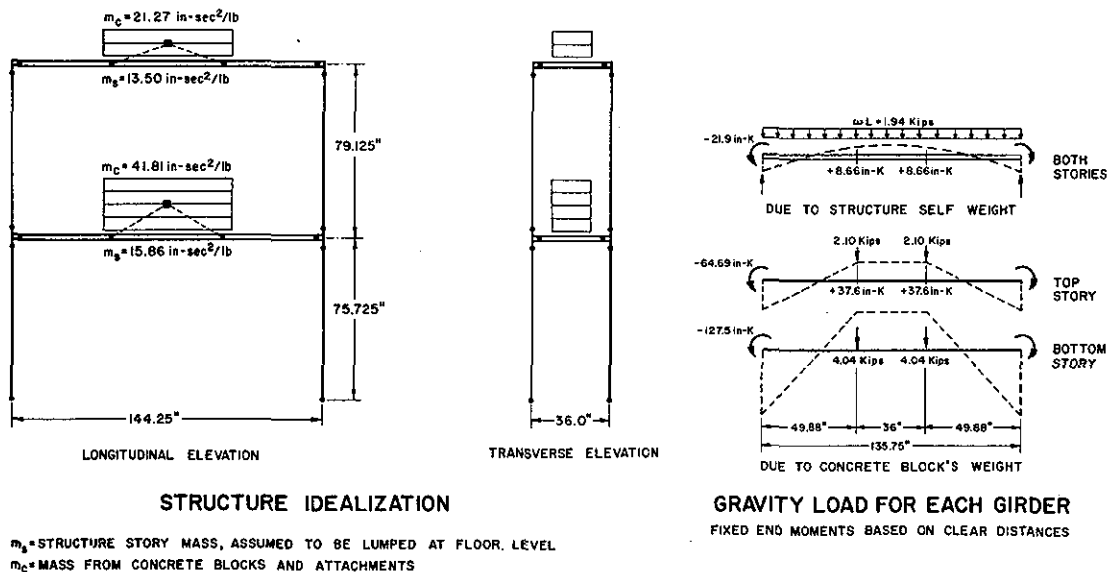
Figure 8.2 Structural idealization, masses, initial forces for analytic model.

reversals are possible. With the large static loads applied at the center of the longitudinal beams, the center segment was continuously subject to a positive (sagging) type moment and an effective I under positive moment could be used. The end segments were for the most part under negative bending and either the negative I value or an average of the negative and positive I's was feasible.

The shaking table is supported by a cushion of compressed air and moved by a system of hydraulic actuators. In addition to the horizontal and vertical active actuators a second set of passive hydraulic cylinders act as a spring-dashpot system, in the vertical direction, to resist table pitching caused by structural overturning moments. The pitch resisting mechanism of the shaking table was modelled by a set of vertical springs under the table itself. If the analysis algorithm were able to accept horizontal and rotational (pitching) type ground accelerations, this table support modelling would be unnecessary. Since the amplitude of motion during the elastic test was small without large overturning moments, very little table pitching motion developed and the springs were considered as rigid.

Computer program:

There are numerous computer solution algorithms which could be used for the elastic frames analysis. In this instance DRAIN2D [13] was selected because the same mathematical model of the structure could be used for elastic and inelastic analyses. DRAIN2D is a general purpose dynamic analysis program for inelastic plane structures, is distributed through the National Information Service for Earthquake Engineering (NISEE), and is frequently used for private commercial analysis. The step by step dynamic analysis procedure and Direct Stiffness Method of stiffness formulation are described in reference [13] which is available from NISEE. The program was used in a completely unmodified condition, as obtained from NISEE. A library of structural elements developed for use with the DRAIN2D program includes an

element intended to model reinforced concrete beams in the inelastic range. It has stiffness degrading rotational springs at the member ends, which are necessary for proper simulation of behavior during inelastic motion. It does not include any type of multi axial interaction effects.

Member stiffness-longitudinal frame:

Stiffnesses, in the form of bending moments of inertia, are described in *Appendix B* for various methods of formulation. Selection of member stiffnesses for the columns and beams in the present situation depends on the past loading history of the frame. The beams, particularly at the lower floor, have been heavily loaded with the sustained dead load of the concrete mass blocks. The dead load moments in the lower beam were 100 in-kips, positive in the center region and negative at the ends, or approximately one third of the section capacity at yield. Cracked section stiffnesses are definitely warranted for the lower beam. The dead load moments in the upper beams are 43 in-k at the center and 59 in-k at the ends. A tensile rupture stress of 7.5 $\sqrt{f_c'}$ (ACI[14]) will develop when the positive moment reaches 21 in-k. However, the beam is under less stress between the points of maximum moment and use of cracked section I over the entire beam length may result in a generally low stiffness estimate. A section of positive cracked section stiffness for the center beam segment and negative gross section stiffness in the end sections was used for the initial analysis.

The frame had already experienced a minor shaking from the T100(1) test. Column moments reached 60-70 in-Kips at the lower level and less at the upper story. Column yield strength was predicted as approximately 200 in-k under 10k axial compression plus bending. The upper and lower story column ends would be expected to have cracked section stiffness but the low stressed material at the column mid-height probably would not yet have experienced cracking. As an initial estimate, cracked section stiffness was selected for the lower column and gross section stiffness for second story columns.

The member stiffnesses selected for the initial frame response analysis are compiled in Table 8.1. Since the test was at a fairly low acceleration level (0.06g's) the yield behavior of the members was ignored by specifying very high yield levels for the inelastic member elements to force elastic analytic behavior.

Damping in an uncracked bare frame concrete structure would be expected to fall between 2 and 5 per cent of critical damping. With an increase in the amplitude of motion, cracking and slip or other energy dissipation mechanisms would require values near the 5% per cent of critical level to properly model the response. In the initial longitudinal analysis values of 2% critical in first mode and 3% in second mode were used to define mass dependent and tangent stiffness dependent damping factors. An integration time step of 0.02 seconds was selected for the analysis, approximately one-fifteenth of the first mode natural period

Analytical results-longitudinal frame:

The analytical response results from the proposed engineering model of the structure are compared with the measured response, in terms of 1st story displacements, in Figure 8.3. For enhanced clarity only the initial portion of the history is shown; the remainder of the predicted

Longitudinal frame- Elastic analysis (1) Model characteristics:		
Member	moment of inertia $(in.^4)$	
Column-lower	150	cracked section
-upper	280	gross section
Beam-lower		
ends	1440	gross section
center	550	cracked section
Beam-upper		
ends	1440	gross section
center	1440	gross section
Damping: specified as 2% first mode 3% second mode combination of mass and tangent stiffness proportional;		

Table 8.1.

FIRST FLOOR DISPLACEMENTS

LONGITUDINAL ELASTIC
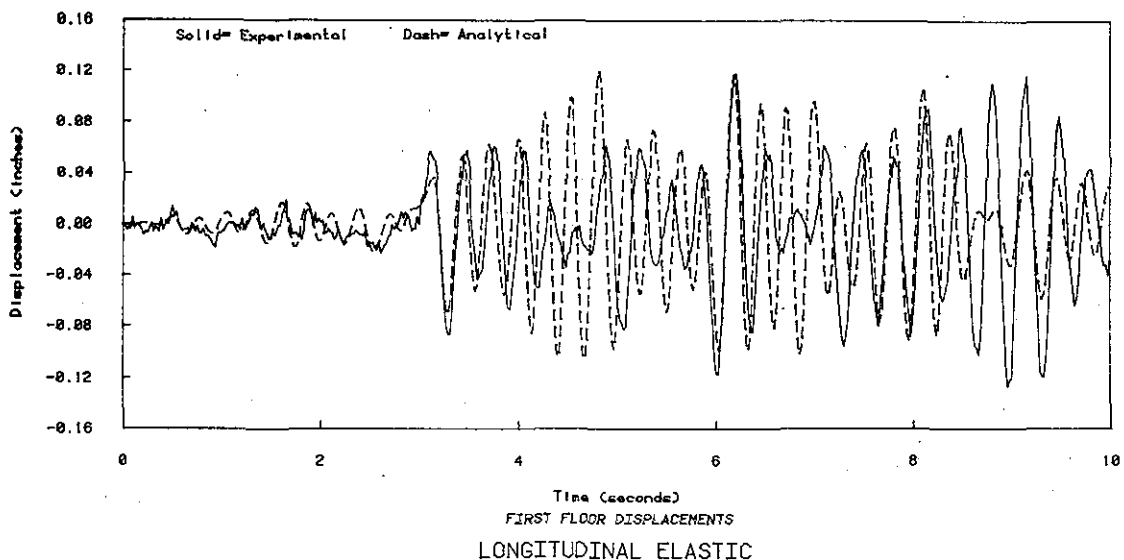
Figure 8.3 Results from first analysis, longitudinal elastic response, T100(2) test.

signal bears as little resemblance to the measured results as that shown, and is of less amplitude. Various conclusions based on comparison of the two response histories may be noted immediately.

1. Counting the number of cycles occurring during a particular interval of time indicates that the experimental response had an average frequency of 3.1Hz, the analytic had an average of 3.6Hz. The mathematical model was too stiff.

2. The rapid buildup of resonant response in the analytical model may indicate that damping was set too low.

The observation made in note 1, above, should have been suspected. With fairly high dead load moments already existing in the longitudinal beams and superimposed earthquake loading, cracked section estimates for moment of inertia in the end segments would have been appropriate. The correct value for damping is   more difficult to estimate. A value twice as high was tried in the second model. The properties used in the second analysis are listed in Table 8.2. Since the moments in the end beam segments generally changed sign from one end to the other, with low moment values in between, a value between the gross and cracked section estimates, though much closer to the latter, was selected and is denoted by cracked section +.

Longitudinal frame- Elastic analysis (2) Model characteristics:		
Member	moment of inertia $(in.^4)$	
Column-lower	150	cracked section
-upper	280	gross section
Beam-lower		
ends	560	cracked section+ **
center	550	cracked section
Beam-upper		
ends	400	cracked section+ **
center	400	cracked section **
Damping: specified as 4% first mode ** 3% second mode		
** *Value modified from first analysis.*		

Table 8.2.

The time-history plot of first floor displacements in Figure 8.4 indicates a fairly good agreement between the floor response measured during the test and predicted by the modified mathematical model. The analytic response peaks tend to be slightly higher than measured, indicating that the damping should probably be increased slightly. However, the results do indicate that a fairly simple model, based on cracked section estimates of stiffness used in a planer frame analysis, is able to simulate the actual response. If interaction between the responses along the structure's transverse axis and longitudinal axis significantly affected longitudinal response, successful planar simulation would not have been obtained.

Member stiffness-transverse frame:

Geometric modelling of the transverse frame may be seen in Figure 8.1. The structure and added masses are again modelled as lumped masses placed at the floor levels. Short transverse beams are replaced by a single beam modelling element, rather than segments, as
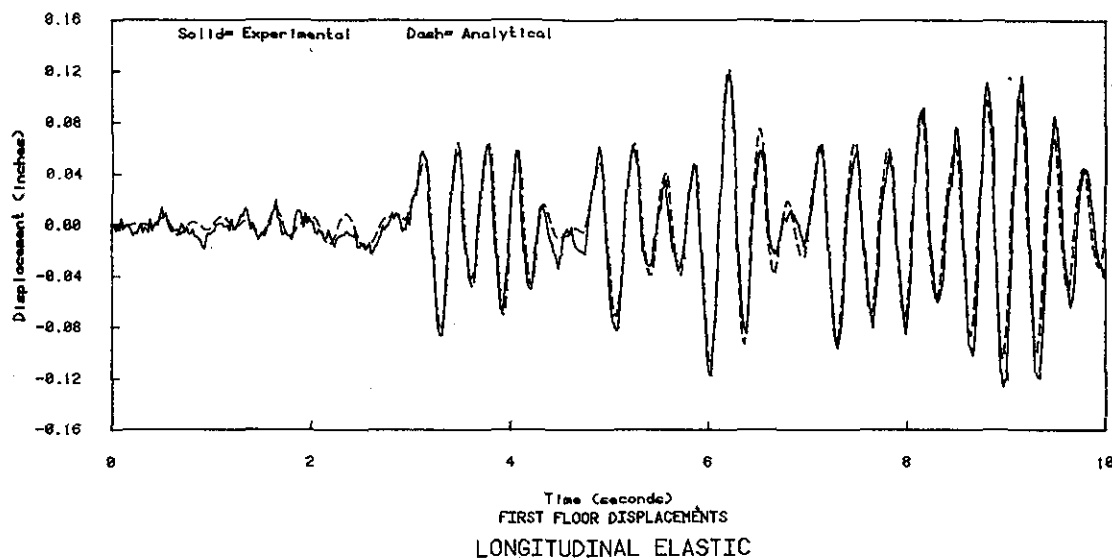
Figure 8.4 Results from second analysis, longitudinal elastic response, T100(2) test.

used in the longitudinal frame. A moment of inertia part way between the I for positive bending (365) and the I for negative bending (333), with a cracked section, was selected. Again, a cracked section stiffness was chosen for the columns as indicated in Table 8.3. Mass and stiffness dependent damping factors were included to give an effective 4% first and 3% second mode damping.

Transverse frame- Elastic analysis (1) Model characteristics:		
Member	moment of inertia $(in.^4)$	
Column-lower	50	cracked section
-upper	50	cracked section
Beams-lower	340	cracked section
upper	340	cracked section
Damping: 4% first mode 3% second mode		

Table 8.3.

Analytic results-transverse frame:

The results for calculated vs measured floor displacement are plotted in Figure 8.5. Only the first portion of the response history is included, however it is representative of the entire sequence.
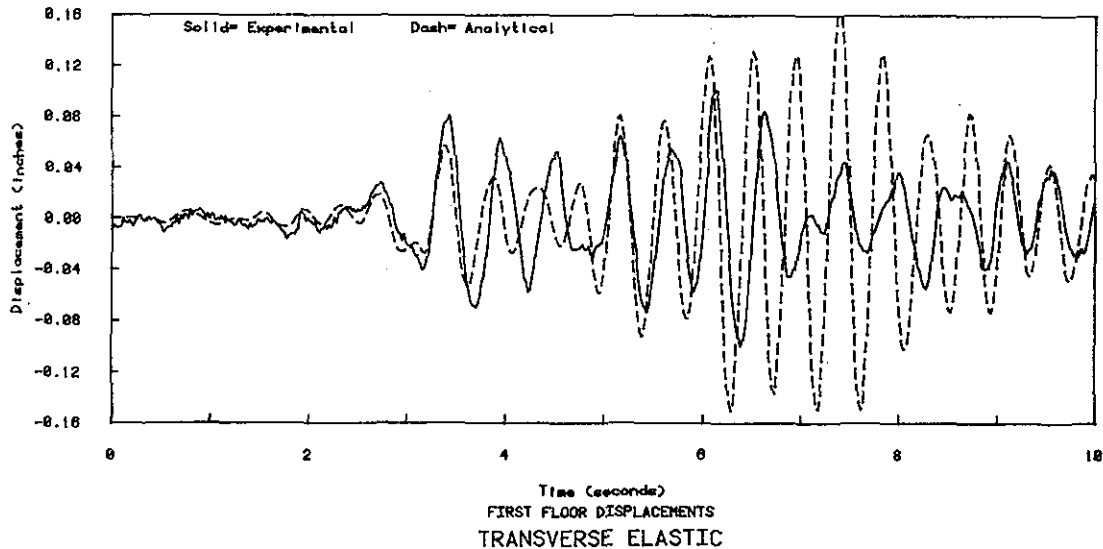
Figure 8.5 Results from first analysis, transverse elastic response, T100(2) test.

The major discrepancy is again a mis-match of frequency caused by high stiffness in the mathematical model. The estimated response frequency predominating in the experimental results (by measuring time interval between peaks) was 1.8 Hz, and in the analytic response, 2.2Hz.

Cracked section stiffnesses were already used in the column and beam elements. The cracked section I used for the column was 50 $in.^4$ while the estimated cracked section I under zero axial load (Appendix B) was 49 $in.^4$. Since overturning moments would develop during earthquake excited motions in the transverse direction, due to the close column spacing and high aspect ratio, the column could be subjected to axial tension forces during intervals in which high accelerations occur. With one column in tension (and having an associated lower stiffness) the overall lateral stiffness of the frame would be slightly decreased.

The beam-column joints provide a second source of flexibility which was neglected in the assumed rigidity of the analytical model. Undoubtedly a finite amount of deformation must occur in any joint under loading and the analyst is faced with a decision regarding the method of modelling non rigid joints and defining the effective length of members meeting at a joint. In the present case the orientation of the columns and transverse beams at the joint is such that the column is wider, out of plane, than the beam, and the continuous column steel is located fully outside of the beam cage. While neglecting shear deformation within the joint, it may be reasonable, for bending purposes, to assume that the effective length to be modelled by the column elements extends into the joint region. Modification reflecting such changes in joint stiffness may be seen in the table of characteristics for the second analysis of the transverse response. (Table 8.4)

Response of the modified analytic model is compared with the experimental history in Figure 8.6. The changes in column stiffness and effective length brought the measured and

Transverse frame- Elastic analysis (2) Model characteristics:		
Member	moment of inertia ($in.^4$)	
Column-lower	45 cracked section ** with 10k axial comp. No eccentricity at top joints, **	Table 8.4
Beams	340 cracked section	
Damping: 4% first mode 3% second mode ** Value modified from first analysis.		

FIRST FLOOR DISPLACEMENTS
TRANSVERSE ELASTIC
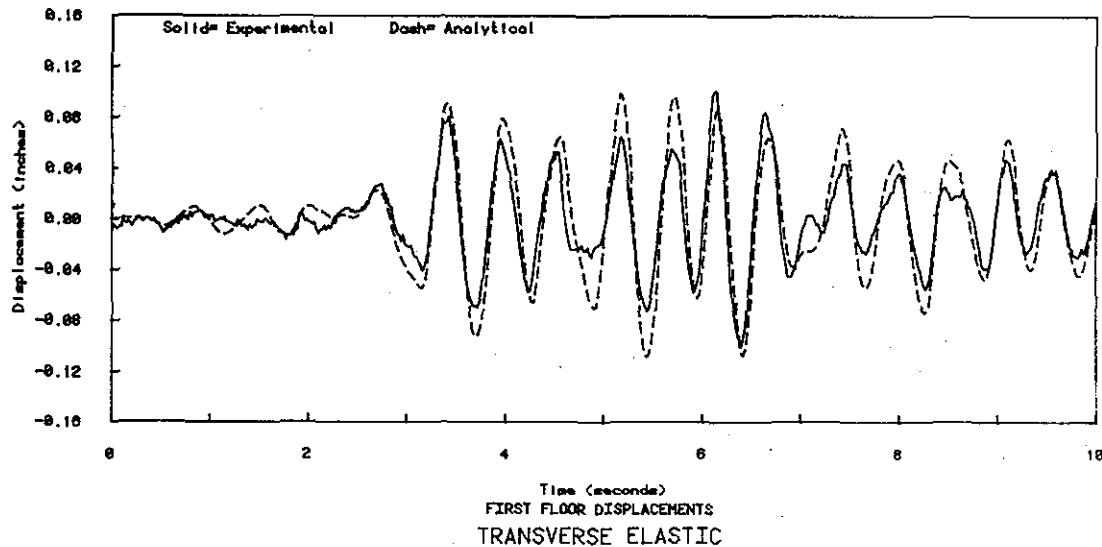
Figure 8.6 Results from second analysis, transverse elastic response, T100(2) test.

mathematically predicted frequencies into close agreement. The amplitudes of the math model are higher than the measured, suggesting that the damping in the analytic model may be set slightly higher than appropriate. Modification of the damping would be expected to bring the displacement amplitudes into close agreement as well.

Once again, the ability of the planar frame mathematical model to simulate the measured response of the three dimensional structure indicates that the motion is relatively free of multiaxial response coupling or interaction. The models were established with a fairly simple approach using calculated section stiffnesses. Selection of the correct section stiffness for the reinforced concrete members, generally not a problem with other materials such as steel, required some consideration of the past load history and anticipated loading. T-beam

sections, with differing stiffnesses under positive and negative moment, require special judgement in selection of correct stiffness to use in various regions along their length.

Inelastic analysis,T1000

Two dimensional frame models, identical in spatial geometry to those detailed in the elastic analysis, were used in mathematical simulation of the T1000 earthquake test which caused significant inelastic behavior. The mathematical models had the same configuration, structural member-element representation and placement of lumped masses as described previously. In addition, specific strength characteristics in the form of resistance capacity at yield and stiffness qualities after yielding were required.

Elastic models- loading past elastic range:

An initial response analysis was attempted using the elastic models with cracked section stiffness described previously. Behavior was artificially kept elastic by prescribed yield levels fifty to one hundred times above the expected. Partial time histories for the two frames may be seen in Figures 8.7 & 8.8. In both directions, the analysis is consistent with measured results until the first major displacement cycle, which initiates yielding in the real structure. It might be noted that the elastic analyses underestimate the first story displacements (longitudinal: actual= 2.12in., predicted= 1.24in., transverse: actual=1.54in., predicted= 1.07in.) though the internal forces which were calculated reached nearly four times the member yield levels. The prediction overestimated structural stiffness and produced a mathematical model with constant higher natural frequencies which were also excited by different sequences of the earthquake motion than the true structure, which had yield softening and degradation of its lateral stiffness causing time variation of frequency.

Nonlinear characterization:

Simulation of the post elastic behavior requires specific knowledge of the strength and stiffness variation of a member resulting from any particular loading history, since the behavior of most materials, and particularly reinforced concrete, are dependent on deformation history if yielding has occurred. Description of the behavior of reinforced concrete is particularly difficult as a result of the various nonlinear phenomena which may occur including:

1   tensile cracking of concrete,

2   yield of tensile reinforcing and residual elongation,

3   compression crushing and spalling of unconfined concrete,

4.   compression crushing of confined concrete,

5.   loss of bar concrete bond at high strains or from cyclic loads,

6.   bar slip at joints,
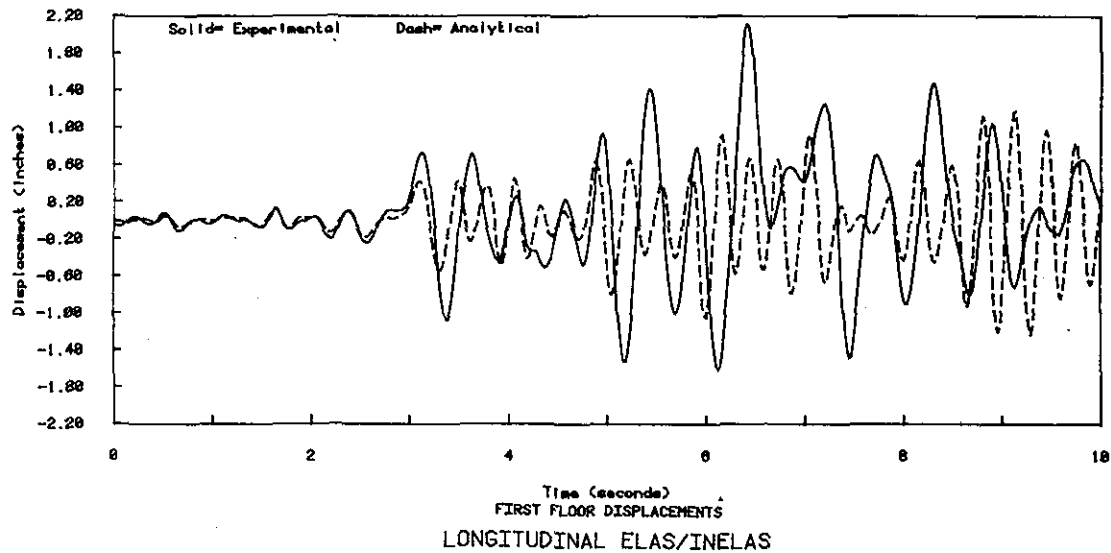
Figure 8.7 Analytic results using elastic analysis, with a motion causing inelastic response, longitudinal, T1000 test.
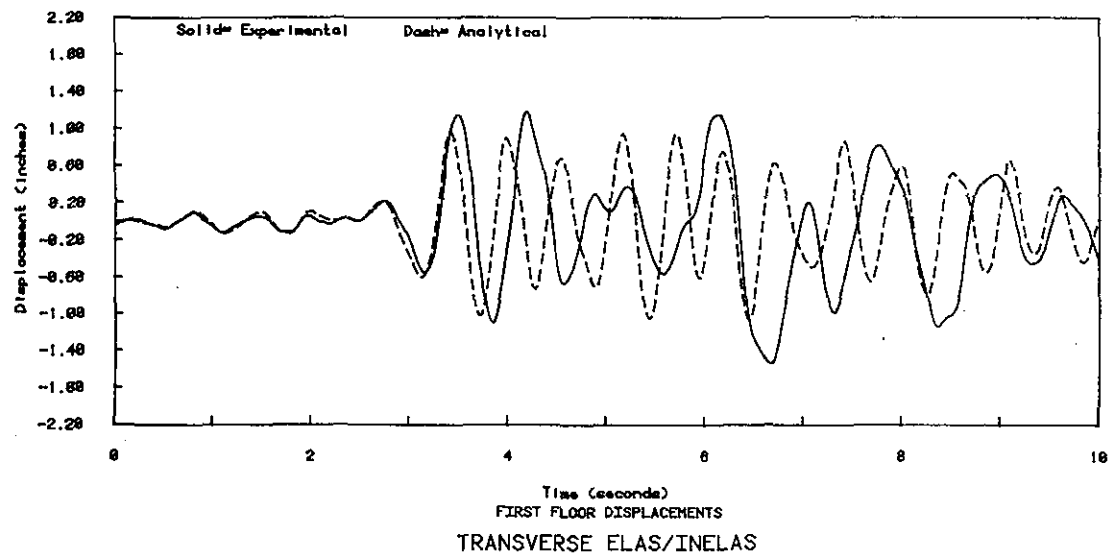
Figure 8.8 Analytic results using elastic analysis, with a motion causing inelastic response, transverse, T1000 test.

7. yield of compression reinforcing and subsequent buckling,

8. apparent strength increase due to visco-elastic behavior with dynamic rates of straining.

Though the list is by no means exhaustive, it is exemplary of the multitude of possible mechanisms which may affect the post-yield response.

The specific mathematical modelling of each of the above occurrences would not only be cumbersome but in certain cases beyond the limits of current ability to generate behavioral rules. The common approach to such modelling is one of including particular components (1,2,3,4) of non linear behavior averaged in a single general deformation mechanism, such as

bending moment-curvature or a moment-end rotation type of relation. Tests have indicated a general pattern for moment-curvature behavior of beam elements as outlined in Figure 8.9. While such a method includes most of the sources of inelasticity which develop within the member, it neglects the other components which allow deformation at the joint interface (5,6) or are normally considered of lessor importance (7,8).

Figure 8.9 Typical moment vs rotation relation for reinforced concrete beams.
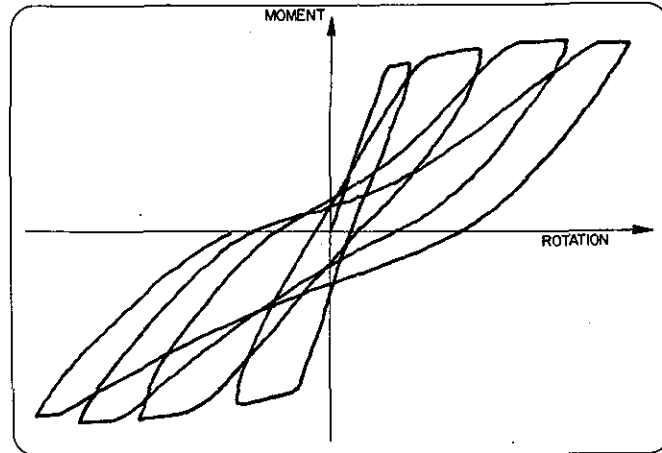
The reinforced concrete beam element available for use in the DRAIN2D computer facilitated analysis package incorporates non-linear rotational springs at the ends of the element. The moment-rotation behavior of the springs is a modified version of the multi-linear degrading hysteresis rule proposed by Takeda[15] and outlined in Figure 8.10. Basic behavior of the model is similar to Fig. 8.9, with the same drawbacks, but also neglects strength deterioration caused by mechanisms '3' and '4' above.

$$\frac{Q^- T}{Q^- V} = \left(\frac{R^+ - R_{REV}}{R^+ - R^-}\right)^{\eta}$$
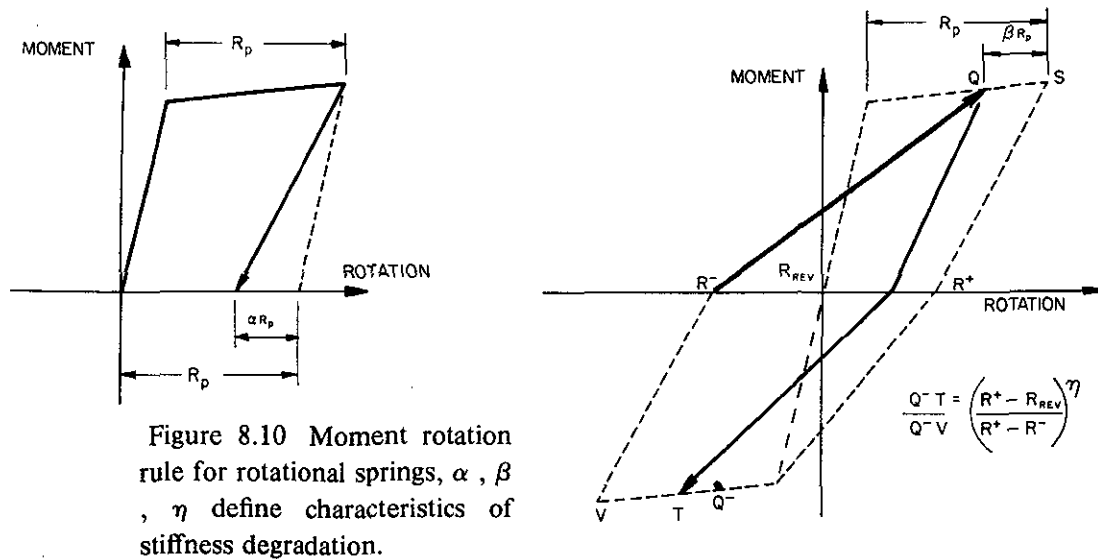
Figure 8.10 Moment rotation rule for rotational springs, α , β , η define characteristics of stiffness degradation.

The parameters which described the moment-rotation rule of Figure 8.10 include:

a.   initial flexural stiffness,

b.   slope of post yield envelope or yielding stiffness,

c.   unloading stiffness parameter α

d.   loading stiffness parameter β

e.   small amplitude cycle parameter η

While selection of the initial flexural and the post-yield stiffness may be accomplished through section analysis, there are no generalized guidelines for selecting appropriate parameters (α β η) to describe the stiffness degradation characteristic of a particular cross section.

This element does not have any provision for including the important interaction effect between axial load and bending moment yield level. Accurate modelling is quite difficult without such an ability. However, a clumsy attempt to incorporate some axial load vs. yield moment interaction was facilitated by a feature of the beam element which allowed differing values of positive and negative yield moments to be defined at each end of the element. Thus, the sign of the bending moment could be foreseen when the frame was displaced in either of the two lateral directions, with an associated compressive or tensile column axial force due to overturning, and values could be assigned for the positive or negative yield moments dependent on the expected column axial force when bending was occurring in that particular direction.

Longitudinal frame- nonlinear analysis:

The section properties derived through the RCCOLA analysis of member cross sections *(Appendix B)* were used to calculate a post-yield stiffness for the non linear rotational springs. The maximum curvature at the column ends was arbitrarily assumed to reach 0.005 radians per inch for calculation of an average post yield stiffness in the degrading rotational springs. Referring to the moment-curvature plots of Figure 7.26 and Figure B.3 from the RCCOLA calculations, moment and curvature values at yield and at a curvature of 0.005 rad/in. were determined for an axial load of 10K compression (the column dead load force). The end deflection values for a cantilever beam of half the column length were calculated through integration of curvature along the beam, assuming a maximum curvature equal to the yield curvature and secondly equal to 0.005 rad/in. at the fixed end. The change in deflection after yield was used to calculate the post-yield stiffness of the rotational spring. It was assumed that the columns would be in reverse bending under the lateral loading: thus the use of half length in the cantilever. Quantities used in calculation of spring properties are included in *Appendix B.*

The remaining parameters, α , β , and η , were somewhat arbitrarily selected since there were no definite guidelines, other than can be obtained by experimental testing and matching response, to describe the degrading stiffness. Based on illustrated moment curvature results of other researchers mentioned in *Appendix A* and results seen in previous tests conducted on the shaking table, [1],[2],[10], the factor β was set to zero. Thus reloading proceeded towards the previous maximum rotation point. Then, with β set to zero, and reloading path always toward the previous maximum, definition of η was not required. The value to be used for α was uncertain, and varying values were used in sequential analysis runs.

The first analytical model assembled for the longitudinal frame used bilinear yielding elements in the beams with a post yield stiffness at 4% of elastic, and multilinear degrading stiffness elements to model the columns with properties, as listed in the accompanying table. (Table 8.5) The specified column-yield moments, 223 and 160 in-k, were calculated assuming that axial forces due to overturning would be 20k compression and 5k tension respectively, at times when yield moment would be reached.

The stiffness and yield level for the lower floor beams, at the beam-column joints, were obtained by neglecting the reinforcing bars in the flanges of the T section, which did not anchor in the column. Previous tests,[1],[2],&[16], have shown a tendency towards formation of diagonal (torsion-shear) cracks, as described in *Chapter6* and noted in Figure 6.6, in the slab above the transverse beams near the column faces; essentially isolating the flanges of the longitudinal beams from the columns. The reduced moment of inertia calculated in this manner is noted as 'cracked section-' in the table.

The previously described elastic analysis employed an integration time step of 0.02 seconds, or one-fifteenth the first mode natural period. Use of the same time step was attempted in the inelastic analysis. However, during the initial computer run the analysis diverged at 5.27 seconds, resulting in sudden displacements beyond a preset limit of 5 inches. Subsequently an integration time step of 0.01 seconds was specified and the analysis was completed successfully albeit more expensively.

Figure 8.11 compares the predicted motion from the analytical model with the measured displacement data. Since the elastic stiffnesses were nearly the same as those used in the previous analyses, it is reasonable to expect the model to be accurate at least in the elastic initial motion, before large displacements cause yielding. The results do agree fairly well until slightly after 3 seconds when the first major displacement occurs. Through the rest of the excitation, the mathematical model retains too high a stiffness while the actual frame degrades considerably.

As a means of increasing the degradation during unloading after yield, the α factor was increased from 0.1 to 0.8 (see Fig. 8.10). And the yield level with additional from overturning was changed from 160in-kips with 5k axial tension to 200in-k with 10k axial compression as noted in Table 8.6.

The results of the second model appear nearly identical to the previous if Figures 8.11 and 8.12 are compared. Apparently the modified α did not have a significant effect on the overall response. An inspection of the moment-curvature behavior of one of the rotational springs at the base of the first floor column (Figure 8.13) indicates that:

1.   very little yielding has occurred in the mathematical model,

2.   the combined α and β parameters have created a model with narrow moment rotation loops and little energy dissipation.

The increase of column yield moment in model 2 was certainly in error since the real structure will have axial tension forces created by the <u>combined</u> overturning moments about the <u>two</u>

Longitudinal frame- Inelastic (1) Model characteristics:		
Member		moment of inertia $(in.^4)$
Column-lower	150	cracked section
-upper	280	gross section
Beam-lower		
ends	350	cracked section-
center	550	cracked section
Beam-upper		
ends	320	cracked section
center	380	cracked section
Member		yield moment (in-k)
Columns	223	under axial comp. (20k)
	160	under axial tension (-5k)
Beam-lower	304	positive-sagging
	356	neg.-humping
at ends	240	negative
Beam-upper	195	positive-sagging
	235	neg.-humping

Table 8.5

Member	rotational nonlinear springs		
	k-post yd.	α	β
Columns	6930in-k/rad	0.10	0.00

Damping: 4% first mode
 3% second mode

structural axes, effectively reducing the axial compression below the 10k dead load (at which the 200 in-k yield was specified). Judging from the types of moment rotation cyclic loops normally seen in beam tests, wider loops with greater energy dissipation would be expected and should be used in the analytical model; requiring a decrease in the value of α .

As mentioned previously, the shaking table itself tends to pitch slightly during testing, particularly when a structure has high induced overturning moments. In essence, table-structure interaction occurs. The modelling of such behavior can be included in the analysis procedure by adding a rigid table with rotational lumped mass on spring elements as described earlier. The spring elements were given a stiffness of 150 k/in each, providing an effective rotational stiffness of 21640 in-k/rad, as used successfully in correlation analyses of previous tests with similar mass characteristics [17].

118
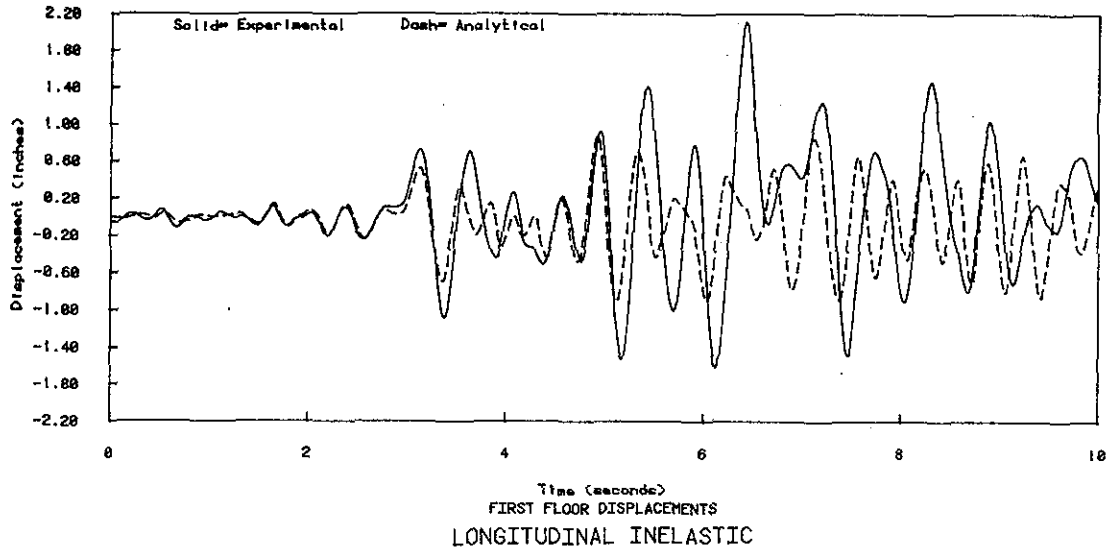
Figure 8.11 Results from first analysis, longitudinal inelastic response, T1000 test.

Longitudinal frame- Inelastic (2) Model characteristics:			
moments of inertia and yield level- same as previous model except:			
Member	yield moment (in-k)		
Columns	200	axial comp. (10k) *	
Member	rotational nonlinear springs k-post yd.	α	β
Columns	6930in-k/rad	0.80	0.00 *
* Value modified from previous analysis.			

Table 8.6.

Inspection of the analytical results of model 2 also indicated that the ends of the lower story beam (modelled with a bi-linear non degrading element) developed maximum rotations of 0.01 radians in their concentrated plastic hinges. Rotations of such magnitude should cause stiffness degradation. Thus the third analysis model used stiffness degrading reinforced concrete beam elements to model the two end segments of the lower level beam with parameters as specified in the Table 8.7. A further modification included in the third analysis involved a change in the stiffness definition for the lower column elements. Axial force in the columns, due to the static dead load, remained constantly at 10kips. Additional axial forces, due to the combination of overturning moments along both of the structure's main axes, varied with a maximum of approximately 35kips, tension and compression. Since the predicted uniaxial column yield moments varied as:
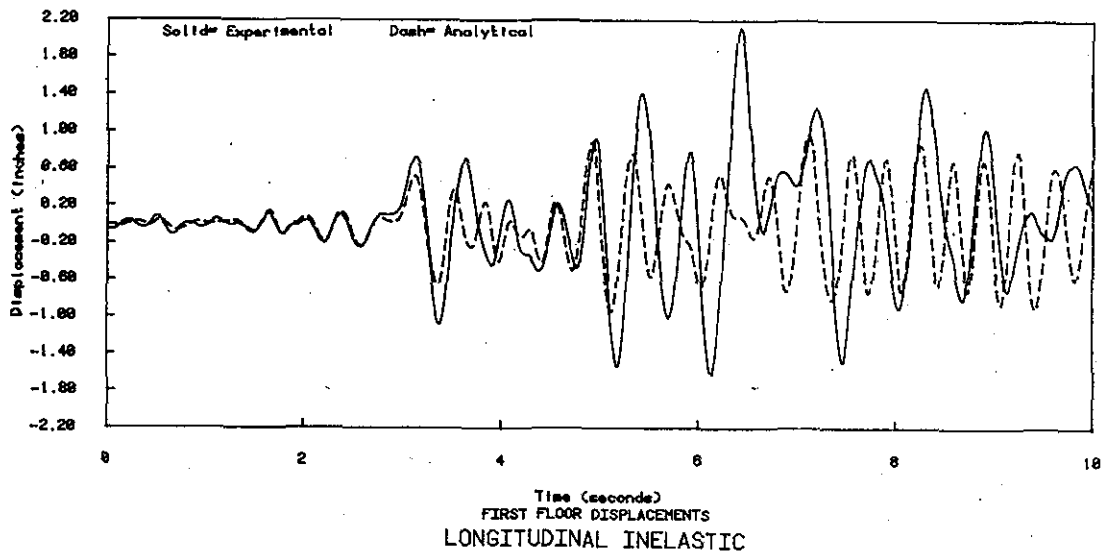
Figure 8.12 Results from second analysis, longitudinal inelastic response, T1000 test.

Figure 8.13 Analytic moment vs curvature for NA column, strong axis, from second run, T1000.
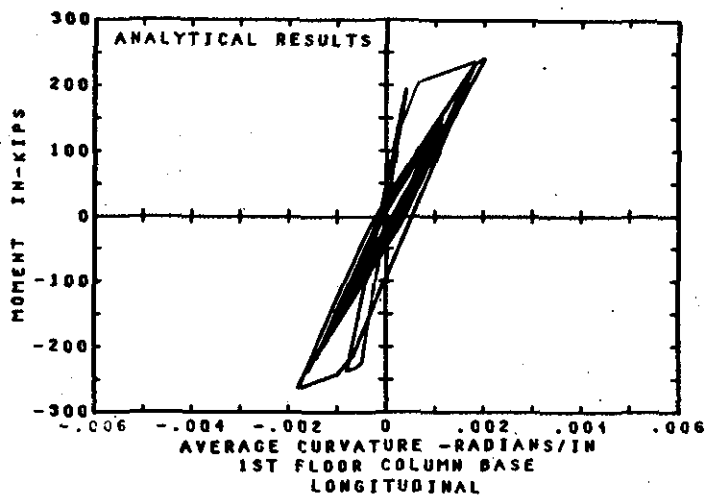
277in-kips at 40k axial compression

168in-kips at 0k axial

109in-kips at 20k axial tension

it seems likely that column yielding, and the stiffness degradation induced, occurred more frequently or to a greater extent when column axial load was reduced by the overturning moment force component. In fact, with the single axis component of overturning moment in the second analysis, the static axial compression was offset, at peaks, by the overturning induced tension. Therefore, the column element properties, and rotational spring stiffness in particular, were reformulated, basing the new parameters on an assumed no axial load situation within the columns (during inelastic excursions the uplift is assumed to cancel deadload). The resulting

parameters are noted in Table 8.7.

Longitudinal frame- Inelastic (3) Model characteristics:			
Member		moment of inertia ($in.^4$)	
Column-lower	146	cracked section, 0 axial **	
-upper	280	gross section	
Beam-lower			
ends	350	cracked section-	
center	550	cracked section	
Beam-upper			
ends	320	cracked section	
center	380	cracked section	
Member		yield moment (in-k)	
Columns	223	under axial comp. (20k)	
	170	no axial load **	
Beam-lower	304	positive-sagging	
	356	neg.-humping	
at ends	240	negative	
Beam-upper	195	positive-sagging	
	235	neg.-humping	
Member	rotational nonlinear springs		
	k-post yd.	α	β
Columns	3214in-k/rad	0.40	0.00
Beam end	91000in-k/rad	0.00	0.00
Damping: 4% first mode 3% second mode			
** *Value modified from previous analysis.*			

Table 8.7.

The results of the third model, plotted in Figure 8.14, match the experimental displacements, and especially their frequency, fairly well, particularly during the first seven seconds, though the amplitudes vary slightly, and an overall drift in the negative (north) direction seems to have developed in the mathematical model and not in the measured data. The later part of the motion shows a greater amount of stiffness degradation, in the associated lower frequency, present in the experimental results. The moment-rotation behavior of the rotational spring at the base of the north column (from the analysis) is included in Figure 8.15. The data is presented in the form of a moment-curvature plot to allow comparison with the experimental
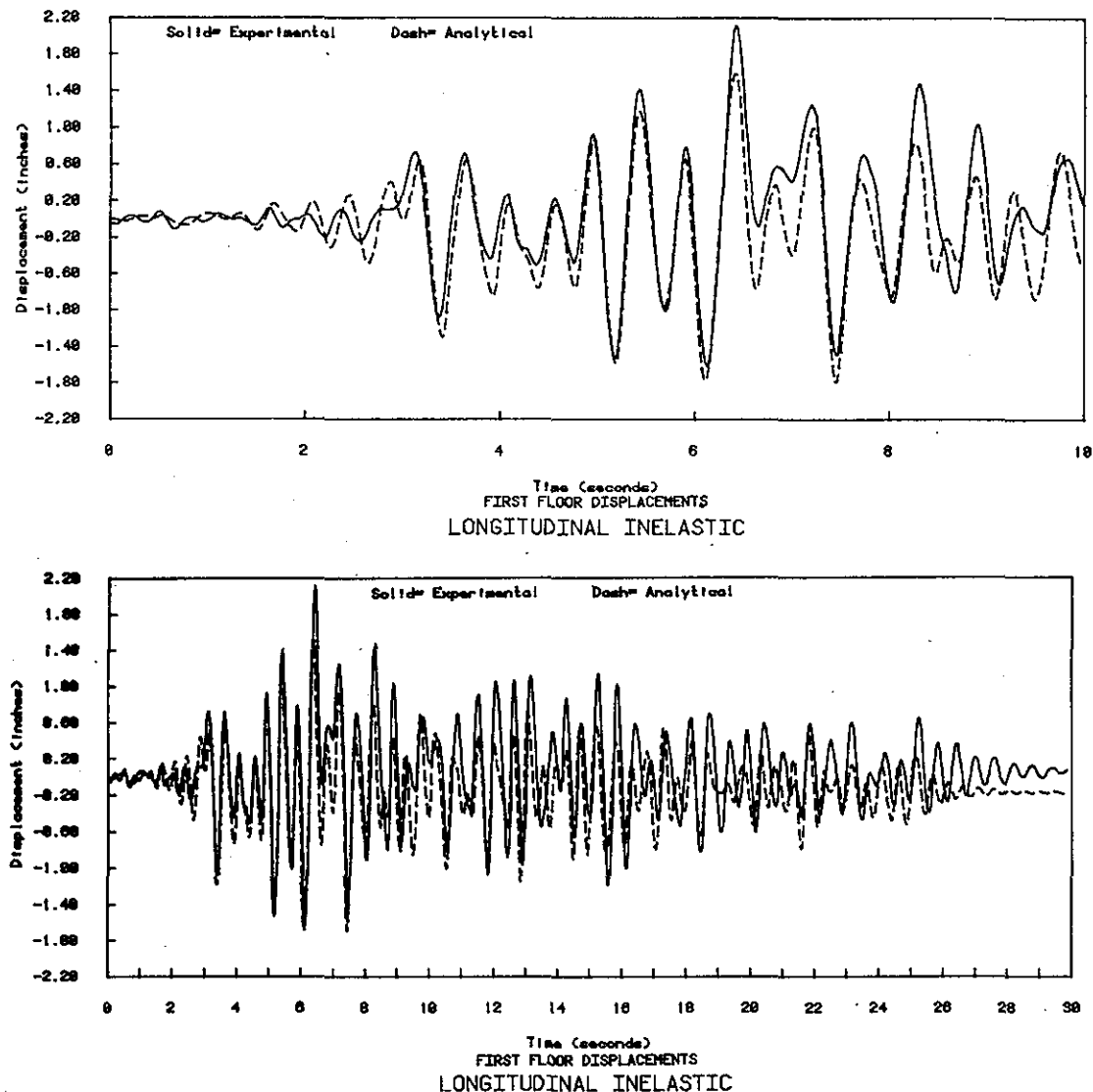
Figure 8.14 Results from third analysis, longitudinal inelastic response, T1000 test, (upper-first ten seconds, lower-full duration).

plots of *Chapter 7.* (Figure 7.16 & .18) Analytic curvature was calculated by combining rotation of the spring divided by 4in. with the elastic curvature. The experimental curvature was based on the rotation measured at the base of the column divided by the 4 in gauge length. Thus both 'pseudo-curvatures' should match. More yielding is apparent and the overall shape of the hysteretic loops look better than that of the previous model, while the general shape and magnitudes compare acceptably with the measured results in Figure 7.16. However certain important deviations should be noted. Comparing the first negative yield cycles in Fig. 8.15 and Fig. 7.16, one of the previously listed shortcomings of the analytic model is apparent. During the actual test yielding in that cycle was followed by a large axial compressive load, causing concrete

crushing and deterioration in strength of the column while it continued to deform, causing a negative slope. The analytic model is incapable of such strength deterioration, but rather, shows strain hardening behavior. The pinching effect in the hysteresis loops is not modelled and the later cycles exhibit less total stiffness degradation than was apparent in the measured results. The hysteretic response of Figure 8.15 has been separated into short segments, with the same time intervals as used in the 'windows' 1 to 8 of *Chapter 7* -Section 2, and can be seen in Figure 8.19 near the end of this chapter.

Figure 8.15 Analytic moment vs curvature for NA column, strong axis, third run, T1000.
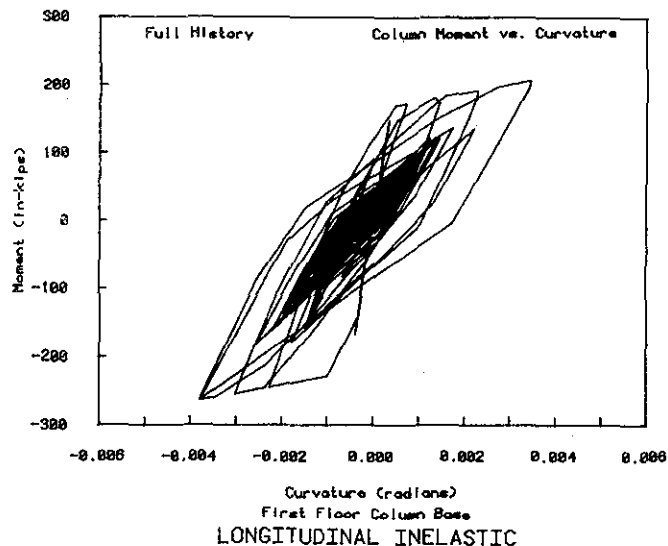
Transverse frame- non linear analysis:

Stiffness values for columns, beams, and rotational springs were calculated for the transverse direction in the same manner as described previously for the longitudinal direction. Bending stiffness in the elastic range was specified as being identical to that used in the elastic correlation analysis. The initial model, with characteristics as in Table 8.8, did not include pitching effects of the shaking table itself.

The overall predicted response using this non linear model, Figure 8.16, seems nearly identical to the results obtained from a pure elastic analysis as shown earlier in Figure 8.8. However, yielding and inelastic deformation did occur at both ends of the lower story columns. The amount of stiffness degradation developed did not begin to approach the amount necessary to match the change in frequency of the test frame. The experimental displacements appear to have a natural frequency of 1.7 Hz, while the measured data has peaks at an average of 1.1 Hz, and, as time increases the true response frequency becomes lower. Maximum first floor displacement predicted by the analysis was 0.91in. compared to a measured peak of 1.54in..

Three possible improvements can be suggested. The results from the first analysis indicate axial tension forces are occurring in the lower story columns in association with dynamic overturning moments. The non linear degrading hinge stiffness used was calculated assuming the columns carried 10 kips of axial compressive load. Recalculation under lower axial load

Transverse frame- Inelastic (1) Model characteristics:			
Member		moment of inertia ($in.^4$)	
Columns	45	cracked section 10k axial tension	
Beams	340	cracked section	
Member		yield moment (in-k)	
Columns	169 103	under axial comp. (40k) under no axial	
Beams	257 252	positive-sagging neg.-humping	
Member	rotational nonlinear springs k-post yd.	α	β
Columns	4666in-k/rad	0.40	0.00
Damping: 4% first mode 3% second mode			

Table 8.8

FIRST FLOOR DISPLACEMENTS

TRANSVERSE INELASTIC

Figure 8.16 Results from first analysis, transverse inelastic response, T1000 test.

may be desirable since the stiffness is reduced, particularly after yield, if no axial load is assumed. The column element yield levels were specified for 40 kip and 0 kip axial loads. Since the maximum axial load listed in the analytic results was 24 kips compression, and since tensile axial loading was indicated, lower yield levels associated with such axial forces should be specified. And thirdly, the pitch effect of the shaking table, which is important when appreciable structural overturning moments are being generated, should be added to the mathematical model.

Transverse frame- Inelastic (2) Model characteristics:			
Member	moment of inertia ($in.^4$)		
Columns	50	cracked section with ** no axial load	
Beams	340	cracked section	
Member	yield moment (in-k)		
Columns	122	under axial comp. (10k) **	
	90	with axial tension (-10k) **	
Beams	257	positive-sagging	
	252	neg.-humping	
Member	rotational nonlinear springs		
	k-post yd.	α	β
Columns	4666in-k/rad	0.40	0.00

Damping: 4% first mode
        3% second mode
** *Value modified from previous analysis.*

Table 8.9

The analytic displacements, plotted with experimental values in Figure 8.17, resulting from the modifications listed in Table 8.9, still show poor correlation. An analytic predicted maximum displacement of 1.05in. is considerably short of the 1.54in. measured. Inspection of the column moment vs. pseudo curvature behavior depicted in Figure 8.18 indicates that the analytic member yields during the first large displacement cycle at 3.40 seconds. During the remainder of the motion no further yielding of the element develops and the column stiffness remains at a constant degraded level. Such predicted behavior is in strong contrast to the experimental results for the NA column seen in Figures 7.19 and 7.20. The actual column has a much higher stiffness degradation effect without any obvious yield sequence. As discussed in *Chapter 7* -Section 2, the weak axis or transverse direction response is strongly affected by the longitudinal axis motion causing an apparent low stiffness. The planar frame analytical model is
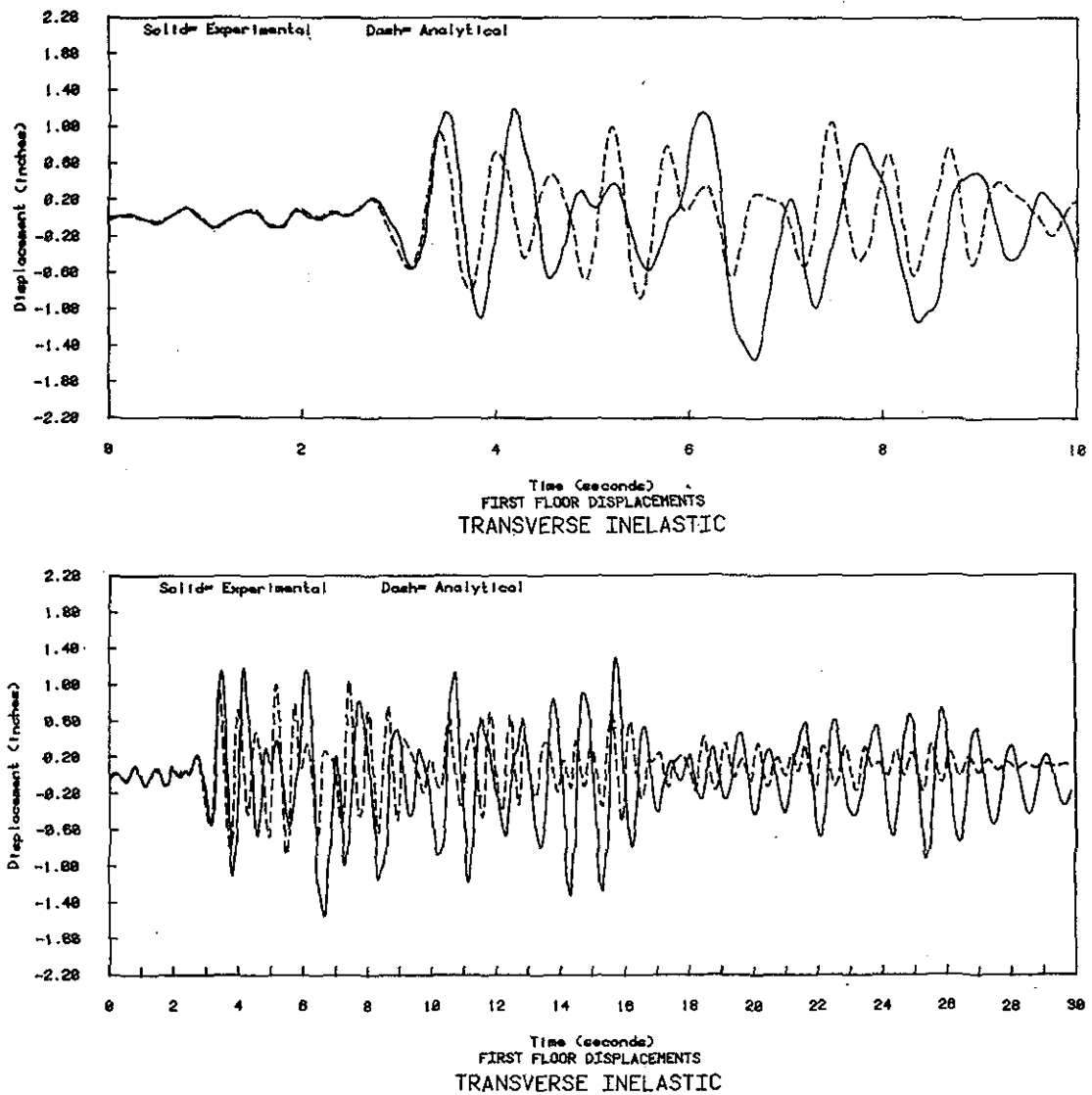
Figure 8.17   Results from second analysis, transverse inelastic response, T1000 test,
(upper- first ten seconds, lower- full duration).

incapable of including such interaction and fails to provide an acceptable correlation with the experimental results.

126

Figure 8.18 Analytic moment vs curvature for NA column, weak axis, second run, T1000.
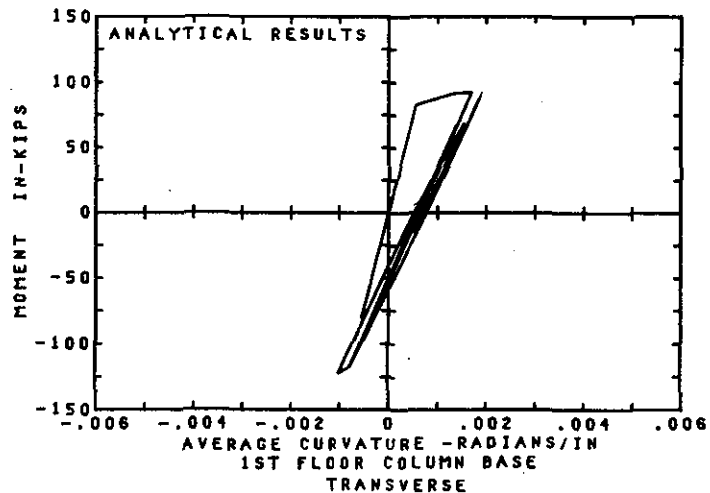
Observations- analytic correlation

Elastic response:

The correlation between predicted response results from the mathematical model and the measured experimental response data was quite successful when the structural deformations remained in the elastic range even though the analytic model used 2D planar frames to simulate a 3D structure. As one might have expected, under low loading, interaction between multi-dimensional loads on members and member response was minimal, allowing uncoupled analysis as long as the material remained nearly elastic. Selection of correct section properties (i.e. gross area or cracked section moment of inertia, effective lengths) requires a degree of knowledge-able judgement based on the past loading history, configuration of structure and expected mode of load resistance. However, the actual calculation of possible section properties is straightforward and easily accomplished.

Non linear response:

The correlation between analytic and measured behavior, once the non-linear deformation range was entered, was fairly poor when attempted using uncoupled planar frames to model 3D frame response with simultaneous multi axial member loading. The uncoupled planar frame analysis was not able to produce the amount of stiffness and strength degradation which occurred in the test frame.

Displacement amplitudes predicted along the longitudinal and transverse axes, using independent planar analyses, were found to be seriously underestimated when compared to measured results. The final analysis in the longitudinal direction predicted a peak displacement of 1.79in., while actual measured displacement of the first floor reached 2.12in., a 16% error. Along the transverse (weak) axis, where considerable interaction had been noted in the experimental data, the prediction accuracy was much poorer. The second analysis resulted in a maximum displacement of 1.05inches, 68% of the experimental first floor displacement, 1.54inches.

In both axes the mathematical model was able to match the initial sequence of low amplitude motion. When large amplitude motion was induced in the models, particularly the transverse, they were unable to match the amount of stiffness degradation which was apparent in the experimental frame. Hence, the natural frequency of vibration, in the inelastic models, invariably differed from the experimental results by the end of the motion.

Pecknold and Suharwardy [31] and Aktan [27] have suggested that biaxial bending effects might be neglected if the system strength is such that predicted 1D or uniaxial loading ductility is less than 2. The 1D lateral displacement ductility predicted in the third inelastic analysis (longitudinal) run was approximately 3.14 (max. displacement = 3.14 times yield displacement). Certainly some interaction effects did occur in the strong axis direction. However, the suggested relation between predicted 1D ductility and actual extent of biaxial interaction effects was not based on experience with rectangular section columns. It is doubtful whether that criteria could serve as an acceptable basis of judging the capability of rectangular section columns to perform during biaxial bending as a part of the design process.

Unfortunately, successful design of columns to resist multi axial load, presupposes an understanding of biaxial response and a biaxial analysis capability. At the present the behavior under randomly oriented cyclical biaxial loading in the inelastic range is just beginning to be interpreted, and existing analysis procedures are lacking in ability to simulate important characteristics of behavior, or are computationally too complex and expensive. While various means have been suggested for evaluating the capacity of columns under biaxial bending [32-34], load-deformation relations are still not understood well enough to describe mathematically.

When modelling reinforced concrete, degradation of the uniaxial mathematical moment vs. curvature or rotation stiffness rule is necessary. The uniaxial concrete beam modelling element used in the correlation analysis had a fairly sophisticated mechanism for including degradation. However, there are no available guidelines for determining or predicting what the characteristics of the degradation should be. Selecting parameters to define the elements' mathematical degradation rule was partly a matter of guesswork. While the stiffness rule incorporated into the element which was used (modified Takeda) is able to model general moment-curvature non linear degradation, it cannot model the effects of bar slip or end rotation after large cracks have formed and the actual hysteresis loops begin to show a pinching type behavior as the moment reverses, associated with less energy dissipation, which some of the column loops started to show near the end of the response.

It is necessary, particularly for reinforced concrete, to consider the effect of axial force interaction on the bending yield moments and on the instantaneous bending stiffness. Certainly there are structural analysis packages, such as ANSR-I and ANSR-II,[18],[19], available with 3D capabilities allowing correct combination of column axial forces from multi-dimensional overturning, and with column elements available which have bi-axial bending and 3D yield surfaces. However, they do not have stiffness degrading characteristics, which may be as important as axial interaction.

The results of *Chapter 7* Indicate the obvious necessity of including biaxial bending interaction effects, as well as those of axial loading, in a proper modelling process. Elements have been proposed and tested in various correlation studies (see *Appendix A*) which have multi-axial interaction and simulate degradation. Probably the most attractive approach, because of its seeming simplicity and elegance, was proposed by Takizawa and Aoyama [20]. The model is of a degrading tril-linear envelope type. Interaction and degradation is achieved through definition of biaxial moment vs moment cracking amplitude and yield amplitude curves which translate and expand during loading. Such an element would be expected to give good results for member cross sections which are circular and have axisymmetric steel location with the reinforcing continuous, or at close discrete spacing around the axis. With a deviation to a square section (which is the closest quadrilateral fit to a circular section) and reinforcing at wider discrete intervals, the results should be acceptable but not as accurate as in a circular case. However, when the section becomes rectangular with a well defined strong and weak axis and widely spaced discrete reinforcing, such as the columns in the present test, it is doubtful whether the model would be appropriate. Simulation of the yielding and residual straining of widely spaced discrete bars, leaving cracks open and creating rocking effects in the weak direction, as described in the analysis of local behavior in *Chapter 7* could not be expected of such a general element. Such local phenomena may be fairly unimportant, however, when in an analysis of a structure with numerous members the overall global behavior is desired, since the irregularities in any single column tend to be masked when combined to define the total lateral load vs. displacement characteristics of the structure.

If simulation of individual column behavior is desired, particularly for an irregularly shaped cross section, the 'finite filament' approach used by Aktan [27] and others [22,26] is preferable. In that method the column cross section is divided into multiple small areas, defining filaments which run the length of the column. Thus each rebar within the section may be modelled separately since the behavior rule for the material in any of the individual area segments may be specified explicitly. In this manner concrete cracking, crushing, and spalling, rebar yield, elongation and buckling may all be simulated. Effects of dynamic straining can be implemented as well by inclusion of appropriate visco-elastic properties. A deflected shape is assumed for the member axis, from which curvature and restoring forces may be calculated based on the individual stress- strain characteristics of the filament materials. The disadvantage of such a method is in the tremendous complexity that is introduced into the analysis process. Computing time and cost become excessive.
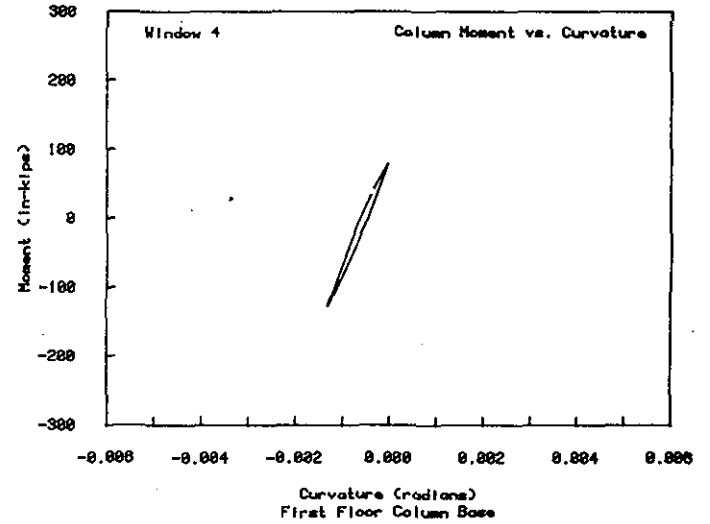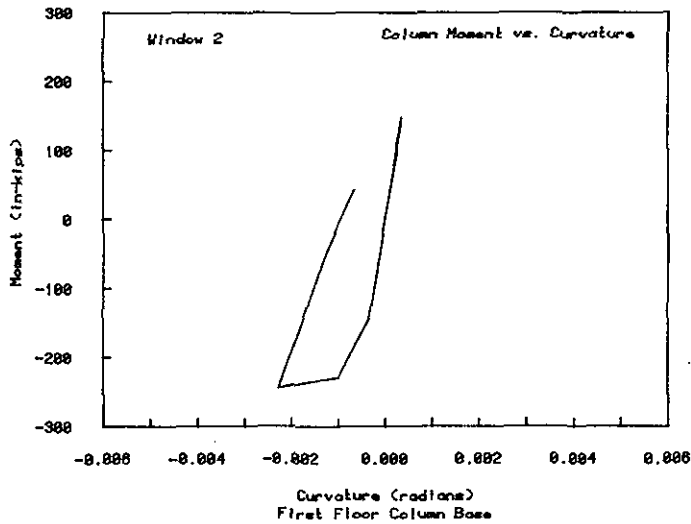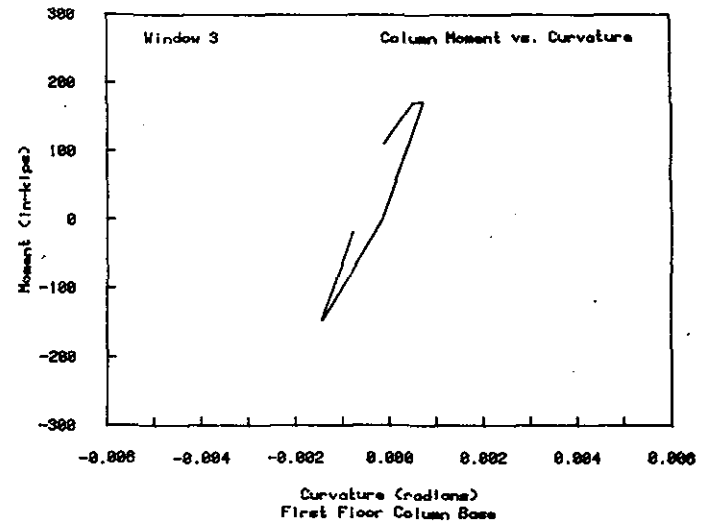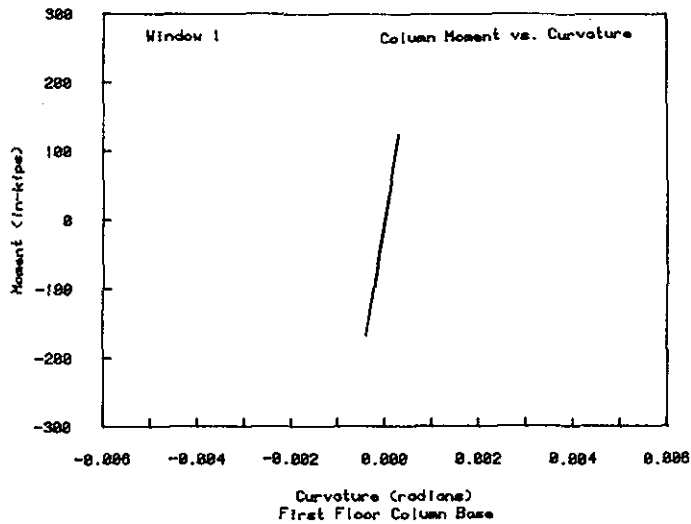
Figure 8.19 *Analytic moment vs curvature for NA column, strong axis, third run- T1000, separated into sequential "windows" as used in Chapter 7.*

130

Window 8 — Column Moment vs. Curvature
Curvature (radians)
First Floor Column Base
LONGITUDINAL INELASTIC

Window 5 — Column Moment vs. Curvature
Curvature (radians)
First Floor Column Base
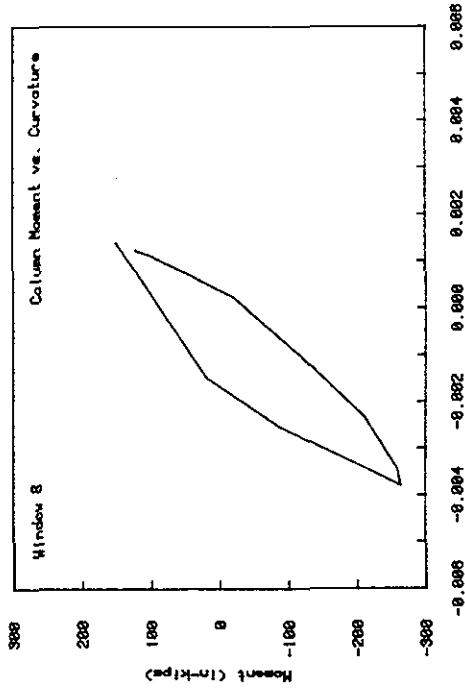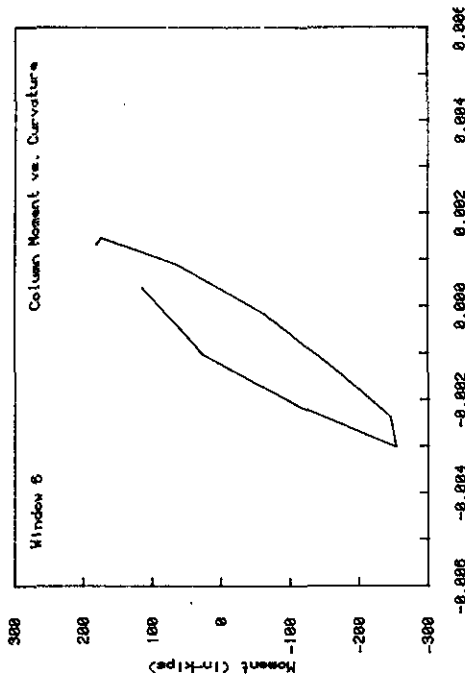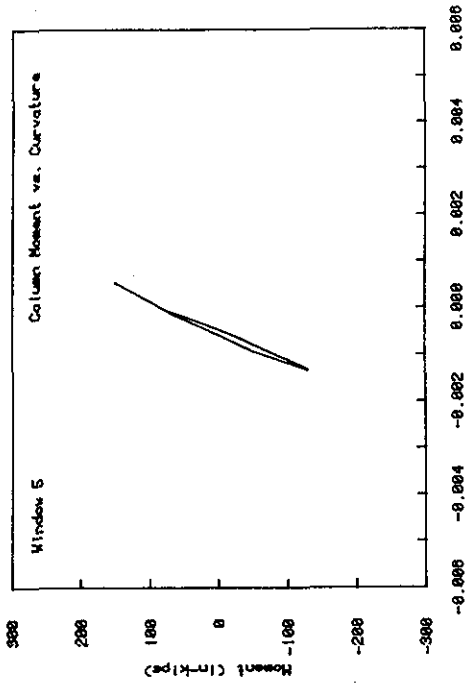
Window 6 — Column Moment vs. Curvature
Curvature (radians)
First Floor Column Base
LONGITUDINAL INELASTIC

Chapter 9

Summary:
Observations, Conclusions, Recommendations

The two story reinforced concrete frame was mounted on the shaking table at a skew angle to induce multiaxial response during testing under earthquake motions. Though the shaking table only had a single horizontal component of motion, the structure responded to different facets of the excitation along its two principal axes, since the lateral natural vibration frequencies in the two axis directions differed.

A weak column-strong girder design was used for the frame. Biaxial moments, deformations and their interrelation were the prime quantities under investigation in the test program and provided a major influence on the overall structural response. Two initial low amplitude tests (accel. 0.06g) were followed by a large amplitude motion (0.68g) using displacements derived from the Taft 1952 earthquake record. Additional testing and repair followed but the investigation of the present program was limited to the former.

The frame's dynamic response was recorded through 140 transducers of various types. Visually apparent damage was noted and frequency tests were conducted after each earthquake sequence. Considerable biaxial effects were detected and the experimental data for a particular column was subjected to detailed analysis to determine mechanisms of the interaction. Catastrophic collapse did not occur, rather, failure was the result of excessive deformation and stiffness degradation.

A brief mathematical vs experimental correlation study was attempted. Independent planar frame analytic models were used in the directions of the frame's two principal axes to simulate the response of the 3-D structure. The second small amplitude earthquake test was simulated using modelling behavior which was linear elastic. The large amplitude test was simulated using behavior with stiffness degrading characteristics.

131

Observations:

Since most existing structures that are susceptible to damage in an earthquake are not instrumented to indicate probable extent, physical observations might be used as a means of judging the degree of destruction. Visual observation did serve to locate possible areas where damage had occurred. However, it was difficult to ascertain whether such damage was superficial or serious. The visible condition certainly did not provide an accurate estimate of the extent of damage after the first Taft 1000 signal. Cracking occurred at the ends of the first floor columns where measured response data indicated the development of inelastic deformation. Very little spalling was seen, yet the strain values indicated corners at the base of the column had reached levels of 0.015, much beyond the crushing strain for unconfined concrete. Probing in the areas of cracking or the chipping away of crushed pieces would make a visual judgement more accurate. This was not undertaken here because further testing, e.g. the Pacoima record as an aftershock, was planned for the damaged frame.

The change in natural frequencies of the structure, as measured before and after each shake, served as an indicator of the model's stiffness. This between test variation, in the lateral displacement vibratory modes, was indicative of damage but provided no information about the type, extent, or location. From the small T100 (2) to the large T1000 tests, natural frequency in the longitudinal direction declined 45%, while the bending stiffness at the lower column bases decreased by over 80%. No interpretation of this frequency decrease could lead directly to a judgement of either column stiffness degradation or damage.

A combination of visual information and frequency measurement provides a definite asset when conjoined with mathematical analysis of a damaged structure. Visual inspection can indicate where inelastic deformation may have occurred (and with probing may give some measure of extent), allowing a mathematical model to be assembled with inelasticity developing in the correct locations. Correlation between measured and predicted frequency should develop when the correct local stiffnesses are selected. These stiffnesses serve as indirect indicators of damage in individual load resisting members of the structure.

A comparison of frequency and changes in frequency during tests on this frame and a previous one, which had only uniaxial displacement, showed that greater frequency shift and accompanying stiffness degradation developed during the present test. In the large Taft 1000 earthquake, the biaxial frame's longitudinal first mode frequency declined from 3.46 to 1.86 Hz, a decrease of 46%, while the uniaxial frame's longitudinal frequency varied from 3.13 to 2.03 Hz, a decrease of 35%. The larger drop in frequency during the biaxial test was attributable to greater stiffness degradation caused by non elastic deformation and damage under the combined multi-axial loading.

An interaction effect of combined loadings in a structure undergoing inelastic motion was immediately apparent when the deformation histories of the uniaxially displaced frame were compared to those of the biaxial frame. The first floor longitudinal displacement histories of the two frames were nearly identical during the initial 6 seconds of the test (Fig. 6.18) Then at 6.2 seconds, the present biaxial frame had simultaneous peak displacements along both its principal axes while the columns were in an in-elastic yield state. Additional damage and stiffness

deterioration developed, greater than that in the uniaxial frame, as evidenced by a decrease in frequency relative to and subsequent motion disjoint from the uniaxial frame's history.

The overall stiffness and strength along the longitudinal axes of the two frames were compared by plotting the column shear vs. first floor displacement. The structures showed identical initial shear-displacement stiffness. Interaction effects in the bi-axial frame were apparent as:

1   lower yield levels than in the uniaxial frame,

2   *greater stiffness degradation,*

even though the individual materials in the biaxial frame had slightly higher yield and/or ultimate strengths.

The resultant column shear force, obtained by vectorially combining the simultaneous shears along the two column principal axes, was 15% below the maximum shear resisted in the uniaxial frame. These results indicate that biaxial loading reduces the total column lateral load capacity (controlled by bending strength in the present case).

The response along the weak direction of the rectangular section columns was severely affected by motions along the strong axis. This significant result of multiaxial force interaction in rectangular columns during inelastic motion became apparent from column shear vs displacement and column local end moment vs. curvature data plots for the two principal column axes. The strong axis lateral restoring force characteristics, with normal yielding, hardening, strength and stiffness degradation, were generally similar to those seen previously in uniaxial lateral displacement tests. The restoring moment vs. curvature characteristics of the weak axis motion *became extremely irregular after initial inelastic deformation had occurred. Weak axis response* exhibited excessive stiffness degradation with intervals of apparent zero and negative bending stiffness.

The irregular behavior observed in the restoring force vs deformation history along the weak axis was attributable to:

1   -concrete cracking caused by combination of biaxial moments and axial loads,

2   -residual rebar deformation, primarily a result of bending yielding in the strong axis direction coupled with weak axis bending and axial load.

These conditions caused formation of unsymmetric section stiffness when concrete in only one corner was carrying compressive load or when a rebar in one corner was yielding. Residual bar deformation (elongation) intermittently left the entire concrete cross section cracked open and supported solely on the reinforcing bars. In such circumstances the column exhibited rocking in the weak axis direction when strong axis loads were changing, particularly when reversing direction, and caused formation of unexpected moments in the weak axis direction.

Unfortunately, the irregular low stiffness behavior in the weak axis direction, which developed without any obvious sign of yielding due to weak axis load, resulted in moment vs. rotation response having hysteretic loops with little enclosed area. Thus, the soft weak axis motion resulted from a local mechanism which did not have the energy dissipation qualities that are desirable in seismic design.

The effect of the extreme interaction measured in the column members was slightly masked when the differing restoring forces in all of the columns were summed and the overall

base shear vs. lateral displacement response was inspected (Figure 7.5b). While the particular irregularities noticed in the response of specific columns are not clearly visible, the general shape of the hysteresis response still clearly shows pinching characteristics indicative of low energy absorption.

Axial loads, developed within the columns due to dynamic overturning moments, were quite sizable and in fact were not typical of a low rise structure. Axial compression reached a maximum of five times the dead load compression, and axial tension developed at certain times. The large axial force variation was created through a combination of overturning moments in the transverse direction, being resisted by columns at a very close spacing (3 ft.), plus the additional axial components from longitudinal overturning, which had also existed in the uniaxial frame. Axial force remained slightly below the "balanced point" of the column axial vs. moment interaction diagrams when under the maximum compression load.

Yield load level, ultimate bending strength, and effective lateral stiffness of the columns were dependent on the simultaneous axial load resisted within the column. The yield moment capacity varied from 277 in-kips with 40 kips axial compression, to 156 in-kips with 5 kips axial tension for strong axis bending and from 169in-kips to 94in-kips, under similar axial load, for weak axis bending. After initiation of cracking and accumulation of residual elongation, existence of axial load could determine whether the section remained with open cracks or closed with effective concrete. This considerably affected section stiffness, especially when under low bending or during moment reversals. Inspection and comparison of the response of various columns under similar deformation indicated that when high axial compression existed in the column, higher lateral load resistance was developed prior to yielding and increased stiffness was apparent.

Relatively high strain rates under the earthquake excited motion occurred in the reinforcing bars. Strain rates as high as 22% per second in the rebars allowed development of strength beyond that elicited from slow rate or "statically" tested material behavior. Correct estimation of member strength would require visco-elastic modelling to include strain rate effects. Statically predicted strengths are, however, generally acceptable in their conservative quality.

An approximate maximum displacement ductility of 2.4 was developed, during the strong amplitude shake, in the structure's longitudinal axis direction. In the transverse, (weak), axis direction quantitative definition of ductility, the ratio of maximum displacement to yield displacement, tends to be meaningless or at least misleading. While column lateral stiffness decreased by two thirds during the test, resulting in large lateral displacements, there was very little actual 'yielding' in the weak axis direction. That ductility implies the occurrence of yield deformation is deceptive in a situation where the development of large deformations along a particular axis is a result of multi-axial interaction without yielding along that axis.

Correlation between the measured structural first floor displacements and those predicted through a mathematical modelling procedure were fairly good for the initial small earthquake test. Predicted displacements along the longitudinal axis were within 11% of each other (0.108 in. experimental vs. 0.120 in predicted, first floor) with excellent agreement in frequency. Transverse displacements could have been just as accurate with a slight modification in the

estimated damping. Frequencies were in good agreement. During that test, the actual frame essentially responded in a low amplitude elastic manner. The analysis procedure simulated response of planar frames oriented along the two axes of the structure independently. The success of such independent modelling indicates that interaction of motions along the frame's principal axes had only minor effects on the overall response under small motion. While good correlation was possible using easily calculated member section properties, poor judgement in estimating the correct status of the section (ie, cracked, uncracked) resulted in prediction of displacements which were 20% low and at an incorrect frequency in one case.

The correlation between mathematically predicted and measured response under the T1000 excitation was poor. The analysis again used two independent planar frames. The longitudinal analysis predicted a first floor displacement of 1.79 in. while the measured maximum was 2.21 in., a 16% error. Local member behavior generally followed the experimental reality. In the transverse axis first floor displacement was 68% of the measured. Frequency matching was quite poor, final measured frequency was 0.95 Hz and the analytic model's was 1.34 Hz. Individual column bending resistance was modelled with a uniaxial inelastic degrading stiffness relation. The analysis did not include the effects of biaxial simultaneous moments and axial load on yield level or stiffness, and did not include strength deterioration, reinforcing bar slip or joint deformation. Degradation in the stiffness of the analytical model could not reach the amount caused by such simultaneous loading and deformation mechanisms, which were induced in the actual test frame. Moreover, the uniaxial degrading stiffness relation used required selection of descriptive parameters for which no estimation guidelines exist, resulting in a guessing procedure.

Conclusions

Biaxial lateral loading effects:

Biaxial bending of reinforced concrete members can be expected to decrease the resultant lateral (bending) stiffness. The combined bending moments cause higher strains to occur in corner rebars with higher residual strains after yielding. Combined concentrated strains in the corner concrete areas are likely to initiate crushing and spalling of unconfined concrete and crushing of confined concrete, with associated section strength deterioration, earlier than under uniaxial loading.

Biaxial bending interaction should be particularly considered in the design and analysis of <u>rectangular</u> columns to be used in moment resisting concrete frame applications subject to lateral cyclic loading. Even when 'strong column-weak girder' design is employed, biaxial over-load causing inelastic deformation may be serious, since the columns of a moment resisting frame will have induced loading from motion along both of the structure's horizontal axes, additional lateral displacement from structural torsion and axial load cause by overturning moments. The results of the tests described herein show that motion along the strong axis of a rectangular section may cause damage and section deterioration which can significantly decrease the weak axis stiffness, resulting in excessive unexpected deformation in that direction under low loads. Unfortunately, such behavior is specifically associated with pinched load deformation hysteresis loops providing a decreased energy dissipation mechanism.

Since weak axis stiffness, under low load, may rely solely on the rebar after concrete cracking and bar residual elongation have developed in the columns, the rebars on the opposing weak axis faces should be placed with as long a distance between them as possible.

Weak axis stiffness degradation and rocking effect noted in the tests, could be reduced by placement of additional reinforcing bars at the center of column faces, particularly along the weak axis column faces, rather than concentrating the steel at the corners where it is more effective in resisting moment because of the high corner straining during biaxial bending. Intermediate bars, at the centers of the weak axis faces, would not yield and develop residual elongations under strong axis bending at the load levels which initiate yielding in the bars at the strong axis faces. Intermediate bars would then serve as ties, tending to constrain the amount of concrete crack opening in the initial strong motion cycles and to reduce the likelihood that all of the bars in a section would develop residual strains due to motion along either axis, while allowing energy dissipation to occur in the highly strained and yielding corner bars. Such a policy, of distributing rebars at close intervals about the periphery, has been recommended as a means of increasing the overall ductility of concrete sections as well.

Mathematical analysis with multi axial loading:

Based on the observed member behavior and attempted correlation studies, an accurate analysis procedure for a reinforced concrete structure under multi-axial loading would require:

a)   3 dimensional structural modelling with coupled simultaneous multiaxial forces and degrees of freedom,

b)   individual member simulation with response behavior rules specifically incorporating:

1.   an inelastic moment-rotation with stiffness degradation,

2.   the effects of biaxial moment and axial load on defining the bending yield level, ie. definition of a yield surface,

3.   axial load effects on increasing or decreasing the effective bending stiffness,

4.   explicit memory of previous yielding and the concrete crack opening status,

5.   a deteriorating strength envelope, particularly if high axial loads exist, which could include the deteriorating effects of concrete crushing and spalling.

In addition to these primary components of biaxial bending response, various other structural mechanisms, such as joint deformation, rebar slip, and visco-elastic simulation to include strain rate effects, could be integrated into the analysis technique. In the present study, inclusion of joint deformation, rebar slip and load interaction could have reduced the 16% error in longitudinal response to the 5%-10% range at the expense of considerably more money and modelling complexity. Transverse axis response, however, simply cannot be modelled reasonably at all without inclusion of load interaction as listed in a, b1, b2, and b4 above. The complexity of an analysis including these characteristics should be quite evident if compared to the correlation technique used in *Chapter 8* which was based solely on the criteria in b1 above.

Existing techniques embodied in computer analysis packages, such as those used in the correlation studies, include fairly sophisticated mathematical "elements" for modeling reinforced concrete beam behavior. The bending moment-bending rotation patterns incorporated in the elements simulate the general type of bending stiffness degradation often seen in reinforced concrete beam tests. The relative availability and apparent sophistication of such elements have made them attractive for commercial use in response analysis of structures under dynamic loading. Unfortunately, even the moderate complexity of the stiffness degrading rule of the present beam element requires definition of parameters for which no guidelines exist. Even with the experimental results in hand, selection of specific parameters was difficult and the resulting response predicted by the analysis varied considerably from the experimental measurements when a parameter was set incorrectly. Such element, or prescribed element behavior, should not be relied upon to predict possible structural response unless rational guidelines are developed to aid in establishing correct degrading parameters for the element behavior rule.

138

Recommendations

Recommendations, concerning use of existing computer assisted analysis programs, experimental and theoretical research, are listed in the order which indicates their priority as viewed by this author.

a) The excessive interaction of strong axis motion or weak axis response for the rectangular section columns was not entirely expected. Previous biaxial tests *(Appendix A)* have used square columns with equal, or nearly equal stiffness and strengths along both axes. Additional biaxial bending tests, pseudo-static, or dynamic and cyclical, should be completed on rectangular column components to verify the degree of strong axis interaction with weak axis behavior noted in the limited tests described herein. In addition to verification of the interaction mentioned, such a program could specifically investigate how variation in the ratio of sections dimensions in a rectangular column can:

-change the weak axis response to one having more favorable energy dissipation characteristics,

-affect when strong axis motion becomes predominant over weak axis response.

A second set of tests should determine how layout of reinforcing within a rectangular section can affect the behavior, again particularly looking for increasing energy dissipation and ductility.

b) Acceptable analytic modelling, as part of the structural design evaluation process, requires the establishment of a general set of guidelines or procedures for estimating the values to be assigned to the various parameters governing the form that the model behavior, in the present study stiffness degradation, will take. Methods of estimation should be based on the section layout and material properties, just as calculation of yield strengths is, not only for biaxial response, but also for existing uniaxial bending response rules. It would seem that a method similar to the finite filament technique, could be used which would model a member cross section divided into small segments of area. Each particular segment could be assigned independent stress-strain properties. Then a specific standard series of cyclic loads, dependent on the section uniaxial capacity, would have to be devised. If results from application of such loads on the analytic section model could be correlated with stiffness degrading characteristics of experimental tests using the same loading, a general rule for establishing characteristic parameters, using the section modeling technique with standard loading, might be developed.

c) Development of a three dimensional reinforced concrete beam -column element, for use in mathematical analysis, which includes 3 D force deformation response defined by multiaxial load levels (effects on stiffness and yield load) with stiffness degradation, will be necessary before accurate member load and deformation can be predicted analytically.

d) The modest analytic correlation program initiated here should be expanded. The ability of various more advanced analysis methods, such as proposed by Takizawa [21], to predict the response should be compared. Effects of inclusion of the various modelling parameters discussed previously (see Conclusions) should be measured, to determine if certain modeling

techniques have a major influence on improving predicted results. Attention should also be directed toward means of duplicating stiffness degradation due to biaxial interaction without causing inherent stability problems in the analysis itself, a result of frequently changing stiffness, which might necessitate use of small, unacceptably expensive, time steps in a dynamic step by step analysis algorithm.

e)   Additional study should be initiated concerning biaxial response behavior with axial loading, and p- Δ effects. The lowered stiffness and additional displacements due to multiaxial column interaction, which were measured in the structure's weak axis, may have important implications regarding creation of a possible failure or collapse situation when the p-Δ effect is important, as in high rise building structures. In the present tests, the column axial loads were low and the p-Δ effect was small. Computer assisted analytical simulation of earthquake response of medium high rise buildings should particularly assess stiffness deterioration effects on stability.

f)   Seismic testing of a similar frame with square column sections would be desirable to compare the earthquake induced response behavior of columns tied together in a frame with existing component result of square columns and to contrast the behavior with the present structure, which used rectangular columns and had a strong and weak axis. While individual component tests have indicated that increased permanent drift occurs under biaxial loading in the yield range, a structure with similar columns tested on the earthquake simulator may show reduced global residual drift due to differing loads in the various columns and slightly varying capacities forcing certain columns to yield before others,dissipating energy, and modifying the overall structural stiffness, which may change the manner of response before subsequent columns yield.

g)   Analytic and experimental studies of structures with multiple bays and frames undergoing biaxial motion should be attempted. Their purpose would be to determine if local response irregularities (as seen along the weak axis of columns in the present test) occurring in any specific rectangular column at a particular instant are significant in affecting the overall global displacement response of the structure. With the multiple column force resisting elements, the irregularities occurring in specific columns may be masked when the overall summed lateral resistance vs. displacement is considered. If so, analysis procedures which are incapable of explicitly modeling such irregularities as crack opening and rocking (e.g. plasticity type approach)may yet be able to predict the overall response of the structure.

Bibliography

[1] Clough, R., Gidwani, J., "Reinforced Concrete Frame 2: Seismic Testing and Analytical Correlation", Earthq. Engng Res. Ctr., EERC 76-15, University of California, Berkeley, 1976.

[2] Hidalgo, P., Clough, R., "Earthquake Simulator Study of a Reinforced Concrete Frame", Earthq. Engng Res. Ctr., EERC 74-13, University of California, Berkeley, 1974.

[3] Kent, D.,Park, R., "Flexural Members with Confined Concrete", *J. Struct. Div., ASCE*, V97, ST7, July 1971.

[4] Mahin, S., Bertero, V., "RCCOLA A Computer Program for Reinforced Concrete Column Analysis", Dept. of Civil Engng., University of California, Berkeley, 1977. †

[5] Rea, D., Abedi-Hayati, S., Takahashi, Y., "Dynamic Analysis of Electrohydraulic Shaking Tables", Earthq. Engng Res. Ctr., EERC 77-29, University of California, Berkeley, 1977.

[6] Jennings, P.,Shepard, R., "Experimental Investigations- Correlation with Analysis", Workshop on Earthquake Resistant Reinforced Concrete Building Construction, University of California, Berkeley, 1977.

[7] "Earthquake Response Spectra, Vol III, Part A", EERL 72-80, California Institute of Technology, Pasadena, 1972.

[8] "Strong Motion Earthquake Accelerograms: Vol II, Corrected Accelerograms and Integrated Ground Velocity and Displacement Curves, Part A", EERL 71-50, California Institute of Technology, Pasadena, 1971.

[9] Shoja-Taheri, J., "Seismological Studies of Strong Motion Records", Earthq. Engng Res. Ctr., EERC 77-04, University of California, Berkeley, 1977.

[10] Clough, R., Oliva, M., "Shear Failure of a Reinforced Concrete Frame Under Shaking Table Tests", Symposium on Nonlinear Behavior of Reinforced Concrete and Prestressed Concrete Structures , ACI Fall Convention, Houston, 1978.

[11] Vallenas, J., Bertero, V., Popov, E., "Concrete Confined by Rectangular Hoops and Subjected to Axial Loads", Earthq. Engng Res. Ctr., EERC 77-13, University of California, Berkeley, 1977.

[12] "Uniform Building Code", International Conference of Building Officials, Pasadena, California

[13] Kanaan, A., Powell, G., "DRAIN2D A General Purpose Computer Program for Dynamic Analysis of Inelastic Plane Structures", Earthq. Engng Res. Ctr., EERC 73-22, University of California, Berkeley, 1973. †

[14] "Building Code Requirements for Reinforced Concrete", (ACI 318-71), American Concrete Institute, Detroit, Michigan, 1971.

[15] Takeda T., Sozen M. , Neilson, N. "Reinforced Concrete Response to Simulated Earthquakes", *J. Struc. Div., ASCE,* V96 ST12, Dec. 1970

[16] Clough, R., Oliva, M., "Shaking Table Tests of an R/C Frame with Column Shear Failure", Earthq. Engng. Res.Ctr., EERC report, University of California, In prep.

[17] Ghanaat, Y., "Study of X Braced Steel Frame Structures Under Earthquake Simulation", Earthq. Engng Res. Ctr. EERC 80-08, University of California, Berkely 1980

[18] Mondkar, D., Powell, G., "ANSR-I General Purpose Program for Analysis of Nonlinear Structural Response", Earthq. Engng Res. Ctr., EERC 75-37, University of California, Berkeley, 1975.†

[19] Mondkar, D., Powell, G., "ANSR-II Analysis of Nonlinear Structural Response", Earthq. Engng. Res. Ctr., EERC 791-17, University of California, Berkeley, 1979

[20] Takizawa, H., Aoyama, H., "Biaxial Effects in M odelling Earthquake Response of R/C Structures", *Int. J. Earthq. Engng. Struc. Dyn.,* V4, 1976

[21] Takizawa, H., "Biaxial and Gravity Effects in Modelling Strong Motion Response of R/C Structures", *Proc. 6th Wld Conf. Earthq. Engng.,* New Delhi, 1977

[22] Takiguchi, K., Kokusho, S., "Hysteretic Behavoir of Reinforced Concrete Members Subject to Biaxial Bending moments", *Proc. 6th Wld Conf. Earthq. Engng.* New Delhi, 1977

[23] Padilla-Mora, R., Schnobrich, W., "Non-linear Response of Framed Structures to Two-Dimensional Earthquake Motion", Civ. Engng. Studies, Struct. Res. Series Report No. 408, University of Illinois, Urbana, 1974

[24] Pecknold, D., Sozen, M., Calculated Inelastic Structural Response to Uniaxial and Biaxial Earthquake Motions", *Proc. 5th Wld Conf. Earthq. Engng.,* Rome, 1973

[25] Aktan, A., Pecknold, D., Sozen, M., "Effects of Two-Dimensional Earthquake Motion on a Reinforced Concrete Column", *Civ. Engng Studies, Struct. Res. Series Report No. 399,* University of Illinois, Urbana, 1973

[26] Okada, T., Seki, M., Asai, S., "Response of Reinforced Concrete Columns to Bi-Directional Horizontal Force and Constant Axial Force", *Bul ERS,* No. 10, University of Tokyo, 1976

[27] Aoyama, H., Sozen, M., "Dynamic Response of a Reinforced Concrete Structure with 'Tied' and 'Spiral' Columns", *Proc. 5th Wld Conf. Earthq. Engng.,* Rome, 1973

[28] Karlson, B., Aoyama, H., Sozen, M.,"Spirally Reinforced Concrete Columns Subjected to Loading Reversals Simulating Earthquake Effects", *Proc. 5th Wld Conf. Earthq. Engng.,* Rome, 1973

[29] Pecknold, D., Inelastic Strcutural Response to 2D Ground Motion", *J. Engng. Mech. Div., ASCE,* V100, N5, Oct. 1974

[30] Suharwardy, M., Pecknold, D., "Inelastic Response of Reinforced Concrete Columns Subject to Two Dimensional Earthquake Motions", Civ. Engng. Studies, Struct. Res. Series Report No. 455, University of Illinois, Urbana, 1978

142

[31] Pecknold, D., Suharwardy, M., "Effects of Two Dimensional Earthquake Motion On Response of R/C Columns", Wrkshp on Earthq. Rstnt. R/C Bldg. Const., University of California, Berkeley, 1977

[32] Row, D., "The Effects of Skew Seismic Response on Reinforced Concrete Frames", Mstr. of Engng. Thesis, University of Canterbury, Christchurch, New Zealand, 1973

[33] Pannell, F., "Failure Surfaces for Members in Compression and Biaxial Bending", *J. Am. Conc. Inst.*, V60 N1, Jan. 1963

[34] Bresler, B., "Design Criteria for Reinforced Concrete Columns under Axial Load and Axial Bending", *J. Am. Conc. Inst.* V32 N5, Nov. 1960

[A1] Ferguson, P., Reinforced Concrete Fundamentals, 3rd ed., John Wiley & Sons,

[A2] Park, R., Paulay, T., *Reinforced Concrete Structures,* John Wliey & Sons, 1975

[A3] Nigam, N., "Inelastic Interactions in the Dynamic Response of Structures", EERL 67-64, California Institute of Technology, Pasadena, 1967

[A4] Selna, L., Lawdor, H., "Biaxial Inelastic Frame's Seismic Behavior", ACI Special Publication, SP-53-17, 1977

[B1] Darwin, D., Pecknold, D., "Inelastic Model for Cyclic Biaxial Loading of Reinforced Concrete", Civ. Engng Studies, Struct. Res. Series No. 409, University of Illinois, Urbana, 1974

[B2] Kent, D., Inelastic Behavior of Reinforced Concrete Members with Cyclic Loading", PhD thesis, University of Canterbury, Christchurch, New Zealand, 1969

[B3] Blume, J., Newmark, N., Corning, L., "Design of Multistory Reinforced Concrete Buildings for Earthquake Motions", Portland Cement Assoc., Skokie, Ill. 1961

[B4] Sargin, M., "Stress Strain Relationships for Concrete and the Analysis of Concrete Sections", SM Study Series N4, Univrsity of Waterloo, Waterloo, Ontario, 1971

[B5] Vallenas, J., Bertero, V., Popov, E., (see [11])

[B6] Karr, P., Corley, W., "Porperties of Confined Confined Concrete for Design of Earthquake Resistant Structures", *Proc. 6th Wld Conf. Earthq. Engng.,* New Delhi, 1977

[B7] Kent, D., Park, R., (see [3])

[B8] Mahin, S., Bertero, V., (see [4])

[B9] Clough, R., Gidwani, J., (see [1])

[B10]Ma, S., Bertero, V., Popov, E., "Experimental and Analytical Studies on the Hysteretic Behavior of Reinforced Concrete Rectangular and T-Beams", Earthq. Engng Res. Ctr., EERC 76-2, University of California, Berkeley, 1976

[B11]Park, R., Kent, D., Sampson, R., "Reinforced Concrete Members with Cyclic Loading", *J. Struct. Div. ASCE,* V98, ST7, July, 1972

[B12]Aktan, A., Karlsson, B., Sozen, M., "Stress-Strain Relationships of Reinforcing Bars Subjected to Large Strain Reversals", Civ. Engng. Studies, Struct. Res. Series No. 397, University of Illinois, Urbana, 1973

[B13]Kanaan, A., Powell, G., (see [13])

† *Distributed through Natl. Inf. Serv. Earthq. Engng., Univ. of Calif., Berkeley*

144

List of Symbols

f_c = maximum stress of concrete test cylinder,

ϵ_c = strain at max. stress f_c,

f_u = ultimate tensile stress of steel bar,

f_y = yield stress of steel reinforcing bar,

M_u = ultimate moment capacity of a section,

M_y = capacity of section when yield starts,

E_{sh} = approximate Young's Modulus during strain hardening,

E_c = Young's modulus for concrete,

ϵ_{sh} = strain at which strain hardening starts in steel,

ϵ_{su} = ultimate strain in steel bar,

ϵ = strain,

ϵ_{cu} = ultimate strain in concrete cylinder test,

ω^2 = rotational frequency,

ν = Poisson ratio

M_{NS} = moment in the north-south direction,

M_{EW} = moment in the east-west direction,

I_{neg} = moment of inertia of a beam in negative bending,

I_{pos} = moment of inertia of a beam in positive bending,

I_x = moment of inertia in the x-axis direction,

I_y = moment of inertia in the y-axis direction,

α β η, = parameters to describe the stiffness degrading spring model,

Δ = lateral displacement,

P = axial force,

Appendix A

Previous Studies of Biaxial Bending in Reinforced Concrete

Capacity with biaxial bending

The non homogeneous character of reinforced concrete sections, concrete combined with discreet steel bars, and the low strength capacity of concrete in tension, make design and analysis more difficult than with most structural materials. Symmetric section design and assumption of no tensile strength for concrete have facilitated design and capacity analysis for uniaxial bending. However, with biaxial bending, location of the neutral axis, which will no longer be parallel to the section's principal axis, and determination of strain distribution become much more difficult. Bresler [34] suggested a general non-dimensional interaction equation which describes a load contour capacity curve relating the simultaneous moments acting along a rectangular section's principal axis when under a given axial load. Pannell [33] developed two equations which define the biaxial moment failure curve in association with any axial load, and include a flattening effect when combined moments create bending along a diagonal to the section's principal axes. As part of a master's thesis, Row [32], authored a computer code to solve the biaxial moment-axial load interaction equations of section capacity and plotted a set of design interaction curves. Basic methods of analyzing sections for capacity under biaxial bending are reviewed by Ferguson [A1] and Park and Paulay [A2].

Experimental investigation of load vs deformation

Though column capacities may be defined by a 3D moment vs moment vs axial load failure surface, as described in the previous section, prediction of the response of a structure under multiaxial loading requires an understanding of the deformations which will be associated with biaxial loading. To this end, researchers have recently begun testing reinforced columns under cyclical biaxial displacement traces to simulate earthquake loading. Karlson et al [28] completed a series of tests on six specimens modelled after spirally reinforced columns damaged under biaxial bending in the Olive View Medical Center during the San Fernando earthquake. However, the tests were with cyclic uniaxial motion. Takiguchi and Kokusho [22] undertook pseudo static testing of 26 square columns with biaxial bending. Constant bending moment was maintained along one of the section's principal axes while reversing moments were applied in the orthogonal axis. Restoring force characteristics about the varying load axis and deformation along the constant moment axis became unstable in cases where large moments were applied. Okada, Seki and Asai [26] tested six square reinforced concrete columns with uniaxial (along principal axis), diagonal (to principal axes), elliptical and circular

displacement traces. They noted significant strength deterioration and loss of ductility due to the biaxial loading. Takizawa and Aoyama [20] referred to a series of tests carried out by Aoyama, Fuji, Umemura and Itoh at the University of Tokyo. Five specimens, square cantilever columns, with constant axial compressive load, were subjected to uniaxial, diagonal, diamond and rectangular shaped (with respect to the section's principal axes) cyclic displacement traces. The restoring force showed distinctive characteristics, most normally not seen in uniaxial tests, such as decrease in restoring force along one axis with constant displacement while movement along the orthogonal axis varies. As would be expected, the square columns exhibited similar behavior along each axis and generally maintained open load-deflection hysteretic loops characteristic of an energy absorbing mechanism. Jirsa, at the University of Texas, has partially completed a test program concerning biaxial bending of square columns which will involve future testing of rectangular concrete columns.

Response analysis

Prediction of the load deformation response of columns under inelastic biaxial bending through mathematical analysis has recently been attempted. Aktan, et al. [25] devised a computer implemented approach to the analysis of column response under multi-axial loading, referred to as a "finite filament method". The column section is divided into numerous small segments of area. Each segment forms an individual prism with the length of the column. Stress-strain properties, such as those of unconfined concrete, confined concrete and the steel rebars, may be specified for each particular filament. The load displacement relation for a column of multiple filaments is then obtained by assuming a general displaced shape. Several check points are established along the length of the column and the geometry of the prescribed displaced shape is used to relate internal deformation at the checkpoints to end displacements, providing a means of stiffness formulation. Comparing the predicted response of a lumped mass on the column system using this biaxial finite filament method with traditional analyses, Aktan determined that predicted 2D response to an earthquake motion exceeded uniaxial predictions by 20 to 200% if the calculated motion of the latter was more than twice the crushing deflection. Okada, et al. [26] used a similar method of analysis and compared predicted results with experimental restoring forces. Given the experimental displacement trace, this analytic model was able to predict restoring forces which matched the experimental results fairly well, except when loading was along the diagonals. Takiguchi and Kokusho reported similar results using a finite filament model in correlation studies with square column tests. Suharwardy [30] simplified the method used by Aktan and reported similar results.

A second general approach to biaxial analysis depends on the definition of a biaxial moment yield curve. Nigam [A3], using this plasticity approach, defined a limiting yield curve for the simultaneous biaxial moments in his column elements. Results indicated that lower yields could be expected under biaxial bending, and permanent drift developed at lower levels of excitation. The increased drift was partly a result of using elastic-perfectly plastic stiffness. Under earthquake motion, his modelling studies suggested that redistribution of energy can be expected when inelastic interaction develops. Nigam postulated that the normal reduction in

stiffness of a structure, due to yield initiation in specific localities as the overall load- displacement relation moves from elastic stiffness to post-yield hardening, may have a significant effect on response prediction. Various other authors have used a similar approach, based on classic plasticity theory, to define the overall yield condition of a member under multi-axial loads [23, A4]. Takizawa and Aoyama [20] extended the plasticity model by using a degrading tri linear moment-rotation stiffness. In addition to the circular or elliptical yield curve, the model used an inscribed cracking curve which defined both cracking and changes in stiffness as functions of the biaxial moments. The elliptic yield curve was allowed to expand as strain hardening and permanent deformation developed after yield. Upon reversal of loading at a point beyond yield, the stiffness degrades in inverse proportion to the post yield deformation amplitude; the unloading and reloading curve is aimed at the maximum deformation point experienced in the opposite direction . Response, predicted with the analytic model, agreed fairly well with results from a set of biaxial column tests. However, in cases where the square cantilever columns were subjected to rectangular and diamond shaped displacement traces, in the plane perpendicular to the member axis, certain discrepancies appeared between the measured and the analytically predicted restoring forces. Under the diamond shaped deflection path, the analytic hysteresis loops were too broad, and with the rectangular path, they were too narrow when compared with the experimental load deflection curves. In both cases, the restoring forces during the virginal displacement trace were overestimated and slightly underestimated in subsequent cycles by the mathematical model. Some inaccuracies were attributed to deviations in the actual displacement traces of the experimental specimens, others may have resulted from incorrect estimates of controlling parametres in the analytical model itself. The experimental results and analytical correlations were based on 3 to 5 cycles of high deformation, while earthquake excited response may involve more cycles of inelastic deformation resulting in considerably higher stiffness and strength deterioration. Takizawa [21] later created a quadrilinear stiffness model which added post crushing stiffness to the tri linear curve proposed previously. Crushing was again defined by an elliptical curve, relating the simultaneous biaxial moments, which contracts and translates in the moment-moment plane. Takizawa additionally included p- Δ effects in reducing the failure level of columns under multi-axial loading. Biaxial effects were found to reduce significantly the input intensities needed to develop ultimate failure. None of the plasticity studies have included varying axial load interaction on definition of yield curves, and the yield curves do not include flattening of sides as mentioned earlier.

Appendix B

Material Tests
Section and Response Calculations
Design Dimensions

Material properties

Reinforcing bar tests

Samples of all the types and sizes of reinforcing steel bars were tested under slow pseudo-static rates of applied axial tension. The specific mechanical quantities measured from analog load deformation plots included:

a.) Young's modulus of elasticity (E) which defines the linear relation between stress and strain under low magnitude elastic stress, stress = E x strain

b.) yield stress, maximum stress beyond which a linear stress-strain relation does not apply,

c.) the strain value, ϵ_{sh}, beyond which strain hardening starts and stresses increase significantly above yield,

d.) the ultimate stress, f_u, whereupon the the steel suffers a tensile rupture,

e.) strain level at which ultimate stress is reached.

The load deformation plot allowed development of a means of approximately describing the stress-strain relation in the strain hardening region as well.

The specimens were pulled in a universal testing machine with axial deformation measured by linear variable differential transformer devices attached to the bars with a two inch gauge length. Results of the individual tests are listed in the following tables.

Table B.1

Tests for Young's Modulus				
	(bar diam. machined to improve grip in test machine)			
original bar type	specimen label	specimen diam. (in.)	average area ($in.^2$)	measured E (ksi)	average E (ksi)
No. 5	A	0.5024	0.1982	30660	
	B	0.5068	0.2017	31230	30880
	C	0.4999	0.1962	30740	
No. 4	A	0.4212	0.1393	30120	
	B	0.4146	0.1350	32450	31080
	C	0.4189	0.1378	30620	
No. 3	A	0.3470	0.0945	28650	29200
	B	0.3530	0.0979	29750	
No. 2	A	0.2570	0.0519	30900	31460
	B	0.2511	0.0495	32030	
Mesh	A	0.2301	0.0416	28800	27600
	B	0.2299	0.0415	26390	

Table B.2

Ultimate Load Tests on Rebars					
bar type	area ($in.^2$)	yield load (kips)	ultimate load (kips)	yield stress (ksi)	ultimate stress (ksi)
No. 5	0.31	15.20	24.5	49.0	79.0
		15.06	24.7	48.6	79.7
		-	24.8	-	80.0
No. 4	0.20	9.74	14.76	48.7	73.8
		9.94	14.73	49.7	73.6
		-	14.76	-	73.8
No. 3	0.11	6.24	8.82	56.7	80.2
		6.24	8.82	56.7	80.2
		6.24	8.80	56.7	80.0
No. 2	0.0498	-	4.22	-	84.7
	0.0519	2.96	4.32	57.0	83.2
	0.0495	2.94	4.32	59.3	87.2
Mesh	0.0230	1.71	1.92	74.2	83.4

Table B.3

Rebars- Inelastic Parameters			
bar type	average ϵ_{sh} (in/in)	average ϵ_{su} (in/in)	approx.* E_{sh} (ksi)
No. 5	0.0090	0.121	1170
No. 4	0.0160	0.121	838
No. 3	0.0185	0.093	902
No. 2	0.0021	0.072	783

* E_{sh} = based on stiffness at onset of strain hardning.

Concrete cylinder tests

Fourteen concrete cylinders, 6in.x12in. (15.2x 30.5cm), were taken during the pouring of the model structure. The cylinders were stored in similar atmospheric conditions to the model. Compression tests, at a standard load rate of 1000 lbs. (4.45 kN) per second, were completed at 7 days, 14 days, 28 days, and near the time of the structural model tests, at 244 days. Three of the cylinders tested at 244 days were fitted with linear variable differential transformers (LVDT's) to measure axial deformation over an 8 inch gauge length and produce an analog plot of load versus deformation from which the initial elastic Young's modulus, strain at maximum $= \epsilon_c$, and strain of the ultimate or crushing load, $= \epsilon_{cu}$, could be measured. Additional LVDT's measured deformation along the radii of the cylinder to define an effective Poisson ratio $= \nu$. Results of the cylinder tests are listed in Table B.4.

Concrete Cylinder Tests				
age	specimen	max load (kips)	max stress (psi)	(MPa)
7	A	48.25	1735	11.96
	B	50.40	1783	12.29
	C	50.55	1788	12.33
14	D	63.75	2292	15.80
28	E	97.25	3497	24.11
	F	93.75	3371	23.24
	G	96.75	3479	23.99
244	H	137.5	4944	34.09
	I	141.0	5070	34.96
	J	120.0	4316	29.76
	K	141.2	5077	35.01
	L	121.8	4380	30.20
	M	130.0	4675	32.23
	N	127.2	4574	31.54
Average stress at 244 days = 4720psi				

Table B.4

Stiffness and Deformation- Spec. H			
E (ksi)	ϵ_c (in/in)	ϵ_{cu} (in/in)	ν
2803	0.00305	0.00511	0.20

Specimen H was taken from the concrete in the truck chute during the pouring of the first floor columns. Its strength and stiffness characteristics, similar in general to the other cylinders, were used to define the material properties in the first floor columns for section property and strength calculations.

The concrete cylinder test results for the previous RCF2 model frame are also listed in Table B.5 to allow comparison with the properties of the present frame's material. While the age at testing (91 days) of the RCF2 frame was less than half the age of the RCF5 frame, (244 days) the average maximum compressive stress from the cylinder tests, 4395 psi and 4720 psi respectively, vary within only 7.5% of one another.

RCF2- Concrete Cylinder Tests		
(age= 91 days, date of model test)		
spec. no.	max stress	ϵ_c
(psi)	(MPa)	(in/in)
1	4465	30.79	0.00330
2	4395	30.30	0.00344
3	4430	30.54	0.00338
4	4465	30.79	0.00350
5	4320	29.79	0.00330
6	4285	29.55	0.00318
avg:	4395	30.29	0.00335

Table B.5

Member section properties

Various theoretical member section properties, including strengths, stiffnesses, and yield loads, may be calculated based on the member dimensions, material properties and expected loading.

Column strength analysis

An accurate estimate of the real strength and stiffness of concrete sections must be based on exact modeling of the various materials within the section, particularly when properties for behavior beyond the elastic range are desired. Of the two materials which are successfully combined to make reinforced concrete a practical structural component, the properties of steel reinforcing are by far the easier to describe. Use of a stress strain relation for the reinforcing which effectively captures the yield and post yield strain hardening behavior of the steel in tension is necessary for acceptable results. This can be efficiently achieved for the present purposes by defining the yield stress, assuming no increase in stress between initial yielding and a given strain at which hardening starts, and defining a strain hardening stiffness for values beyond that point. Since the maximum steel strains measured during the test sequence were less than 2% or 0.02 in/in and strain hardening started at 0.009 in/in, the total amount of strain hardening was relatively small and stress could be fairly well predicted by a linear relation after the strain hardening point, using an initial tangent stiffness. An exact modeling of the steel behavior under compression is slightly more difficult, particularly under deformations beyond the yield strain where the low yielding stiffness allows little resistance to buckling. In this case, the buckling strength of the longitudinal bars depends on the spacing of the lateral hoop-tie reinforcing and the integrity of the confining concrete cover. Since concrete spalling and loss of

cover occur at strains of approximately the bar yield, for most of the inelastic range the concrete confinement of the rebar is small. However, lateral reinforcing in the form of spirals and ties can significantly increase buckling resistance if closely spaced along the longitudinal bars. In the present columns the lateral hoop spacing of 1 3/8 in. was assumed to provide sufficient restraint against buckling, allowing a moderate amount of inelastic deformation to occur in compression under a stress-strain relation identical to that in tension.

Realistic definition of the mechanics for the concrete, including the concrete cover outside the reinforcing cage and the concrete confined within the cage, under tension and compression stress is a considerably more complex problem. Various researchers have tried to develop model stress-strain relations for concrete [B1], [B2], [B3], [B4], [B5], [B6], [B7], under differing loads, member configuration, and type of loading. Experimental results described by Vallenas et al [B5], are compared with predictions from relations developed by Kent [B2], Blume [B3], and Sargin [B4] for uniaxial compressive loading in the Vallenas report.

The concrete cover is most easily assumed to respond to the same stress strain characteristics seen in compression tested concrete cylinders. It is certain that variations from the cylinder result will occur, such as earlier crushing or spalling due to the plane of weakness at the reinforcing cage and due to lateral expansion of the cage and confined core under loading. However, minor variations in the cover mechanisms will have only small effects on the overall section behavior.

The confined concrete tends to show various mechanical characteristics distinctly different from the compression test results, depending on the effectiveness of the confinement, including:

a)   A higher maximum compressive stress, greater than f_c ,

b)   Maximum compressive stress occurring at a higher strain,

c)   Continued load capacity beyond the max strain measured in a cylinder test,

The effect of these variations may be seen in Figure B.1 where possible confined and unconfined stress-strain plots are compared. The extent to which such variations occur was shown to be related to the existence of both lateral and longitudinal reinforcement by Vallenas [B5] in columns under pure axial loading. In beam-column members under moment and axial loading, the low stressed material near the neutral axis could be expected to provide additional confinement for the highly stressed material under post-crushing strains in the outer regions.

Because of the uncertainty in defining definite properties for the concrete material, assorted analyses were completed for the columns used in the present model frame, varying parameters such as the maximum compressive stress, and strain level at which the maximum compressive stress occurs. The concrete was assumed incapable of carrying any tension stresses. Stress-strain characteristics for the rebar were assumed to be generally defined by the axial tension tests and modeled as having a linear relation at strains below yielding, constant stress at strains between the yield and strain hardening level, and a curve with cubic equation based on the initial tangent slope at onset of strain hardening, and zero slope at maximum

Figure B.1 Typical stress-strain curves for confined and unconfined concrete.
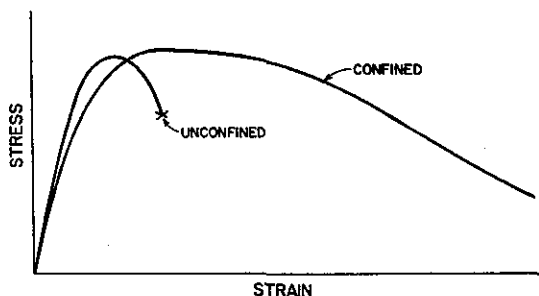
strain, for values beyond the hardening point. All of the column analyses were achieved using the RCCOLA [B8] analysis program including axial loading and uniaxial bending.

Column analysis- type 1

A first prediction of the column strength used the average of measured column dimensions from all of the lower story columns. The strength and stiffness from this "average" prediction would provide the logical values to use for modeling the whole frame in a computer analysis sequence if the actual dimensions of the columns had not been explicitly obtained. Material properties were described as :

-concrete cover with stress-strain relation as obtained from cylinder tests,

-confined concrete with Kent [B2,B7] type stress-strain relation; assumes that lateral reinforcing provides sufficient confinement, which allows concrete to continue carrying load at a decreased magnitude, beyond the crushing strain,

-steel with stress-strain relations from tensile tests as mentioned previously.

Axial-moment interaction and predicted moment-curvature plots from the analysis may be seen in Figures B.3 along the strong and weak column axes. Though the column capacity under axial load is predicted as nearly 300 kips the actual forces in the test frame varied between a maximum compression of 45 kips, below the "balanced", to 20 kips tension during large dynamic overturning cycles. Thus the axial interaction plot near the zero load axis is the only relevant segment for the present frame. Similar interaction plots for the RCF2 frame, based on average column dimensions and measured material properties, with Kent modeling for confined concrete may be seen in Figure B.2.
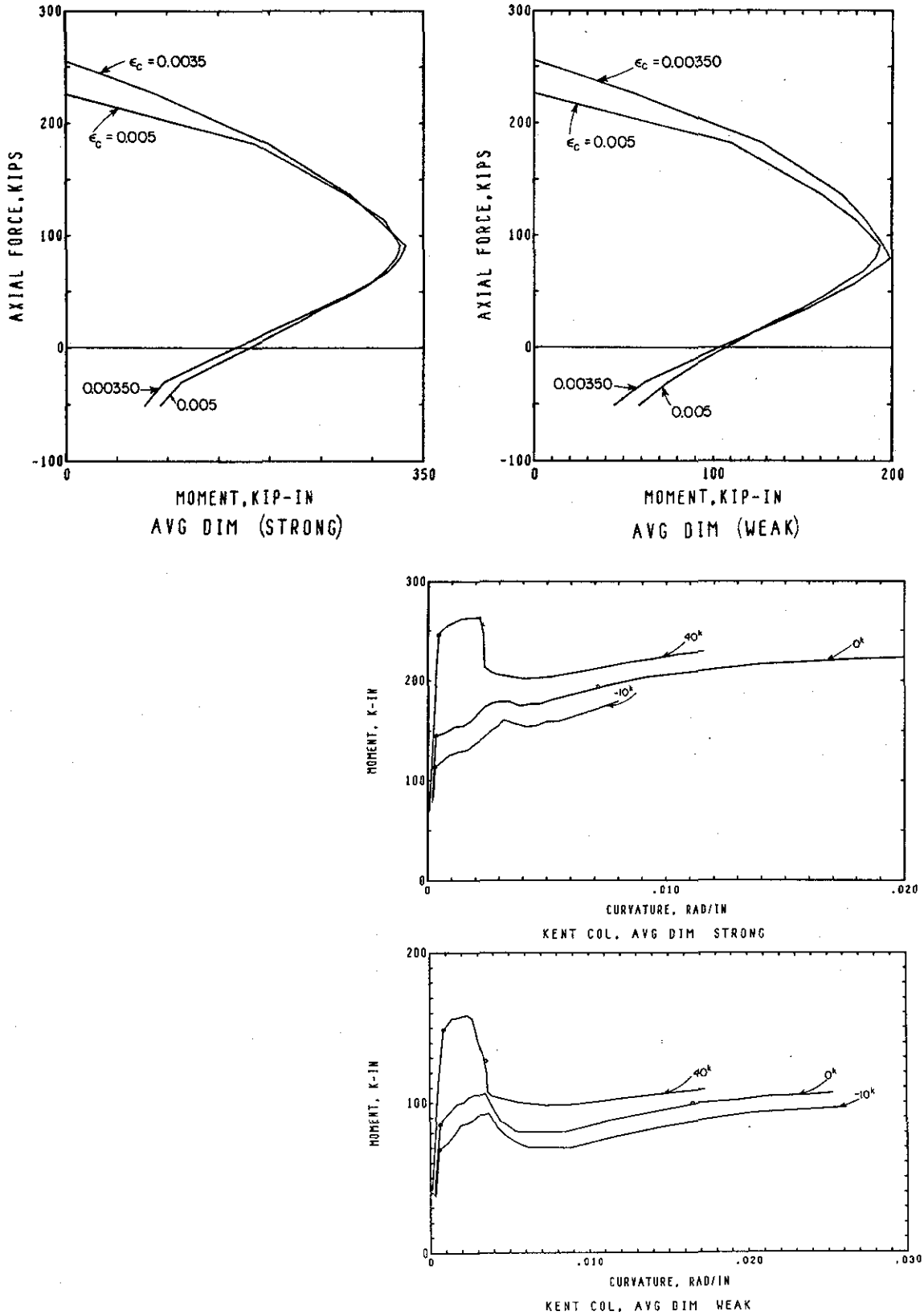
Figure B.2 Predicted moment-axial load interaction curves, moment and curvature relations with axial load, columns from RCF2.
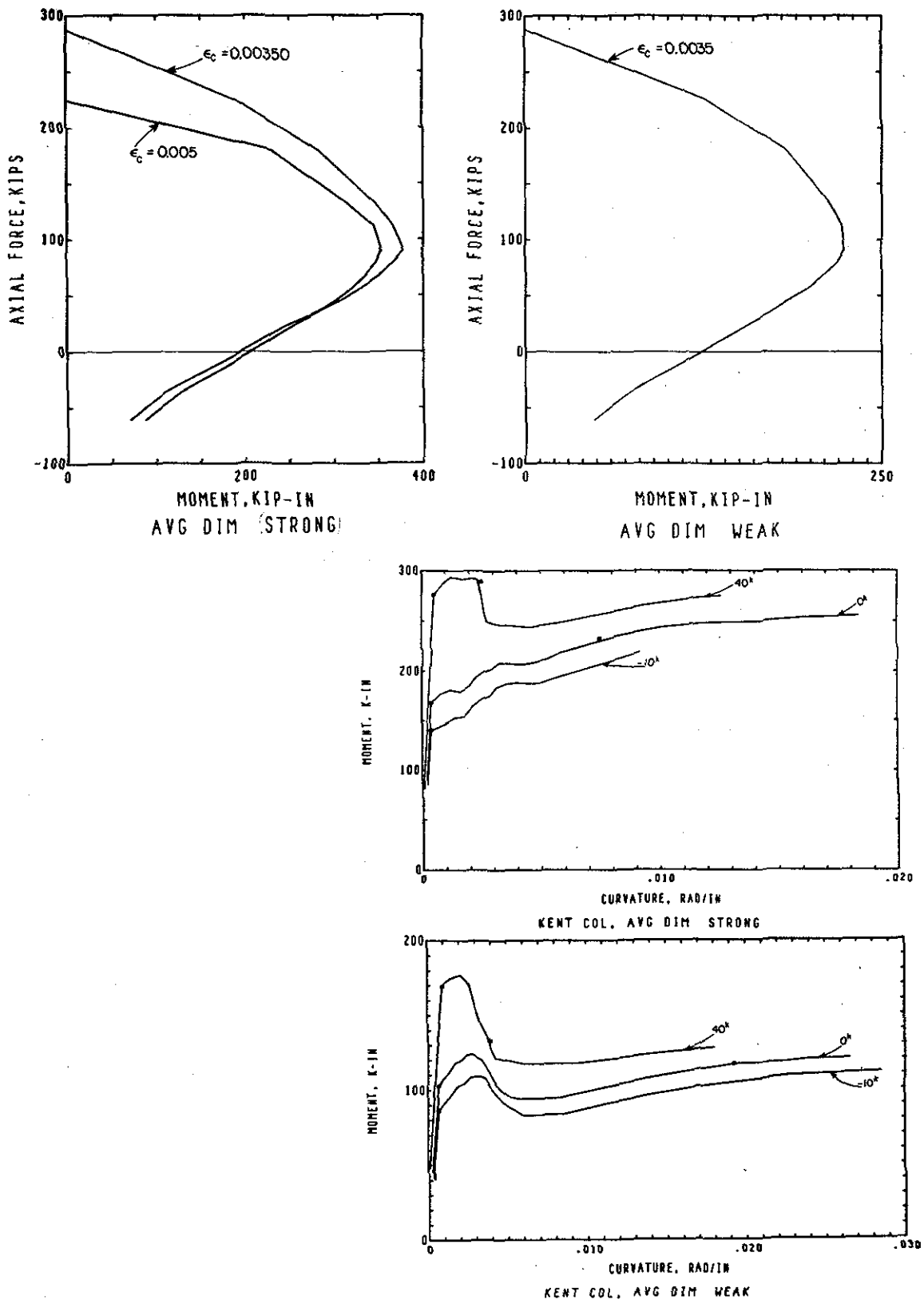
Figure B.3 Predicted moment axial load interaction curves, moment and curvature relations with axial load, columns from present frame.

Column analysis-type 2

A second analysis used the actual measured dimensions and steel locations in the north A frame column, rather than average dimensions, to provide a close comparison between predicted and actual column strength and deformation on a local level. In fact, the average dimensions for the strong direction (NS) were the same as the actual dimensions in the 1NAB column; the weak axis dimensions (EW) varied slightly from the average. Material properties were modeled in the same manner as in type 1. Results for the weak axis are plotted in Figure B.4. The results of this analysis are nearly identical to those of type 1, except for small deviations due to non symmetrical placement of the bars.

Figure B.4 Predicted moment-axial load interaction, actual dimensions of NA column.
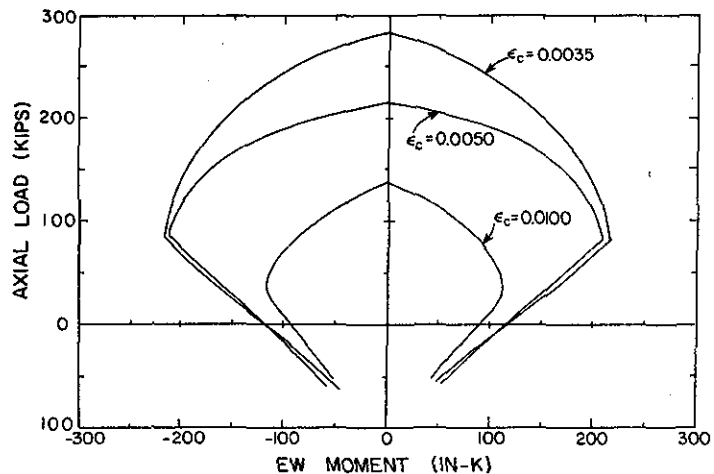
Column analysis-type 3

With confinement provided by the lateral reinforcing, longitudinal bars and low stressed concrete near the neutral axis (in bending plus axial load), it is to be expected that the concrete may actually reach a higher strength [B5] than measured in the cylinder test and used in the normal Kent model. The confined concrete in this analysis was assumed to reach a strength of 1.1 times the measured cylinder strength. Material properties were:

- confined concrete, Kent type relationship with maximum stress of 1.1 times the maximum test cylinder strength,

-unconfined concrete and steel, same as previous types.

The actual 1NAB column dimensions were used again and the analysis was applied in only the weak (EW) direction.

Column analysis-type 4

The Kent model assumes that the actual stress in the confined concrete is attained at a strain of 0.0020. Since the strain at max stress in the cylinder tests was 0.00305 this third variation of the Kent relation defined the max stress to be at a strain of 0.00305 as compared to the normal Kent curve (used in analysis types 1&2) which is illustrated in Figure B.5. In this analysis, the material properties were assumed to be:
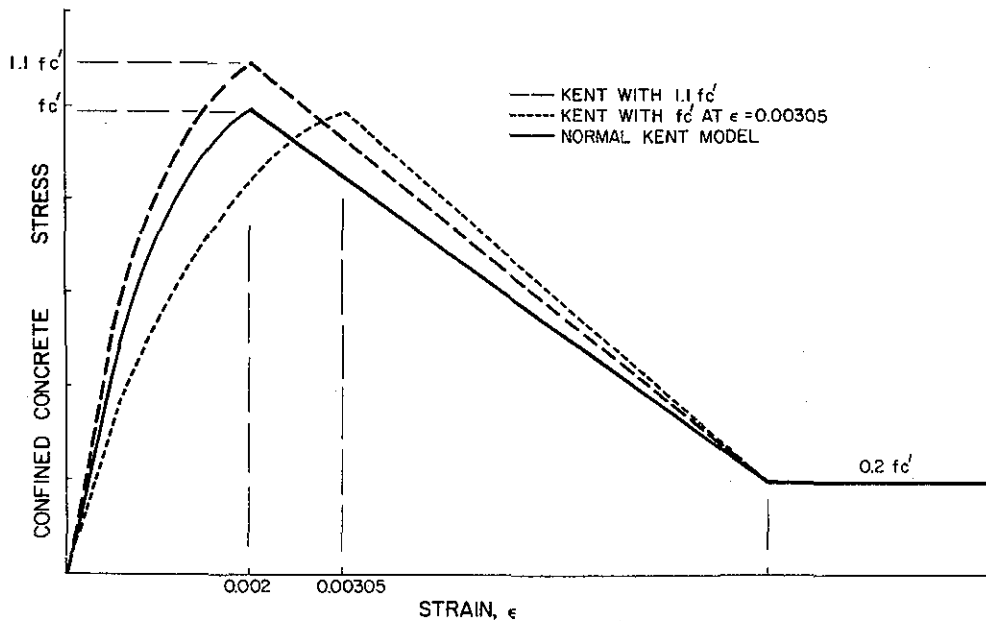
Figure B.5 Stress-strain rules for confined concrete used in types 1-4 analyses.

-confined concrete- similer to Kent model with max stress occurring at a strain of 0.00305,

-unconfined concrete and steel- same as previous analysis.

The actual 1NAB column dimensions were used with the analysis applied only in the weak column direction.

Figure B.6 Predicted moment-axial load interaction for model type 2, model type 3, and model type 4 analyses.
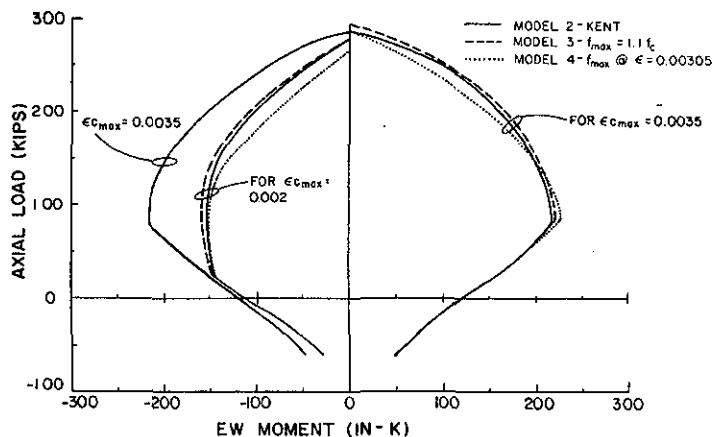
Results of the type 2 analysis are compared with the variations of the Kent model, analyses 3&4, in Figure B.6. The variations on the Kent model made no identifiable differences in the column strength when axial loads were less than 25 kips. At higher axial load the strength was slightly higher in the 1.1 f_c model. While these models vary the size and strain at which maximum concrete stress occurs, they do not significantly change the behavior beyond the

maximum strength point. The actual slope or rate of loss of strength at at high strain may be less than described by Kent if the confining effect of the low strained concrete near the neutral axis, and the lateral stirrups, remains intact; however, after cyclical bending reversals, the confining will be effectively reduced and the slope of the stress-strain curve at high values will increase.

Section stiffnesses

Bending and axial stiffness, in terms of the moment of inertia and area, were calculated for the column strong axis direction and the longitudinal girders in the report on the RCF2 test series [B9]. Those results and results of additional calculations for the column weak axis and the transervse girders are presented in Table B.6 and are based on the section dimensions described at the end of this appendix.

Section properties based on transformed full section: ·

Cracked section properties:

Column   Area = 58 $in.^2$
            I_x = 149 $in.^4$ (weak axis)
            I_y = 357 $in.^4$ (strong axis)

Longitudinal girder

1st floor   Area = 169 $in.^2$
               I = 1749 $in.^4$

2nd floor   A = 166 $in.^2$
               I = 1650 $in.^4$

Transverse girder   A = 103 $in.^2$
                     I = 1127 $in.^4$

Column I_x = 58 $in.^4$ at 20k axial
          = 49 $in.^4$ at 0k axial
          = 45 $in.^4$ at -10k axial (tension) .

          I_y = 160 $in.^4$ at 20k axial
          = 146 $in.^4$ at 0k axial
          = 136 $in.^4$ at -10k axial (tension)

Longitudinal girder

1st floor I_{pos} = 558 $in.^4$ (sagging)
             I_{neg} = 445 $in.^4$ (humping)
             I_{neg}* = 330 $in.^4$ (hump)

2nd floor I_{pos} = 379 $in.^4$
             I_{neg} = 318 $in.^4$

Section properties based on gross area:

Column   A = 49 $in.^2$
          I_x = 135 $in.^4$
          I_y = 294 $in.^4$

Longitudinal girders   A = 152 $in.^2$
                        I = 1440 $in.^4$

Transverse girders   A = 77 $in.^2$
                      I = 886 $in.^4$

Trans. girders I_{pos} = 365 $in.^4$
               I_{neg} = 333 $in.^4$

*Neglecting tensile steel in flanges of T,

Table B.6

Yield moments

The cracked section stiffnesses and predicted member yield levels were derived (as in Table B.7) from the bending axial load interaction analyses of RCCOLA [B8]. Since the columns resist varying axial loads, their yield-moment and to a lesser extent, stiffness, depend on the instantaneous loading. The yield loads listed were developed using average section dimensions, steel stress-strain behavior based on the tensile tests, unconfined concrete stress-strain similar to tested cylinders, and confined concrete behaving as described in the Kent model [B2,B7,B8].

Predicted yield moments:

Table B.7

Columns- strong axis	277in-k at 40k axial
	223in-k at 20k axial
	197in-k at 10k axial
	168in-k at 0k axial
Columns- weak axis	169in-k at 40k axial
	138in-k at 20k axial
	122in-k at 10k axial
	103in-k at 0k axial
Long. girders-lower	+304in-k (sagging)
	-356in-k (humping)
	(-240in-k hump)*
Long. girders-upper	+195in-k
	-235in-k
Transverse girders	+257in-k
	-252in-k

Steel in flanges neglected,

Stress in reinforcing bars

The restoring force characteristics of columns depend extensively on the behavior of the reinforcing steel. Correlation and explanation of the column load versus deformation response required an indication of the resistance provided at any instant by the steel. Thus it was necessary to develop an estimate of the steel stresses corresponding to the measured strains. Since the motion in the test series was of an inelastic cyclical nature, the bar stress-strain relation became history dependent after first yield.

A number of researchers have proposed rules for relating steel stress to measured strain, often based on some variation of the Ramberg-Osgood type of formulation as described by Ma [B10] or Park et al [B11]. The model proposed in Ma's report was able to follow experimental cyclical testing of individual reinforcing bars quite well. However, uncertainties in bar strains at particular locations (as described in Chapter 7-Part 1) caused by discrete cracking in the concrete, and bridging between cracks may make a complex modeling unwarranted, especially

when the main use of the results is to define the approximate stiffness state at any instant.

Based on the results of the previously quoted researchers, and simplified models examined by Aktan [B12], a simple linear algorithm was written to estimate the bar stress and stiffness state based on the measured bar strains. The cyclic stress strain loops were modelled by three line segments representing initial elastic stiffness, Bauschinger softening and yielding, as shown in Figure B.7. Bauschinger effects were included in cycles after the first yield and started when the stress came within a fixed percentage (25%) of the initial yield stress from reaching the new yield level. The slope in the softened range was 20% of the initial elastic stiffness. After yield, a strain hardening stiffness of 712 ksi or 2.3% of the elastic stiffness was maintained.
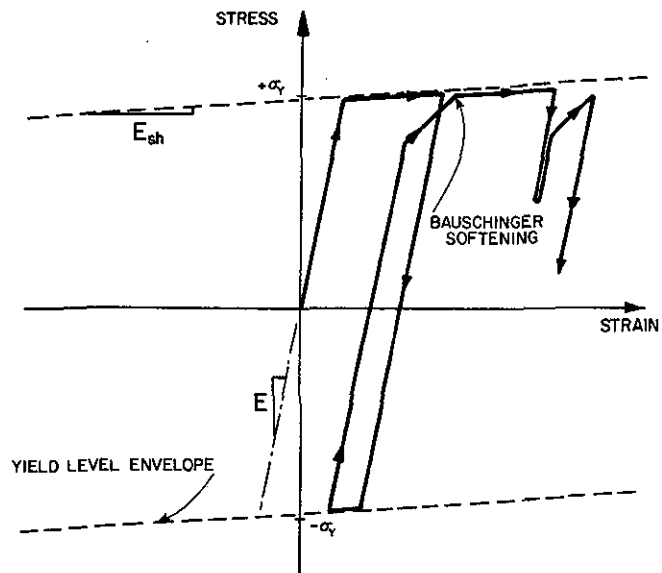
Figure B.7 Stress strain rule for calculating stress from measured rebar strain.

Calculation of degrading rotational spring stiffness

Concentrated rotational springs were used in the correlation analyses, with the DRAIN 2D [B13] computer program, to simulate inelastic deformation and stiffness degradation of the columns. Properties for the springs were calculated by:

1. assuming a maximum curvature expected at the column ends,

2. determining the curvature distribution along the length of the column, based on predicted uniaxial moment-curvature results for specific axial loads from the RCCOLA analysis described previously, assuming the column was in double curvature with equal and opposite end moments,

3. integrating curvature over half the column length to calculate tip displacement and rotation of an imaginary cantilever beam half the length of the columns,
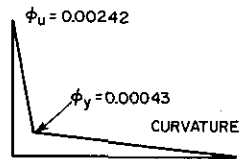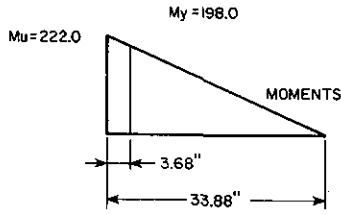
Figure B.8 Strong axis (1)
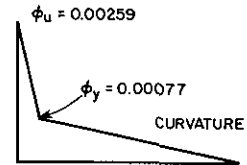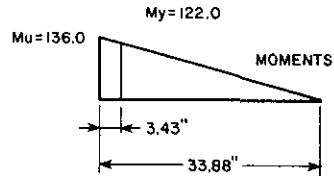
Figure B.10 Weak axis (1).
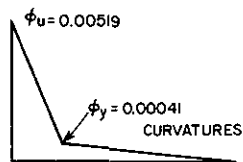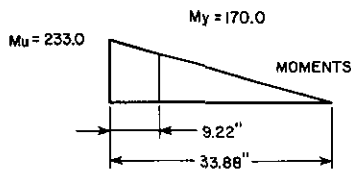
Figure B.9 Strong axis (2).
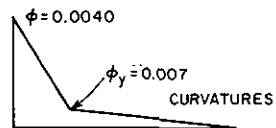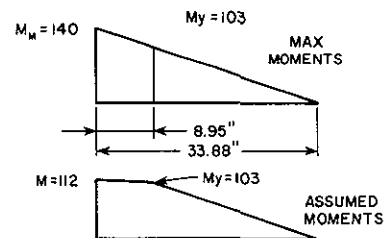
Figure B.11 Weak axis (2).

Figures B.8-B.11 Moment and curvature distributions assumed over columns for use in defining characteristics of rotational inelastic springs used in frame analyses.

4.   assuming that the difference in tip rotation and deflection of the imaginary beam, when the fixed end curvature is increased from yield to to the assumed maximum curvature, is due to rotation of a concentrated spring at the beam fixed end and calculating the stiffness from the change in tip configuration and the increase in end moment over the yield moment.

A first calculation was completed assuming the column carried a 10 kip axial compressive load and a maximum curvature ductility of 5. Column moments and curvatures in the strong and weak axis, respectively, are drawn in Figure B.8 and B.10. Resulting spring stiffnesses were used in the initial inelastic models of *Chapter 8* and are listed in Tables 8.5 and 8.8.

A second calculation assumed no axial load was present and used higher assumed maximum curvatures. Moment and curvature distributions are drawn in Figures B.9 and B.11 for this case. Since the moment capacity at a maximum curvature of 0.004 RAD/in in the weak axis direction (112 in-K) is less than the maximum capacity (136 in-k at 0.0026 rad/in), as may be noted in Figure 7.28, calculation of hinge length (8.95in) was based on a 140 in-kip maximum moment which would have occurred if the initial inelastic slope of the moment-curvature relation had continued rather than deteriorating. Resulting spring properties are listed in Tables 8.7 and 8.9.

Calculation of structural relative displacements

Installation of the displacement measuring potentiometers on reference frames off the shaking table, to avoid vibration of the mounting frames and potentiometers, was described in *Chapter 4* and illustrated in Figure 4.1. The potentiometers provide a calibrated electrical output which varies proportionally to the distance a cable is pulled out of the instrument. As the instruments were mounted, Figure 4.1, the cable extensions of one unit would have been exactly equal to a pure longitudinal floor displacement, and the cable extension or retraction of the remaining two units, at each floor level, would have been exactly equal to a pure transverse floor displacement; such were defined as the primary sensitivities. Unfortunately, each instrument was also sensitive to displacements in directions perpendicular to the directions of prime sensitivity, e.g.- cross sensitivities.Definition of the frame's lateral motion, two horizontal displacements and torsion at each floor, based on extensions measured at the three potentiometers per floor resulted in three simultaneous second order equations. A Newton-Raphson iteration technique was used to solve for estimates of the instantaneous displacements at each data time step.

Plans- design dimensions

Dimensions of the present biaxially tested frame and of a frame previously tested under uniaxial motion [B9] were identical except in design of the footings which were stressed to the shaking table. Original contract drawings (not to scale) are included in Figures B.12 thru B.19.
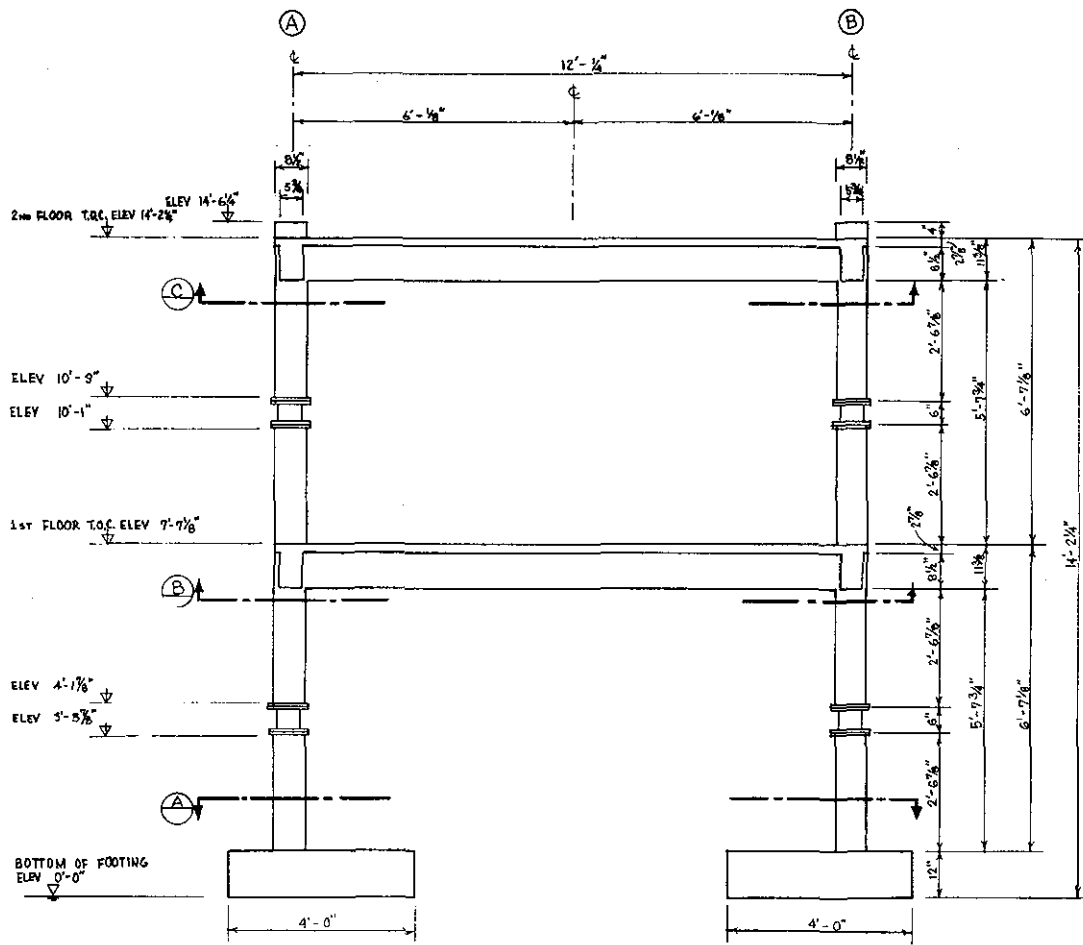
NORTH ELEVATION
SCALE ½"=1'-0"
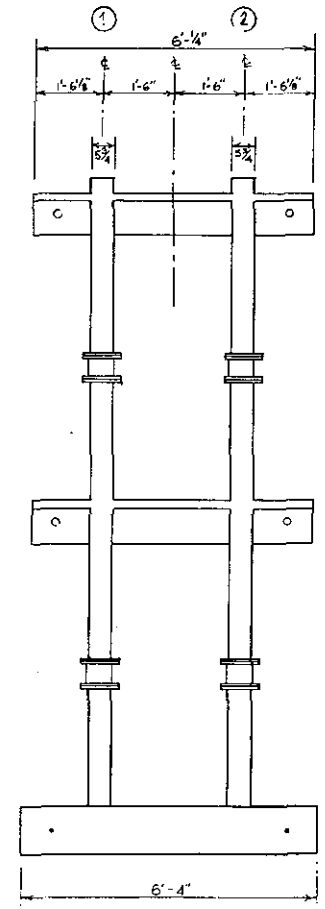
EAST/WEST ELEVATION
SCALE ½"=1'-0"

Figure B.12 Elevation drawings of biaxial test frame.

Ⓐ Ⓑ

12'-¼"

C2

① BEAM B201

SLAB S201

B202

② C2 BEAM B201

C2

1'-6½"

3'-0"

1'-6½"

2ᴺᴰ STORY CEILING ~ SECTION Ⓒ
SCALE ½"=1'-0"

12'-¼"

C12

B101

C15

S101

B102

C15 B101

C12

1'-6½"

3'-0"

1'-6½"

1ˢᵀ STORY CEILING ~ SECTION Ⓑ
SCALE ½"=1'-0"

8½"

5³/₈"

4#5

STIRRUP #2

COLUMN C1 or C2

SLAB S101 or S201

BEAM B101 or B201

#3 BARS (CONTINUING INTO TRANSVERSE
BEAM B102 or B202)

*SEE CROSS SECTION BEAMS B102 & B202
ON THIS PAGE

5³/₄"

TOP BARS - 2#3
BOTTOM BARS - B101 - 2#5
B201 - 2#4

SEE NOTE #

#2 STIRRUP

4#5 BARS
2 TOP, 2 BOTTOM

BEAM B102 or B202

BEAM/COLUMN JOINT (TYP)
1"=0'-6"

COLUMN C1, BEAM B101 & B102
COLUMN C2, BEAM B201 & B202

Figure B.14 Reinforcing
detail, beam-column joint
(above).
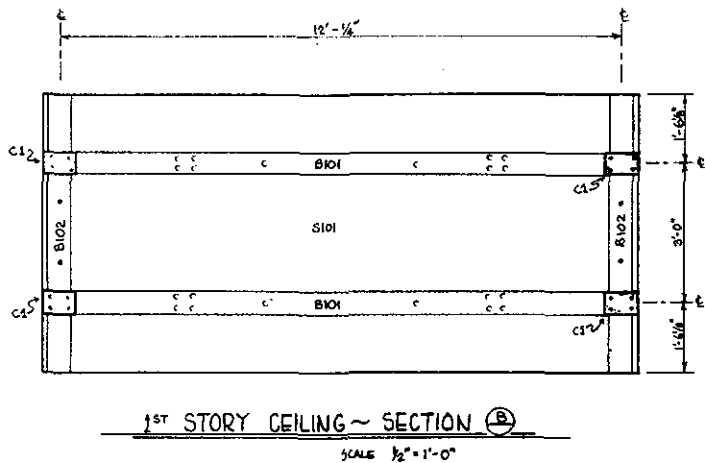
Figure B.13 First and second
story ceiling plans (left).

Figure B.15 Column reinforcing, column sections.
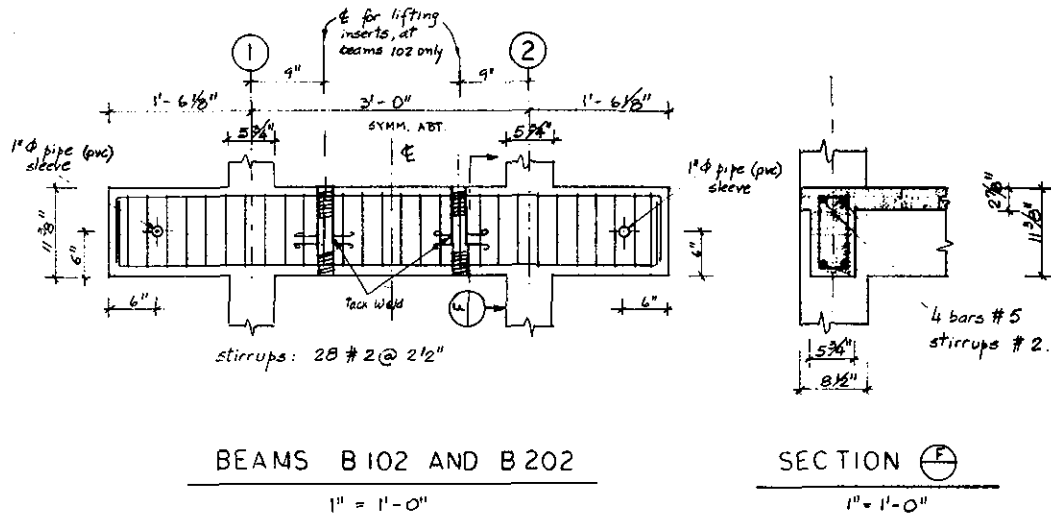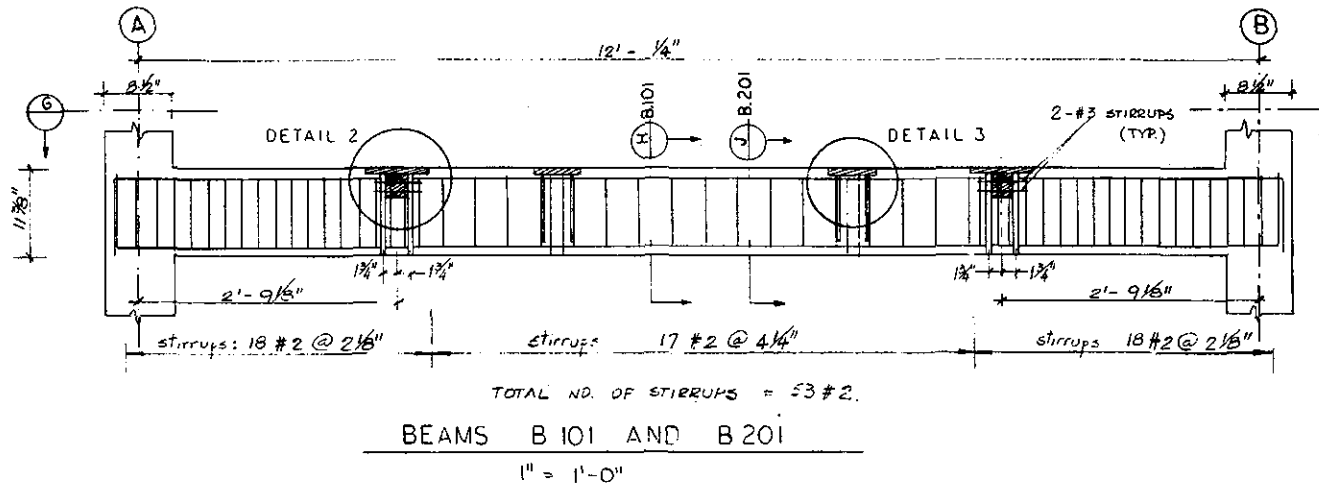
Figure B.16 Transverse and longitudinal beam reinforcing.

BEAM 101 – SECTION (H)

1" = 1'-0"

6 bars # 3

2 bars # 5

stirrup #2

stirrup #2

Both stirrups at same spacing

SLABS S101 AND S201

1" = 1'-0"

TOP AND BOTTOM REINFORCEMENT
WIRE FABRIC 4"X 4" SPACING
GAUGE OF WIRE: 4
(RYERSON TWO-WAY REINFORCEMENT
SHEETS OR EQUIVALENT)
CONCRETE COVER FOR WIRE MESH = ½"

BEAM 201 – SECTION (J)

1" = 1'-0"

4 bars # 3

2 bars # 4

stirrup #2

stirrup #2

Both stirrups at same spacing
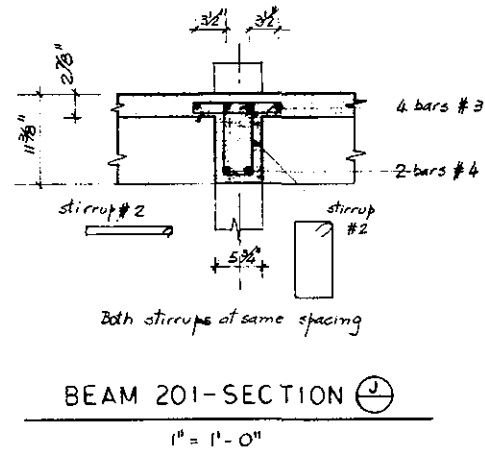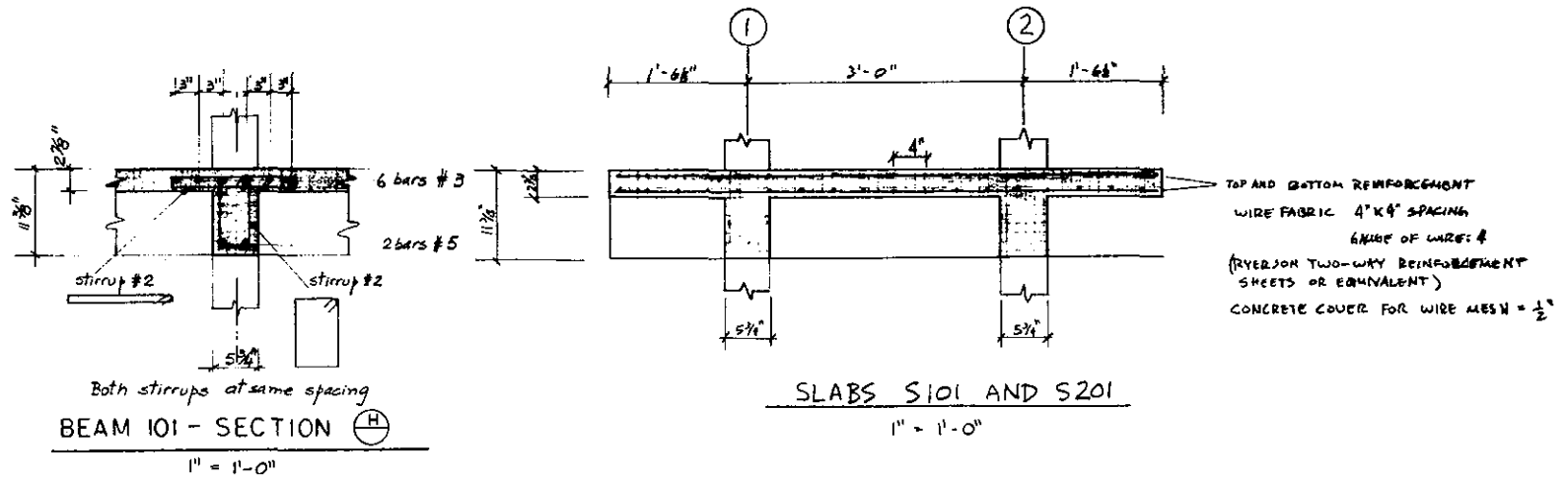
Figure B.17 Sections through longitudinal beams and slab, (above) section through slab, (below) section through lower and upper story beams.
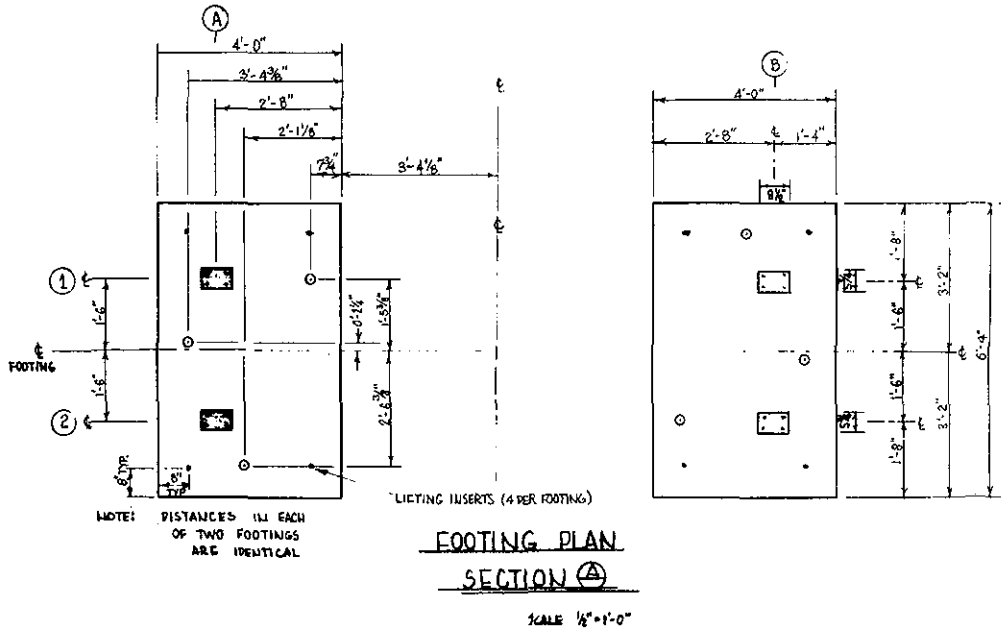
Figure B.18 Footing plan (above) and reinforcing (below).

COLUMN
STIRRUPS

SYMM. ABT. ℄

SYMM. ABT. ℄

21 #2 @ 1 3/8"

4 #2 @ 2 3/4"

3 #2

4 #2 @ 2 3/4"

29 #2 @ 1 3/8"

4 #2 @ 2 3/4"

3 #2

4 #2 @ 2 3/4"

15 #2 @ 1 3/8"

18 #2 @ 2 1/8"   8 #2 @ 4 1/4"

GIRDER STIRRUPS

18 #2 @ 2 1/8"   8 #2 @ 4 1/4"

GIRDER STIRRUPS

10"x 9"x 1" END PLATES
SHEAR KEY AND # 5 BARS
WELDED TO THEM (TYP.)

11 # 4 BARS

14 #2 @ 2 1/2"
GIRDER STIRRUPS

1"x 3"x 3 1/2"
SHEAR KEY
(TYP)

14 #2 @ 2 1/2"
GIRDER STIRRUPS

8 # 4 BARS

FRONT ELEVATION

SIDE ELEVATION

8 1/2"   2 7/8"

5 3/4"

4 # 5 BARS
STIRRUPS #2

11 3/8"

4 # 5 BARS
STIRRUPS #2

5 3/4"

SECT ① COLUMN

SECT ④ TRANSV. GIRDER

6 # 3 BARS

11 3/8"   2 7/8"

2 # 5 BARS
STIRRUPS #2

5 3/4"

SECT ② BOTTOM STORY GIRDER

4 # 3 BARS

11 3/8"   2 7/8"

2 # 4 BARS
STIRRUPS # 2

5 3/4"

SECT ③ TOP STORY GIRDER

SLAB REINFORCEMENT:

4"x 4" WIRE MESH ON TOP & BOTTOM
AREA=0.120 in.²/ft. IN EACH DIRECTION,
EACH LAYER; φ WIRE = 0.225 in.

Figure B.19 Design dimensions and reinforcing of previous (RCF2) uniaxially tested frame.

Instrumentation- Description and Response Characteristics

The accuracy of data collected during experimental testing depends on the accuracy of calibration of the instruments, the suitability of the instruments for the particular application, the quality of the instruments themselves, and the degree to which their attachment changes the response of the model from that which would occur without their presence.

The *accuracy* of the manufacturer's specified *calibration* for the instruments used in the test program was verified at the time of procurement. Short recalibration of each instrument (other than strain gauges) was undertaken before the instruments were mounted on the test frame. Such recalibration primarily checked the linearity of the instrument with a three point calibration procedure and established a voltage vs. measured units rule. The force transducers were subjected to an exhaustive adjustment under numerous multi-axial loadings.

The *suitability* of the instrumentation in this test is primarily a function of:

a) the natural dynamic characteristics of the individual measuring instruments versus those of the test model,

b) the amplitude of the quantities to be measured versus the range of the instrument.

The frequency range within which an instrument's output can be directly related to the measured quantity, preferably through a linear rule, must coincide with the range of frequencies of interest in the test model. Based on the manufacturer's listed specifications, all of the instruments used in this test had frequency characteristics (as will be listed) appropriate to motions in the structure's basic first and second translational modes along each axis (frequencies from 0.9 to 20Hz). And secondly, individual instruments were selected with a measuring range of approximately twice the expected amplitude of motions to avoid accidental overloading, while maintaining a good proportion of the full scale output under expected motion.

The *quality* of the individual instrument is generally a function of the linearity of its output versus the measured quantity over the full range. For any given movement within the measuring range of the instrument, the output must be proportional to that motion in a describable manner. While responding with a preferably linear output to the motions being studied, the instrument should show no response to displacements other than those to be measured (i.e.- zero cross sensitivity). All of the instruments used had very good linearity and cross sensitivity characteristics except the single active arm strain gauges as will be described later.

The amount of *model instrument interaction* or the degree to which which the added mass, stiffness or movement of the attached instrument changes the response of the model from what it would be without the instrument must be minimized. The mass and stiffness of the

instruments used in this test were trivial relative to the model's characteristics. However, the strain gauges attached to the reinforcing bars caused some interaction, as mentioned in the strain gauge characterization of this appendix.

Figure C.1 Accelerometer mounted on concrete added mass block.
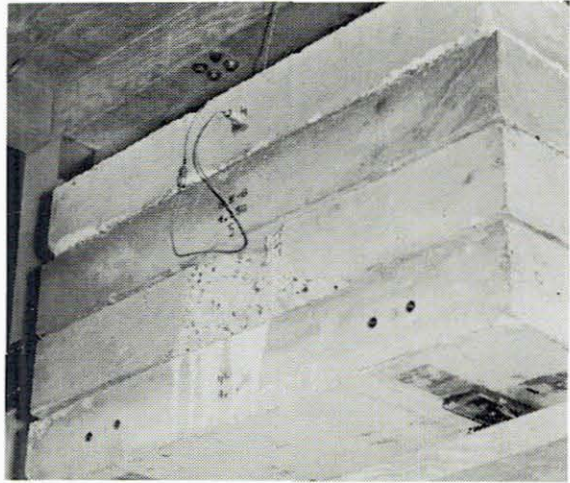
Figure C.2 Accelerometer mount at south end of first floor.
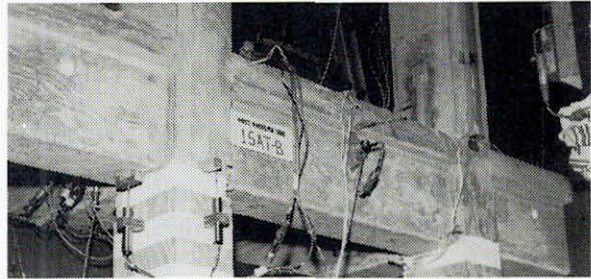
Accelerometers

Two basic types were used- electronic servo accelerometers and open loop strain gauged mechanical accelerometers. They were mounted directly to the floor slabs at center span in both axes of the frame near floor level, and to the sides of the top mass blocks as shown in Figures C.1 and C.2. Mounting elevations of the accelerometers are indicated in Figure C.3.

Figure C.3 Accelerometer mounting positions.
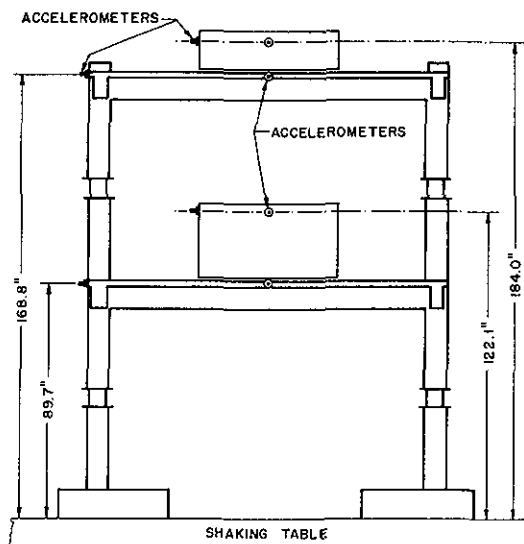
Servo accelerometers

Four precision (Kistler) servo-accelerometers using a closed loop feedback were located to measure motion along the north-south axis of the frame. The response characteristics, well within the necessary range, for the electronically damped instruments follow: (based on manufacturers' specifications)

> frequency response .... within 5%, 0 to 200 Hz
> -3db at 470Hz
> noise... less than 1mv, RMS
> (accelerometer and amplifier)
> transverse sensitivity ....less than 0.005g per g.
> static linearity deviation 0.05%

Strain gauge accelerometers-

These linear accelerometers (Statham) incorporated an unbonded, balanced, fully active strain gauge bridge. Four such instruments were used to monitor frame motion along the frame's east-west axis. The accelerometers were damped to of 70% of critical with a viscous liquid medium, producing the relatively flat response curve of Figure C.4.

Figure C.4 Flat response curve at 70% damping.
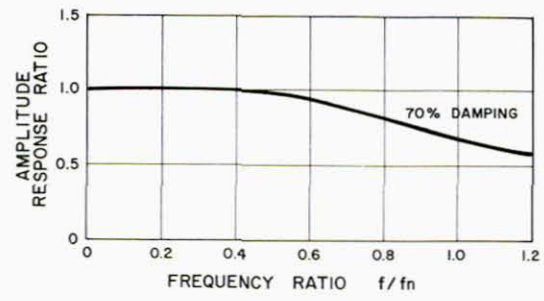
characteristics

range 5g to -5g

natural frequency 375Hz

non-linearity and hysteresis 0.75% full scale

transverse sensitivity less than 0.01g per g

DC-LVDT's

Displacement measuring, direct current, linear variable, differential transformers were used extensively to measure member rotations through small differential displacements on opposite sides of members. A typical beam mounting is shown in Figure C.5. Typical column DCDT displacement amplitudes measured during the Taft 1000 test were on the order of 0.1 to 0.2in (0.25 to 0.51cm). The instrument's displacement range is linear from +0.5in. to -0.5in from the null or centered position.
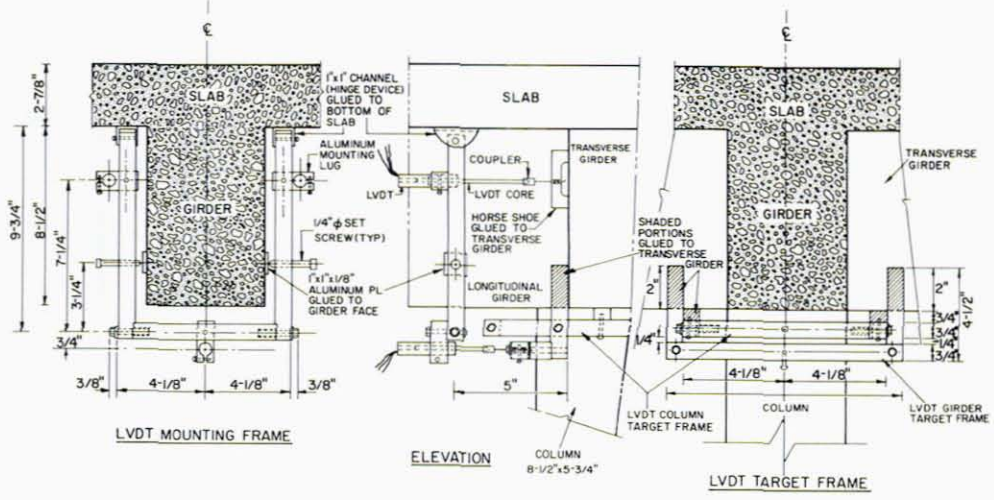
Figure C.5 Mounting system for DCDTs (LVDT) on beams.

maximum non linearity = 0.5% of full scale

internal carrier frequency = 2.4kHz

frequency response down 3 db at 135 Hz

   (function of filter frequency)

calibrated to within 1 milli-inch at 0.500in.

Potentiometers

     Linear variable potentiometers were mounted on reference frames off the shaking table with leads attached to the structure to monitor frame motion (from which relative displacements are calculated by subtracting table motion). The large displacements expected (to 8 in, 20.3cm) and necessity of a flexible connection suggested the use of cable actuated potentiometers. The mechanical limitations of the retracting system dictated that the maximum acceleration of the actuating cable be less than four g's. The manufacturer's specifications are:

linearity = within 0.020%

sensitivity = 62.8 mV/inch/volt excitation

nominal resistance = 0 to 500 ohms output

calibration to within 0.01in. at 10.00 inches

maximum cable travel = 15 in.

Strain Gauges

Individual reinforcing bars are monitored at critical locations through strain gauges attached to the bars before pouring . Gauge attachment, wiring, and waterproofing techniques, designed to allow large bar strains and concrete cracking without harming the gauge operation, are shown in Figures C.6 and C.7.
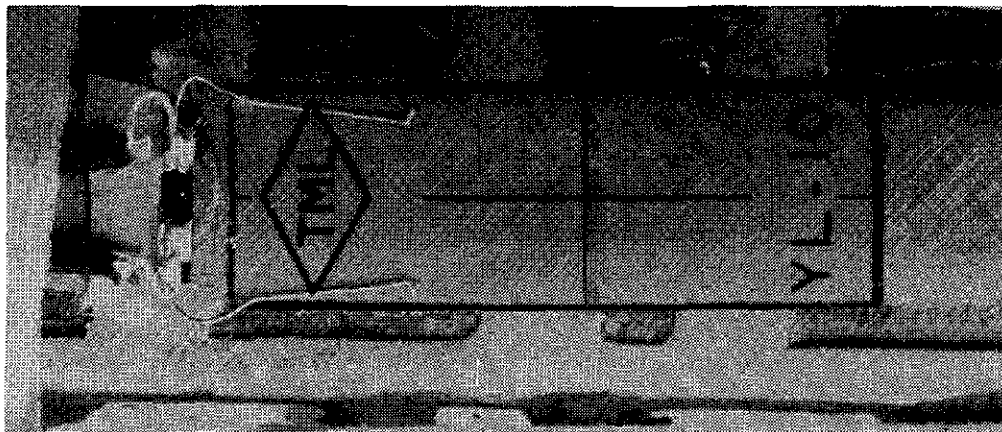
Figure C.6 Strain gauge attachment to reinforcing bar.
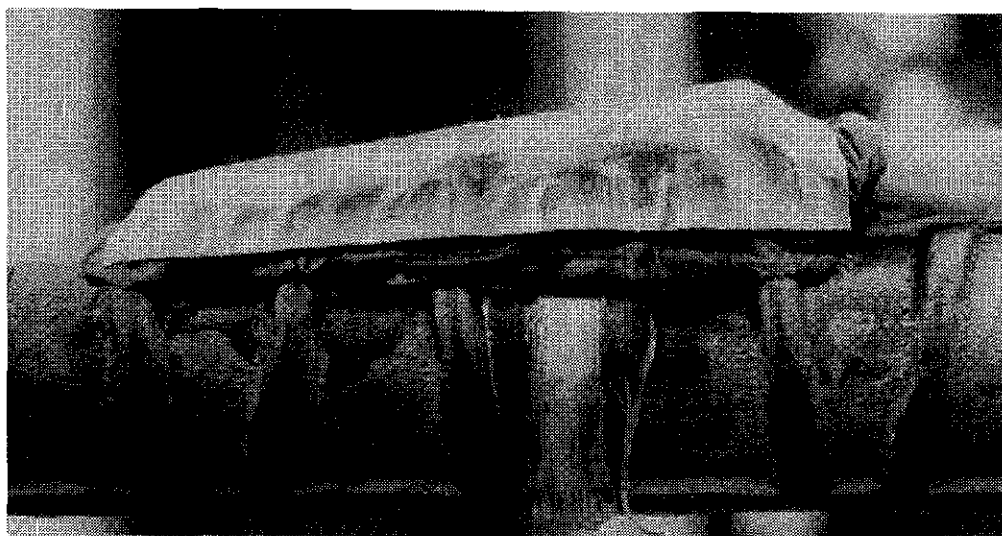
Figure C.7 Strain gauge on rebar with protective coating.

The possible disruptive effect of a data measuring instrument upon the system which it monitors is evident from these figures. In addition to a slight weakening effect due to removing bar deformations in the gauge mounting region, is the more obvious loss of concrete to bar bond in the area of the protective coating. The inaccuracies induced by these effects are difficult to avoid, particularly on small diameter bars, but must be kept in mind when evaluating data.

Additional errors, though small, are due to Wheatstone bridge non-linearities. All of the gauges attached to reinforcing bars are used in single active arm (1/4 bridge) Wheatstone

bridge circuits. The bridges are initially balanced through signal conditioner circuits but any subsequent loading and straining causes resistive change in the single arm. Under single active arm operation, current change in the half bridge containing the active arm causes a small non-linearity between bridge output and actual induced strain. At the level of straining measured in the present tests, the error is inconsequential (ie. at .015 strain error is 0.00023 strain or 2% error).

Various types of gauges were used, including post yield operable gauges. Attachment was with cyanoacrylate glue or 100% solids epoxy- both allowing high elongation and cyclic strain. Gauges denoted as MM were manufactured by Micro-Measurements, the YL-10 by Tokyo-Sokki-Kenyujo. All strain gauges had resistances of 120 ohms and were connected with low resistance cables to the data acquisition system.

Gauge types:

name	gauge length	gauge factor	cross sens.	max. strain	type
MMEA125	.125in.	2.065	0.9%	5%	constantin foil
MMEA250	.25in.	2.110	0.2%	5%	constantin foil
MMEP250	.25in.	2.070	0.6%	20%	annealed " "
YL-10	.39in.	2.02	n.a.	20%ten 5%comp	Cu-Ni wire

Force transducers

The force transducers were intended to provide the actual flexural moment and shear histories along the two column axes at mid-height. The individual transducers were made of hollow rectangular steel sections as drawn in Figure C.8 and shown in Figure C.9.

Figure C.8 Section through column force transducers, (steel).
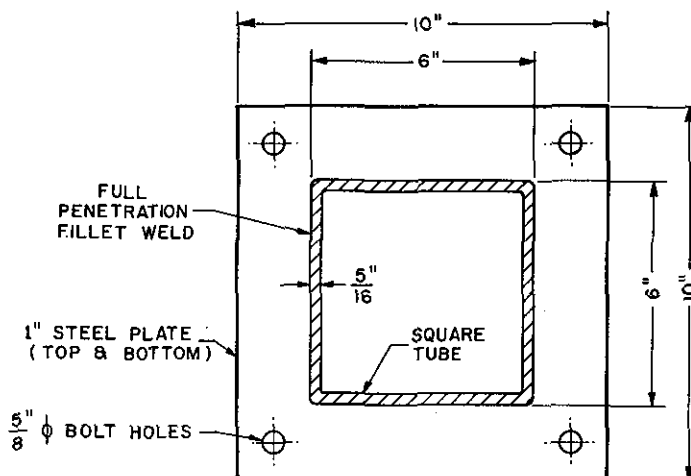
Bending was monitored by a half bridge strain gauge circuit comprised of one gauge mounted in the direction of compression stress on the compression flange and a second in the tensile

Figure C.9 Force transducer mounted at mid-height of column.
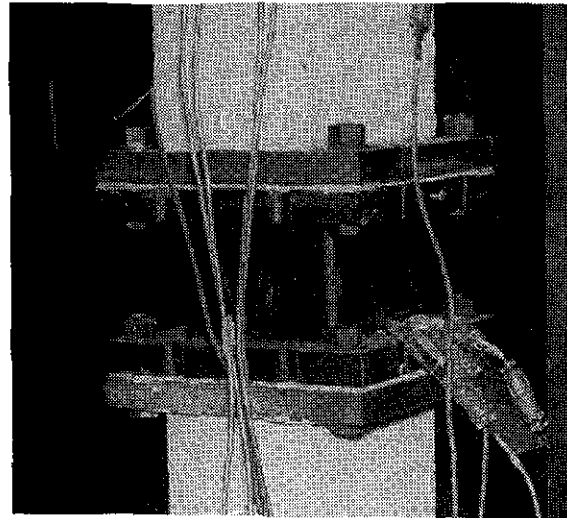
direction on the tension flange. This particular Wheatstone bridge configuration (Figure C.10), in contrast to the 1/4 bridge mentioned previously, exhibits a linear correspondence between strain and bridge output voltage. Shear was monitored by a full bridge circuit with two gauges mounted at 90 degrees to each other on each of two shear webs, as shown in Figure C.11.

Figure C.10 Strain gauge bridge configuration to measure bending.
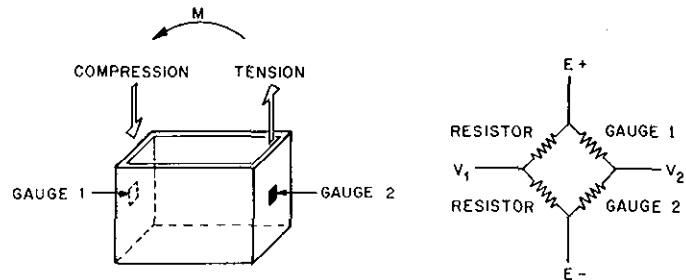
Figure C.11 Strain gauge bridge configuration for shear measurement.
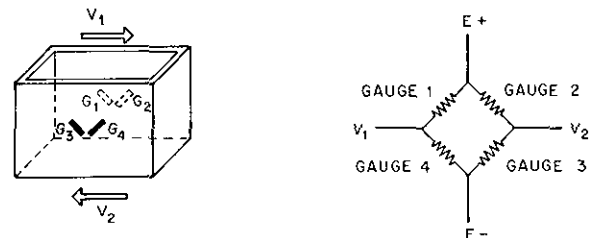
The four active gauges, subjected to opposite strains, again form a Wheatstone bridge configuration which produces linear shear strain vs. voltage output, and are arranged to eliminate effects of normal forces due to bending and shear strains due to torsional loading. A constant correction factor for exact shear strain should be applied to eliminate cross sensitivity if shear strain is desired.

The transducers were subjected to a rigorous calibration procedure including various combined loadings of shear, moment and axial load applied simultaneously. Data from the calibration was analyzed graphically and through a statistical multiple regression to define prime and cross sensitivities directly in moment or shear units as a function of voltage output from the prime circuit and the three other secondary circuits. Typical results from a single transducer are listed below.

Calibration factors, transducer 2
(Actual force quantity = sum of factors x output quantities)

> AVNS = actual shear in north-south axis
>
> etc.
>
> RVEW = transducer output shear along east-west axis
>
> RMNS = transducer output moment in north-south direction
>
> etc.

desired channel	output channel				square of correlation
	RVNS	RVEW	RMNS	RMEW	
AVEW	-.0469	.9195	0	0	.995
AVNS	1.0229	0	0	0	.994
AMEW	0	0	0	.9662	.997
AMNS	0	0	.9125	-.0241	.991

Calibration:
maximum applied shear: 14kips (62.3kN)
maximum applied moment: 140in-k (15.8kN-m)

Neff data acquisition system

The data acquisition network is based on a Neff System 620 analog signal processor. Important characteristics of this unit are listed below. The processor amplifies an instrument's analog signals, applying variable gains, multiplex-scans channels and converts data to digital form. The sampling scan rate of 50Hz was definitely sufficient to detect motions in the structure's frequency range.

Gain- preamplifier per channel:

accuracy- 0.012%

linearity- 0.02%

Analog-digital converter:

crosstalk 0.001% at 20kHz, 50kHz capability,

Noise, peak to peak,:

50 micro volts at 10Hz

Overload:

settles to 0.05% in 1 millisecond

  from 1000% overload-preamplifier

input overload on 1 channel will not affect any other channel

    by more than 0.006%

Appendix D

Data Channel Description

One hundred and forty one data channels, each providing a unique response history, were recorded during the earthquake shaking tests. The channels contained accelerometer, force transducer, strain gauge, displacement measuring potentiometer and differential transformer output signals converted to digital form at 0.01952 second intervals in each channel. A detailed listing of the data measured and identity of each channel follows.

Mnemonics

The mnemonics used to describe locations of the various measuring devices normally consist of a four digit sequence QRST in which the digits have the following meaning (refer to Figure D.1).
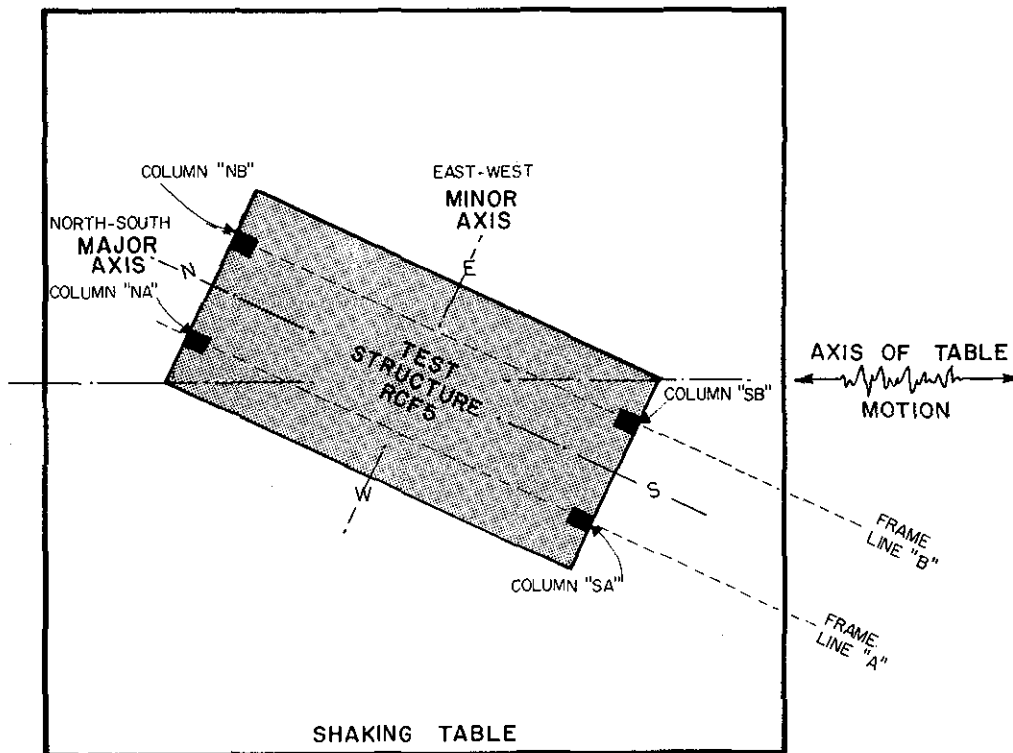
Figure D.1   Key to column and frame notation

(Q) denotes story level, either 1 (first) or 2 (second),

(R) denotes north or south end of structure (N or S),

(S) denotes longitudinal frame, either frame A or frame B,

(T) denotes location, particularly for columns, either T (top) or B (bottom).

As an example, the mnemonic '1NAB column' refers to the lower story (1), north end (N), A frame (A), column bottom (B).

<div align="center">Channels- EERC Data Acquisition System</div>

Chn. no.	Name	Description	Units	Polarity
1	Av H T Disp	Average horizontal N-S table displacement	in.	+S
2	Av V T Disp	Average vertical table displacement	in.	+up
3	Av H T Acc	Average horizontal table NS acceleration	g	+S
4	Av V T Acc	Average vertical table acceleration	g	+up
5	Pitch Acc	Table pitching angular acceleration	rad/s/s	+E
6	Roll Acc	Table roll angular acceleration	rad/s/s	+N
7	Twist Acc	Table twist angular acceleration	rad/s/s	+down
8	Acc-S-F1	NS accelerometer at S end, first floor	g	+N
9	Acc-S-B1	NS accelerometer at S end, lower blocks	g	+N
10	Acc-S-F2	NS accelerometer at S end, second floor	g	+N
11	Acc-S-B2	NS accelerometer at S end, upper blocks	g	+N
12	Acc-E-F1	EW accelerometer at E side, first floor	g	+W
13	Acc-E-B1	EW accelerometer at E side, lower blocks	g	+W
14	Acc-E-F2	EW accelerometer at E side, second floor	g	+W
15	Acc-E-B2	EW accelerometer at E side, upper blocks	g	+E
16	Disp-S1	Potentiometer, south end, first floor, displ.	in.	+extend
17	Disp-S2	Potentiometer, south end, second floor, displ.	in.	+extend
18	C-LB-TB	DCDT on A frame long. beam at 1NA column, top, B side	in.	1
19	C-TB-TS	DCDT on N trans. beam at 1NA column, top, S side	in.	1
20	Disp-SE1	EW pot, SE frame corner, first floor, displ.	in.	+extend
21	Disp-SE2	EW pot, SE frame corner, second floor, displ.	in.	+extend
22	Disp-NW1	EW pot, NW frame corner, first floor, displ.	in.	+extend
23	Disp-NW2	EW pot, NW frame corner, second floor, displ.	in.	+extend
24	C-1NAB-N	Col. DCDT at 1NAB at N face	in.	1
25	C-1NAB-E	Col. DCDT at 1NAB at E face	in.	1
26	C-1NAB-S	Col. DCDT at 1NAB at S face	in.	1
27	C-1NAB-W	Col. DCDT at 1NAB at W face	in.	1
28	S-1NAB-NWB	Col. strain, 1NAB, NW bar, bottom gauge	mil/in	2
29	S-1NAB-NWM	Col. strain, 1NAB, NW bar, middle gauge, at joint	mil/in	2
30	S-1NAB-NWT	Col. strain, 1NAB, NW bar, top gauge	mil/in	2
31	S-1NAB-NE	Col. strain, 1NAB, NE bar, at joint	mil/in	2

Channels- EERC Data Acquisition System

Chn. no.	Name	Description	Units	Polarity
32	S-1NAB-SEB	Col. strain, 1NAB, SE bar, bottom gauge	mil/in	2
33	S-1NAB-SEM	Col. strain, 1NAB, SE bar, mid gauge, at joint	mil/in	2
34	S-1NAB-SET	Col. strain, 1NAB, SE bar, top gauge	mil/in	2
35	S-1NAB-SW	Col. strain, 1NAB, SW bar, at joint	mil/in	2
36	V-NS-1NA	Transducer output, col. 1NA, NS-shear	kips	A
37	V-EW-1NA	Transducer output, col. 1NA, EW-shear	kips	B
38	M-NS-1NA	Transducer output, col. 1NA, NS-moment	in-kips	C
39	M-EW-1NA	Transducer output, col. 1NA, EW-moment	in_kips	D
40	S-1NAT-NW	Col. strain, 1NAT, NW bar, at joint	mil/in	2
41	S-1NAT-NE	Col. strain, 1NAT, NE bar, at joint	mil/in	2
42	S-1NAT-SE	Col. strain, 1NAT, SE bar, at joint	mil/in	2
43	S-1NAT-SW	Col. strain, 1NAT, SW bar, at joint	mil/in	2
44	Acc-Lat	Horizontal EW table acceleration	g	+W
45	S-LB-TB	Long. beam strain, at 1NA col., top B side bar	mil/in	2
46	S-LB-BB	Long. beam strain, at 1NA col., bottom B side bar	mil/in	2
47	S-LB-BA	Long. beam strain, at 1NA col., bottom A side bar	mil/in	2
48	S-TB-TN	Trans. beam strain, at 1NA col., top N side bar	mil/in	2
49	S-TB-TS	Trans. beam strain, at 1NA col., top S side bar	mil/in	2
50	S-TB-TS	Trans. beam strain, at 1NA col., bottom S side bar	mil/in	2
51	S-TB-BN	Trans. beam strain, at 1NA col., bottom N side bar	mil/in	2
52	S-2NAB-NW	Col. strain, 2NAB, NW bar at joint	mil/in	2
53	S-LB-SAT	Long. beam strain, at 1SA col., top A side	mil/in	2
54	S-2NAB-SE	Col. strain, 2NAB, SE bar at joint	mil/in	2
55	S-2NAB-SW	Col. strain, 2NAB, SW bar at joint	mil/in	2
56	C-1NAT-N	Col. DCDT, 1NAT at N face	in.	1
57	C-1NAT-E	Col. DCDT, 1NAT at E face	in.	1
58	C-1NAT-S	Col. DCDT, 1NAT at S face	in.	1
59	C-1NAT-W	Col. DCDT, 1NAT at W face	in.	1
60	C-LB-T	Long. beam DCDT, at 1NA col., top A side	in.	1
61	C-LB-B	Long. beam DCDT, at 1NA col., bottom A side	in.	1
62	C-TB-T	Trans. beam DCDT, at 1NA col., top N side	in.	1
63	C-TB-B	Trans. beam DCDT, at 1NA col., bottom N side	in.	1
64	C-2NAB-N	Col. DCDT, 2NAB, on N face	in.	1
65	C-2NAB-E	Col. DCDT, 2NAB, on E face	in.	1
66	C-2NAB-S	Col. DCDT, 2NAB, on S face	in.	1
67	C-2NAB-W	Col. DCDT, 2NAB, on W face	in.	1
68	V-NS-2NA	Transducer output, col. 2NA, NS-shear	kips	A
69	V-EW-2NA	Transducer output, col. 2NA, EW-shear	kips	B
70	M-NS-2NA	Transducer output, col. 2NA, NS-moment	in-kips	C

Channels- EERC Data Acquisition System

Chn. no.	Name	Description	Units	Polarity
71	M-EW-2NA	Transducer output, col. 2NA, EW-moment	in-kips	D
72	V-NS-2SA	Transducer output, col. 2SA, NS-shear	kips	A
73	V-EW-2SA	Transducer output, col. 2SA, EW-shear	kips	B
74	M-NS-2SA	Transducer output, col. 2SA, NS-moment	in-kips	C
75	M-EW-2SA	Transducer output, col. 2SA, EW-moment	in-kips	D
76	C-1SAT-N	Col. DCDT, 1SAT, N face	in.	1
77	C-1SAT-E	Col. DCDT, 1SAT, E face	in.	1
78	C-1SAT-S	Col. DCDT, 1SAT, S face	in.	1
79	C-1SAT-W	Col. DCDT, 1SAT, W face	in.	1
80	V-NS-1SA	Transducer output, col. 1SA, NS-shear	kips	A
81	V-EW-1SA	Transducer output, col. 1SA, EW-shear	kips	B
82	M-MS-1SA	Transducer output, col. 1SA, NS-moment	in-kips	C
83	M-EW-1SA	Transducer output, col. 1SA, EW-moment	in-kips	D
84	C-1SAB-N	Col. DCDT, 1SAB, N face	in.	1
85	C-1SAB-E	Col. DCDT, 1SAB, E face	in.	1
86	C-1SAB-S	Col. DCDT, 1SAB, S face	in.	1
87	C-1SAB-W	Col. DCDT, 1SAB, W face	in.	1
88	C-1NBB-N	Col. DCDT, 1NBB, N face	in.	1
89	C-1NBB-E	Col. DCDT, 1NBB, E face	in.	1
90	C-1NBB-S	Col. DCDT, 1NBB, S face	in.	1
91	C-1NBB-W	Col. DCDT, 1NBB, W face	in.	1
92	V-NS-1NB	Transducer output, col. 1NB, NS-shear	kips	A
93	V-EW-1NB	Transducer output, col. 1NB, EW-shear	kips	B
94	M-NS-1NB	Transducer output, col. 1NB, NS-moment	in-kips	C
95	M-EW-1NB	Transducer output, col. 1NB, EW-moment	in-kips	D
96	V-NS-2NB	Transducer output, col. 2NB, NS-shear	kips	A
97	V-EW-2NB	Transducer output, col. 2NB, EW-shear	kips	B
98	M-NS-2NB	Transducer output, col. 2NB, NS-moment	in-kips	C
99	M-EW-2NB	Transducer output, col. 2NB, EW-moment	in-kips	D
100	V-NS-2SB	Transducer output, col. 2SB, NS-shear	kips	A
101	V-EW-2SB	Transducer output, col. 2SB, EW-shear	kips	B
102	M-NS-2SB	Transducer output, col. 2SB, NS-moment	in-kips	C
103	M-EW-2SB	Transducer output, col. 2SB, EW-moment	in-kips	D
104	V-NS-1SB	Transducer output, col. 1SB, NS-shear	kips	A
105	V-EW-1SB	Transducer output, col. 1SB, EW-shear	kips	B
106	M-NS-1SB	Transducer output, col. 1SB, NS-moment	in-kips	C
107	M-EW-1SB	Transducer output, col. 1SB, EW-moment	in-kips	D
108	C-1SBB-N	Col. DCDT, 1SBB, N face	in.	1
109	C-1SBB-E	Col. DCDT, 1SBB, E face	in.	1

Channels- EERC Data Acquisition System

Chn. no.	Name	Description	Units	Polarity
110	C-1SBB-S	Col. DCDT, 1SBB, S face	in.	1
111	C-1SBB-W	Col. DCDT, 1SBB, W face	in.	1
112	C-1SAM-N	Col. DCDT, middle 1SA col., N face	in.	1
113	C-1SAM-E	Col. DCDT, middle 1SA col., E face	in.	1
114	C-1SAM-S	Col. DCDT, middle 1SA col., S face	in.	1
115	C-1SAM-W	Col. DCDT, middle 1SA col., W face	in.	1
116	OKUBA-1			
117	OKUBA-2			
118	OKUBA-3			
119	OKUBA-4			
120	Displ-L	First floor, relative long. (NS) displacement	in.	+S
121	Displ-T	First floor, relative trans. (EW) displacement	in.	+W

Notes:

1. DCDT polarity: + for extension,

2. Strain gauge polarity: + for extension,

A) Force transducer, north-south shear, + with shear acting from north to south in column when section viewed from above,

B) Force transducer, east-west shear, + with shear acting from east to west in column when section viewed from above,

C) Force transducer, north-south moment, + when compression stress formed in south face of column,

D) Force transducer, east-west moment, + when compression stress formed in west face of column.

Channels- High Speed Scanner System

Ch. no.	Name	Description	Units	Polarity
1	S-1SAB-NW	Col. strain, 1SAB, NW bar at joint	mil/in	2
2	S-1SAB-NE	Col. strain, 1SAB, NE bar at joint	mil/in	2
3	S-1SAB-SE	Col. strain, 1SAB, SE bar at joint	mil/in	2
4	S-1SAB-SW	Col. strain, 1SAB, SW bar at joint	mil/in	2
5	S-1SAT-NWB	Col. strain, 1SAT, NW bar, bottom gauge	mil/in	2
6	S-1SAT-NWM	Col. strain, 1SAT, NW bar, mid, at joint	mil/in	2
7	LB-S-AB	Long. beam strain, at 1SA col., bottom A side bar	mil/in	2
8	S-1SAT-NE	Col. strain, 1SAT, NE bar at joint	mil/in	2
9	S-1SAT-SEB	Col. strain, 1SAT, SE bar, bottom gauge	mil/in	2
10	S-1SAT-SEM	Col. strain, 1SAT, SE bar, mid, at joint	mil/in	2
11	S-1SAT-SET	Col. strain, 1SAT, SE bar, top gauge	mil/in	2
12	S-1SAT-SW	Col. strain, 1SAT, SW bar, at joint	mil/in	2
13	LB-S-StirrupB	Long. beam stirrup strain, at 1SA col., B side	mil/in	2
14	LB-S-StirrupA	Long. beam stirrup strain, at 1SA col., A side	mil/in	2
15	LB-N-BA-BM	Long. beam strain, at 1NA col., A side bottom, in beam	mil/in	2
16	LB-N-TA-BM	Long. beam strain, at 1NA col., A side bottom, in beam	mil/in	2
17	TB-TS-BM	Trans. beam strain, at 1NA col., S side top, in beam	mil/in	2
18	TB-BS-BM	Trans. beam strain, at 1NA col., S side bottom, in beam	mil/in	2
19	LB-S-BT	Long. beam strain, at 1SA col., B side top bar	mil/in	2
20	LB-S-BB	Long. beam strain, at 1SA col., B side bottom bar	mil/in	2
21	AHTACC	Average horizontal table acceleration (same as EERC channel no. 3)	g	+S

2   Strain gauge polarity: + for extension,
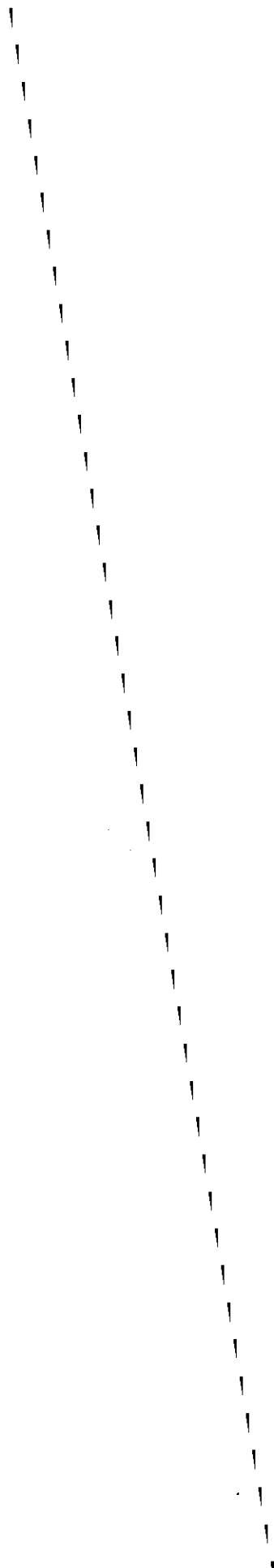
EARTHQUAKE ENGINEERING RESEARCH CENTER REPORTS

NOTE: Numbers in parenthesis are Accession Numbers assigned by the National Technical Information Service; these are followed by a price code. Copies of the reports may be ordered from the National Technical Information Service, 5285 Port Royal Road, Springfield, Virginia, 22161. Accession Numbers should be quoted on orders for reports (PB --- ---) and remittance must accompany each order. Reports without this information were not available at time of printing. Upon request, EERC will mail inquirers this information when it becomes available.

EERC 67-1   "Feasibility Study Large-Scale Earthquake Simulator Facility," by J. Penzien, J.G. Bouwkamp, R.W. Clough and D. Rea - 1967 (PB 187 905)A07

EERC 68-1   Unassigned

EERC 68-2   "Inelastic Behavior of Beam-to-Column Subassemblages Under Repeated Loading," by V.V. Bertero - 1968 (PB 184 888)A05

EERC 68-3   "A Graphical Method for Solving the Wave Reflection-Refraction Problem," by H.D. McNiven and Y. Mengi - 1968 (PB 187 943)A03

EERC 68-4   "Dynamic Properties of McKinley School Buildings," by D. Rea, J.G. Bouwkamp and R.W. Clough - 1968 (PB 187 902)A07

EERC 68-5   "Characteristics of Rock Motions During Earthquakes," by H.B. Seed, I.M. Idriss and F.W. Kiefer - 1968 (PB 188 338)A03

EERC 69-1   "Earthquake Engineering Research at Berkeley," - 1969 (PB 187 906)A11

EERC 69-2   "Nonlinear Seismic Response of Earth Structures," by M. Dibaj and J. Penzien - 1969 (PB 187 904)A08

EERC 69-3   "Probabilistic Study of the Behavior of Structures During Earthquakes," by R. Ruiz and J. Penzien - 1969 (PB 187 886)A06

EERC 69-4   "Numerical Solution of Boundary Value Problems in Structural Mechanics by Reduction to an Initial Value Formulation," by N. Distefano and J. Schujman - 1969 (PB 187 942)A02

EERC 69-5   "Dynamic Programming and the Solution of the Biharmonic Equation," by N. Distefano - 1969 (PB 187 941)A03

EERC 69-6   "Stochastic Analysis of Offshore Tower Structures," by A.K. Malhotra and J. Penzien - 1969 (PB 187 903)A09

EERC 69-7   "Rock Motion Accelerograms for High Magnitude Earthquakes," by H.B. Seed and I.M. Idriss - 1969 (PB 187 940)A02

EERC 69-8   "Structural Dynamics Testing Facilities at the University of California, Berkeley," by R.M. Stephen, J.G. Bouwkamp, R.W. Clough and J. Penzien - 1969 (PB 189 111)A04

EERC 69-9   "Seismic Response of Soil Deposits Underlain by Sloping Rock Boundaries," by H. Dezfulian and H.B. Seed 1969 (PB 189 114)A03

EERC 69-10   "Dynamic Stress Analysis of Axisymmetric Structures Under Arbitrary Loading," by S. Ghosh and E.L. Wilson 1969 (PB 189 026)A10

EERC 69-11   "Seismic Behavior of Multistory Frames Designed by Different Philosophies," by J.C. Anderson and V. V. Bertero - 1969 (PB 190 662)A10

EERC 69-12   "Stiffness Degradation of Reinforcing Concrete Members Subjected to Cyclic Flexural Moments," by V.V. Bertero, B. Bresler and H. Ming Liao - 1969 (PB 202 942)A07

EERC 69-13   "Response of Non-Uniform Soil Deposits to Travelling Seismic Waves," by H. Dezfulian and H.B. Seed - 1969 (PB 191 023)A03

EERC 69-14   "Damping Capacity of a Model Steel Structure," by D. Rea, R.W. Clough and J.G. Bouwkamp - 1969 (PB 190 663)A06

EERC 69-15   "Influence of Local Soil Conditions on Building Damage Potential during Earthquakes," by H.B. Seed and I.M. Idriss - 1969 (PB 191 036)A03

EERC 69-16   "The Behavior of Sands Under Seismic Loading Conditions," by M.L. Silver and H.B. Seed - 1969 (AD 714 982)A07

EERC 70-1   "Earthquake Response of Gravity Dams," by A.K. Chopra - 1970 (AD 709 640)A03

EERC 70-2   "Relationships between Soil Conditions and Building Damage in the Caracas Earthquake of July 29, 1967," by H.B. Seed, I.M. Idriss and H. Dezfulian - 1970 (PB 195 762)A05

EERC 70-3   "Cyclic Loading of Full Size Steel Connections," by E.P. Popov and R.M. Stephen - 1970 (PB 213 545)A04

EERC 70-4   "Seismic Analysis of the Charaima Building, Caraballeda, Venezuela," by Subcommittee of the SEAONC Research Committee: V.V. Bertero, P.F. Fratessa, S.A. Mahin, J.H. Sexton, A.C. Scordelis, E.L. Wilson, L.A. Wyllie, H.B. Seed and J. Penzien, Chairman - 1970 (PB 201 455)A06

EERC 70-5   "A Computer Program for Earthquake Analysis of Dams," by A.K. Chopra and P. Chakrabarti – 1970 (AD 723 994)A05

EERC 70-6   "The Propagation of Love Waves Across Non-Horizontally Layered Structures," by J. Lysmer and L.A. Drake 1970 (PB 197 896)A03

EERC 70-7   "Influence of Base Rock Characteristics on Ground Response," by J. Lysmer, H.B. Seed and P.B. Schnabel 1970 (PB 197 897)A03

EERC 70-8   "Applicability of Laboratory Test Procedures for Measuring Soil Liquefaction Characteristics under Cyclic Loading," by H.B. Seed and W.H. Peacock – 1970 (PB 198 016)A03

EERC 70-9   "A Simplified Procedure for Evaluating Soil Liquefaction Potential," by H.B. Seed and I.M. Idriss – 1970 (PB 198 009)A03

EERC 70-10   "Soil Moduli and Damping Factors for Dynamic Response Analysis," by H.B. Seed and I.M. Idriss – 1970 (PB 197 869)A03

EERC 71-1   "Koyna Earthquake of December 11, 1967 and the Performance of Koyna Dam," by A.K. Chopra and P. Chakrabarti 1971 (AD 731 496)A06

EERC 71-2   "Preliminary In-Situ Measurements of Anelastic Absorption in Soils Using a Prototype Earthquake Simulator," by R.D. Borcherdt and P.W. Rodgers – 1971 (PB 201 454)A03

EERC 71-3   "Static and Dynamic Analysis of Inelastic Frame Structures," by F.L. Porter and G.H. Powell – 1971 (PB 210 135)A06

EERC 71-4   "Research Needs in Limit Design of Reinforced Concrete Structures," by V.V. Bertero – 1971 (PB 202 943)A04

EERC 71-5   "Dynamic Behavior of a High-Rise Diagonally Braced Steel Building," by D. Rea, A.A. Shah and J.G. Bouwkamp 1971 (PB 203 584)A06

EERC 71-6   "Dynamic Stress Analysis of Porous Elastic Solids Saturated with Compressible Fluids," by J. Ghaboussi and E. L. Wilson – 1971 (PB 211 396)A06

EERC 71-7   "Inelastic Behavior of Steel Beam-to-Column Subassemblages," by H. Krawinkler, V.V. Bertero and E.P. Popov 1971 (PB 211 335)A14

EERC 71-8   "Modification of Seismograph Records for Effects of Local Soil Conditions," by P. Schnabel, H.B. Seed and J. Lysmer – 1971 (PB 214 450)A03

EERC 72-1   "Static and Earthquake Analysis of Three Dimensional Frame and Shear Wall Buildings," by E.L. Wilson and H.H. Dovey – 1972 (PB 212 904)A05

EERC 72-2   "Accelerations in Rock for Earthquakes in the Western United States," by P.B. Schnabel and H.B. Seed – 1972 (PB 213 100)A03

EERC 72-3   "Elastic-Plastic Earthquake Response of Soil-Building Systems," by T. Minami – 1972 (PB 214 868)A08

EERC 72-4   "Stochastic Inelastic Response of Offshore Towers to Strong Motion Earthquakes," by M.K. Kaul – 1972 (PB 215 713)A05

EERC 72-5   "Cyclic Behavior of Three Reinforced Concrete Flexural Members with High Shear," by E.P. Popov, V.V. Bertero and H. Krawinkler – 1972 (PB 214 555)A05

EERC 72-6   "Earthquake Response of Gravity Dams Including Reservoir Interaction Effects," by P. Chakrabarti and A.K. Chopra – 1972 (AD 762 330)A08

EERC 72-7   "Dynamic Properties of Pine Flat Dam," by D. Rea, C.Y. Liaw and A.K. Chopra – 1972 (AD 763 928)A05

EERC 72-8   "Three Dimensional Analysis of Building Systems," by E.L. Wilson and H.H. Dovey – 1972 (PB 222 438)A06

EERC 72-9   "Rate of Loading Effects on Uncracked and Repaired Reinforced Concrete Members," by S. Mahin, V.V. Bertero, D. Rea and M. Atalay – 1972 (PB 224 520)A08

EERC 72-10   "Computer Program for Static and Dynamic Analysis of Linear Structural Systems," by E.L. Wilson, K.-J. Bathe, J.E. Peterson and H.H. Dovey – 1972 (PB 220 437)A04

EERC 72-11   "Literature Survey – Seismic Effects on Highway Bridges," by T. Iwasaki, J. Penzien and R.W. Clough – 1972 (PB 215 613)A19

EERC 72-12   "SHAKE-A Computer Program for Earthquake Response Analysis of Horizontally Layered Sites," by P.B. Schnabel and J. Lysmer – 1972 (PB 220 207)A06

EERC 73-1   "Optimal Seismic Design of Multistory Frames," by V.V. Bertero and H. Kamil – 1973

EERC 73-2   "Analysis of the Slides in the San Fernando Dams During the Earthquake of February 9, 1971," by H.B. Seed, K.L. Lee, I.M. Idriss and F. Makdisi – 1973 (PB 223 402)A14

EERC 73-3   "*Computer Aided Ultimate Load Design of Unbraced Multistory Steel Frames*," by M.B. El-Hafez and G.H. Powell
1973 (PB 248 315)A09

EERC 73-4   "Experimental Investigation into the Seismic Behavior of Critical Regions of Reinforced Concrete Components
as Influenced by Moment and Shear," by M. Celebi and J. Penzien - 1973 (PB 215 884)A09

EERC 73-5   "Hysteretic Behavior of Epoxy-Repaired Reinforced Concrete Beams," by M. Celebi and J. Penzien - 1973
(PB 239 568)A03

EERC 73-6   "General Purpose Computer Program for Inelastic Dynamic Response of Plane Structures," by A. Kanaan and
G.H. Powell - 1973 (PB 221 260)A08

EERC 73-7   "A Computer Program for Earthquake Analysis of Gravity Dams Including Reservoir Interaction," by
P. Chakrabarti and A.K. Chopra - 1973 (AD 766 271)A04

EERC 73-8   "Behavior of Reinforced Concrete Deep Beam-Column Subassemblages Under Cyclic Loads," by O. Küstü and
J.G. Bouwkamp - 1973 (PB 246 117)A12

EERC 73-9   "Earthquake Analysis of Structure-Foundation Systems," by A.K. Vaish and A.K. Chopra - 1973 (AD 766 272)A07

EERC 73-10   "Deconvolution of Seismic Response for Linear Systems," by R.B. Reimer - 1973 (PB 227 179)A08

EERC 73-11   "SAP IV: A Structural Analysis Program for Static and Dynamic Response of Linear Systems," by K.-J. Bathe,
E.L. Wilson and F.E. Peterson - 1973 (PB 221 967)A09

EERC 73-12   "Analytical Investigations of the Seismic Response of Long, Multiple Span Highway Bridges," by W.S. Tseng
and J. Penzien - 1973 (PB 227 816)A10

EERC 73-13   "Earthquake Analysis of Multi-Story Buildings Including Foundation Interaction," by A.K. Chopra and
J.A. Gutierrez - 1973 (PB 222 970)A03

EERC 73-14   "ADAP: A Computer Program for Static and Dynamic Analysis of Arch Dams," by R.W. Clough, J.M. Raphael and
S. Mojtahedi - 1973 (PB 223 763)A09

EERC 73-15   "Cyclic Plastic Analysis of Structural Steel Joints," by R.B. Pinkney and R.W. Clough - 1973 (PB 226 843)A08

EERC 73-16   "QUAD-4: A Computer Program for Evaluating the Seismic Response of Soil Structures by Variable Damping
Finite Element Procedures," by I.M. Idriss, J. Lysmer, R. Hwang and H.B. Seed - 1973 (PB 229 424)A05

EERC 73-17   "Dynamic Behavior of a Multi-Story Pyramid Shaped Building," by R.M. Stephen, J.P. Hollings and
J.G. Bouwkamp - 1973 (PB 240 718)A06

EERC 73-18   "Effect of Different Types of Reinforcing on Seismic Behavior of Short Concrete Columns," by V.V. Bertero,
J. Hollings, O. Küstü, R.M. Stephen and J.G. Bouwkamp - 1973

EERC 73-19   "Olive View Medical Center Materials Studies, Phase I," by B. Bresler and V.V. Bertero - 1973 (PB 235 986)A06

EERC 73-20   "Linear and Nonlinear Seismic Analysis Computer Programs for Long Multiple-Span Highway Bridges," by
W.S. Tseng and J. Penzien - 1973

EERC 73-21   "*Constitutive Models for Cyclic Plastic Deformation of Engineering Materials*," by J.M. Kelly and P.P. Gillis
1973 (PB 226 024)A03

EERC 73-22   "DRAIN - 2D User's Guide," by G.H. Powell - 1973 (PB 227 016)A05

EERC 73-23   "Earthquake Engineering at Berkeley - 1973," (PB 226 033)A11

EERC 73-24   Unassigned

EERC 73-25   "Earthquake Response of Axisymmetric Tower Structures Surrounded by Water," by C.Y. Liaw and A.K. Chopra
1973 (AD 773 052)A09

EERC 73-26   "Investigation of the Failures of the Olive View Stairtowers During the San Fernando Earthquake and Their
Implications on Seismic Design," by V.V. Bertero and R.G. Collins - 1973 (PB 235 106)A13

EERC 73-27   "Further Studies on Seismic Behavior of Steel Beam-Column Subassemblages," by V.V. Bertero, H. Krawinkler
and E.P. Popov - 1973 (PB 234 172)A06

EERC 74-1   "Seismic Risk Analysis," by C.S. Oliveira - 1974 (PB 235 920)A06

EERC 74-2   "Settlement and Liquefaction of Sands Under Multi-Directional Shaking," by R. Pyke, C.K. Chan and H.B. Seed
1974

EERC 74-3   "Optimum Design of Earthquake Resistant Shear Buildings," by D. Ray, K.S. Pister and A.K. Chopra - 1974
(PB 231 172)A06

EERC 74-4   "*LUSH - A Computer Program for Complex Response Analysis of Soil-Structure Systems*," by J. Lysmer, T. Udaka,
H.B. Seed and R. Hwang - 1974 (PB 236 796)A05

EERC 74-5   "Sensitivity Analysis for Hysteretic Dynamic Systems: Applications to Earthquake Engineering," by D. Ray 1974 (PB 233 213)A06

EERC 74-6   "Soil Structure Interaction Analyses for Evaluating Seismic Response," by H.B. Seed, J. Lysmer and R. Hwang 1974 (PB 236 519)A04

EERC 74-7   Unassigned

EERC 74-8   "Shaking Table Tests of a Steel Frame - A Progress Report," by R.W. Clough and D. Tang - 1974 (PB 240 869)A03

EERC 74-9   "Hysteretic Behavior of Reinforced Concrete Flexural Members with Special Web Reinforcement," by V.V. Bertero, E.P. Popov and T.Y. Wang - 1974 (PB 236 797)A07

EERC 74-10   "Applications of Reliability-Based, Global Cost Optimization to Design of Earthquake Resistant Structures," by E. Vitiello and K.S. Pister - 1974 (PB 237 231)A06

EERC 74-11   "Liquefaction of Gravelly Soils Under Cyclic Loading Conditions," by R.T. Wong, H.B. Seed and C.K. Chan 1974 (PB 242 042)A03

EERC 74-12   "Site-Dependent Spectra for Earthquake-Resistant Design," by H.B. Seed, C. Ugas and J. Lysmer - 1974 (PB 240 953)A03

EERC 74-13   "Earthquake Simulator Study of a Reinforced Concrete Frame," by P. Hidalgo and R.W. Clough - 1974 (PB 241 944)A13

EERC 74-14   "Nonlinear Earthquake Response of Concrete Gravity Dams," by N. Pal - 1974 (AD/A 006 583)A06

EERC 74-15   "Modeling and Identification in Nonlinear Structural Dynamics - I. One Degree of Freedom Models," by N. Distefano and A. Rath - 1974 (PB 241 548)A06

EERC 75-1   "Determination of Seismic Design Criteria for the Dumbarton Bridge Replacement Structure, Vol. I: Description, Theory and Analytical Modeling of Bridge and Parameters," by F. Baron and S.-H. Pang - 1975 (PB 259 407)A15

EERC 75-2   "Determination of Seismic Design Criteria for the Dumbarton Bridge Replacement Structure, Vol. II: Numerical Studies and Establishment of Seismic Design Criteria," by F. Baron and S.-H. Pang - 1975 (PB 259 408)A11 (For set of EERC 75-1 and 75-2 (PB 259 406))

EERC 75-3   "Seismic Risk Analysis for a Site and a Metropolitan Area," by C.S. Oliveira - 1975 (PB 248 134)A09

EERC 75-4   "Analytical Investigations of Seismic Response of Short, Single or Multiple-Span Highway Bridges," by M.-C. Chen and J. Penzien - 1975 (PB 241 454)A09

EERC 75-5   "An Evaluation of Some Methods for Predicting Seismic Behavior of Reinforced Concrete Buildings," by S.A. Mahin and V.V. Bertero - 1975 (PB 246 306)A16

EERC 75-6   "Earthquake Simulator Study of a Steel Frame Structure, Vol. I: Experimental Results," by R.W. Clough and D.T. Tang - 1975 (PB 243 981)A13

EERC 75-7   "Dynamic Properties of San Bernardino Intake Tower," by D. Rea, C.-Y. Liaw and A.K. Chopra - 1975 (AD/A008 406) A05

EERC 75-8   "Seismic Studies of the Articulation for the Dumbarton Bridge Replacement Structure, Vol. I: Description, Theory and Analytical Modeling of Bridge Components," by F. Baron and R.E. Hamati - 1975 (PB 251 539)A07

EERC 75-9   "Seismic Studies of the Articulation for the Dumbarton Bridge Replacement Structure, Vol. 2: Numerical Studies of Steel and Concrete Girder Alternates," by F. Baron and R.E. Hamati - 1975 (PB 251 540)A10

EERC 75-10   "Static and Dynamic Analysis of Nonlinear Structures," by D.P. Mondkar and G.H. Powell - 1975 (PB 242 434)A08

EERC 75-11   "Hysteretic Behavior of Steel Columns," by E.P. Popov, V.V. Bertero and S. Chandramouli - 1975 (PB 252 365)A11

EERC 75-12   "Earthquake Engineering Research Center Library Printed Catalog," - 1975 (PB 243 711)A26

EERC 75-13   "Three Dimensional Analysis of Building Systems (Extended Version)," by E.L. Wilson, J.P. Hollings and H.H. Dovey - 1975 (PB 243 989)A07

EERC 75-14   "Determination of Soil Liquefaction Characteristics by Large-Scale Laboratory Tests," by P. De Alba, C.K. Chan and H.B. Seed - 1975 (NUREG 0027)A08

EERC 75-15   "A Literature Survey - Compressive, Tensile, Bond and Shear Strength of Masonry," by R.L. Mayes and R.W. Clough - 1975 (PB 246 292)A10

EERC 75-16   "Hysteretic Behavior of Ductile Moment Resisting Reinforced Concrete Frame Components," by V.V. Bertero and E.P. Popov - 1975 (PB 246 388)A05

EERC 75-17   "Relationships Between Maximum Acceleration, Maximum Velocity, Distance from Source, Local Site Conditions for Moderately Strong Earthquakes," by H.B. Seed, R. Murarka, J. Lysmer and I.M. Idriss - 1975 (PB 248 172)A03

EERC 75-18   "The Effects of Method of Sample Preparation on the Cyclic Stress-Strain Behavior of Sands," by J. Mulilis, C.K. Chan and H.B. Seed - 1975 (Summarized in EERC 75-28)

EERC 75-19 "The Seismic Behavior of Critical Regions of Reinforced Concrete Components as Influenced by Moment, Shear and Axial Force," by M.B. Atalay and J. Penzien - 1975 (PB 258 842)A11

EERC 75-20 "Dynamic Properties of an Eleven Story Masonry Building," by R.M. Stephen, J.P. Hollings, J.G. Bouwkamp and D. Jurukovski - 1975 (PB 246 945)A04

EERC 75-21 "State-of-the-Art in Seismic Strength of Masonry - An Evaluation and Review," by R.L. Mayes and R.W. Clough 1975 (PB 249 040)A07

EERC 75-22 "Frequency Dependent Stiffness Matrices for Viscoelastic Half-Plane Foundations," by A.K. Chopra, P. Chakrabarti and G. Dasgupta - 1975 (PB 248 121)A07

EERC 75-23 "Hysteretic Behavior of Reinforced Concrete Framed Walls," by T.Y. Wong, V.V. Bertero and E.P. Popov - 1975

EERC 75-24 "Testing Facility for Subassemblages of Frame-Wall Structural Systems," by V.V. Bertero, E.P. Popov and T. Endo - 1975

EERC 75-25 "Influence of Seismic History on the Liquefaction Characteristics of Sands," by H.B. Seed, K. Mori and C.K. Chan - 1975 (Summarized in EERC 75-28)

EERC 75-26 "The Generation and Dissipation of Pore Water Pressures during Soil Liquefaction," by H.B. Seed, P.P. Martin and J. Lysmer - 1975 (PB 252 648)A03

EERC 75-27 "Identification of Research Needs for Improving Aseismic Design of Building Structures," by V.V. Bertero 1975 (PB 248 136)A05

EERC 75-28 "Evaluation of Soil Liquefaction Potential during Earthquakes," by H.B. Seed, I. Arango and C.K. Chan - 1975 (NUREG 0026)A13

EERC 75-29 "Representation of Irregular Stress Time Histories by Equivalent Uniform Stress Series in Liquefaction Analyses," by H.B. Seed, I.M. Idriss, F. Makdisi and N. Banerjee - 1975 (PB 252 635)A03

EERC 75-30 "FLUSH - A Computer Program for Approximate 3-D Analysis of Soil-Structure Interaction Problems," by J. Lysmer, T. Udaka, C.-F. Tsai and H.B. Seed - 1975 (PB 259 332)A07

EERC 75-31 "ALUSH - A Computer Program for Seismic Response Analysis of Axisymmetric Soil-Structure Systems," by E. Berger, J. Lysmer and H.B. Seed - 1975

EERC 75-32 "TRIP and TRAVEL - Computer Programs for Soil-Structure Interaction Analysis with Horizontally Travelling Waves," by T. Udaka, J. Lysmer and H.B. Seed - 1975

EERC 75-33 "Predicting the Performance of Structures in Regions of High Seismicity," by J. Penzien - 1975 (PB 248 130)A03

EERC 75-34 "Efficient Finite Element Analysis of Seismic Structure - Soil - Direction," by J. Lysmer, H.B. Seed, T. Udaka, R.N. Hwang and C.-F. Tsai - 1975 (PB 253 570)A03

EERC 75-35 "The Dynamic Behavior of a First Story Girder of a Three-Story Steel Frame Subjected to Earthquake Loading," by R.W. Clough and L.-Y. Li - 1975 (PB 248 841)A05

EERC 75-36 "Earthquake Simulator Study of a Steel Frame Structure, Volume II - Analytical Results," by D.T. Tang - 1975 (PB 252 926)A10

EERC 75-37 "ANSR-I General Purpose Computer Program for Analysis of Non-Linear Structural Response," by D.P. Mondkar and G.H. Powell - 1975 (PB 252 386)A08

EERC 75-38 "Nonlinear Response Spectra for Probabilistic Seismic Design and Damage Assessment of Reinforced Concrete Structures," by M. Murakami and J. Penzien - 1975 (PB 259 530)A05

EERC 75-39 "Study of a Method of Feasible Directions for Optimal Elastic Design of Frame Structures Subjected to Earthquake Loading," by N.D. Walker and K.S. Pister - 1975 (PB 257 781)A06

EERC 75-40 "An Alternative Representation of the Elastic-Viscoelastic Analogy," by G. Dasgupta and J.L. Sackman - 1975 (PB 252 173)A03

EERC 75-41 "Effect of Multi-Directional Shaking on Liquefaction of Sands," by H.B. Seed, R. Pyke and G.R. Martin - 1975 (PB 258 781)A03

EERC 76-1 "Strength and Ductility Evaluation of Existing Low-Rise Reinforced Concrete Buildings - Screening Method," by T. Okada and B. Bresler - 1976 (PB 257 906)A11

EERC 76-2 "Experimental and Analytical Studies on the Hysteretic Behavior of Reinforced Concrete Rectangular and T-Beams," by S.-Y.M. Ma, E.P. Popov and V.V. Bertero - 1976 (PB 260 843)A12

EERC 76-3 "Dynamic Behavior of a Multistory Triangular-Shaped Building," by J. Petrovski, R.M. Stephen, E. Gartenbaum and J.G. Bouwkamp - 1976 (PB 273 279)A07

EERC 76-4 "Earthquake Induced Deformations of Earth Dams," by N. Serff, H.B. Seed, F.I. Makdisi & C.-Y. Chang - 1976 (PB 292 065)A08

EERC 76-5   "Analysis and Design of Tube-Type Tall Building Structures," by H. de Clercq and G.H. Powell - 1976 (PB 252 220) A10

EERC 76-6   "Time and Frequency Domain Analysis of Three-Dimensional Ground Motions, San Fernando Earthquake," by T. Kubo and J. Penzien (PB 260 556)A11

EERC 76-7   "Expected Performance of Uniform Building Code Design Masonry Structures," by R.L. Mayes, Y. Omote, S.W. Chen and R.W. Clough - 1976 (PB 270 098)A05

EERC 76-8   "Cyclic Shear Tests of Masonry Piers, Volume 1 - Test Results," by R.L. Mayes, Y. Omote, R.W. Clough - 1976 (PB 264 424)A06

EERC 76-9   "A Substructure Method for Earthquake Analysis of Structure - Soil Interaction," by J.A. Gutierrez and A.K. Chopra - 1976 (PB 257 783)A08

EERC 76-10   "Stabilization of Potentially Liquefiable Sand Deposits using Gravel Drain Systems," by H.B. Seed and J.R. Booker - 1976 (PB 258 820)A04

EERC 76-11   "Influence of Design and Analysis Assumptions on Computed Inelastic Response of Moderately Tall Frames," by G.H. Powell and D.G. Row - 1976 (PB 271 409)A06

EERC 76-12   "Sensitivity Analysis for Hysteretic Dynamic Systems: Theory and Applications," by D. Ray, K.S. Pister and E. Polak - 1976 (PB 262 859)A04

EERC 76-13   "Coupled Lateral Torsional Response of Buildings to Ground Shaking," by C.L. Kan and A.K. Chopra - 1976 (PB 257 907)A09

EERC 76-14   "Seismic Analyses of the Banco de America," by V.V. Bertero, S.A. Mahin and J.A. Hollings - 1976

EERC 76-15   "Reinforced Concrete Frame 2: Seismic Testing and Analytical Correlation," by R.W. Clough and J. Gidwani - 1976 (PB 261 323)A08

EERC 76-16   "Cyclic Shear Tests of Masonry Piers, Volume 2 - Analysis of Test Results," by R.L. Mayes, Y. Omote and R.W. Clough - 1976

EERC 76-17   "Structural Steel Bracing Systems: Behavior Under Cyclic Loading," by E.P. Popov, K. Takanashi and C.W. Roeder - 1976 (PB 260 715)A05

EERC 76-18   "Experimental Model Studies on Seismic Response of High Curved Overcrossings," by D. Williams and W.G. Godden - 1976 (PB 269 548)A08

EERC 76-19   "Effects of Non-Uniform Seismic Disturbances on the Dumbarton Bridge Replacement Structure," by F. Baron and R.E. Hamati - 1976 (PB 282 981)A16

EERC 76-20   "Investigation of the Inelastic Characteristics of a Single Story Steel Structure Using System Identification and Shaking Table Experiments," by V.C. Matzen and H.D. McNiven - 1976 (PB 258 453)A07

EERC 76-21   "Capacity of Columns with Splice Imperfections," by E.P. Popov, R.M. Stephen and R. Philbrick - 1976 (PB 260 378)A04

EERC 76-22   "Response of the Olive View Hospital Main Building during the San Fernando Earthquake," by S. A. Mahin, V.V. Bertero, A.K. Chopra and R. Collins - 1976 (PB 271 425)A14

EERC 76-23   "A Study on the Major Factors Influencing the Strength of Masonry Prisms," by N.M. Mostaghel, R.L. Mayes, R. W. Clough and S.W. Chen - 1976 (Not published)

EERC 76-24   "GADFLEA - A Computer Program for the Analysis of Pore Pressure Generation and Dissipation during Cyclic or Earthquake Loading," by J.R. Booker, M.S. Rahman and H.B. Seed - 1976 (PB 263 947)A04

EERC 76-25   "Seismic Safety Evaluation of a R/C School Building," by B. Bresler and J. Axley - 1976

EERC 76-26   "Correlative Investigations on Theoretical and Experimental Dynamic Behavior of a Model Bridge Structure," by K. Kawashima and J. Penzien - 1976 (PB 263 388)A11

EERC 76-27   "Earthquake Response of Coupled Shear Wall Buildings," by T. Srichatrapimuk - 1976 (PB 265 157)A07

EERC 76-28   "Tensile Capacity of Partial Penetration Welds," by E.P. Popov and R.M. Stephen - 1976 (PB 262 899)A03

EERC 76-29   "Analysis and Design of Numerical Integration Methods in Structural Dynamics," by H.M. Hilber - 1976 (PB 264 410)A06

EERC 76-30   "Contribution of a Floor System to the Dynamic Characteristics of Reinforced Concrete Buildings," by L.E. Malik and V.V. Bertero - 1976 (PB 272 247)A13

EERC 76-31   "The Effects of Seismic Disturbances on the Golden Gate Bridge," by F. Baron, M. Arikan and R.E. Hamati - 1976 (PB 272 279)A09

EERC 76-32   "Infilled Frames in Earthquake Resistant Construction," by R.E. Klingner and V.V. Bertero - 1976 (PB 265 892)A13

UCB/EERC-77/01   "PLUSH - A Computer Program for Probabilistic Finite Element Analysis of Seismic Soil-Structure Inter-action," by M.P. Romo Organista, J. Lysmer and H.B. Seed - 1977

UCB/EERC-77/02   "Soil-Structure Interaction Effects at the Humboldt Bay Power Plant in the Ferndale Earthquake of June 7, 1975," by J.E. Valera, H.B. Seed, C.F. Tsai and J. Lysmer - 1977 (PB 265 795)A04

UCB/EERC-77/03   "Influence of Sample Disturbance on Sand Response to Cyclic Loading," by K. Mori, H.B. Seed and C.K. Chan - 1977 (PB 267 352)A04

UCB/EERC-77/04   "Seismological Studies of Strong Motion Records," by J. Shoja-Taheri - 1977 (PB 269 655)A10

UCB/EERC-77/05   "Testing Facility for Coupled-Shear Walls," by L. Li-Hyung, V.V. Bertero and E.P. Popov - 1977

UCB/EERC-77/06   "Developing Methodologies for Evaluating the Earthquake Safety of Existing Buildings," by No. 1 - B. Bresler; No. 2 - B. Bresler, T. Okada and D. Zisling; No. 3 - T. Okada and B. Bresler; No. 4 - V.V. Bertero and B. Bresler - 1977 (PB 267 354)A08

UCB/EERC-77/07   "A Literature Survey - Transverse Strength of Masonry Walls," by Y. Omote, R.L. Mayes, S.W. Chen and R.W. Clough - 1977 (PB 277 933)A07

UCB/EERC-77/08   "DRAIN-TABS: A Computer Program for Inelastic Earthquake Response of Three Dimensional Buildings," by R. Guendelman-Israel and G.H. Powell - 1977 (PB 270 693)A07

UCB/EERC-77/09   "SUBWALL: A Special Purpose Finite Element Computer Program for Practical Elastic Analysis and Design of Structural Walls with Substructure Option," by D.Q. Le, H. Peterson and E.P. Popov - 1977 (PB 270 567)A05

UCB/EERC-77/10   "Experimental Evaluation of Seismic Design Methods for Broad Cylindrical Tanks," by D.P. Clough (PB 272 280)A13

UCB/EERC-77/11   "Earthquake Engineering Research at Berkeley - 1976," - 1977 (PB 273 507)A09

UCB/EERC-77/12   "Automated Design of Earthquake Resistant Multistory Steel Building Frames," by N.D. Walker, Jr. - 1977 (PB 276 526)A09

UCB/EERC-77/13   "Concrete Confined by Rectangular Hoops Subjected to Axial Loads," by J. Vallenas, V.V. Bertero and E.P. Popov - 1977 (PB 275 165)A06

UCB/EERC-77/14   "Seismic Strain Induced in the Ground During Earthquakes," by Y. Sugimura - 1977 (PB 284 201)A04

UCB/EERC-77/15   "Bond Deterioration under Generalized Loading," by V.V. Bertero, E.P. Popov and S. Viwathanatepa - 1977

UCB/EERC-77/16   "Computer Aided Optimum Design of Ductile Reinforced Concrete Moment Resisting Frames," by S.W. Zagajeski and V.V. Bertero - 1977 (PB 280 137)A07

UCB/EERC-77/17   "Earthquake Simulation Testing of a Stepping Frame with Energy-Absorbing Devices," by J.M. Kelly and D.F. Tsztoo - 1977 (PB 273 506)A04

UCB/EERC-77/18   "Inelastic Behavior of Eccentrically Braced Steel Frames under Cyclic Loadings," by C.W. Roeder and E.P. Popov - 1977 (PB 275 526)A15

UCB/EERC-77/19   "A Simplified Procedure for Estimating Earthquake-Induced Deformations in Dams and Embankments," by F.I. Makdisi and H.B. Seed - 1977 (PB 276 820)A04

UCB/EERC-77/20   "The Performance of Earth Dams during Earthquakes," by H.B. Seed, F.I. Makdisi and P. de Alba - 1977 (PB 276 821)A04

UCB/EERC-77/21   "Dynamic Plastic Analysis Using Stress Resultant Finite Element Formulation," by P. Lukkunapvasit and J.M. Kelly - 1977 (PB 275 453)A04

UCB/EERC-77/22   "Preliminary Experimental Study of Seismic Uplift of a Steel Frame," by R.W. Clough and A.A. Huckelbridge 1977 (PB 278 769)A08

UCB/EERC-77/23   "Earthquake Simulator Tests of a Nine-Story Steel Frame with Columns Allowed to Uplift," by A.A. Huckelbridge - 1977 (PB 277 944)A09

UCB/EERC-77/24   "Nonlinear Soil-Structure Interaction of Skew Highway Bridges," by M.-C. Chen and J. Penzien - 1977 (PB 276 176)A07

UCB/EERC-77/25   "Seismic Analysis of an Offshore Structure Supported on Pile Foundations," by D.D.-N. Liou and J. Penzien 1977 (PB 283 180)A06

UCB/EERC-77/26   "Dynamic Stiffness Matrices for Homogeneous Viscoelastic Half-Planes," by G. Dasgupta and A.K. Chopra - 1977 (PB 279 654)A06

UCB/EERC-77/27   "A Practical Soft Story Earthquake Isolation System," by J.M. Kelly, J.M. Eidinger and C.J. Derham - 1977 (PB 276 814)A07

UCB/EERC-77/28   "Seismic Safety of Existing Buildings and Incentives for Hazard Mitigation in San Francisco: An Exploratory Study," by A.J. Meltsner - 1977 (PB 281 970)A05

UCB/EERC-77/29   "Dynamic Analysis of Electrohydraulic Shaking Tables," by D. Rea, S. Abedi-Hayati and Y. Takahashi 1977 (PB 282 569)A04

UCB/EERC-77/30   "An Approach for Improving Seismic - Resistant Behavior of Reinforced Concrete Interior Joints," B. Galunic, V.V. Bertero and E.P. Popov - 1977 (PB 290 870)A06

UCB/EERC-78/01   "The Development of Energy-Absorbing Devices for Aseismic Base Isolation Systems," by J.M. Kelly and D.F. Tsztoo - 1978 (PB 284 978)A04

UCB/EERC-78/02   "Effect of Tensile Prestrain on the Cyclic Response of Structural Steel Connections, by J.G. Bouwkamp and A. Mukhopadhyay - 1978

UCB/EERC-78/03   "Experimental Results of an Earthquake Isolation System using Natural Rubber Bearings," by J.M. Eidinger and J.M. Kelly - 1978 (PB 281 686)A04

UCB/EERC-78/04   "Seismic Behavior of Tall Liquid Storage Tanks," by A. Niwa - 1978 (PB 284 017)A14

UCB/EERC-78/05   "Hysteretic Behavior of Reinforced Concrete Columns Subjected to High Axial and Cyclic Shear Forces," by S.W. Zagajeski, V.V. Bertero and J.G. Bouwkamp - 1978 (PB 283 858)A13

UCB/EERC-78/06   "Inelastic Beam-Column Elements for the ANSR-I Program," by A. Riahi, D.G. Row and G.H. Powell - 1978

UCB/EERC-78/07   "Studies of Structural Response to Earthquake Ground Motion," by O.A. Lopez and A.K. Chopra - 1978 (PB 282 790)A05

UCB/EERC-78/08   "A Laboratory Study of the Fluid-Structure Interaction of Submerged Tanks and Caissons in Earthquakes," by R.C. Byrd - 1978 (PB 284 957)A08

UCB/EERC-78/09   "Model for Evaluating Damageability of Structures," by I. Sakamoto and B. Bresler - 1978

UCB/EERC-78/10   "Seismic Performance of Nonstructural and Secondary Structural Elements," by I. Sakamoto - 1978

UCB/EERC-78/11   "Mathematical Modelling of Hysteresis Loops for Reinforced Concrete Columns," by S. Nakata, T. Sproul and J. Penzien - 1978

UCB/EERC-78/12   "Damageability in Existing Buildings," by T. Blejwas and B. Bresler - 1978

UCB/EERC-78/13   "Dynamic Behavior of a Pedestal Base Multistory Building," by R.M. Stephen, E.L. Wilson, J.G. Bouwkamp and M. Button - 1978 (PB 286 650)A08

UCB/EERC-78/14   "Seismic Response of Bridges - Case Studies," by R.A. Imbsen, V. Nutt and J. Penzien - 1978 (PB 286 503)A10

UCB/EERC-78/15   "A Substructure Technique for Nonlinear Static and Dynamic Analysis," by D.G. Row and G.H. Powell - 1978 (PB 288 077)A10

UCB/EERC-78/16   "Seismic Risk Studies for San Francisco and for the Greater San Francisco Bay Area," by C.S. Oliveira - 1978

UCB/EERC-78/17   "Strength of Timber Roof Connections Subjected to Cyclic Loads," by P. Gülkan, R.L. Mayes and R.W. Clough - 1978

UCB/EERC-78/18   "Response of K-Braced Steel Frame Models to Lateral Loads," by J.G. Bouwkamp, R.M. Stephen and E.P. Popov - 1978

UCB/EERC-78/19   "Rational Design Methods for Light Equipment in Structures Subjected to Ground Motion," by J.L. Sackman and J.M. Kelly - 1978 (PB 292 357)A04

UCB/EERC-78/20   "Testing of a Wind Restraint for Aseismic Base Isolation," by J.M. Kelly and D.E. Chitty - 1978 (PB 292 833)A03

UCB/EERC-78/21   "APOLLO - A Computer Program for the Analysis of Pore Pressure Generation and Dissipation in Horizontal Sand Layers During Cyclic or Earthquake Loading," by P.P. Martin and H.B. Seed - 1978 (PB 292 835)A04

UCB/EERC-78/22   "Optimal Design of an Earthquake Isolation System," by M.A. Bhatti, K.S. Pister and E. Polak - 1978 (PB 294 735)A06

UCB/EERC-78/23   "MASH - A Computer Program for the Non-Linear Analysis of Vertically Propagating Shear Waves in Horizontally Layered Deposits," by P.P. Martin and H.B. Seed - 1978 (PB 293 101)A05

UCB/EERC-78/24   "Investigation of the Elastic Characteristics of a Three Story Steel Frame Using System Identification," by I. Kaya and H.D. McNiven - 1978

UCB/EERC-78/25   "Investigation of the Nonlinear Characteristics of a Three-Story Steel Frame Using System Identification," by I. Kaya and H.D. McNiven - 1978

UCB/EERC-78/26   "Studies of Strong Ground Motion in Taiwan," by Y.M. Hsiung, B.A. Bolt and J. Penzien - 1978

UCB/EERC-78/27   "Cyclic Loading Tests of Masonry Single Piers: Volume 1 - Height to Width Ratio of 2," by P.A. Hidalgo, R.L. Mayes, H.D. McNiven and R.W. Clough - 1978

UCB/EERC-78/28   "Cyclic Loading Tests of Masonry Single Piers: Volume 2 - Height to Width Ratio of 1," by S.-W.J. Chen, P.A. Hidalgo, R.L. Mayes, R.W. Clough and H.D. McNiven - 1978

UCB/EERC-78/29   "Analytical Procedures in Soil Dynamics," by J. Lysmer - 1978

UCB/EERC-79/01   "Hysteretic Behavior of Lightweight Reinforced Concrete Beam-Column Subassemblages," by B. Forzani, E.P. Popov, and V.V. Bertero - 1979

UCB/EERC-79/02   "The Development of a Mathematical Model to Predict the Flexural Response of Reinforced Concrete Beams to Cyclic Loads, Using System Identification," by J.F. Stanton and H.D. McNiven - 1979

UCB/EERC-79/03   "Linear and Nonlinear Earthquake Response of Simple Torsionally Coupled Systems," by C.L. Kan and A.K. Chopra - 1979

UCB/EERC-79/04   "A Mathematical Model of Masonry for Predicting Its Linear Seismic Response Characteristics," by Y. Mengi and H.D. McNiven - 1979

UCB/EERC-79/05   "Mechanical Behavior of Lightweight Concrete Confined by Different Types of Lateral Reinforcement," by M.A. Manrique, V.V. Bertero and E.P. Popov - 1979

UCB/EERC-79/06   "Static Tilt Tests of a Tall Cylindrical Liquid Storage Tank," by R.W. Clough and A. Niwa - 1979

UCB/EERC-79/07   "The Design of Steel Energy Absorbing Restrainers and Their Incorporation Into Nuclear Power Plants for Enhanced Safety: Volume 1 - Summary Report," by P.N. Spencer, V.F. Zackay, and E.R. Parker - 1979

UCB/EERC-79/08   "The Design of Steel Energy Absorbing Restrainers and Their Incorporation Into Nuclear Power Plants for Enhanced Safety: Volume 2 - The Development of Analyses for Reactor System Piping," "Simple Systems" by M.C. Lee, J. Penzien, A.K. Chopra, and K. Suzuki "Complex Systems" by G.H. Powell, E.L. Wilson, R.W. Clough and D.G. Row - 1979

UCB/EERC-79/09   "The Design of Steel Energy Absorbing Restrainers and Their Incorporation Into Nuclear Power Plants for Enhanced Safety: Volume 3 - Evaluation of Commerical Steels," by W.S. Owen, R.M.N. Pelloux, R.O. Ritchie, M. Faral, T. Ohhashi, J. Toplosky, S.J. Hartman, V.F. Zackay, and E.R. Parker - 1979

UCB/EERC-79/10   "The Design of Steel Energy Absorbing Restrainers and Their Incorporation Into Nuclear Power Plants for Enhanced Safety: Volume 4 - A Review of Energy-Absorbing Devices," by J.M. Kelly and M.S. Skinner - 1979

UCB/EERC-79/11   "Conservatism In Summation Rules for Closely Spaced Modes," by J.M. Kelly and J.L. Sackman - 1979

UCB/EERC-79/12   "Cyclic Loading Tests of Masonry Single Piers Volume
                  3 - Height to Width Ratio of 0.5," by P.A. Hidalgo,
                  R.L. Mayes, H.D. McNiven and R.W. Clough - 1979

UCB/EERC-79/13   "Cyclic Behavior of Dense Coarse-Grained Materials in
                  Relation to the Seismic Stability of Dams," by N.G.
                  Banerjee, H.B. Seed and C.K. Chan - 1979

UCB/EERC-79/14   "Seismic Behavior of Reinforced Concrete Interior Beam-Column
                  Subassemblages," by S. Viwathanatepa, E.P. Popov and
                  V.V. Bertero - 1979

UCB/EERC-79/15   "Optimal Design of Localized Nonlinear Systems with
                  Dual Performance Criteria Under Earthquake Excitations,"
                  by M.A. Bhatti - 1979

UCB/EERC-79/16   "OPTDYN - A General Purpose Optimization Program for
                  Problems with or without Dynamic Constraints," by
                  M.A. Bhatti, E. Polak and K.S. Pister - 1979

UCB/EERC-79/17   "ANSR-II, Analysis of Nonlinear Structural Response,
                  Users Manual," by D.P. Mondkar and G.H. Powell - 1979

UCB/EERC-79/18   "Soil Structure Interaction in Different Seismic
                  Environments," A. Gomez-Masso, J. Lysmer, J.-C. Chen
                  and H.B. Seed - 1979

UCB/EERC-79/19   "ARMA Models for Earthquake Ground Motions," by M.K.
                  Chang, J.W. Kwiatkowski, R.F. Nau, R.M. Oliver and
                  K.S. Pister - 1979

UCB/EERC-79/20   "Hysteretic Behavior of Reinforced Concrete Structural
                  Walls," by J.M. Vallenas, V.V. Bertero and E.P.
                  Popov - 1979

UCB/EERC-79/21   "Studies on High-Frequency Vibrations of Buildings I:
                  The Column Effects," by J. Lubliner - 1979

UCB/EERC-79/22   "Effects of Generalized Loadings on Bond Reinforcing Bars
                  Embedded in Confined Concrete Blocks," by S. Viwathanatepa,
                  E.P. Popov and V.V. Bertero - 1979

UCB/EERC-79/23   "Shaking Table Study of Single-Story Masonry Houses,
                  Volume 1: Test Structures 1 and 2," by P. Gülkan,
                  R.L. Mayes and R.W. Clough - 1979

UCB/EERC-79/24   "Shaking Table Study of Single-Story Masonry Houses,
                  Volume 2: Test Structures 3 and 4," by P. Gülkan,
                  R.L. Mayes and R.W. Clough - 1979

UCB/EERC-79/25   "Shaking Table Study of Single-Story Masonry Houses,
                  Volume 3: Summary, Conclusions and Recommendations,"
                  by R.W. Clough, R.L. Mayes and P. Gülkan - 1979

UCB/EERC-79/26   "Recommendations for a U.S.-Japan Cooperative Research
                  Program Utilizing Large-Scale Testing Facilities," by
                  U.S.-Japan Planning Group - 1979

UCB/EERC-79/27   "Earthquake-Induced Liquefaction Near Lake Amatitlan,
                  Guatemala," by H.B. Seed, I. Arango, C.K. Chan,
                  A. Gomez-Masso and R. Grant de Ascoli - 1979

UCB/EERC-79/28   "Infill Panels: Their Influence on Seismic Response of
                  Buildings," by J.W. Axley and V.V. Bertero - 1979

UCB/EERC-79/29   "3D Truss Bar Element (Type 1) for the ANSR-II Program,"
                  by D.P. Mondkar and G.H. Powell - 1979

UCB/EERC-79/30   "2D Beam-Column Element (Type 5 - Parallel Element
                  Theory) for the ANSR-II Program," by D.G. Row, G.H. Powell
                  and D.P. Mondkar

UCB/EERC-79/31   "3D Beam-Column Element (Type 2 - Parallel Element
                  Theory) for the ANSR-II Program," by A. Riahi, G.H. Powell
                  and D.P. Mondkar - 1979

UCB/EERC-79/32   "On Response of Structures to Stationary Excitation," by
                  A. Der Kiureghian - 1979

UCB/EERC-79/33   "Undisturbed Sampling and Cyclic Load Testing of Sands,"
                  by S. Singh, H.B. Seed and C.K. Chan - 1979

UCB/EERC-79/34   "Interaction Effects of Simultaneous Torsional and
                  Compressional Cyclic Loading of Sand," by P.M. Griffin
                  and W.N. Houston - 1979

UCB/EERC-80/01   "Earthquake Response of Concrete Gravity Dams Including
                  Hydrodynamic and Foundation Interaction Effects," by
                  A.K. Chopra, P. Chakrabarti and S. Gupta - 1980

UCB/EERC-80/02   "Rocking Response of Rigid Blocks to Earthquakes,"
                  by C.S. Yim, A.K. Chopra and J. Penzien - 1980

UCB/EERC-80/03   "Optimum Inelastic Design of Seismic-Resistant Reinforced
                  Concrete Frame Structures," by S.W. Zagajeski and V.V.
                  Bertero - 1980

UCB/EERC-80/04   "Effects of Amount and Arrangement of Wall-Panel
                  Reinforcement on Hysteretic Behavior of Reinforced
                  Concrete Walls," by R. Iliya and V.V. Bertero - 1980

UCB/EERC-80/05   "Shaking Table Research on Concrete Dam Models," by
                  A. Niwa and R.W. Clough - 1980

UCB/EERC-80/06   "Piping With Energy Absorbing Restrainers: Parameter
                  Study on Small Systems," by G.H. Powell, C. Oughourlian
                  and J. Simons - 1980

UCB/EERC-80/07   "Inelastic Torsional Response of Structures Subjected to Earthquake Ground Motions," by Y. Yamazaki - 1980

UCB/EERC-80/08   "Study of X-Braced Steel Frame Structures Under Earthquake Simulation," by Y. Ghanaat - 1980

UCB/EERC-80/09   "Hybrid Modelling of Soil-Structure Interaction," by S. Gupta, T.W. Lin, J. Penzien and C.S. Yeh - 1980

UCB/EERC-80/10   "General Applicability of a Nonlinear Model of a One Story Steel Frame," by B.I. Sveinsson and H. McNiven - 1980

UCB/EERC-80/11   "A Green-Function Method for Wave Interaction with a Submerged Body," by W. Kioka - 1980

UCB/EERC-80/12   "Hydrodynamic Pressure and Added Mass for Axisymmetric Bodies," by F. Nilrat - 1980

UCB/EERC-80/13   "Treatment of Non-Linear Drag Forces Acting on Offshore Platforms," by B.V. Dao and J. Penzien - 1980

UCB/EERC-80/14   "2D Plane/Axisymmetric Solid Element (Type 3 - Elastic or Elastic-Perfectly Plastic) for the ANSR-II Program," by D.P. Mondkar and G.H. Powell - 1980

UCB/EERC-80/15   "A Response Spectrum Method for Random Vibrations," by A. Der Kiureghian - 1980

UCB/EERC-80/16   "Cyclic Inelastic Buckling of Tubular Steel Braces," by V.A. Zayas, E.P. Popov and S.A. Mahin - June 1980

UCB/EERC-80/17   "Dynamic Response of Simple Arch Dams Including Hydrodynamic Interaction," by C.S. Porter and A.K. Chopra - July 1980

UCB/EERC-80/18   "Experimental Testing of a Friction Damped Aseismic Base Isolation System with Fail-Safe Characteristics," by J.M. Kelly, K.E. Beucke and M.S. Skinner - July 1980

UCB/EERC-80/19   "The Design of Steel Energy-Absorbing Restrainers and their Incorporation into Nuclear Power Plants for Enhanced Safety (Vol 1B): Stochastic Seismic Analyses of Nuclear Power Plant Structures and Piping Systems Subjected to Multiple Support Excitations," by M.C. Lee and J. Penzien - 1980

UCB/EERC-80/20   "The Design of Steel Energy-Absorbing Restrainers and their Incorporation into Nuclear Power Plants for Enhanced Safety (Vol 1C): Numerical Method for Dynamic Substructure Analysis," by J.M. Dickens and E.L. Wilson - 1980

UCB/EERC-80/21   "The Design of Steel Energy-Absorbing Restrainers and their Incorporation into Nuclear Power Plants for Enhanced Safety (Vol 2): Development and Testing of Restraints for Nuclear Piping Systems," by J.M. Kelly and M.S. Skinner - 1980

UCB/EERC-80/22   "3D Solid Element (Type 4-Elastic or Elastic-Perfectly-Plastic) for the ANSR-II Program," by D.P. Mondkar and G.H. Powell - 1980

UCB/EERC-80/23   "Gap-Friction Element (Type 5) for the ANSR-II Program," by D.P. Mondkar and G.H. Powell - 1980

UCB/EERC-80/24   "U-Bar Restraint Element (Type 11) for the ANSR-II Program," C. Oughourlian and G.H. Powell - 1980

UCB/EERC-80/25   "Testing of a Natural Rubber Base Isolation System by an Explosively Simulated Earthquake," by J.M. Kelly 1980

UCB/EERC-80/26   "Input Identification from Structural Vibrational Response," by Y. Hu - 1980

UCB/EERC-80/27   "Cyclic Inelastic Behavior of Steel Offshore Structures," by V.A. Zayas, S.A. Mahin and E.P. Popov - 1980

UCB/EERC-80/28   "Shaking Table Testing of a Reinforced Concrete Frame with Biaxial Response," M.G. Oliva and R.W. Clough 1980